IS-T 1766

Line Narrowing Spectroscopic Studies of DNA-carcinogen adducts and DNA-dye Complexes

by

Suh, Myungkoo

PHD Thesis submitted to Iowa State University

Ames Laboratory, U.S. DOE

Iowa State University

Ames, Iowa 50011

Date Transmitted: December 6, 1995

This report has been reproduced directly from the best available copy.

AVAILABILITY:

To DOE and DOE contractors: Office of Scientific and Technical Information
P.O. Box 62
Oak Ridge, TN 37831

prices available from: (615) 576-8401
FTS: 626-8401

To the public: National Technical Information Service
U.S. Department of Commerce
5285 Port Royal Road
Springfield, VA 22161

Line narrowing spectroscopic studies of DNA-carcinogen adducts

and DNA-dye complexes

Myungkoo Suh

Major Professor: Dr. Gerald J. Small

Iowa State University

Laser-induced fluorescence line narrowing (FLN) and non-line narrowing (NLN) spectroscopic methods were applied to conformational studies of stable DNA adducts of the 7β,8α-dihydoxy-9α,10α-epoxy-7,8,9,10-tetrahydrobenzo[*a*]pyrene (*anti*-BPDE). Stereochemically distinct (+)-*trans*-, (-)-*trans*-, (+)-*cis*- and (-)-*cis* adducts of *anti*-BPDE bound to exocyclic amino group of the central guanine in the oligonucleotide, 5'-d(CCATCGCTACC) · (GGTAGCGATGG), exist in a mixture of conformations in frozen aqueous buffer matrices. The (+)-*trans* adduct adopts primarily an external conformation with a smaller fraction (~25%) exists in a partially base-stacked conformation. Both *cis* adducts were found to be intercalated with significant π-π stacking interactions between the pyrenyl residues and the bases. Conformations of the *trans*-adduct of (+)-*anti* -BPDE in 11-mer oligonucleotides d(CTATG$_1$G$_2$G$_3$TATC) were studied as a function of flanking bases. In single stranded form the adduct at G$_2$ or G$_3$ (5'-flanking base guanine) adopts a conformation with strong interaction with the bases. In contrast, the adduct with a 5'-flanking thymine exists in a primarily helix-external conformation. Similar differences were observed in the double stranded oligonucleotides. The nature of the 3'-flanking base has little influence on the conformational equilibrium of the (+)-*trans-anti* BPDE-dG adduct. The formation and

repair of BPDE-N^2-dG in DNA isolated from the skin of mice treated topically with benzo[*a*]pyrene (BP) was studied. Low-temperature fluorescence spectroscopy of the intact DNA identified the major adduct as (+)-*trans-anti*-BPDE-N^2-dG, and the minor adduct fraction consisted mainly of (+)-*cis-anti*-BPDE-N^2-dG. The (+)-*cis*- adducts were repaired more slowly than most other adducts. Moreover, the (+)-*trans*-adducts exhibited a broad distribution of base-stacked, partially base-stacked, and helix-external conformations and the adducts with the base-stacked conformation are repaired less readily than the others.

Optical and hole burning properties of the DNA binding fluorescent dye TO-PRO-3 were studied using absorption and fluorescence spectroscopy. We found that saturated hole depth of TO-PRO-3 decreased dramatically when bound to DNA. The saturated hole depth and hole growth kinetics of the dye bound to DNA also changed depending on DNA types, sequences and lengths all of which affect the interaction between the dye and DNA. Unlike the saturated hole depth and hole growth kinetics, the hole width of the dye bound to DNA remained practically the same. It is concluded that the dye binds to DNA in various modes, and the binding mode of the dye can be external and partially intercalated. The distribution of the binding modes and the coupling of the dye with its environment are found to be responsible for differences in the observed hole burning properties. The hole growth kinetic property of the homodimeric dye TO-TO-3 also depended on its environment.

TABLE OF CONTENTS

CHAPTER 1. GENERAL INTRODUCTION

1.1 DNA damage by the potent carcinogen benzo[a]pyrene

1.1.1 Formation of DNA-BPDE adducts

Various organic and inorganic compounds are known to be potential carcinogens. Among the most potent and widely distributed chemical carcinogens are the polycyclic aromatic hydrocarbons (PAHs), which are found mostly in petroleum and combustion products derived from heat and power generation and motor vehicle exhausts [1]. Since the first investigation into the tumorigenic properties of PAH occurred about 200 years ago with the report that chimney sweeps developed scrotal cancer due to their occupational exposure to soot [2], carcinogenesis by PAHs has been the subject of numerous investigations [3-5]. Later [6], the compound responsible for the scrotal cancer was identified as benzo[a]pyrene (BP). BP is the most extensively studied environmental carcinogen [7]: in the United States its emission into the air is estimated about 900-1300 tons per year as the result of combustion of fossil fuels [1,8].

It is believed that the initial event in cancer is adduct formation between cellular DNA and carcinogens [7]. However, PAHs are chemically inert toward DNA, therefore, metabolic activation by biological enzyme systems is necessary to convert them to reactive electrophiles. In cells, BP can be activated by two major mechanisms, monooxygenation to yield bay-region diol epoxides [9-11] and one-electron-oxidation to yield radical cations [12-14]. The schematic representation of the BP activation pathway leading to the formation of electrophilic 7,8-dihydroxy-9,10-epoxy-7,8,9,10-tetrahydrobenzo[a]pyrene (BPDE), which eventually forms the major stable adducts to DNA, is illustrated in Figure 1-1. Upon its introduction into certain cells, BP is readily oxidized to a 7,8-oxide [15] by a microsomal
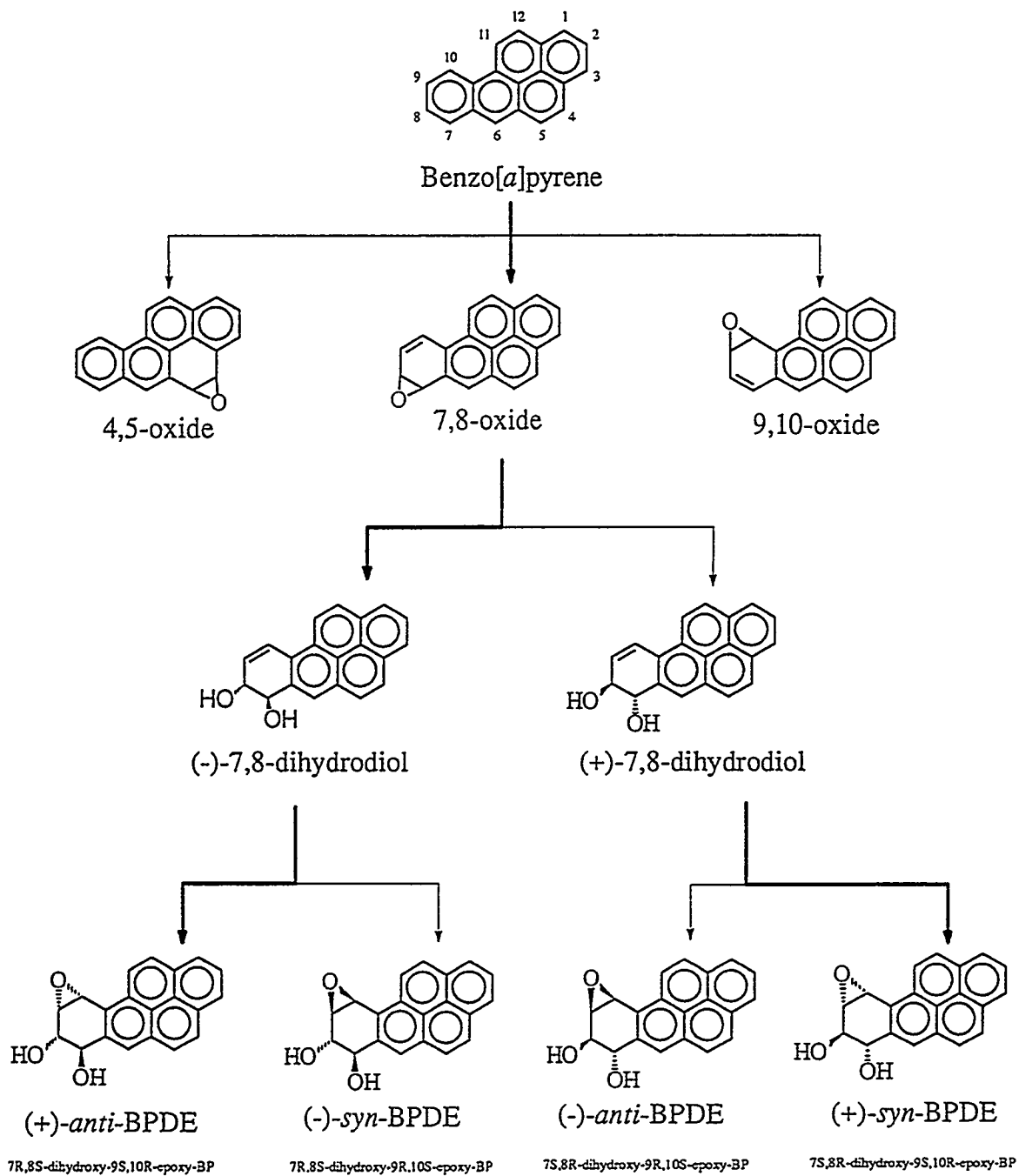
Figure 1-1. The metabolic pathways of benzo[a]pyrene to epoxides, dihydrodiol and 7,8-dihydrodiol-9,10-epoxides. The thick solid lines indicate the major pathways.

system which includes cytochrome p-450 and epoxide hydrolase. The resulting arene oxides are then transformed to the corresponding (±)-*trans*-7,8-dihydrodiols [16,17], which might be transformed further to various metabolites. The BP 7,8-dihydrodiols are further metabolized to reactive metabolites, 7,8-diol 9,10-epoxides (BPDEs), which are known to bind covalently to DNA [18,19].

Among the four different isomeric BPDEs, (+)-*anti*-BPDE is believed to be the predominant isomer produced metabolically (90%), but minor amounts of (-)-*anti*-BPDE and (±)-*syn*-BPDE are also formed [9]. The preferred reaction of (+)-*anti*-BPDE to DNA occurs via the formation of a covalent bond between the electrophilic C10 carbon of BPDE and the exocyclic N^2-amino group of guanine base in DNA (N^2-dG adduct), which accounts for ~90 % of its adducts with DNA [20]. Other minor adducts such as N^6-adenine and O^6-guanine and N^7-guanine adducts are also formed. The adduct formation of (-)-*anti*-BPDE to DNA is less regiospecific, yielding only 50 % of the N^2-dG products along with substantial amounts of other adducts. The N^2-dG adducts can be formed via *trans* or *cis* addition of N^2-amino group of guanine base to C10 position with respect to the epoxides, and the resulting four *trans*- and *cis-anti*-BPDE-N^2-dG adducts are shown in Figure 1-2. The ratio of *trans* to *cis* addition adducts is very high, 94:1, for (+)-*anti*-BPDE while in the case of (-)-*anti*-BPDE the ratio is substantially reduced to 63:22 [21].

1.1.2 Biological activity of DNA-BPDE adducts

Racemic *anti*-BPDE is reported to be more mutagenic than (±)-*syn*-BPDE [22,23]. Moreover, (+)- and (-)-enantiomers of *anti*-BPDE exhibit striking differences in biological activities. The results of tumorigenicity studies on mouse skin indicated that the (+)-*anti*-BPDE possesses 60-70% of the skin tumor-initiating activity of benzo[*a*]pyrene diol epoxide whereas the (-)-*anti*-BPDE, as well as the two enantiomers of syn-BPDE, were either very

(+)-*trans-anti*-BPDE-N^2-dG

(+)-*cis-anti*-BPDE-N^2-dG

(+)-*anti*-BPDE

7R,8S-dihydroxy-9S,10R-epoxy-BP

(-)-*trans-anti*-BPDE-N^2-dG

(-)-*cis-anti*-BPDE-N^2-dG

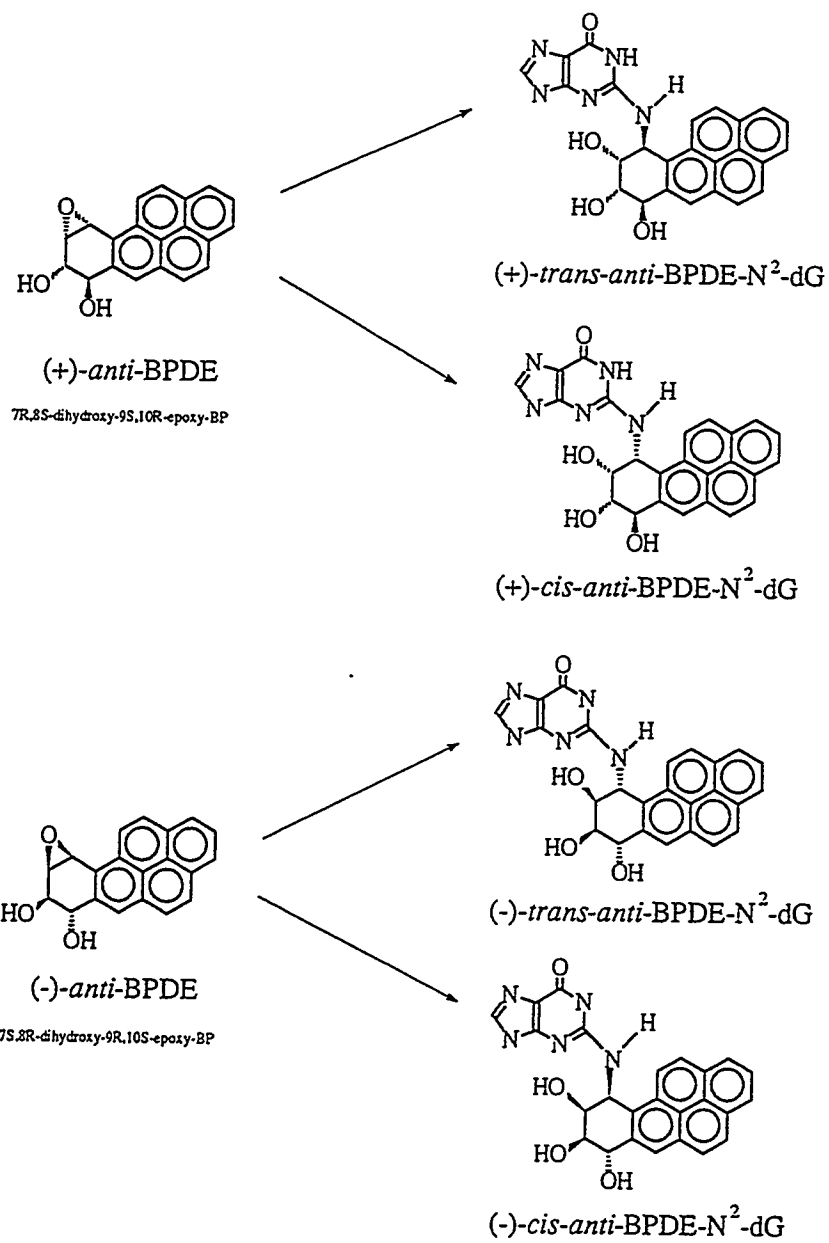(-)-*anti*-BPDE

7S,8R-dihydroxy-9R,10S-epoxy-BP

Figure 1-2. Structures of the four stereoisomeric *anti*-BPDE-N^2-dG adducts.

weakly tumorigenic or were essentially inactive [24]. Detailed studies on the tumorigenicity of BPDEs in newborn mice have confirmed that the (+)-*anti*-BPDE was more than 30-fold more potent in inducing lung adenomas in newborn mice than benzo[*a*]pyrene, (-)-*anti*- and (±)-*syn*-BPDE when each compound was administered to newborn mice at equal dose [25,26]. In this *in vivo* model, it was also established that (+)-*anti*-BPDE is the ultimate carcinogenic metabolite of benzo[*a*]pyrene. However, the mutagenic efficiencies of the two enantiomers, (+)-*anti*- and (-)-*anti*-BPDE, are different depending on the selected bacterial and mammalian cell systems studied: in *S. typhimurium* cells (strain TA98), the mutagenic activities of (+)-and (-)-enantiomers are almost identical, but in TA100 strain, as well as in mammalian Chinese hamster ovary cells (v79 cells), the activity of (+)-*anti*-BPDE is 4-6 times greater than that of (-)-*anti*-BPDE [27,28]. Although the same adduct distributions are found in both the bacterial and human cells, the relative mutagenicity of (+)-*anti*-BPDE is about 7 times higher than that of the (-)-enantiomer in diploid human fibroblasts [29]. The differences in the mutagenicity imply that the same lesions are processed differently in human and bacterial cells.

The covalent binding of BPDE to DNA induces errors in DNA replication and transcription. Detailed *in vitro* studies of BPDE-dG lesions in DNA using site-specific and stereospecific BPDE-N^2-dG oligonucleotide adducts as templates reported that the DNA and RNA polymerase activity as well as the type of mutations depends strongly on the stereochemistry of the BPDE-N^2-dG lesion [30,31]. DNA polymerase I (Klenow fragment) showed relatively easy bypass of the (-)-*trans-anti*-BPDE-N^2-dG lesion with misincorporation of dAMP (GC →AT transversion), while in the case of (-)-*cis-anti*-BPDE-N^2-dG lesion, very poor bypass with base deletion was observed [31]. Also, in the same study, if the 5' flanking base of the lesion site was changed from dC to dT, the frequency of one base deletion increased 9.3-fold. On the other hand, T7 DNA polymerase (Sequenase

2.0) and human polymerase α were strongly blocked by (+)-*trans* - and (+)-*cis*-BPDE adducts and a small amount of dCMP was preferentially incorporated opposite to lesion [30]. These different behaviors of DNA polymerases with the same BPDE lesion indicate that the mutational spectra are influenced by the types of DNA polymerases and may explain in part why the mutagenicity of the same BPDE adduct is different in mammalian cells and in bacterial cells. An investigation of the influences of site-specific and stereospecific BPDE-DNA adducts on transcription using T7 RNA polymerase revealed that the transcription is significantly inhibited in the order of (+)-*trans-* > (-)-*trans-* > (+)-*cis-* > (-)-*cis*-BPDE-N^2-dG at the lesion site [32].

1.1.3 Conformations of DNA-BPDE adducts

There have been many studies of the conformations of *anti*-BPDE-N^2-dG adducts in DNA using various techniques [5,33-35] aimed at investigating carcinogen structure and biological function relationship. In this section, however, only very recent findings, mostly studied with high resolution NMR spectroscopies, will be discussed. Using molecular mechanics methods and the energy-minimization computational program DUPLEX with extensive conformational searches, Singh et al. obtained molecular structures of the (+)- and (-)-*trans-anti*-BPDE-N^2-dG lesions in a duplex dodecamer $(dG-dC)_6 \cdot (dG-dC)_6$ [36]. This theoretical study successfully predicted that both (+)- and (-)-*trans* adducts were positioned externally in the minor groove of DNA and that the pyrenyl ring system pointed towards the 5' side of the modified strand for (+)-*trans* adducts while in (-)-*trans* adducts the pyrenyl ring system pointed towards the 3' side of the modified strand. The solution structures of (+)- and (-)-*trans-anti*-BPDE-N^2-dG oligonucleotides were determined by two-dimensional NMR spectroscopic techniques by Cosman et al. [37] and de los Santos et al. [38], respectively. The refined structures of (+)- and (-)-*trans-anti*-BPDE-N^2-dG modified

oligonucleotides are shown in Figure 1-3. As predicted by Singh et al. [36], the pyrenyl ring systems of these adducts are located at the minor groove with their long axes directed towards the 5' side and 3' side of the modified strands for the (+)- and (-)-*trans* adducts, respectively. The angle between the long axis of the pyrenyl ring and the average helix axis is about 45° in the (+)-*trans-anti*-BPDE modified oligonucleotide d(CCATC**G**CTACC) d(GGTAGCGATGG), where bold typesetting is used for the BPDE lesion site, and is approximately 40° in the (-)-*trans-anti*-BPDE modified duplex. All base pairs are intact, despite the fact that the minor groove is widened to ~8 Å in order to accommodate the pyrenyl ring system of both (+)- and (-)-*trans* adducts.

The solution structure of the (+)-*cis-anti*-BPDE adduct in the same duplex oligonucleotide was reported as an intercalative complex of pyrenyl ring [39]. The NMR study of the (+)-*cis-anti*-BPDE modified duplex oligonucleotide shows (see Figure 1-4) that the benzylic ring of the covalently bound BPDE moiety is inserted between adjacent base pairs. The modified dG residue is displaced into the minor groove, and stacked over the sugar ring of the adjacent cytosine residue on the 5' side. The partner C residue on the complementary strand is displaced from the center of the duplex towards the major groove. The base pair at the -**G**C-site is disrupted, while all other base pairs are intact and of the Watson-Crick type. The long axis of the BPDE ring is orthogonal to the flanking dG:dC base pair and spans both grooves of the helix. In this conformation, there is a larger extent of pyrenyl-base stacking interaction than in the *trans*-BPDE modified duplexes. While the solution structure of the (-)-*cis-anti*-BPDE-N^2-dG adduct has not yet been determined by high-resolution NMR methods, optical spectroscopic studies carried out with polynucleotides and oligonucleotides modified covalently with (+)- and (-)-*anti*-BPDE suggest that both *cis* adducts are characterized by intercalative conformation with strong pyrenyl-base stacking interaction [34].

A

(-)-trans-*anti*-BPDE-N²-dG

B

(+)-trans-*anti*-BPDE-N²-dG
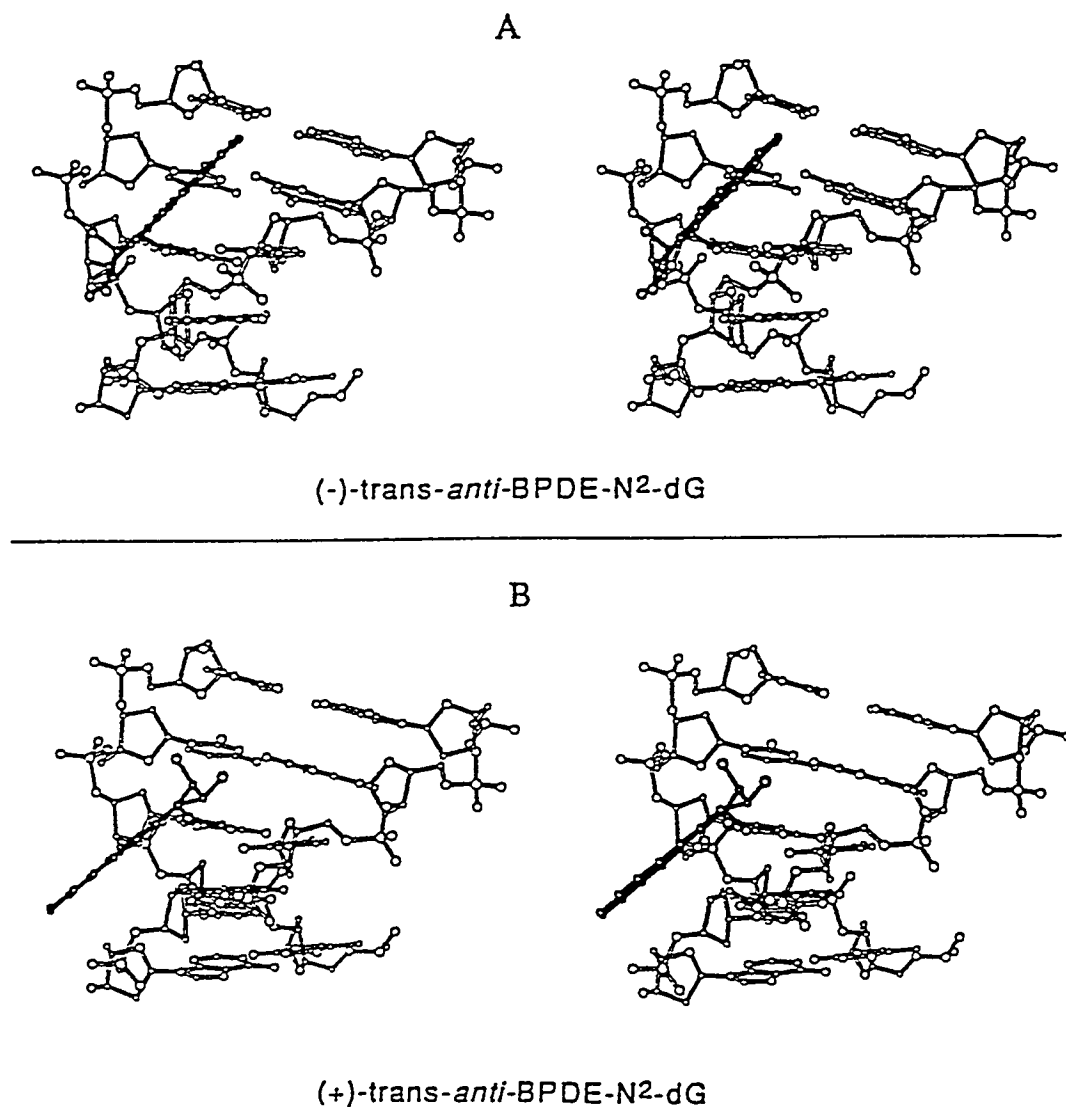
Figure 1-3. Stereo pairs of (-)-*trans*- (frame A) and (+)-*trans-anti*-BPDE-N²-dG (frame B) adducts to a duplex oligonucleotide in solution. Only the central d-(TCGCT)·d-(AGCGA) segment is shown. The BPDE moiety is shown with darkened bonds. 3'-Thymine is the base in the upper left-hand corner. The long axis of the pyrenyl system is directed toward the 3'-end of the modified strand for the (-)-*trans* adduct and is directed toward the 5'-end of the modified strand for the (+)-*trans* adduct.
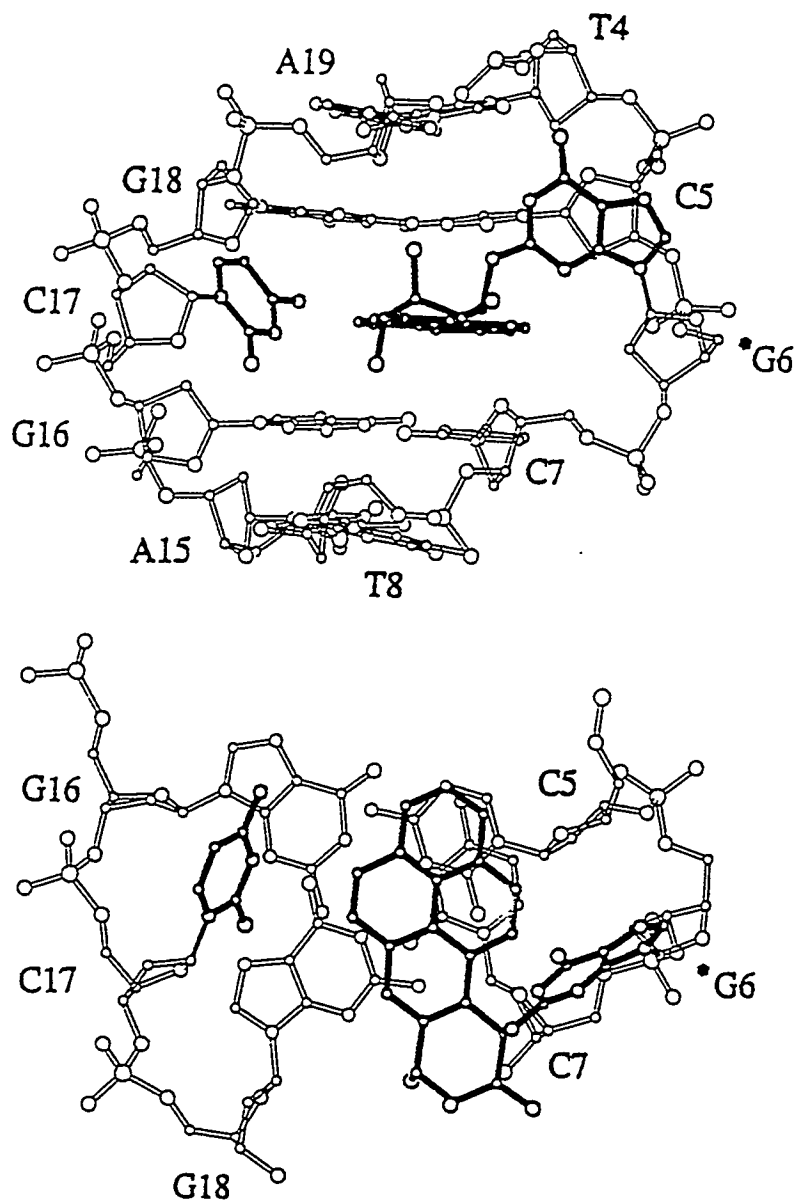
Figure 1-4. Solution structures of the (+)-*cis-anti*-BPDE-N^2-dG adduct in a duplex oligonucleotide. Only the central d-(TCGCT)·d-(AGCGA) segment is shown. Base numbering is d(T4-C5-G6-C7-T8)·d(A15-G16-C17-G18-A19) with T4 corresponding to the 5' end of the segment. (Top) A view looking into the minor groove and normal to the helix axis. (Bottom) A view looking down the helix axis.

1.1.4 Enzymatic repair of BPDE-adducts

Removal of DNA-carcinogen adducts by cellular DNA repair enzymes is as important as formation of DNA-carcinogen adducts in carcinogenesis. The importance of repair of DNA-BPDE adducts was demonstrated by Pelling and Slaga in their study with ($\pm$)-*syn* and *anti*-BPDE topically applied to mice [40]. The modification levels of DNA by ($\pm$)-*syn*- and ($\pm$)-*anti*-BPDE in the mouse basal cell layer at 3,12 and 24 hours after topical treatment with the corresponding BPDE were equivalent. However, the BPDE levels of the two diastereomers at macromolecules (DNA, RNA and proteins) in whole epidermis showed two different time courses: at 3 hours after the treatment, 3 times more racemic ($\pm$)-*syn*-BPDE adducts was bound to DNA isolated from whole epidermis (also RNA and proteins showed a similar binding ratio pattern), while 12 hours after treatment the two diastereomers bound to the same extent. The 24 hours sample contained ~2 times more ($\pm$)-*anti*-BPDE adducts than *syn* isomers. The absence of any observable difference between the amount of *anti*- and *syn*-diastereomer bound to basal DNA suggested that the previously reported difference in carcinogenicities of the two diastereomers is rather due to the preferential removal of *syn* adducts and not to the difference in the extent of DNA binding. The preferential removal of the *syn*- over the *anti*-diastereomer was later supported by the finding of Mcleod et al. in their study of ($\pm$)-*syn*- and ($\pm$)-*anti*-BPDE adduct removal in Chinese hamster ovary (CHO) cells. The *syn*-diastereomer was found to be removed twice as fast as the *anti*-BPDE adducts [41].

The importance of repair efficiency in carcinogenesis was further demonstrated in the repair study of cyclobutane pyrimidine dimers (CPD) in mammalian cells using Southern (DNA) blot techniques and the ligation-mediated polymerase chain reaction [42,43]. It was reported that the CPD repair is gene-specific and is more efficient on transcribed strand of active genes than untranscribed ones [43,44]. Also, seven of eight positions frequently

mutated in skin cancer were repaired more slowly than those at the surrounding positions on the same strand. Similar preferential adduct repair on the transcribed strand was observed with (+)-*anti*-BPDE adducts in human diploid fibroblasts [45]. Base sequence dependence of incision repair activity of UVRABC nuclease from *E. coli* at BPDE lesion sites was also observed [46].

1.2 Fluorescence Line Narrowing Spectroscopy

1.2.1 Optical line- and spectral shapes in solid state spectroscopy

In the solid state, all guest molecules (sample) are frozen, therefore, they have no freedom of translation and rotation, and at sufficiently low temperature generally only the lowest molecular vibrational mode is populated. Hence, it might be expected that molecular spectra at low temperature are much simpler than gaseous or liquid samples. However, the interaction between a guest molecule and its surrounding matrix molecules (host) affects the line and band shapes resulting in broadening of spectral bands. For simplicity, in the following discussion the guest molecules are assumed to be isolated by the matrix at low temperature.

In solid state molecular systems, there are two types of spectral broadening: homogeneous and inhomogeneous broadenings. First, the interaction between the guest molecules and the lattice vibrations (phonons) of the host results in homogeneous line broadening by "dephasing". The strongly temperature-dependent, periodical movements of the matrix molecules result in destruction of the phase relations between the ground state and excited state involved in the transition. The total temperature dependent homogeneous bandwidth of the spectral band is given by :

$$\Gamma_{hom} = (\pi \tau_2 c)^{-1}$$

where $1/\tau_2 = 1/(2\tau_1) + 1/\tau_2'$, τ_2 is the total dephasing time, τ_1 is the life time of the excited state, τ_2' is the pure dephasing time, and c is the speed of light. As the dephasing is mediated by phonons that are excited by thermal motion, it is strongly temperature dependent. Since Γ_{hom} determines the ultimate spectral resolution attainable, low temperature is required for high resolution spectroscopy to minimize the number of thermally populated low-frequency phonons responsible for Γ_{hom}. For moderate to good fluorophores, the homogeneous broadening from τ_1 is very small compared to τ_2' . For glass hosts, it is now firmly established that Γ_{hom} from pure dephasing is ≤ 0.1 cm^{-1} at 4.2 K [47,48]. The coupling between the electronic transitions of the guest molecules and the matrix phonons also has marked effects on the general shape of the spectral lines. In solid state spectroscopy, the spectral line consists of a narrow line, the "zero-phonon line (ZPL)", accompanied by a broad band, the "phonon wing (PW)", at its low energy side in the emission spectrum. The phonon wing is the result of the electron-phonon coupling which will be discussed separately in the next section.

Secondly, the energies of the electronic states of guest molecules are affected by static interactions with the lattice [49]. If the host lattice is perfect, the interaction is the same for all guest molecules resulting in a single spectral line as shown in Figure 1-5 A. The single line has a Lorentzian line shape and a homogeneous line width, Γ_{hom}. However, the immediate environments (sites) of the guest molecules in an amorphous lattice are inequivalent as shown in Figure 1-5 B. The statistical distribution of the inequivalent sites leads to a Gaussian distribution of frequencies for any given vibronic transition. The full width at half maximum (FWHM) of the Gaussian distribution is referred to as inhomogeneous line width, Γ_{inh}. Spectra of molecules dissolved in amorphous solids (such as glasses and polymers) usually exhibit a bandwidth, Γ_{inh}, of hundreds of cm^{-1}, $\approx 100 - 300$ cm^{-1} . In contrast, for crystalline hosts, Γ_{inh} is reduced by about 2 orders of magnitude.
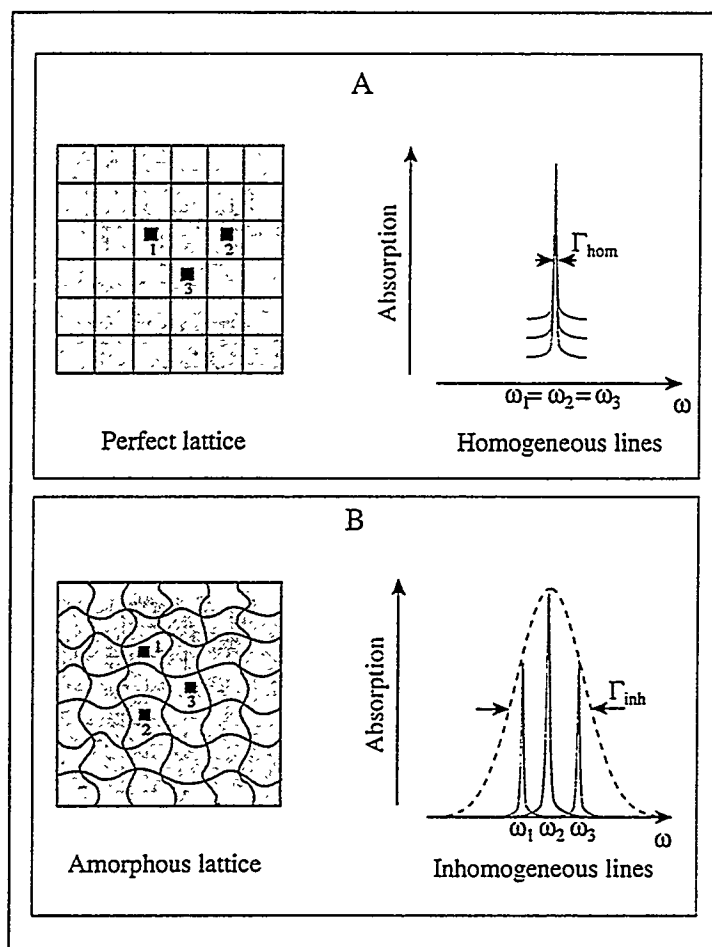
Figure 1-5. Schematic view of the optical absorption lines of three (identical) guest molecules in a perfect crystal (A) and in an amorphous host (B).

In order to achieve high resolution in solid state spectroscopy, the inhomogeneous broadening, Γ_{inh}, must be eliminated or reduced. This can be accomplished in two ways. 1) One can incorporate the guest molecule in a more uniform matrix. For example, by dissolving polycyclic aromatic hydrocarbons either in a single crystal of another hydrocarbon with approximately the same molecular dimension (mixed crystal technique) or in a suitable n-alkane (Shpol'skii technique), one can achieve the linewidths of a few cm^{-1}. 2) More generally applicable techniques are laser-based line-narrowing spectroscopies. Narrow lines with a homogeneous linewidth can be extracted from an inhomogeneously broadened band by using selective narrow line excitation. Fluorescence line narrowing spectroscopy (FLNS) is a low temperature solid state spectroscopic technique which eliminates or significantly reduces the contribution from Γ_{inh} to the vibronic fluorescence bandwidth. Also, spectral hole burning spectroscopy is another member of this class. Both fluorescence line narrowing and spectral hole burning spectroscopy will be discussed in separate sections later in this chapter.

1.2.2 Electron-Phonon Coupling

The theoretical background of electron-phonon coupling has been discussed extensively in the literature [50,51]. In this section, only a brief summary of the most relevant features will be given. Figure 1-6 illustrates transitions between two electronic states. The electronic ground state with energy E_0 and the first excited state with energy E_1 of a guest molecule are depicted in interaction with a matrix phonon i (energy $h\nu_i$). A number of phonon quanta are described by the harmonic oscillator model. Along the horizontal axis, the lattice normal coordinate q_i belonging to phonon mode i is plotted. Because the interaction with the matrix is influenced by the electronic distribution of the guest, the minima in the curves for ground and excited electronic states generally lie at
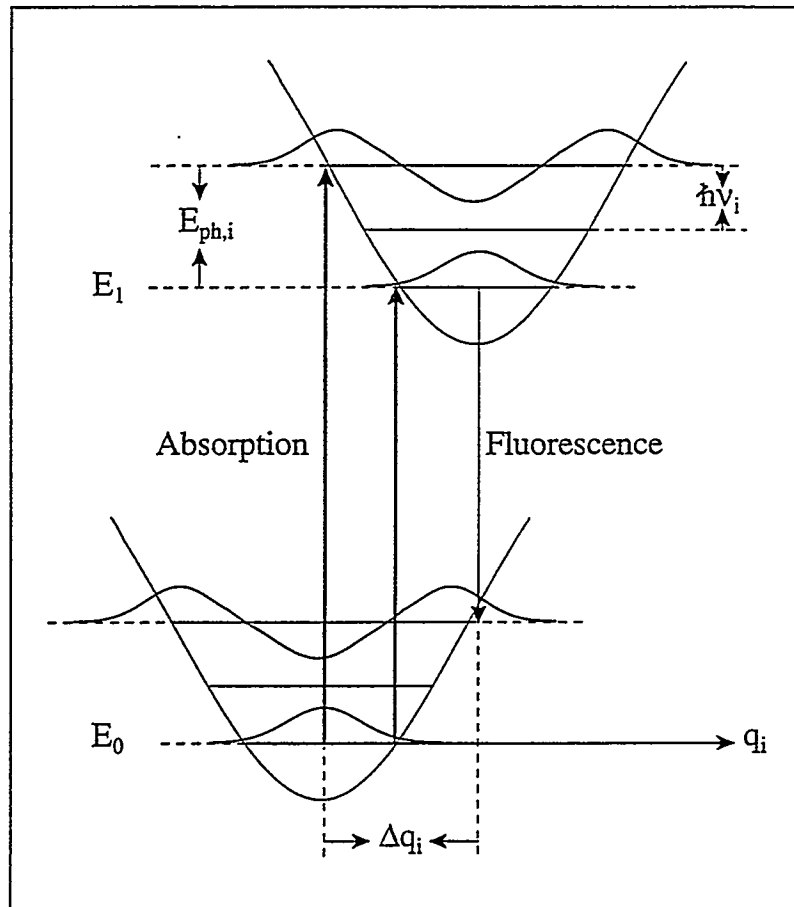
15

Figure 1-6. Energy diagram for illustrating the origin of phonon sidebands in solid state electronic spectra in terms of configurational coordinates. Electronic (E_0, E_1) and phonon ($h\nu_i$) energy levels are represented. q_i is a normal coordinate of the lattice.

different values of q_i with the difference Δq_i. The corresponding energy change of electronic

excitation from E_0 to E_1 is proportional to the force constant $K_i = m_i v_i^2$ of the harmonic

oscillator with frequency v_i and mass m_i:

$$E_{ph,i} = \frac{1}{2} K_i (\Delta q_i)^2 = \frac{1}{2} m_i v_i^2 (\Delta q_i)^2$$

The energy $E_{ph,i}$ corresponds to half of the Stokes-shift between the maxima of the

absorption and emission spectra. Similar to the intramolecular vibronic transitions, the

Franck-Condon principle applies in this case, i.e. the electronic transitions take place so fast

that the nuclear positions can be considered fixed. Thus, the electronic transitions are

represented by vertical lines in Figure 1-6. As illustrated in the figure, a number of

transitions can occur with simultaneous change of the vibrational state of the host and the

electronic state of the guest. The relative probabilities of the transitions can be well

approximated by the Franck-Condon overlap integrals of the harmonic phonon wave

functions. Evidently, a very large number of normal coordinates q_i, each with its

characteristic frequency v_i, are needed to describe the vibrational movements of the matrix.

Therefore, for the overall transition, one has to sum over a large number of phonon modes.

In practice, there are many phonons which are so close together that their states can be

considered as a quasi-continuum. The summation over all these phonon states leads to the

typical lineshape shown in Figure 1-7.

In the following theoretical description of electron-phonon coupling, only the

electronic transitions in which the intramolecular vibrations do not change will be considered

for simplicity. For fluorescence, the probability of the transition from phonon mode i with

quantum number n = 0 in the first excited electronic state to phonon mode i in the electronic
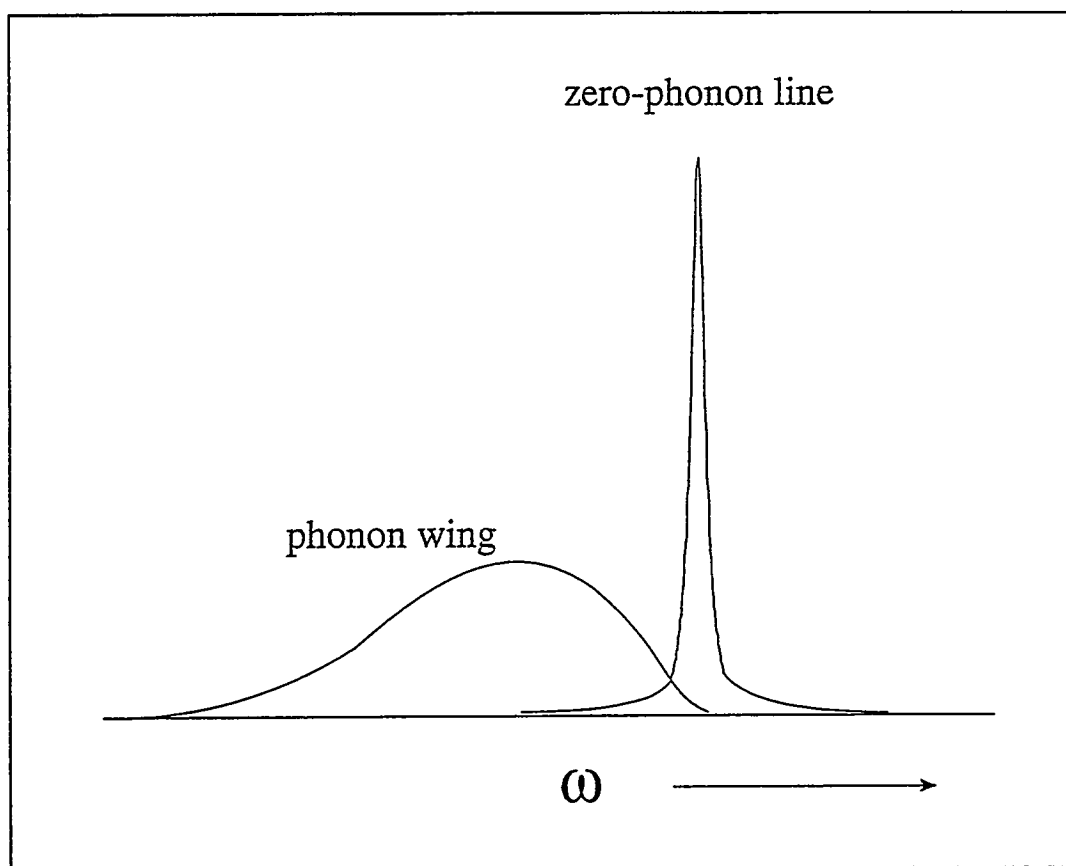
ground state can be written as

Figure 1-7. Schematic representation of the shape of a vibronic band in the luminescence spectrum of a guest molecule in a solid matrix.

$$P_{10,0i}(n) \sim |<\chi_{ph,1i}(0)\,|\,\chi_{ph,0i}(n)>|^2 \cdot |<\varphi_1^0|\bar{\mu}|\varphi_0^0>|^2 \cdot g(E\text{-}E_1 + nh\nu_i)$$

The function $g(E\text{-}E_1 + nh\nu_i)$ is a line form function which ensures sharp spectral features with distance $h\nu_i$ in the fluorescence spectrum. $\chi_{ph,1i}$ and $\chi_{ph,0i}$ represent the phonon wave functions for mode i in the electronic excited state and ground state, respectively. φ_1^0 and φ_0^0 are the electronic wave functions of the excited and ground state, respectively. The total intensity per phonon quantum requires a summation over all phonon modes. In order to calculate the overlap integrals $<\chi_{ph,1i}(0)\,|\,\chi_{ph,0i}(n)>$, the harmonic approximation which assumes that all phonon modes are independent of each other and are described by parabolic potentials is used. The overlap between two displaced harmonic oscillators has been derived by Keil [52].

The ratio of the intensities of the sharp zero-phonon line (ZPL) and the broad phonon wing (PW) is expressed as the Debye-Waller factor, α :

$$\alpha = \frac{I_{ZPL}}{I_{ZPL}+I_{PW}} = \sum_i |<\chi_{ph,1i}(0)\,|\,\chi_{ph,0i}(0)>|^2$$

This factor can be calculated for the very low temperature limit, $T \to 0$:

$$\alpha\,(T=0) = \exp(-S)$$

$$\text{where} \quad S\,(T=0) = \frac{1}{2}\sum_i \Delta q_i^2 \frac{2\pi\mu_i\nu_i}{h}$$

μ_i and ν_i are reduced mass and frequency of the mode i, respectively. The Huang-Rhys parameter S is a dimensionless quantity that indicates the strength of the electron-phonon coupling for a particular guest-host system. For strong electron-phonon coupling ($S \gg 1$), no narrow zero-phonon line will be observed in the spectra. In the limit of low temperature, the temperature dependence of the zero-phonon line intensity can be expressed as:

$$I_{ZPL} \sim \exp(-S) \exp{-[8S(kT/h\nu_D)^2]}$$

In this equation, it is assumed that the Debye distribution gives a good description of the density of states of the phonons with the Debye frequency (ν_D) for the matrix under consideration. Consequently, at very low temperature, the ZPL intensity decreases approximately quadratically with increasing temperature. This decrease is accompanied by a broadening and increase in intensity of the phonon wing.

The electron-phonon coupling theory described above in principle applies to perfect crystals since it uses the Debye theory to describe the phonon density of states. Thus, the theory explains the features of mixed crystal and Shpol'skii spectra very well. However, it is less accurate for FLN spectra. The discrepancies can be accounted for by the fact that amorphous materials also possess many quasi-localized modes of very low-frequency apart from the delocalized acoustic phonon modes [53]. It may also be explained by modeling the amorphous solid as a broad distribution of two-level systems [54,55] which is coupled to the guest molecules levels [56]. Such theoretical aspects will be discussed further in the following hole burning sections.

1.2.3   Principles of FLNS

In 1970, Szabo [57] for the first time reported narrow lines in the fluorescence spectrum of Cr^{3+} ions in ruby upon narrow band laser excitation at 4.2 K. Later, Personov et al. [58,59] observed the same effect for perylene in an ethanol glass at 4.2 K. Since then, it has been a subject for many studies and reviews [60-63]. The physical background of FLN spectroscopy is reasonably well understood and the technique can be applied to diminish inhomogeneous broadening to a large extent in a wide variety of guest-host systems.

The basic principles of FLN can be understood from Figure 1-8. Figure 1-8 is a schematic representation of an inhomogeneously broadened electronic absorption origin band (0,0) at low temperature. The relatively sharp dashed bands are zero-phonon lines (ZPLs) corresponding to the (0,0) transitions of the "guest" molecules occupying inequivalent sites. Building to the higher energy side of each ZPL in the figure is a broader phonon wing referred to as phonon side band (PSB). First, we note that if a broad band excitation source is used to excite the (0,0) band, all sites will be excited and the excited sites will fluoresce resulting in a broad fluorescence spectrum characterized by a bandwidth equal to Γ_{inh}. If a laser of frequency ω_L and line width $\Delta\omega_L$ is used, $\Delta\omega_L \ll \Gamma_{inh}$, only a subset of guest molecules whose transition frequency overlap with the laser profile will be excited. In the absence of intermolecular energy transfer, only this "isochromat" will fluoresce resulting in a "line-narrowed" fluorescence spectrum. The spectrum consists of an origin ZPL coincident with ω_L and to lower energy numerous ZPLs corresponding to transitions to vibrational sublevels of the ground electronic states. Note that as ω_L is tuned across the inhomogeneously broadened absorption, the origin ZPL ,and therefore, the entire fluorescence spectrum will "track" ω_L. For origin band excitation, the fluorescence of the origin ZPL is not a useful analytical line due to interference from scattered laser light. For this reason and others related to selectivity, it proves advantageous to excite into vibronic bands (vibronically excited FLN).

The vibronically excited FLN is demonstrated in Figure 1-9A, in which the electronic ground and excited states are labeled as S_0 and S_1. For simplicity, the vibrational energy level of S_0 is depicted as isoenergetic for all sites. The site inhomogeneous broadening for the (0,0) absorption transition is indicated by the "slanted" solid line for S_1. The magnitude of Γ_{inh} is indicated to the left side of the S_1 state. The slanted dashed lines for the S_1 state denote vibrational sublevels 1, 2, 3. The absorption transitions to the vibrational levels of
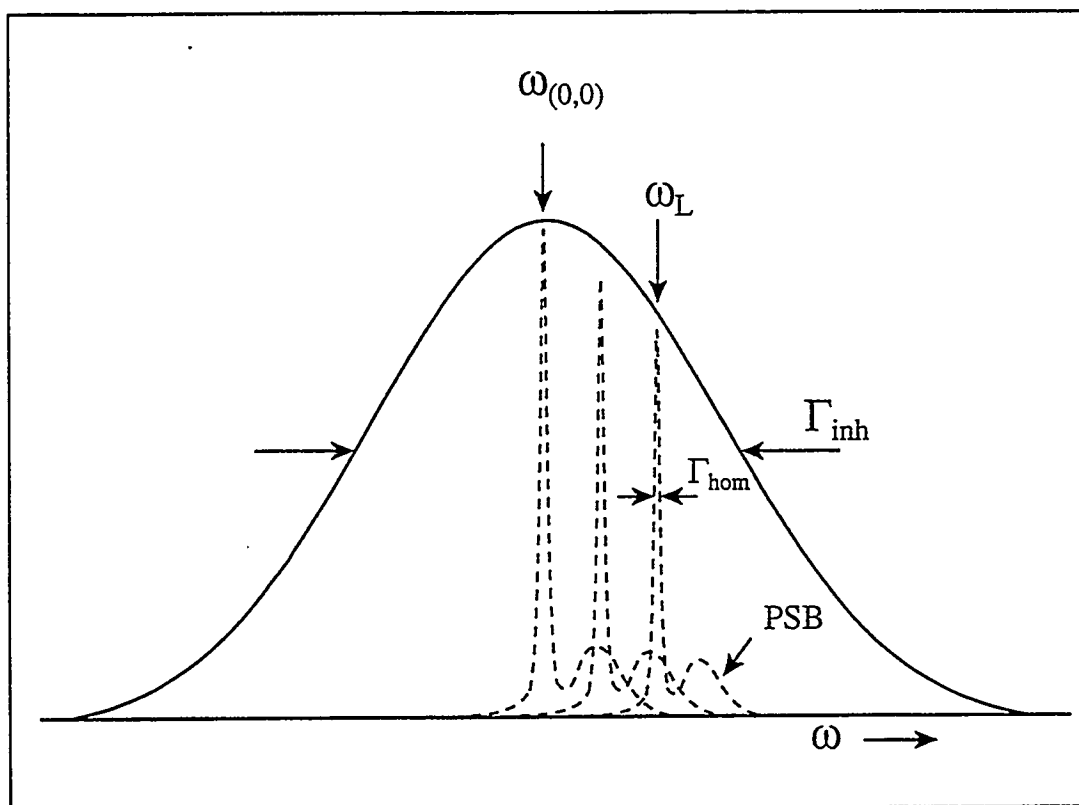
Figure 1-8. Schematic representaion of homogeneous (Γ_{hom}) and inhomogeneous (Γ_{inh}) broadening. Profiles of the zero-phonon lines (ZPL) and their associated phonon side bands (PSB) for specific sites at different frequencies are enlarged compared to the inhomogeneous line to provide more detail. ω_L is the laser frequency which selectively excites a narrow isochromat of an inhomogeneously broadened absorption band.
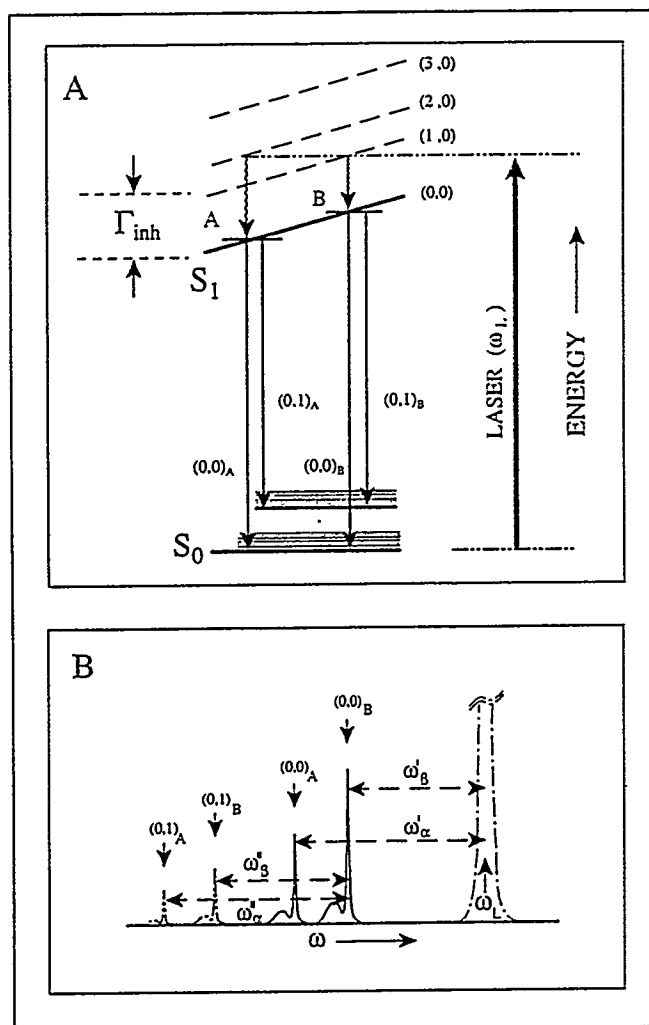
Figure 1-9. Schematic for vibronically excited fluorescence line narrowing. A: The slope of excited-state levels represents the variation of their energies as a function of site. Γ_{inh} denotes the inhomogeneous broadening of the (0,0) transition. Using laser excitation of frequency ω_L, two subsets of molecules within Γ_{inh} are selectively excited. B: Schematic of the resulting fluorescence spectrum. Fluorescence from two isochromats results in a doubling of the (0,0) transitions as well as the (0,1) vibronic transitions.

the excited state are labeled as (1,0), etc., where the zero indicates the absorption originates from the zero-point level of S_0 (it is assumed that at low temperature, all molecules reside at the zero-point level of the ground state). The thick solid vertical arrow is the laser excitation frequency (ω_L) chosen to excite isochromats A and B belonging to (1,0) and (2,0) transitions, respectively. The intersections of the horizontal dash-dot line with the dashed lines are the locations of the isochromats in the sites with the same excitation energy but at different vibrational sublevels. The two initially excited isochromats rapidly relax (squiggly downward arrows) to their respective and correlated zero-point distribution in the S_1 site (A and B). The fluorescence transitions from these two positions to the zero point and a vibrational level of S_0 are shown as solid arrows. The resulting line-narrowed fluorescence spectrum is given in Figure 1-9B. Note that the pure electronic transition (0,0) and a transition to the first vibronic level (0,1) are doublets. If the dissolved molecules have several closely spaced vibronic levels near the laser frequency (ω_L) in the excited state, the corresponding more complex "multiplet" appears in the (0,0) transition region of the fluorescence spectrum. More importantly, the spectrum yields both the ground and excited-state vibrational frequencies. For example, the displacements of $(0,0)_A$ and $(0,0)_B$ from ω_L yield the excited state vibrational frequencies (ω_α' and ω_β') and the displacements of $(0,1)_A$ and $(0,1)_B$ from corresponding $(0,0)_A$ and $(0,0)_B$ yield the ground state vibrational frequencies (ω_α'' and ω_β''). The $(0,0)_A$ and $(0,0)_B$ lines comprise what will be referred to as multiplet origin structure. By varying the excitation frequency ω_L, different multiplet origin structure will be observed; it is possible to determine all active excited-state fundamental intramolecular vibrations by appropriate variations of ω_L. The intramolecular vibrational sublevels of S_1 have a lifetime of ~1 psec due to rapid relaxation to the zero-point level of S_1. Therefore, the multiplet origin bands will generally be not sharper than ~5 cm^{-1}.

The relatively broad PSB that builds on the ZPL in absorption and fluorescence is contributed by 1-, 2-, ⋯ phonon transitions. The Franck-Condon factor for the ZPL is $\exp(-S) \equiv P_0$ while that for the r-phonon process is $[\exp(-S)]S^r/r! \equiv P_r$. Noting that $\Sigma P_r = 1$, it is easy to show that for $S < 1$ (weak coupling), the ZPL is dominant while for $S > 1$, (strong coupling) the PSB is dominant. For large S, the ZPL becomes Franck-Condon forbidden and FLN will not be possible.

Since the first publication of the FLN spectrum of perylene in ethanol in 1972, a large number of compounds in a variety of matrices have been studied [64-68]. Especially, many polycyclic aromatic hydrocarbons and biological compounds (e.g. porphyrins and chlorophylls, adducts to DNA) have been measured [69-73]. The fact that many polar and even ionic species yield FLN spectra in suitable solvents presents a very strong advantage of this line narrowing technique to achieve vibrationally resolved high resolution spectroscopy.

1.3 Spectral Hole Burning Spectroscopy

Solid state spectral hole burning is another example of a line narrowing technique which reduces or eliminates the effects of inhomogeneous broadening while retaining the advantages of utilizing glassy matrices. The observation of spectral holes requires a mechanism by which electronic excitation of a chromophore can alter its transition energy. As mentioned previously in section 1.2.3, irradiation into an inhomogeneously broadened line with a narrow-band laser of frequency ω_L excites a group of molecules with the same transition energy. The electronic transition energy of these molecules can be changed by one of several mechanisms, resulting in depletion of these chromophores which can be excited at the excitation frequency ω_L. Depending on the mechanism, there are three types of hole burning: photochemical hole burning (PHB), nonphotochemical hole burning (NPHB), and

population bottleneck hole burning. The mechanisms of these three types of hole burning will be discussed in the next section.

A zero-phonon transition is an electronic transition with no net change in the number of phonons. The ultimate spectral resolution is determined by the homogeneous linewidth, Γ_{hom}, which is related to the total dephasing time τ_2 by $\Gamma_{hom} = (\pi\tau_2 c)^{-1}$ (see section 1.2.1). Figure 1-10 illustrates a hole burned spectrum for the origin band and a vibronic excitation. In the absorption spectrum shown in Figure 1-10A, a laser with a frequency ω_L (the burn frequency) irradiates an isochromat in the (0,0) or origin band. However, the sites that contribute to the origin isochromat also contribute to the $(1_\alpha,0)$ and $(1_\beta,0)$ vibronic bands. Thus, a zero phonon hole (ZPH) burned at ω_L can be accompanied by higher energy vibronic satellite holes, as indicated in the Δ-absorbance spectrum. Since the zero phonon line (ZPL) in absorption is accompanied by a phonon side band (PSB), the ZPH is accompanied by phonon side band holes (PSBH). The PSBH at the higher energy side of the ZPH is readily understood and is referred to as the real-PSBH. The PSBH appearing at the lower energy side of the ZPH is called a pseudo-PSBH. The pseudo-PSBH is due to sites whose ZPL frequencies lie to the lower energy side of ω_L and which absorb the laser light by virtue of their PSB.

Pseudo-vibronic hole structure can also be generated. The basic idea is very similar to that involved in vibronically excited FLN spectroscopy. In Figure 1-10B, the laser (ω_L) excites two isochromats (α and β) belonging to the first and second vibration, respectively. Since the time constant for hole burning is long relative to the vibrational relaxation time, the vibrational isochromats relax to their respective zero point positions in the (0,0) band prior to hole burning. Two ZPHs, $(0,0)_A$ and $(0,0)_B$, are produced, while both also lead to a hole at ω_L. The relative intensities of the former two and the latter hole at ω_L depend, in part, on
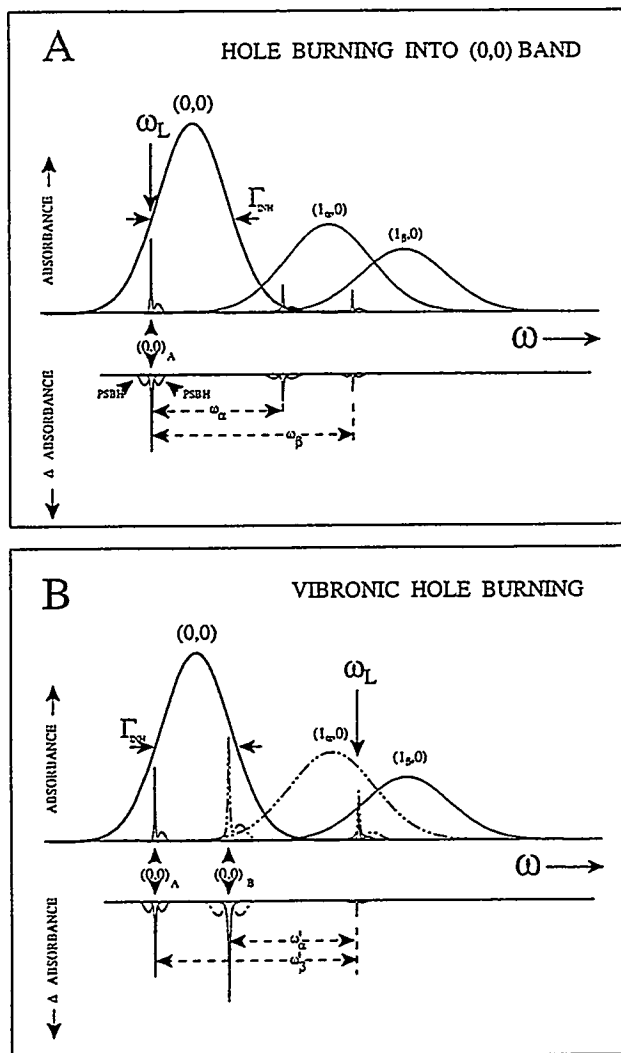
Figure 1-10. Schematic hole burning into the origin band (A) and into the vibronic region (B) (see explanation in text).

the Franck-Condon factors for the vibrations α and β. The displacement of the vibronic "satellite" holes from the burn frequency yields the excited state vibrational frequencies.

1.3.1 Hole Burning Mechanisms

Three basic hole-burning mechanisms, photochemical hole burning (PHB), nonphotochemical hole burning (NPHB), and population bottleneck hole burning, will be discussed in this section. PHB describes hole burning which results from a chemical reaction initiated in an excited state of the chromophore. For PHB, therefore, photoreactivity of the absorbing chromophore is required. PHB can be observed in both amorphous and crystalline hosts. The reaction initiated by photoexcitation can be tautomerization, bond-breaking, isomerization and so on. Via this mechanism, selective photobleaching of the absorption spectrum can be achieved. Photochemical hole burning was first observed for free base phthalocyanine in n-octane, where the PHB is caused by an intramolecular hydrogen tautomerization. In PHB, the antihole (absorption increase due to products) is usually not near the zero-phonon hole and is much broader than its parent hole because of the inhomogeneous broadening of the zero phonon lines of the photoproducts.

Unlike photochemical hole burning, non-photochemical hole burning involves only the modification of the interaction between the microscopic environment (host) and the impurity (guest) molecules. On excitation, a reorientation of the guest molecule with respect to its environment takes place. Since the host configurations need to be changed, NPHB is a characteristic of amorphous systems with a few exceptions [48]. NPHB is a reversible process, and nonphotochemical holes often disappear after increasing the temperature. The absorption positions of the products (antiholes) for nonphotochemical processes are located not very far from the original absorption position. In 1972, Anderson et al. [54] and Phillips [55], independently, proposed the so-called two-level system (TLS). The proposed TLS

theory is that in any glass system, there should be a certain number of atoms or groups of atoms which may occupy, with nearly equal probability, two equilibrium positions separated by an energy barrier. At very low temperatures, atoms or groups of atoms cannot be thermally activated over the barrier, but can bypass the barrier by tunneling. In 1978, the two-level system model based on the coupling of the electronic transition of the guest to the glass (TLS_{ext}) was utilized to explain the NPHB mechanism [74]. In this mechanism, extrinsic TLSs (TLS_{ext}) are suggested to be strongly associated with the absorbing center and are responsible for the initiation of hole burning. The rate-determining step for hole formation is phonon-assisted tunneling within TLS_{ext}. The intrinsic bistable configuration of the host itself is denoted by TLS_{int}, and the intrinsic TLSs (TLS_{int}) were proposed to be responsible for optical dephasing [48,74]. The standard TLS_{ext} model for NPHB is illustrated in Figure 1-11. The superscripts α and β denote the potential energy curve for TLS_{ext} coupled to the ground and excited electronic state of the guest. The asymmetry parameter (Δ) and the barrier height (V) are used to describe the TLS_{ext} system. In the figure, excitation of the zero-phonon transition is pictured as occurring on the left (L) with the critical $L \rightarrow R$ relaxation taking place in the excited electronic state (β). There is a distribution of the tunneling frequency, W, depends on the tunneling parameter λ by $W = \omega_0 exp(-\lambda)$. It is assumed that λ value is Gaussian distributed with mean value λ_0 and variance σ_λ^2 [75]. Note that the transition frequency of the absorber in the postburn configuration is higher than the one for the preburn configuration. The mechanistic model for NPHB was further developed by Shu et al. [76]. In their NPHB model, it was proposed that NPHB occurs as a result of an outside-in hierarchy of dynamical events which are triggered by electronic excitation and result in an increase in the free volume of the probe for the postburn configuration. The free volume increase for the guest in its inner shell of host molecules was proposed to occur following relatively fast configurational relaxation

$$W = \omega_0 \exp(-\lambda)$$

TLS_{ext}^{β}

Δ_β

L   R

ω_B

E

TLS_{ext}^{α}

V

Δ_α

d

q
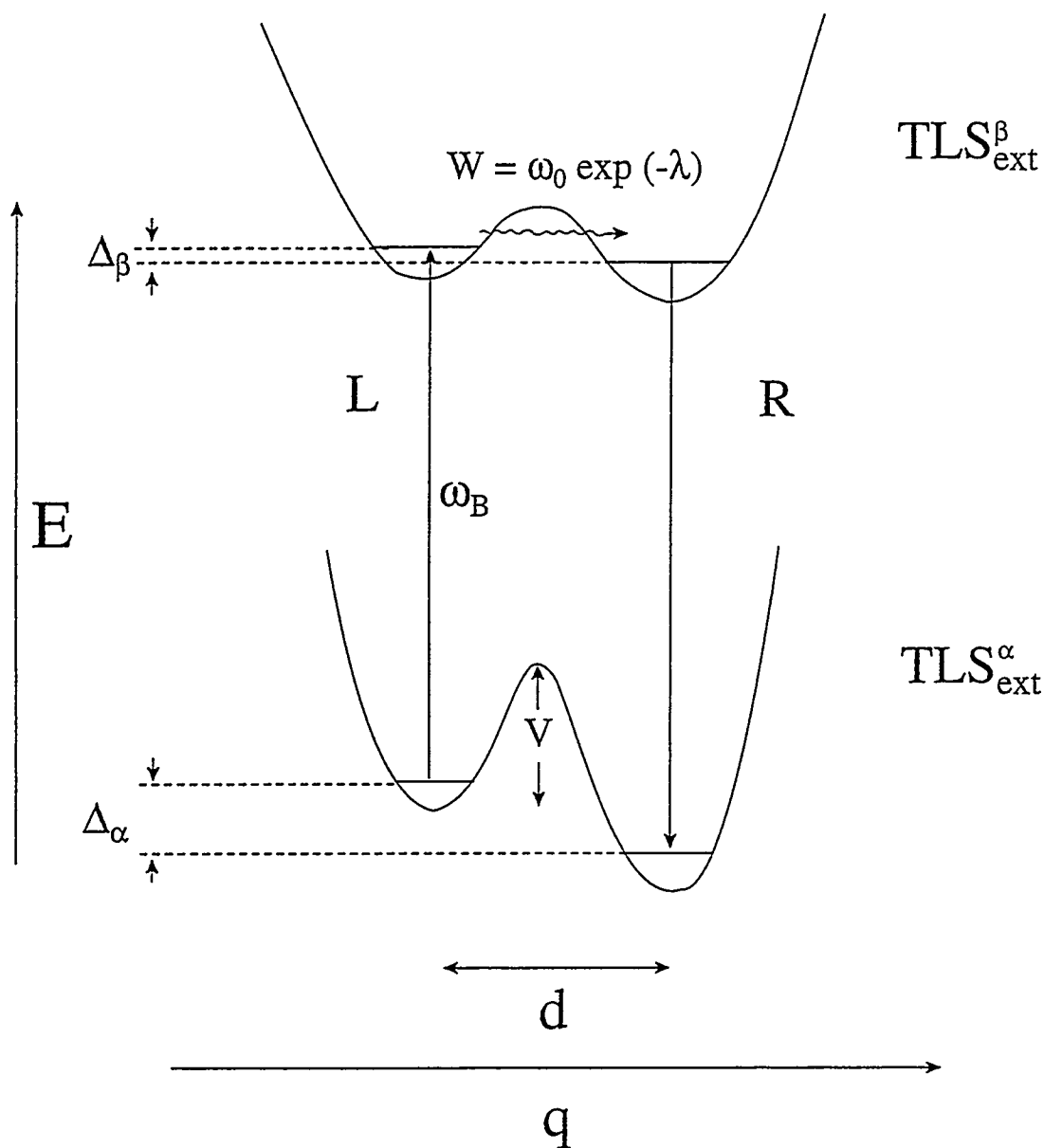
Figure 1-11. Potential energy diagrams for a two-level system (TLS) coupled to a guest molecule in its ground state (α) and excited electronic state (β). Δ is the asymmetry parameter; V, the barrier height; and q, the intermolecular coordinate. The tunneling frequency, W, depends on the tunneling parameter λ which is defined as $d(2mV)^{1/2}/h$, where m is the tunneling mass. ω_B is the laser burn frequency.

processes in the outer shell which lead to a reduction in the excess free volume of the outer shell.

Population bottleneck hole burning utilizes a third, long-lived, level to store the population depleted from the ground state [77,78]. The technique was first described for Pr^{3+} in a LaF_3 crystal, in which nuclear hyperfine levels provided the bottleneck state [79]. In the case of zinc porphyrin in n-octane [80], the long-lived triplet level was used as a population reservoir to observe a hole in the $S_1 \leftarrow S_0$ transition. As expected, the hole lifetime was shown to be the same as the triplet lifetime.

1.3.2 Dispersive Nonphotochemical Hole Growth Kinetics

The dispersive kinetics of zero-phonon hole growth is based on the hole burning mechanism proposed by Shu and Small [76,81]. The rate determining step for hole formation is phonon-assisted tunneling of TLS_{ext}^{β} (β denotes the excited electronic state of the guest), and the intrinsic disorder of the glass leads to a distribution of tunneling frequencies. The tunneling is strongly biased toward processes that involve phonon emission, that is, the excited-state energy of the probe molecule in the postburn configuration is lower than that in the preburn configuration [76]. For a single TLS_{ext}^{β}, the downward phonon-assisted relaxation rate, R, is [47,82]:

$$R = (3f^2W^2E/16\pi\rho c^5\hbar^5)(<n_E>_T + 1)$$

where $E^2 = \Delta^2 + W^2$, E is the tunneling splitting, Δ and W are the asymmetry parameter and tunneling frequency, respectively (see Figure 1-11), ρ is the sample density and c is an average sound velocity. The average phonon thermal occupation number $<n_E>_T = (exp(E/kT) -1)^{-1}$. The f parameter is related to the TLS_{ext} deformation potential.

In cases where the antihole is significantly shifted away from the ZPL which is burned, the tunnel splitting E may be replaced by Δ. Because the tunneling frequency W depends exponentially on the tunnel parameter λ, $W = \omega_0 \exp(-\lambda)$, and λ depends on several parameters subject to statistical fluctuations due to disorder, the distribution of relaxation rates (R) can be assumed to be derived from the distribution function for W. Thus, R can be written:

$$R = \Omega_0 \exp(-2\lambda)$$

where $\Omega_0 = 3 <f^2\Delta> \omega_0^2/16\pi\rho c^5 \hbar^5$. Because $\lambda \geq 0$, $R_{max} = \Omega_0$. We define f(R) as the normalized distribution function for the TLS_{ext} relaxation rate so that

$$D(t) = \int_0^{\Omega_0} dR\, f(R)\, \exp\left(-\sigma P\phi(R)t\right)$$

1 - D(t) is the fractional ZPH depth following a burn for time t with a burn photon flux P. σ is the peak absorption cross section for the ZPL and $\phi(R) = R/(R + k)$ is the NPHB quantum yield for a probe excited state lifetime of k^{-1}. The expression for D(t) is valid for a burn laser with frequency width much narrower than the homogeneous line width of the ZPL.

For kinetic simulations, it is convenient to employ a particular form for D(t) which is equivalent to the expression above:

$$D(t) = [(\sqrt{2\pi})\sigma_\lambda]^{-1}\int_{+\infty}^{-\infty} d\lambda\, \exp[-(\lambda - \lambda_0)^2 / \sigma_\lambda^2]\, \exp[-P\sigma\phi(\lambda)t]$$

and by defining $x = (\lambda - \lambda_0)/\sigma_\lambda$, D(t) becomes:

$$D(t) = (2\pi)^{-1/2}\int_{-\infty}^{+\infty} dx\, \exp[-x^2 /2]\, \exp[-\Sigma_0\xi(x)t]$$

where $\Sigma_0 = P\sigma\Omega_0\tau$ and $\xi(x) = \exp[-2(\lambda_0-\sigma_\lambda x)]$. When fitting the equation to the experimental hole growth curves, a renormalization is necessary to take into account the

off-set due to electron-phonon coupling: the maximum fractional hole depth is exp(-S) where S is the Huang-Rhys factor.

1.3.3 Applications of Spectral Hole Burning to Biological Systems

Spectral hole-burning spectroscopies (nonphotochemical, photochemical and population bottleneck) have been applied to many photosynthetic antenna and reaction center protein-cofactor (e.g. chlorophyll) complexes with considerable success [77]. During the past several years, it has been established that NPHB is a general and facile phenomenon for chromophores in proteins (chlorophylls, caratenoids, pheophytins and hemes) and for dye molecules such as rhodamine 640, cresyl violet and nile blue in hydrogen bonding hosts (e.g. glycerol, ethanol, polyvinyl alcohol). Also, NPHB was shown to be facile for DNA-PAH adducts and for molecules intercalated into DNA [83,84].

Recently, Hayes and Small showed that NPHB can be used to investigate the structural details of various materials [85-87]. They also proposed that NPHB can be applied as a probe for imaging biological systems (DNA, proteins, membranes, nuclei, organelles of the cell, cell ensembles and tissues), since the many hole burning characteristics of chromophores are very sensitive to their environments. The ZPH width depends on the total dephasing time of the optical transition. A ZPH burned into the origin absorption band has homogeneous width 2γ, where γ is the homogeneous width of the associated ZPL in absorption. As discussed in the previous section, γ is given by $\gamma = (\pi \tau_2 c)^{-1}$ where τ_2 is the total dephasing time of the chromophore's optical transition. There are many studies showing that the width of the ZPH depends strongly on the amorphous host in which the chromophore is imbedded [88-90]. In the case of polymer hosts, it has been shown that the ZPH width is reduced as the rigidity of the polymer is increased [91]. Also, the pressure dependence of the hole width [92] can be a probe for detecting abnormal cells since a change

in compressibility of the host is believed to accompany the gross structural change of the cell transforming from normal to abnormal. Also the hole growth rate was reported to depend strongly on the host environment [86].

1.4 Dissertation Organization

This dissertation contains the candidate's original work on line narrowing spectroscopic studies of DNA-carcinogen adducts and DNA-dye complexes. Chapter 1 contains a general introduction about BPDE (benzo[a]pyrene diol epoxide), fluorescence line-narrowing spectroscopy and hole burning spectroscopy. Chapter 2 describes the experimental apparatus used for the dissertation work. Chapter 3, 4 and 5 contain published papers about BPDE-N^2-dG adducts in oligonucleotides *in vitro* and in the DNA of mouse skin *in vivo*. Chapter 6 contains a spectroscopic study of TO-PRO-3-DNA complexes using absorption and fluorescence spectroscopy in conjunction with nonphotochemical hole burning. The additional hole burning data of TO-PRO-3 bound to various DNAs are contained in Appendix A. References are found at the end of each chapter. Future prospects are also suggested in each chapter.

References

1. Baum,E.J. In *Polycyclic Hydrocarbons and cancer* (Harvey,R.G. Ed) (1978) Academic Press, New York, pp 45-62.

2. Pott,P. (1775) Reprinted in *National Cancer Inst. Monogr.* 1963, **10**, 7.

3. Thakker,D.R., Yagi,H,, Kevin,W., Wood,A.W., Conney,A.H. and Jerina,D.M. (1985) In *Bioactivation of Foreign Compounds* (Anders,M.W. Ed.) Academic Press, New York, pp177-245

4. Miller,E.C., and Miller,J.A. (1981) *Cancer* **47**, 2327.

5. Gräslund,A., and Jernström.B. (1989) *Quart. Rev. Biophys.* **22**, 1.

6. Cook,J.W., Hewett,C.L., and Hieger,I. (1933) *J. Chem. Soc.* 395.

7. Phillips,D.H. (1983) *Nature* **303**, 468.

8. Commitee on Biologic Effects of Atmospheric Pollutants, *Particulate Polycyclic Organic Matter*, National Academy of Sciences, Washington D.C., 30.

9. Conney,A.H. (1982) *Cancer Res.* **42**, 4875.

10. Sims,P., and Grover,P.L. (1981) In *Polycyclic Hydrocarbons and Cancer* (Gelbon,N.V., Ts'o,P.O.P. Eds) Academic Press, New York, Vol, 3. pp 117-181.

11. Weinstein,I.B., Jeffrey,A.M., Jennette,K.W., Blobstein,S.H., Harvey,R.G., Harris,C., Autrup,H., Kasai,H., and Nakanishi,K. (1976) *Science* **193**,592.

12. Cavalieri,E.L., and Rogan,E.G. (1990) *Free Rad, Res, Comms.* **11**,77.

13. Cavalieri,E.L., and Rogan,E.G. (1985) *Environ. Health. Perspect.* **64**, 69.

14. Cavalieri,E.L., and Rogan,E.G. (1985) In *Polycyclic hydrocarbons and Carcinogenesis* (Harvey,R.G. Ed) ACS Press, Washington D.C., Chapter 11.

15. Boyd,D.R., Jerina,D.M. (1984) In *Small Ring Heterocycles* (Hassner,A. Ed.) Wiley, New York, Part 3, p197-282.

16. Jerina,D.M., Daly,J.W., Witkot,B., Zaltzman-Nirenberg,P. and Udenfriend,S. (1968) *Arch.Biochem. Biophys.* **128**, 176.

17. Lu,A.T.H., Jerina,D.M., and Levin,W.J. (1977) *J. Biol. Chem.* **252**, 3715.

18. Sims,P., Grover,P.L., Swaisland,A., Pal,K., and Hewer,A. (1974) *Nature* **252**,326.

19. Borgen,A.O., Dover,H., Costagnoli,N, Crucker, T.T., Rasmussen,R,C. and Wong,I.Y. (1973) *J. Med, Chem.* **16**, 502.

20. Osborne,M.R., Jacobs,S., Harvey,R.G., and Brookes,P. (1981) *Carcinogenesis* 2, 553.

21. Cheng,S.C., Hilton,B.D., Roman,J.M., and Dipple,A. (1989) *Chem. Res. Toxicol.* 2, 334.

22. Huberman,E., Sachs,L., Yang,S.K., and Gelboin,H.V. (1976) *Proc. Natl. Acad. Sci. USA* 73, 607.

23. Newbold,R.F.and Brookes,P. (1976) *Nature* **261**, 52.

24. Slaga,T.J., Bracken,W.J., Gleason,G., Levin,W., Yagi,H., Jerina,D.M., and Conney,A.H. (1979) *Cancer Res.* **39**, 67.

25. Buening,M.K., Wislocki,P.G., Levin,W., Yagi,H., Thakker,D.R., Akagi,H., Koreeda,M., Jerina,D.M., and Conney,A.H. (1978) *Proc. Natl. Acad. Sci. USA* **75**, 5358.

26. Kapitulnik,J., Wislocki,P.G., Levin,W., Yagi,H., Thakker,D.R., Akagi,H., Koreeda,M., Jerina,D.M. and Conney,A.H. (1978) *Cancer Res.* **38**, 2661.

27. Wood,A.W., Chang,R.L., Levin,W., Yagi,H., Thakker,D.R., Jerina,D.M, and Conney,A.H. (1977) Differences in mutagenicity of the optical enantiomers of the diastereomeric benzo[a]pyrene 7,8-diol-9,10-epoxides. *Biochem. Biophys. Res. Commun.* **77**, 1389-1396.

28. Brookes,P and Osborne,M.R. (1982) Mutation in mammalian cells by stereoisomers of *anti*-benzo[*a*]pyrene-diolepoxide in relation to the extent and nature of the DNA reaction products. *Carcinogenesis* **3**, 1223-1226.

29. Stevens,C.W., Bouck,N., Burgess,J.A., and Fahl,W.E. (1985) *Mutation Res.* **152**, 615.

30. Hruszkewycz,A.M., Canella,K.A., Peltonen,K., Kotrappa,L., and Dipple,A. (1992) *Carcinogenesis* **13**, 2347.

31. Shibutani, S., Margulis, L. A., Geacintov, N. E., and Grollman, A. (1993) *Biochemistry* **32**, 7531.

32. Choi,D.-J., Marino-Alessandri,D.J, Geacintov,N.E., and Scicchitano,D.A. (1994) *Biochemistry* **33**, 780.

33. Eriksson,M., Nordén,B., Jernström,B., and Gräslund,A. (1988) *Biochemistry* **27**, 1213.

34. Geacintov,N.E., Cosman,M., Mao,B., Alfano,A., Ibanez,V., and Harvey,R.G. (1991) *Carcinogenesis* **12**, 2099.

35. Roche,C.J., Geacintov,N.E., Ibanez,V., and Harvey,R.G. (1989) *Biophys. Chem.* **33**, 277.

36. Singh,S.B., Hingerty,B.E., Singh,U.C., Greenberg,J.P., Geacintov,N.E., and Broyde,S. (1991) *Cancer Res.* **51**, 3482.

37. Cosman,M., de los Santos,C., Fiala,R., Hingerty,B.E., Singh,S.B., Ibanez,V., Margulis,L.A., Live,D., Geacintov,N.E, Broyde,S., and Patel,D.J. (1992) *Proc. Natl. Acad. Sci. USA* **89**, 1914.

38. de los Santos,C., Cosman,M., Hingerty,B.E., Ibanez,V., Margulis,L.A., Geacintov,N.E., Broyde,S., and Patel,D.J. (1992) *Biochemistry* **31**, 5245.

39. Cosman,M., de los Santos,C., Fiala,R., Hingerty,B.E., Ibanez,V., Luna,E., Harvey,R.G., Geacintov,N.E, Broyde,S., and Patel,D.J. (1993) *Biochemistry* **32**, 4145.

40. Pelling,J.C. and Slaga,T.J. (1982) *Carcinogenesis* **3**, 1135.

41. MacLeod,M.C., Daylong,A., Adair,G., and Humphrey,R.M. (1991) *Mutation Res.* **261**, 267.

42. Bohr,V.A., Smith,C.A., Okumoto,D.S. and Hanawalt, P.C. (1985) *Cell* **40**, 359.

43. Tornaletti, S., and Pfeifer,G.P. (1994) *Science* **263**, 1436.

44. Gao,S., Drouin,R., and Holmquist,G.P. (1994) *Science* **263**, 1438.

45. Chen,R.-H., Maher,V.M., Brouwer,J., van de Putte,P., and McCormick,J.J. (1992) *Proc. Natl. Acad. Sci. USA.* **89**, 5413.

46. Tang,M., Pierce,J.R., Doisy,R.P., Nazimiec,M.E., and MacLeod,M.C. (1992) *Biochemistry* **31**, 8429.

47. Hayes,J.M., Jankowiak,R., and Small,G.J. (1987) In *Topics in Current Physics, Persistent Spectral Hole Burning: Science and Applications* (Moerner,W.E., Ed.) Vol. 44, Chapter 5, pp 153-202, Springer-Verlag, New York.

48. Jankowiak,R., and Small,G.J. (1987) *Science* **237**, 618.

49. Sapozhnikov,M.N. (1976) *Phys.Stat. Sol.* **B75**, 11.

50. Rebane,K.K., (1970) *Impurity Spectra of Solids* Plenum, New York.

51. O'sadko,I.S. (1983) In *Spectroscopy and Excitation Dynamics of Condensed Molecular Systems,*(Agranovich,V.M., and Hochstrasser,R.M. Eds) North-Holland, Amsterdam.

52. Keil,T. (1965) *Phys. Rev.* **140** A601.

53. Winterling,G. (1975) *Phys. Rev.* B **12**, 2432.

54. Anderson,P.W., Halperin,B.I., and Varma,C.M. (1972) *Phil. Mag.* **25**, 1.

55. Phillips,W.A. (1972) *J Low Temp. Phys.* **7**, 531.

56. Morawitz,H., and Reineker,P. (1982) *Solid State Comm.* **42**, 609.

57. Szabo,A. (1970) *Phys. Rev. Lett.* **25**, 924.

58. Personov,R.I., Al'Shits,E.I., and Bykovskaya,L.A. (1972) *Opt. Commun.* **6**, 169.

59. Personov,R.I., Al'Shits,E.I., and Bykovskaya,L.A. (1972) *JETP Lett.* **15**, 431.

60. Kohler,B.E. (1979) In *Chemical and Biochemical Applications of Lasers* (Moore,C.B. Ed.) Vol. 4, Academic Press, New York, P31.

61. Personov,R.I. (1981) *J. Lumin.* **24/25**. 475.

62. Weber,M.J. (1981)In *Laser Spectroscopy in Solids* (Yen,W.M. and Selzer.P.M. Eds.) Springer, Berlin, Heidelberg, New York. Chapter 6.

63. Personov,R.I. (1983) *Sepctrochim. Acta* **38 B**, 1533.

64. Personov,R.I. (1983) In *Spectroscopy and Excitation Dynamics of Condensed Molecular Systems*,(Agranovich,V.M., and Hochstrasser,R.M. Eds) North-Holland, Amsterdam. Chapter 10.

65. Selzer,P.M. (1986) In *Laer Spectroscopy of Solids* Springer-Verlag, Berlin, Chapter 4.

66. Hofstraat,J.W. (1988) *High-Resolution Molecular Fluorescence Spectroscopy in Low Temperature Matrices: Principles and Analytical Application* Free University Press, Amsterdam.

67. Jankowiak,R. and Small,G.J. (1989) *Anal. Chem.* **61**, 1023A.

68. Jankowiak,R. and Small,G.J. (1991) *Chem. Res. Toxicol.* **4**, 256.

69. Warren,J.A., Hayes,J.M. and Small.G.J. (1987) *Biochim. Biophys. Acta* **932**, 287.

70. Hofstraat,J.W., Gooijer,C., and Velthorst,N.H. (1988) In *Molecular Luminescence Spectroscopy, Methods and Applications, Part 2* (Schulman,S.G. Ed.) John Wiley & Sons, New York, pp 283-459.

71. Avarmaa,R.A., and Rebane,K.K. (1985) *Spectrochim, Acta* **41A**, 1365.

72. Renge,I., Mauring,K., and Avarmaa,R. (1987) *J Lumin.* **37**, 207.

73. Heisig,V., Jeffrey,A.M. McGlade,M.J., and Small,G.J. (1984) *Science* **223**,289.

74. Hayes,J.M. and Small,G.J. (1978) *Chem. Phys.* **27**, 151.

75. Jankowiak,R., Small,G.J., and Athreya,K.B. (1986) *J. Phys. Chem.* **90**, 3896.

76. Shu,L., and Small,G.J. (1990) *Chem. Phys.* **141**, 447.

77. Jankowiak,R., Hayes,J.M., and Small,G.J. (1993) *Chem. Rev.* **93**, 1472.

78. Jankowiak,R. and Small,G.J. (1993) In *The Photosynthetic Reaction Center*, Vol. 2, (Deisenhofer,J, and Norris,J. Eds.) Academic Press, New York, p 133.

79. Erickson,L.E. (1975) *Phys. Rev. B.* **11**, 4512.

80. Shelby,R.M., and MacFarlane,R.M. (1979) *Chem. Phys. Lett.* **64**, 545.

81. Shu,L., and Small,G.J. (1992) *J. Opt. Soc. Am. B.* **9**, 724.

82. Phillips,W.A. Ed. (1981) *Amorphous Solids-Low Temperature Properties*, Springer, Berlin.

83. Jankowiak.R., Cooper,R.S., Zamzow,D., Small, G.J., Doskocil,J., and Jeffrey, A.M. (1988) *Chem. Res. Toxicol.* **1**, 60.

84. Flöser,G., and Haarer,D. (1988) *Chem. Phys. Lett.* **147**, 288.

85. Kenney,M.J., Jankowiak,R., and Small,G.J. (1990) *Chem. Phys.*, **146**, 40.

86. Kim,W.-H., Reinot,T., Hayes,J.M. and Small,G.J. (1995) *J. Phys. Chem.* **99**, 7300.

87. Hayes,J.M. and Small,G.J. (1995) *SPIE* **2385**, 115.

88. Narasimhan,L.R., Littau,K.A., Pack,D.W., Bai,Y.S., Elschner,A., and Fayer,M.D. (1990) *Chem. Rev.* **90**, 439.

89. Völker,S. (1989) *Annu. Rev. Phys. Chem.* **40**, 499.

90. Meijers,H.C., and Wiersma,D., (1992) *Phys. Rev. Lett.* **68**, 381.

91. Furusawa,A. Horie,K., Suzuki,T., Madrida,S., and Mita,I. (1990) *Appl. Phys. Lett.* **57**, 1.

CHAPTER 2. INSTRUMENTATION

2.1 Fluorescence Line Narrowing (FLN) and Non Line Narrowing (NLN) Spectroscopy

A block diagram of the fluorescence line narrowing (FLN) spectroscopy and the low resolution fluorescence (non-line narrowing, NLN) measurement apparatus is shown in Figure 2-1. The excitation source used is a Lambda-Physik FL-2002 tunable dye laser pumped by a Lambda Physik Lextra 100 XeCl excimer laser system. The excimer laser system provides high energy (200 mJ/pulse) pulses with a repetition rate of up to 100 Hz at 308 nm. For gated mode detection, a Lambda Physik EMG-97 zero-drift controller is used to trigger a high voltage gate pulse generator (Princeton Instruments FG-100), which controls both the adjustable delay time and the width of a temporal detection window. The corresponding dye laser uses a grating in a Littrow geometry for wavelength selection which provides 0.22 cm^{-1} spectral line width. For dye laser, p-terphenyl (332-350 nm) and DMQ (346-377 nm) dyes from Exciton Inc. were employed to select the excitation wavelength. Typically, the attenuated laser output (50 mW/cm^2 intensity) was used for the FLN and NLN measurement. The laser beam is shaped into a 7 mm × 2 mm beam by using a quartz biconvex cylindrical lens for complete irradiation of samples. A 3-liter double-nested glass low temperature cryostat manufactured by H. S. Martin Inc. was used for both 4.2 K (FLN) and 77 K (NLN) optical experiments. A sample in a quartz tube (2 mm i.d.) was directly immersed in liquid helium (or liquid nitrogen) to obtain spectra at 4.2 K (or 77 K). Fluorescence was collected at right angle to the excitation. The collected fluorescence was dispersed by a McPherson 2016 1-meter focal length monochromator and detected by a Princeton Instruments IRY 1024/G/B intensified photodiode array. For the FLN measurement, the monochromator was equipped with a 2400 grooves/mm grating providing
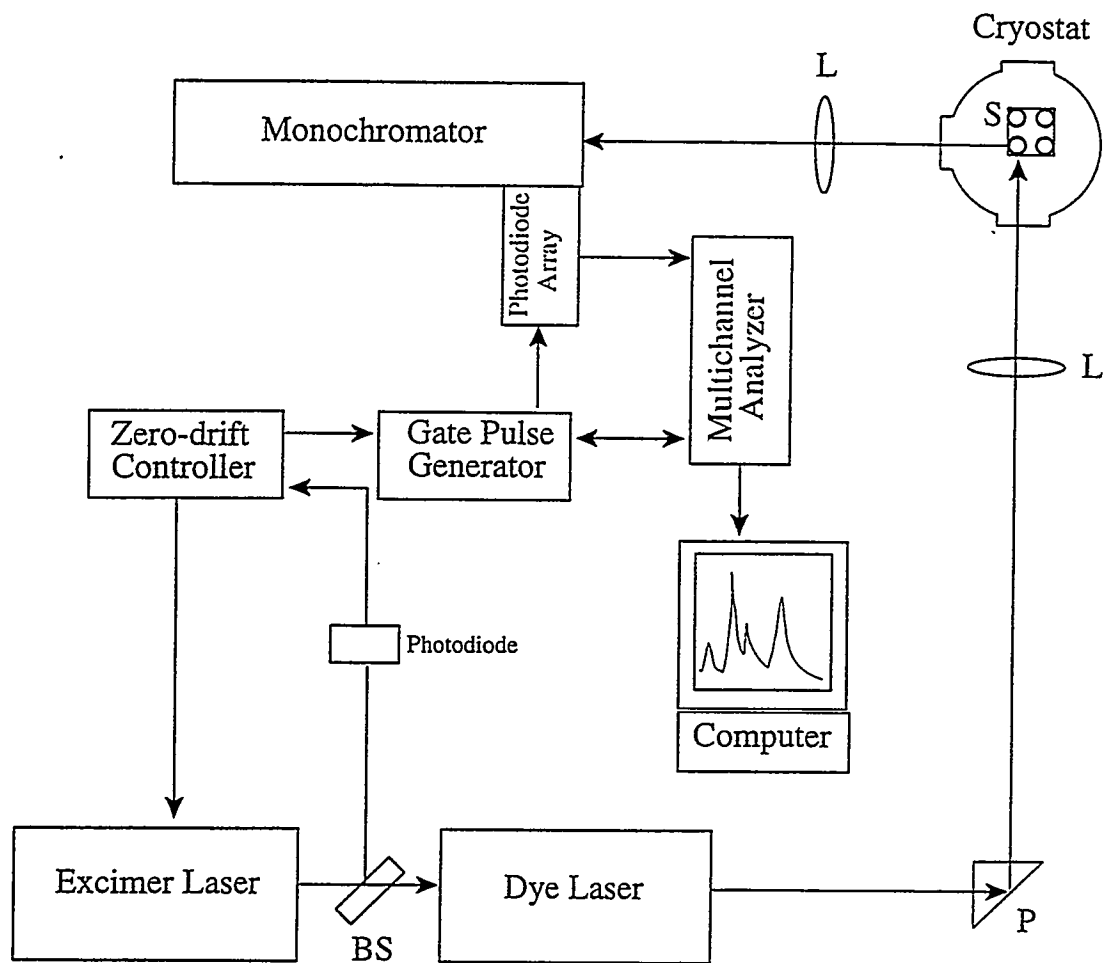
Figure 2-1. Block diagram of FLN and NLN spectroscopy instrumentation: S, sample in a copper holder; L, lens; P, prism; BS, beam splitter.

an 18 nm spectral window at 0.1 nm resolution. For the low resolution fluorescence (NLN) emission spectra, a 150 grooves/mm grating was employed to provide a 150 nm window and 0.8 nm resolution. In the case of FLN measurement at 620 nm - 650 nm excitation wavelength, the laser output from Coherent 699-29 ring dye laser system (DCM Special dye from Exciton) pumped with an argon ion laser (6 W output) was used as an excitation source.

2.2 Spectral Hole Burning Spectroscopy

Absorption and fluorescence excitation spectroscopy were used for the spectral hole burning studies in this work. The laser output from Coherent 699-29 ring dye laser pumped by an argon ion laser (6 W output) was used as an excitation source for the hole burning and the fluorescence excitation spectroscopy. DCM Special dye (Exciton) was used giving a tuning range from 615 to 706 nm. A block diagram of the apparatus used for measuring the fluorescence excitation spectra is shown in Figure 2-2. For long-range scans of the excitation spectrum, the intracavity etalon was removed from the ring dye laser and the wavelength was scanned by rotating the birefringent filter stack. In this configuration, the laser line width was 0.1 cm^{-1}. For hole burning and high resolution scans (scanning for hole width), the intracavity etalons were reinstalled giving a laser line width of ≤ 20 MHz. The wavelength was continuously monitored with a Burleigh wavemeter. Dye laser output power was stabilized with a laser amplitude stabilizer (Cambridge Research and Instrumentation, model LS.100) and monitored with a power meter (Newport Co. model 1825-C) equipped with a diode (Newport Co. model 818-SL). The laser power density for the hole burning was varied with density filters from 250 nW/cm^2 to 300 μW/cm^2. For the fluorescence excitation spectra before and after burning, the laser was attenuated to ~250 nW/cm^2. The laser illuminated ~0.35 cm^2 area of a sample. The sample solutions in quartz
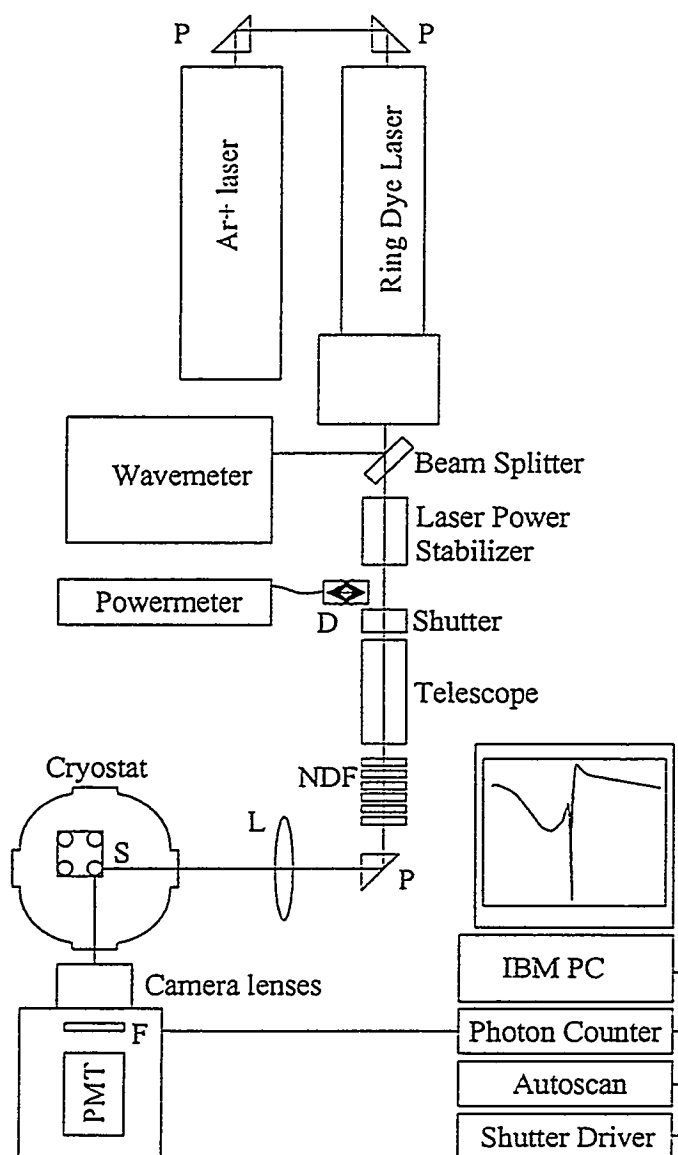
Figure 2-2. Block diagram of fluorescence excitation spectroscopy instrumentation: S, sample in a copper holder; L, lens; P, prism; BS, beam splitter; D, photodiode; F, long-pass filter; NDF, neutral density filter; PMT, photomultiplier tube.

tubes (2 mm i.d.) were first cooled slowly to liquid nitrogen temperature, then cooled to liquid helium temperature in a Janis model 8-DT Super Vari-Temp cryostat. A temperature lower than 4.2 K was achieved by pumping the cryostat filled with liquid helium. The temperature was measured with a silicon diode thermometer (Lake Shore Cryotronics Inc. model DT-470-SD-13) mounted on a copper frame which holds the sample. Fluorescence from the sample was long pass filtered and detected with an RCA C31034 GaAs photomultiplier tube. The signal from the photomultiplier tube was amplified (Stanford Research Systems SR-445 preamplifier) and digitized with a Stanford Research Systems SR-400 photon counter.

Absorption spectra of samples were measured with Bruker IFS 120 HR Fourier transform infrared spectrometer (FT-IR) as shown in Figure 2-3. With a tungsten light source, a CaF beam splitter and a silicon diode detector, spectra over the range from 25000 to 10000 cm^{-1} were acquired with a resolution of 1 or 4 cm^{-1}. The sample solution was placed between two quartz plates separated by an o-shaped teflon spacer (1 mm thick) and the quartz plates were mounted in a copper sample holder with screws. The hole burning light source was the same as the one for the fluorescence excitation spectroscopy. The sample solutions were first cooled slowly to liquid nitrogen temperature in order to produce good glassy samples, then cooled to liquid helium temperature in a Janis model 8-DT Super Vari-Temp cryostat for hole burning studies or kept in liquid nitrogen temperature for a simple low temperature absorption measurement. The sample temperature was measured with a silicon diode thermometer (Lake Shore Cryotronics model DT-500K) mounted on the copper sample holder. The sample was placed to make a 45 degree angle to both the burning laser beam and the probe beam from FT-IR. The burning laser beam was defocused to illuminate the whole sample while the probe beam was not.
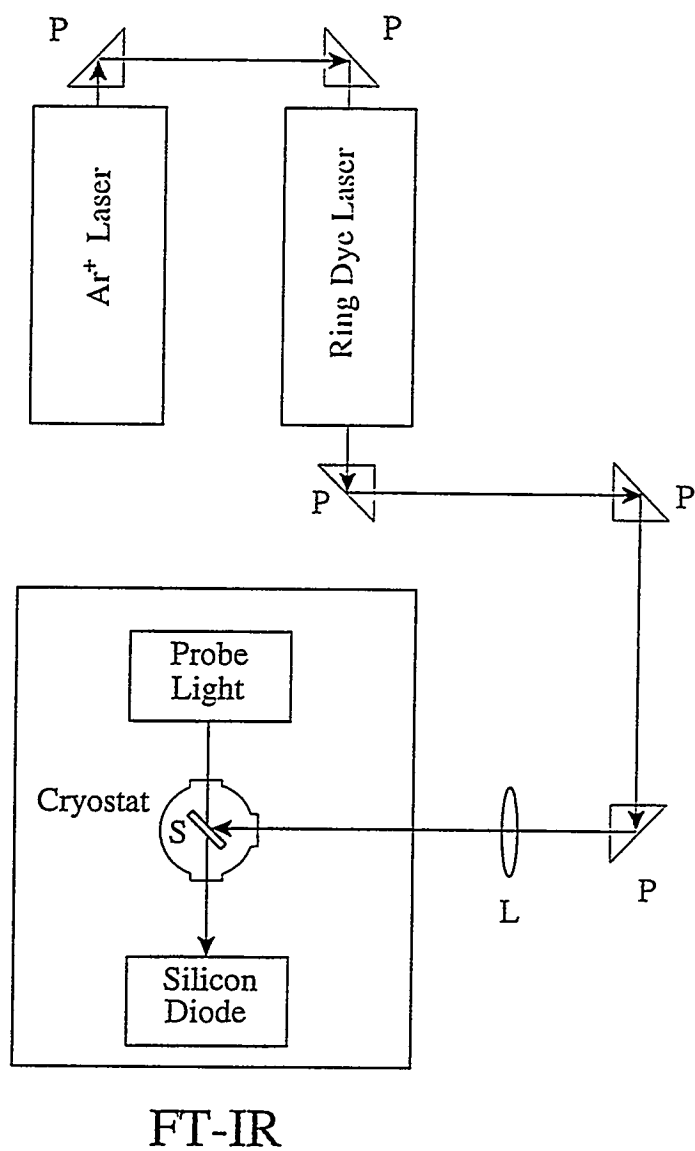
P   P

Ar⁺ Laser

Ring Dye Laser

P   P

Probe
Light

Cryostat   S

L   P

Silicon
Diode

FT-IR

Figure 2-3. Block diagram of absorption measurement: S, sample which was placed between two quartz plates (1.3 cm × 1.3 cm) with a teflon spacer (1 mm thick) and mounted in a copper holder with screws; L, lens; P, prism.

CHAPTER 3. CONFORMATIONAL STUDIES OF THE (+)-*TRANS*-, (-)-*TRANS*-, (+)-*CIS*-, AND (-)-*CIS* ADDUCTS OF ANTI-BENZO[a]PYRENE DIOLEPOXIDE TO N^2-dG IN DUPLEX OLIGONUCLEOTIDES USING POLYACRYLAMIDE GEL ELECTROPHORESIS AND LOW-TEMPERATURE FLUORESCENCE SPECTROSCOPY

Myungkoo Suh, Freek Ariese, Gerald J. Small, and Ryszard Jankowiak,

Tong-Ming Liu, and Nicholas E. Geacintov

ABSTRACT

Using polyacrylamide gel electrophoresis (PAGE) and low temperature, laser-induced fluorescence line narrowing (FLN) and non-line narrowing (NLN) spectroscopic methods, the conformational characteristics of stereochemically defined and site-specific adducts derived from the binding of 7β,8α-dihydoxy-9α,10α-epoxy-7,8,9,10-tetrahydrobenzo[a]pyrene (*anti*-BPDE, a metabolite of the environmental carcinogen benzo[a]pyrene), to DNA were studied. The focus of these studies was on the four stereochemically distinct *anti*-BPDE-modified duplexes 5'-d(CCATCGCTACC) · (GGTAGCGATGG), where G denotes the lesion site derived from *trans* or *cis* addition of the exocyclic amino group of guanine to the C10 position of either (+) or (-)-*anti*-BPDE. PAGE experiments under non-denaturing conditions showed that the (+)-*trans* adduct causes a significantly greater retardation in the electrophoretic mobility than the other three adducts, probably the result of important

adduct-induced distortions of the duplex structure. Low-temperature fluorescence studies in frozen aqueous buffer matrices showed that the (+)-*trans* adduct adopts primarily an external conformation with only minor interactions with the helix, but a smaller fraction (~25%) appears to exists in a partially base-stacked conformation. The (-)-*trans* adduct exists almost exclusively (~97%) in an external conformation. Both *cis* adducts were found to be intercalated; strong electron-phonon coupling observed in their FLN spectra provided additional evidence for significant π-π stacking interactions between the pyrenyl residues and the bases. FLN spectroscopy is shown to be suitable for distinguishing between *trans* and *cis* adducts, but lesions with either (+)- or (-)-*trans*, or (+)- or (-)-*cis* stereochemical characteristics showed very similar vibrational patterns. Addition of glycerol (50%, v/v) to the matrix caused a partial disruption of the chromophore-base stacking interactions for most adducts, but the (-) *cis* isomer showed a strong blue-shift and unusual vibrational frequencies. Low-temperature fluorescence spectroscopy techniques are most suitable for distinguishing between different conformational benzo[*a*]pyrene diol epoxide-DNA adduct types; because of the sensitivity of these methods, they may provide important information necessary for an understanding of the biological effects of the stereochemically distinct BPDE-guanine lesions.

INTRODUCTION

Benzo[*a*]pyrene is one of the most intensively studied environmental carcinogens [1,2]. Several enzymatic pathways have been reported to catalyze the binding of this compound or its metabolites to DNA, including monooxygenation [3] and one-electron oxidation routes [4]. Stable DNA adducts are mainly formed via covalent binding of the exocyclic amino group of guanine or adenine to the biologically most active and

chemically reactive metabolic intermediate 7,8-dihydroxy-9,10-epoxy-7,8,9,10-tetrahydrobenzo[a]pyrene [5]. There are two diastereomeric forms of this molecule, 7β,8α-dihydoxy-9α,10α-epoxy-7,8,9,10-tetrahydrobenzo[a]pyrene (anti-BPDE), and the 7β,8α,9α,10β-stereoisomer (syn-BPDE). Each of these diastereomers can be resolved into (+) and (-) enantiomers, and each enantiomer can react via cis or trans addition at the C10 position with the exocyclic amino groups of guanine and adenine residues [6,7]. In mammalian cells, racemic (±)-anti-BPDE is more mutagenic than (±)-syn-BPDE [8,9]. Furthermore, (+)-anti BPDE is strongly tumorigenic while (-)-anti BPDE is not [10,11]. These differences in biological activity are believed to be related to different conformations of the carcinogen-DNA adducts [12]. BPDE adducts may adopt various conformations depending on the stereochemistry of the adduct [13] and also depending on the nature of the flanking bases [14,15].

BPDE-DNA adduct conformations have been studied by several techniques, including circular/linear dichroism [14,16], fluorescence spectroscopy [15,17,18], polyacrylamide gel electrophoresis (PAGE) [19], high resolution NMR methods [20], and molecular modelling [21]. In the case of randomly modified BPDE-DNA adducts, the interpretation of data is complicated whenever (1) racemic (±)-anti BPDE is used, (2) mixtures of cis- and trans adducts are formed, (3) different DNA bases are modified, and (4) the sequence contexts in which the different lesions are embedded are not defined. In order to overcome these difficulties it is necessary to synthesize stereochemically pure BPDE adducts bound to a specific group of a given base in a well defined oligonucleotide sequence. Geacintov and coworkers have developed a direct synthetic approach in which BPDE is reacted with a given single stranded oligonucleotide [13,22]. The resulting mixture of BPDE-modified and unmodified oligonucleotide strands with different bases modified and/or different adduct

stereochemistries are separated from ane another by means of HPLC techniques, and annealed with the complementary strand. This approach was recently used for studying the effects of flanking bases on the characteristics of (+)-trans-anti BPDE-N^2-dG adducts [15,23]. For our present study in which conformational differences are investigated as a function of adduct stereochemistry, the same approach was used to synthesize the oligonucleotide d(CCATCGCTACC) · (GGTAGCGATGG) containing the (+)-*trans*-, (-)-*trans*-, (+)-*cis*, and (-)-*cis*- adducts of *anti*-BPDE bound to the exocyclic aminogroup of the central dG. The chemical structures of the four adducts are presented in Fig. 3-1. The solution conformations of three of these adducts, bound to the same duplex oligonucleotide, have recently been established by high resolution NMR and molecular mechanics modeling techniques. It was found that the (+)-*trans* and (-)-*trans* adducts are both located in the minor groove, but point in opposite directions (towards the 3' and 5' end of the modified strand, respectively) [20,24]. The (+)-*cis* adduct, on the other hand, was found to be characterized by a base-displacement intercalation model, in which the pyrenyl residue is intercalated, while the modified guanine residue and cytidine residue on the partner strand are displaced into the minor and major grooves, respectively [25].

In this paper we describe conformational studies of these four stereoisomeric BPDE adducts, employing low temperature laser induced fluorescence spectroscopy under line narrowing (FLN) and non-line narrowing (NLN) conditions [26], as well as polyacrylamide gel electrophoresis [19]. The determination of BPDE-DNA adduct conformations by NMR techniques requires milligram quantities of purified BPDE-modified oligonucleotides. Fluorescence techniques on the other hand are very sensitive and subnanogram quantities of adducts are often sufficient for identification of the types of adducts [4,26] or their conformational characteristics [15,18,19,27,28]. In addition,
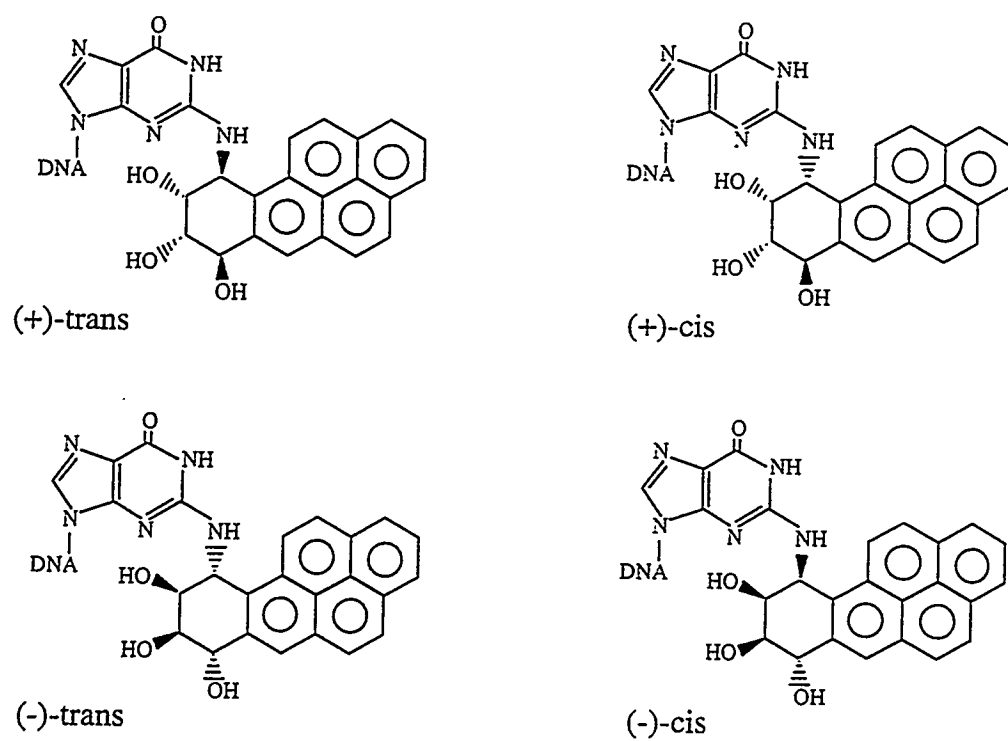
49

(+)-trans

(+)-cis

(-)-trans

(-)-cis

Figure 3-1. Stereochemical configurations of the four isomeric adducts of *anti*-BPDE.

fluorescence techniques are capable of distinguishing conformational equilibria on nanosecond and submicrosecond time scales. By comparing results obtained for identical BPDE-modified oligonucleotide duplexes obtained by NMR and by fluorescence methods, more exact interpretations of the lower resolution but higher sensitivity optical spectroscopic techniques such as UV absorbance [29] and fluorescence (this work) become feasible.

MATERIALS AND METHODS

Preparation of the stereospecifically pure adducted oligonucleotides.

Racemic *anti*-BPDE was purchased from the National Cancer Institute Chemical Carcinogen Reference Standard Repository (Chemsyn, Inc.), Lot no. CSL-91-320-29-17A, batch 15. The synthesis of the covalent *trans* adducts bound to the d(CCATCGCTACC) sequence at dG was carried out starting from racemic *anti*-BPDE using previously described methods [13,22,30]. Briefly, the stereochemically different 11-mer oligonucleotide adducts were separated and purified by reverse phase HPLC methods. The stereochemical characteristics of the adducts were ascertained by enzymatically digesting the BPDE-modified oligonucleotides to the BPDE-dG mononucleoside levels, and comparing their HPLC retention times and CD spectra with those of (+)-*trans*-, (-)-*trans*-, (+)-*cis*-, and (-)-*cis*-*anti*-BPDE-N^2-dG adduct standards as described by Cheng et al. [7]. The stereochemically pure BPDE-modified oligonucleotide strands 5'-d(CCATCGCTACC) were mixed with equimolar amounts of the complementary strands 5'-d(GGTAGCGATGG), heated to 65 °C, and slowly cooled to room temperature. The melting points, T_m, of the duplexes are above 40 °C; typical melting profiles have been published [29].

For low-temperature spectroscopic measurements, samples in aqueous buffer (20 mM sodium phosphate, 0.1 M NaCl, pH 7.0) or 50:50 mixed with glycerol, were transfered to 30 μL quartz sample tubes, sealed with rubber septa, and stored at -20 °C until further use. Adduct concentrations of all samples were 4×10^{-6} M in aqueous buffer or 2×10^{-6}M in 50 % glycerol.

Low temperature fluorescence measurements

The instrumentation used for low-temperature laser-excited fluorescence spectroscopy has been described elsewhere [26]. Here, only the most important specifications of the apparatus are summarized. The excitation source was a Lambda Physik EMG 103 MSC XeCl excimer laser/FL-2002 dye laser system. Adduct samples were probed with the laser under non-line-narrowing conditions (77 K, $S_2 \leftarrow S_0$ excitation) or line-narrowing conditions (4.2 K, $S_1 \leftarrow S_0$ excitation). Fluorescence was dispersed by a McPherson 2061 1-m monochromator; for NLN measurements the resolution was 0.6 nm (100 μm slit and 150 G/mm grating), while FLN spectra were recorded using a resolution of 0.08 nm (200 μm slit and 2400 G/mm grating. Depending on the grating used the spectral window covered by the active part of the Princeton Instruments IRY-1024/GRB intensified photodiode array detector was 160 nm, or 8 nm, respectively. For gated detection the output of a reference photodiode was used to trigger a Princeton Instruments FG-100 high-voltage pulse generator. Most spectra were recorded using a 45 ns delay and a 400 ns gate width. Before the measurements, samples were thawed from -20 °C to room temperature, then first slowly cooled on ice before rapid cooling by the cryogenic liquid. This procedure had previously been found to yield maximum duplexation [15].

Polyacrylamide gel electrophoresis

The oligonucleotide-BPDE adducts, complementary strands, and unmodified oligonucleotides (controls) were labeled separately with [γ-^{32}P]ATP (New England Nuclear) using T4 polynucleotide Kinase from Sigma Inc. Labeling was terminated by incubation at 80 °C for 25 minutes. Electrophoresis of duplex oligomers was carried out in two ways: labeled oligonucleotide-BPDE adducts were annealed to the corresponding unlabeled complementary strand, while labeled complementary oligonucleotides were annealed to non-labeled adducted oligonucleotides. In both cases the non-labeled strands were in slight molar excess. Annealing solutions were cooled down from 70 °C to 4 °C over 2 hours and kept at 4 °C for additional 20 minutes, then dried under a vacuum in a Speed Vac concentrator. The dried pellets were resuspended in loading buffer (pH 8.3) containing 9 mM tris-borate, 0.2 mM Na$_2$EDTA, xylene cyanole FF tracking dye (Sigma), and 30% glycerol (v/v).

20% native polyacrylamide gel (19:1 acrylamide:bis-acrylamide v/v in 53 mM tris-borate, 1.2 mM Na$_2$EDTA, 50 mM NaCl, pH = 8.3 buffer solution) was prepared for the 38 cm × 50 cm Bio-Rad Sequi-Gen Nucleic Acids Sequencing system. Thickness was 0.4 mm. The gel was polymerized at ambient temperature, then placed in a cold room (4°C) and incubated in the running buffer overnight before electrophoresis. Separation was carried out for 60 hours at 320 V and ~ 15 mA. The gel was kept at 4 ± 1 °C in the cold room throughout the separation. Autoradiography of gels using various exposure times was done at ambient temperature using Kodak X-ray films.

RESULTS AND DISCUSSION

PAGE analysis of modified oligonucleotide structures

The autoradiogram in Fig.3-2 demonstrates that the PAGE separation of single stranded oligonucleotide samples was excellent, and therefore could be used as an independent purity check. No cross-contamination was observed for the (+)-*trans*, (+)-*cis*, and (-)-*cis* adducts; overexposure revealed only a very low level of contamination (< 0.1 %) in the (-)-*trans* sample. Adduct decomposition by hydrolysis would produce a benzo[*a*]pyrene tetrol and the unmodified oligonucleotide, but this was not observed for any of the samples.

In single stranded form, all modified strands move significantly slower than the unmodified control. The retardation of the BPDE-modified oligonucleotides was in the order (+)-*trans*- > (-)-*trans*- > (+)-*cis*- > (-)-*cis* anti-BPDE adduct (see Fig. 3-2; lanes 1, 2, 3 and 4, respectively). Similar results, but with less pronounced differences in mobilities, were obtained by Shibutani et al. [30] for the same adducts embedded in an 18-mer oligonucleotide. The mobilities must reflect different translational friction coefficients since molecular weight and charge are the same for each adducted strand. However, adduct conformations in single stranded oligonucleotides are not the focus of this paper.

In the case of double stranded modified oligonucleotides, the same mobilities were observed independent of whether the modified strand or the complement strand was labeled (only the mobilities of the former are shown in Fig. 3-2). This indicates that under our experimental conditions (native gel, T = 4 °C) the modified 11-mer oligonucleotides were in complete duplex form, in agreement with the thermal melting studies of Ya et al. [29]. As shown in Fig. 3-2, the (-)-*trans*-, (+)-*cis*- and (-)-*cis-anti*-
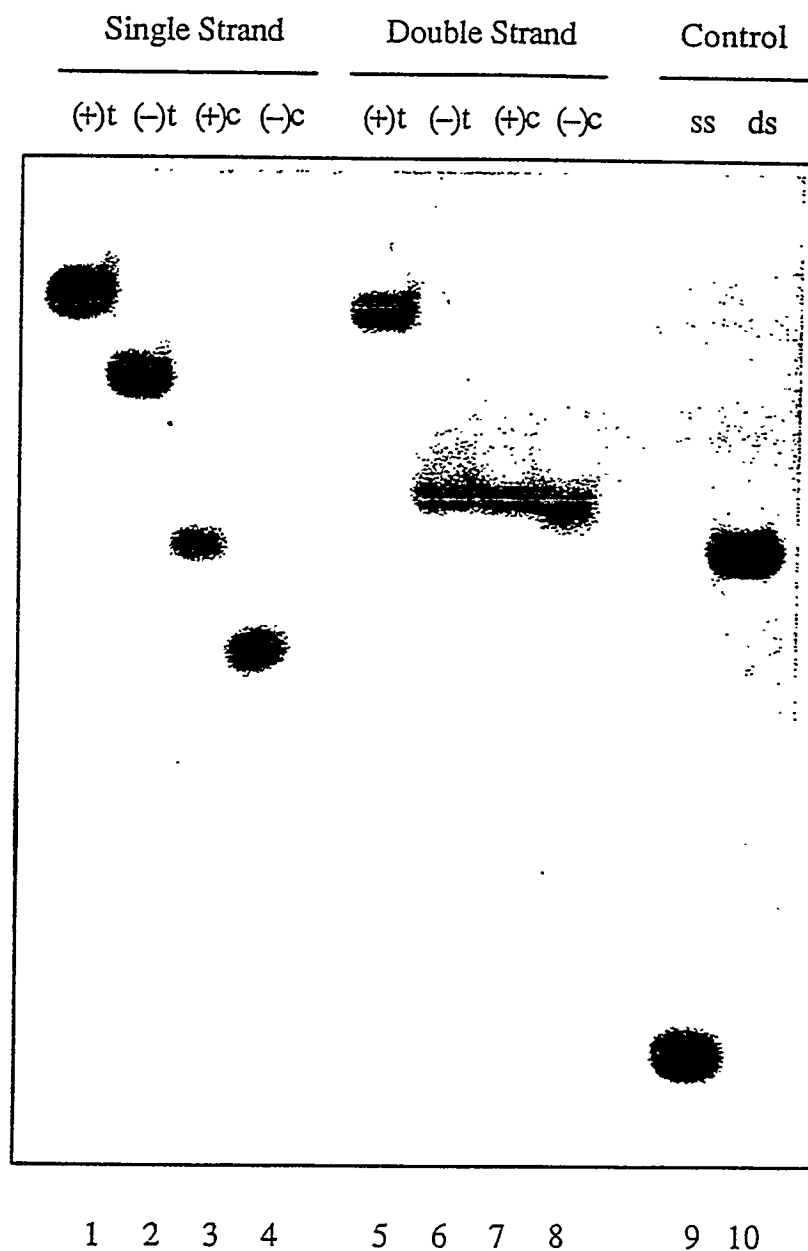
Figure 3-2.   Autoradiogram showing electrophoretic mobilities (migration direction downwards) of single strand (lanes 1 through 4) and duplex (lanes 5 through 8) oligonucleotides modified by (+)-*trans* (lanes 1 and 5), (-)-*trans* (lanes 2 and 6), (+)-*cis* (lanes 3 and 7), and (-)-*cis* (lanes 4 and 8) adducts of *anti*-BPDE. Lanes 9 and 10 represent the single stranded and duplex unmodified controls, respectively. Conditions: T = 4° C, native 20% polyacrylamide slab gel, 50 mM NaCl, 0.6X TBE buffer.

BPDE-adducted duplexes (lanes 6, 7 and 8, respectively) move slightly slower than the unmodified duplex (lane 10). Considering the molecular weight increase (5%) by adduct formation, these three adducts show minimal deviation in mobility from the duplex unmodified oligonucleotide. On the other hand, the mobility of the (+)-*trans* adduct (lane 5) was drastically reduced. According to the NMR studies of Cosman et al. [20] and de los Santos et al. [24], the extent of solvent exposure of the (+)-*trans*- and (-)-*trans-anti*-BPDE adducts are comparable; for both adducts the aromatic moiety is located in the minor groove with one side exposed to the solvent. On the other hand, for the (+)-*cis* adduct (and also for the (-)-*cis* adduct as will be shown below) the pyrenyl system is embedded within the double helix. Thus, there seems to be no clear correlation between the observed gel mobilities and the external/internal character of the adduct. If the observed mobilities of the double stranded modified oligonucleotides are not governed by adduct-solvent interactions, then they must be the result of different adduct-induced distortions of the duplex structure. Several experimental findings indicate bending of the helix at the site of the (+)-*trans-anti*-BPDE adduct. Linear dichroism studies of BPDE-DNA adducts with external character, which is characteristic for the (+)-*trans-anti*-BPDE adducts, suggested that there is a kink or flexible joint at the site of lesion [31,32]. It was also reported that DNA (145 - 185 base pairs) modified with (+)-*anti*-BPDE showed reduced electrophoretic mobility, and bending of the helix was suggested [33]. In addition, theoretical molecular dynamics simulation studies reported that the (+)-*trans-anti*-BPDE adduct produced severe helical bending in a duplex dodecamer, while the (-)-*trans-anti*-BPDE adduct caused only minimal distortion [21]. Our PAGE results confirm those findings, showing that the (+)-*trans-anti*-BPDE adduct causes indeed a severe distortion of the overall helix structure, but that the helical structures of the duplex oligonucleotides modified with (-)-*trans*-, (+)-*cis*- or

(-)-*cis-anti*-BPDE are minimally disturbed. These results are also consistent with those of Mao [34] and Xu et al. [35] who have shown that upon ligation of BPDE-modified oligonucleotides 11-23 base pairs long, only the (+)-*trans* BPDE-modified oligonucleotides are capable of forming small, covalently closed minicircles. This clearly indicates that only the (+)-*trans*-BPDE-N^2-dG lesions are associated with a flexible hinge joint or bend at the site of the lesion.

General remarks concerning low-temperature matrices

Before we discuss the NLN and FLN spectra of the different adduct stereoisomers a short discussion of low-temperature fluorescence measurements and the matrices used in our experiments is appropriate. Compared to conventional fluorescence spectrometry at room temperature, carrying out the measurements at 77K under non-line narrowing conditions offers several advantages for these types of adducts. Reduced spectral broadening is important in order to observe the sometimes subtle differences in fluorescence spectra. Furthermore, quenching phenomena, affecting the fluorescence of intercalated adducts less strongly than that of external adducts [13,16,17], play only a minor role at cryogenic temperatures; all adduct types exhibit comparable fluorescence lifetimes (ranging from 150-200 ns). Apart from the obvious increase in signal intensity, this also means that when non-selective excitation is applied to a mixture of different conformations all adduct types can be observed with similar sensitivities. The relative intensities of different emission bands thus give a direct indication of the relative concentrations of the particular species.

All samples were studied in two matrices: aqueous buffer and aqueous buffer/glycerol 50:50 v/v ("glass"). Obviously the conformations encountered in aqueous buffer mimick the situation in a cellular environment most closely. The

addition of glycerol serves several purposes: it increases the solvent compatibility towards the aromatic moiety of the adduct and has a destabilizing effect on the DNA structure. Conformational changes induced by the addition of glycerol thus provide qualitative information regarding the stability of the adduct conformation in aqueous buffer. At the same time the decrease in base-chromophore interactions (weaker electron-phonon coupling) usually leads to better resolved FLN spectra [18], which is useful if the frequencies of the vibrational modes are to be used for identification purposes [4,19,36].

An important question is whether fluorescence line-narrowing spectroscopy is also applicable to frozen aqueous samples that could lead to a crystalline environment. However, due to the presence of buffer salts [37] and also the flexible nature of the oligonucleotides the direct surrounding of the chromophore moieties is highly disordered, as reflected in our FLN spectra (see below), and also our preliminary hole burning experiments (data not shown). An ordered environment could cause matrix-induced (Shpol'skii-type) line-narrowing, but that was never observed for adduct samples in aqueous buffer. Thus, aromatic fluorophores bound to DNA or oligonucleotides in frozen aqueous buffer matrices experience a matrix inhomogeneity similar to that of common low-temperature glasses. Apparently, the occurrence of polycrystalline regions away from the oligonucleotides has no influence on the spectroscopic properties of the adducts. It should also be mentioned that light scattering problems in partially polycrystalline aqueous samples are easily overcome if time-resolved detection can be used.

It should be emphasized that during the cooling procedure only conformations that are thermally accessible at ambient temperature can be trapped. At elevated temperatures the adducts will show a broad distribution of conformations, and some

higher-energy conformations may not be trapped during cooling. However, the conformations corresponding to an absolute or local minumum of the potential energy surface will also exist at cryogenic temperatures. Therefore, if two or more distinct molecular conformations are observed in a low temperature fluorescence experiment, it can be concluded that these conformations do contribute to the conformational equilibrium in solution at biological temperatures, but they may not represent the full room temperature distribution. Since the matrix in the immediate vicinity of the adduct is of an amorphous nature, the possibility that otherwise improbable conformations are being induced by matrix crystallization can be excluded.

Non-line-narrowing ($S_2 \leftarrow S_0$) fluorescence spectroscopy

In this section non-line narrowed (NLN) fluorescence spectra will be shown for BPDE adducts bound to double stranded oligonucleotides or to deoxyguanosine only. Based on the extent of the red-shift of the fluorescence origin band, we define three different adduct conformations as ($\pm$)-1, ($\pm$)-2, and ($\pm$)-3 [18,27]. These conformations are characterized by increasing stacking interactions with the bases and decreasing accesibility to quenchers, and are assigned as external, partially base stacked, and intercalated adduct types, respectively [18,27]. Most NLN spectra were obtained using excitation at 308 or 343 nm, wavelengths with poor selectivity that one can use to excite external, partially base stacked, and intercalated conformations at the same time with roughly comparable efficiencies (at cryogenic temperatures all adduct types exhibit similar fluorescence lifetimes, while the molar extinction coefficients are not significantly different). Excitation at 355 nm is used to selectively excite intercalated adducts [13]. Selective excitation of external adducts is not possible; the existence of such conformations can only be infered via spectral deconvolution (see below).

(+)-trans-anti BPDE adduct

NLN fluorescence spectra obtained for the (+)-*trans* isomer in double stranded oligonucleotide, as well as bound to the nucleoside dG only, are shown in Fig. 3-3. The solvent matrices were aqueous buffer (curves a, b, d) or aqueous buffer/glycerol 50:50 (curve c). For comparison, curve 3d is the NLN spectrum of the (+)-*trans* adduct bound to guanosine only, showing the typical spectral characteristics (emission maximum 376.3 nm, bandwidth ∼130 cm^{-1} FWHM) of the BPDE adduct in the absence of interaction with the DNA helix. Emission maxima and widths of the 0-0 origin bands of all adduct isomers are listed in Table 3-1. Spectrum a in Fig. 3-3 with its relatively broad 0-0 band (∼350 cm^{-1}) corresponds to a mixture of conformations. The major one with its maximum at 378.6 nm (a moderate red shift compared to the mononucleoside adduct in spectrum 3d) is assigned, based on our previous nomenclature [18,27], as a (+)1 external conformation. This agrees very well with the data, reported for this adduct in solution by Cosman et al [20], showing that the pyrenyl moiety is located in the minor groove with one side exposed to the solvent. However, the skewed peak shape of the fluorescence origin band in spectrum 3a indicates that the sample was not conformationally pure, as revealed by selective excitation at 355 nm (see spectrum 3b). This fraction, with its maximum at 380.3 and band width $\Gamma = $ ∼240 cm^{-1} is assigned as a (+)-2 type, partially base-stacked conformation; its relative abundance is estimated to be ∼25% (see Table 3-1). This is an unexpected finding, since the NMR spectra recorded by Cosman et al. [20] showed no indication of a heterogeneous equilibrium of conformations. The differences in the apparent conformational adduct heterogeneities observed by the fluorescence and high resolution NMR methods are presently not well understood. We note, however, some important experimental
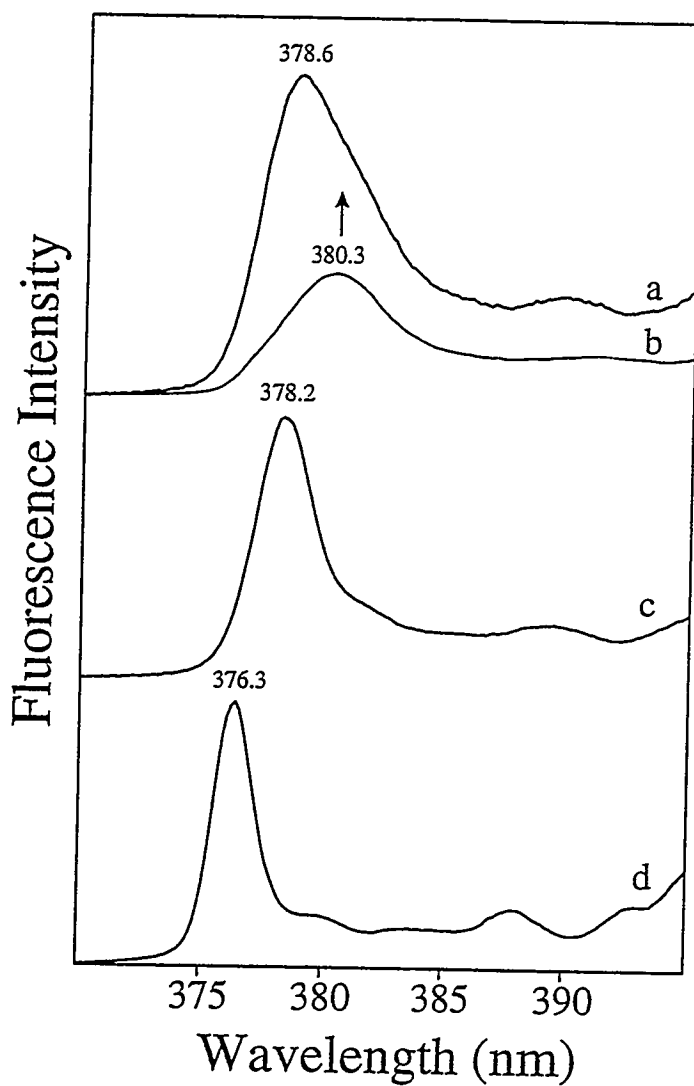
Figure 3-3. Non-line narrowed (0,0) fluorescence origin bands of the (+)-*trans*-adduct of *anti*-BPDE in duplex oligonucleotide (T = 77 K) Curve a: spectrum in aqueous buffer; λex = 343 nm. Curve b: spectrum in aqueous buffer; λex = 355 nm. Curve c: spectrum in 50 % glycerol matrix; λex = 343 nm. Curve d: spectrum of the same adduct bound to dG only; aqueous buffer; λex = 308 nm.

Table 3-1. Spectral characteristics of the *anti*-BPDE adduct conformations

	(+)-*trans*			(-)-*trans*			(+)-*cis*			(-)-*cis*		
	Conform. type Abundance[c]	(0,0)[a]	Γ[b]	Conform. type Abundance	(0,0)	Γ	Conform. type Abundance	(0,0)	Γ	Conform. type Abundance	(0,0)	Γ
Oligonucleotides in aqueous buffer	(+)-1 major(~75%)	378.4	180	(-)-1 major(~97%)	378.4	170	(+)-1 minor(~6%)	~378		(-)-1 minor(~8%)	378.5	
	(+)-2 minor(~25%)	380.3	~240	(-)-2 minor(~3%)	380.4	~300	(+)-3 major(~94%)	381.0	300	(-)-3 major(~92%)	381.3	270
Oligonucleotides in 50% glycerol	(+)-1	378.3	200	(-)-1	377.7	200	(+)-1 minor(~12%)	377.8	230	(-)-1*[d] minor(~15%)	375.7	160
							(+)-3 major(~88%)	381.4	330	(-)-3 major(~85%)	381.1	300
Mononucleosides in aqueous buffer		376.3	130		376.3	130		376.3	130		376.3	130
Mononucleosides in 50% glycerol		376.5	150		376.5	150		376.5	160		376.5	160

a Maximum of fluorescence (0,0) origin band after deconvolution (in nm).
b Γ is the FWHM obtained by doubling the half width at half maximum measured at the high energy side of the band (in cm^{-1}).
c Relative abundances are estimates obtained upon deconvolution of non-selectively excited NLN spectra.
d For this adduct the conformation of the saturated ring is believed to have undergone an important change (see text).

differences in these two experiments, for instance, time scales and concentrations. A search for an explanation for these conformational heterogeneity effects would have to begin with an investigation of some of these variables, but was beyond the scope of this work.

As observed in previous studies for partially base stacked conformations [38], the addition of glycerol disrupted the weak stacking interactions and the minor (+)-2 contribution observed in aqueous buffer disappeared, leaving a purely external (+)-1 type conformation. This effect is believed to be due to an increased solvent compatibility towards the aromatic moiety. The resulting spectrum, presented in Fig. 3-3c, is narrower (~ 200 cm^{-1}) and does not show any dependence on the excitation wavelength .

NLN spectra of the single stranded (+)-*trans* adduct sample (not shown) indicates that in aqueous buffer a very broad distribution of external and base-stacked conformations exists (bandwidth ~ 430 cm^{-1}; emission maximum ~ 381 nm). Upon dilution from 4×10^{-6} M to 2×10^{-7} M a significant spectral narrowing and a blue-shift to 376.7 nm is observed. Similar effects were observed upon dilution of the single stranded samples of the (-)-*trans* and (+)-*cis* adducts, but not for the (-)-cis adduct. Studies in progress are expected to clarify these phenomena for single stranded oligonucleotides. In this paper we focus only on structural properties of adducts in duplex oligonucleotides.

(-)-*trans-anti* BPDE adduct

NLN spectra of the double stranded (-)-*trans* adduct, obtained using non-selective excitation at 343 nm, are shown in Fig. 3-4, curves a and b. The emission
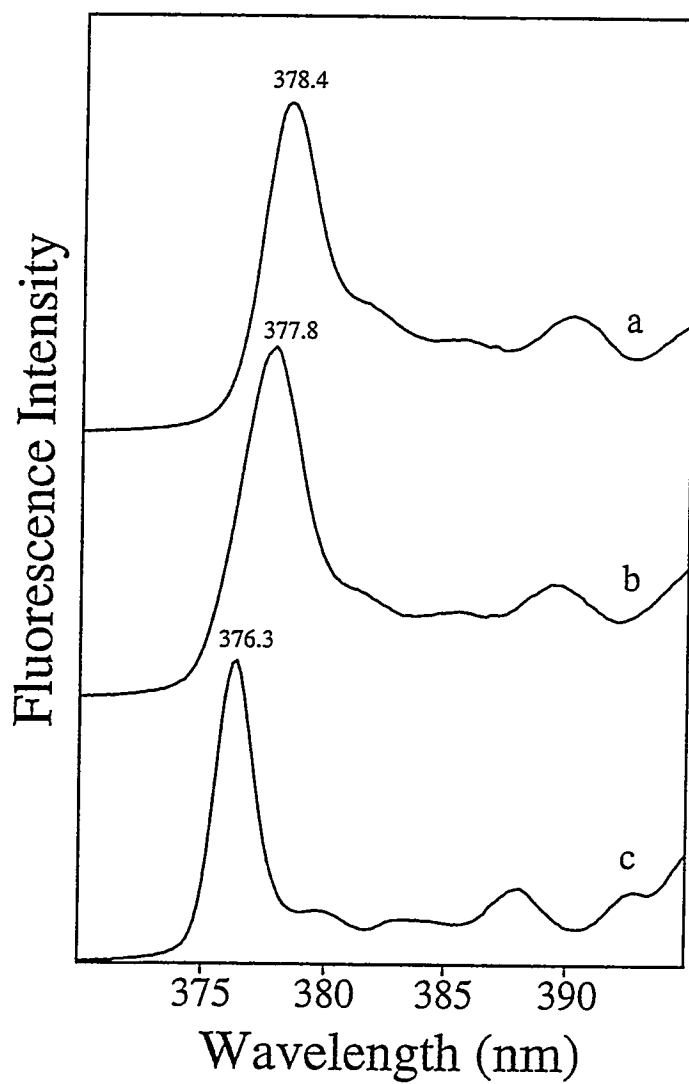
63

Figure 3-4.   Non-line narrowed (0,0) fluorescence origin bands of the (-)-*trans*-adduct of *anti*-BPDE in duplex oligonucleotide (T = 77 K). Curve a: spectrum in aqueous buffer; λex = 343 nm. Curve b: spectrum in 50 % glycerol matrix; λex = 343 nm. Curve c: spectrum of the same adduct bound to dG only; aqueous buffer; λex = 308 nm.

maximum at 378.4 nm observed in aqueous buffer (spectrum 4a) corresponds to a (-)-1 external adduct type with only weak interactions with the DNA helix. The 0-0 origin band of the (-)-*trans* adduct is very narrow ($\sim$170 cm^{-1}), indicating minimal heterogeneity. Excitation wavelength dependence was practically absent; a very small contribution with a red-shifted emission was observed when 355 nm excitation was employed (spectrum not shown). Addition of glycerol to the sample did not have a large impact on the width of its NLN spectrum (compare spectrum 4b with 4a). However, the (0-0) origin band was found to undergo a 0.7 nm blue-shift, which was not observed for the (+)-*trans* adduct. The bottom curve 4c shows the NLN spectrum of the (-)-*trans* adduct to dG for comparison. Our conformational assignment as a (-)-1 external adduct is in agreement with the studies of de los Santos et al. [24], who reported that the (-)-*trans* adduct is located in the minor groove with one face of the aromatic moiety exposed to the solvent. The fact that the two *trans* adducts behave differently upon the addition of glycerol indicates that the interactions with the DNA are not identical.

(+)-*cis-anti* BPDE adduct

The NLN spectra of the *cis* adduct of (+)-*anti* BPDE are shown in Fig. 3-5. In aqueous buffer matrix (spectrum 5a, employing non-selective excitation at 308 nm) the major conformation showed strong chromophore-base interactions: the width is ca. 300 cm^{-1}, while the emission maximum at 381.0 nm is significantly red-shifted compared to those of the two *trans* adducts discussed above. This indicates that in the duplex oligonucleotide the adduct is held in an internal (+)-3 type conformation. These results agree with the findings of Cosman et al. [25], who recently established the major solution conformation of this adduct to be of the intercalated type, with the pyrenyl moiety being sandwiched between the two neighboring cytosine bases and displacing not
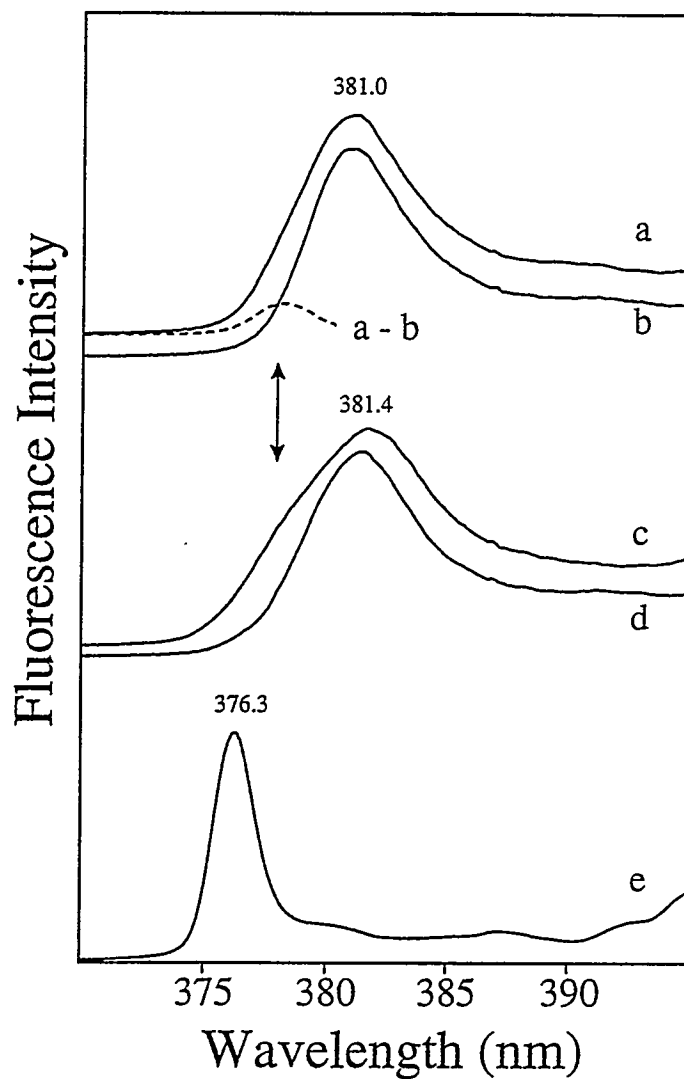
Figure 3-5. Non-line narrowed (0,0) fluorescence origin bands of the (+)-*cis*-adduct of *anti*-BPDE in duplex oligonucleotide (T = 77 K). Curve a: spectrum in aqueous buffer; λex = 308 nm. Curve b: spectrum in aqueous buffer; λex = 355 nm. Dashed curve: difference spectrum 5a - 5b. Curve c: spectrum in 50 % glycerol matrix; λex = 308 nm. Curve d: spectrum in 50 % glycerol matrix; λex = 355 nm. Curve e: spectrum of the same adduct bound to dG only; aqueous buffer; λex = 308 nm.

only the adducted guanine into the minor groove, but also the opposite cytosine residue on the partner strand into the major groove. When using selective excitation at 355 nm a minor conformational heterogeneity is observed, as can be seen by comparing spectra 5a and 5b. The dashed curve represents the difference spectrum. This minor fraction, with its origin band around 378 nm, is less efficiently excited at 355 nm, indicating that its conformation must be of the external type [13]. Also Cosman et al. [25] noticed the existence of a minor, non-intercalative conformation in their NMR study, in agreement with our findings.

Addition of glycerol to the aqueous sample increases the solvent compatibility towards the aromatic moiety and may also disrupt the helical structure. Both effects can be illustrated in the case of the (+)-*cis* adduct. The very broad origin band of the duplex sample in 50% glycerol indicates a mixture of external and intercalated adducts (see Fig. 3-5c). The glycerol causes a larger fraction of the adduct molecules to adopt an external conformation (larger shoulder around 378 nm in spectrum 5c than in spectrum 5a). The fact that the major origin band is still at 381.4 nm shows that, unlike the partially base-stacked (+)-2 conformation observed for the (+)-*trans* adduct, the truly intercalated (+)-3 type conformation is relatively stable in this matrix, as was previously demonstrated for these adducts in double stranded oligonucleotides [38] and in DNA [27]. The 30 cm^{-1} increase in spectral bandwidth of the intercalated conformation (compare curves 5d and 5b, both obtained employing selective excitation at 355 nm; see also Table 3-1) presumably reflects a destabilization of the helical structure in the 50% glycerol matrix, leading to a broader distribution of intercalated structures. Again the bottom curve 5e shows the NLN spectrum of the (+)-*cis-anti* BPDE-dG adduct for comparison.

(-)-*cis-anti* BPDE adduct

NLN spectra of the (-)-*cis-anti* adduct are shown in Fig. 3-6. The spectrum of the duplex sample in aqueous buffer (curve 6a) is very similar to that of the (+)-*cis* adduct. The 0-0 band is red-shifted to 381.3 nm, which according to our nomenclature corresponds to a (-)-3 type internal adduct conformation [18,27], and almost as broad as that of the (+)-cis adduct. For this adduct no independent structure characterization by means of high resolution NMR spectroscopy has yet been published, but based on the similarity between the spectral properties of the two *cis*-adducts we conclude that also the (-)-*cis* anti-BPDE adduct adopts an intercalated conformation [13]. Further evidence will be provided in the next section by means of FLN spectroscopy. The sample showed only minor excitation wavelength dependence, as can be seen by comparing curves 6a and 6b. The dashed curve represents the difference spectrum 6a-6b. As in the case of the (+)-*cis* adduct, a minor contribution (~5 %) of an adduct with an external conformation can be discerned around 378.5 nm. In the 50 % glycerol matrix the majority of the adduct molecules are still intercalated, which means that also for this adduct the intercalated conformation is relatively stable (see curve 6c). However, an important fraction has adopted a conformation that shows an emission maximum around 375.7 nm, more blue-shifted than observed for the external fractions of the other three adduct samples and even more blue-shifted than the mononucleotide adduct (curve 6e). When 355 nm excitation is used only the intercalated fraction of the conformational mixture is observed (spectrum 6d). More information on the nature of this peculiar conformational equilibrium was obtained using FLN spectroscopy (see below).

Finally, we note that under NLN conditions the spectra of the single nucleoside adducts are very similar for all four stereoisomers (compare the bottom spectra of Figs. 3-3 and 3-6), and practically independent of the solvent matrix used (see Table 3-1).
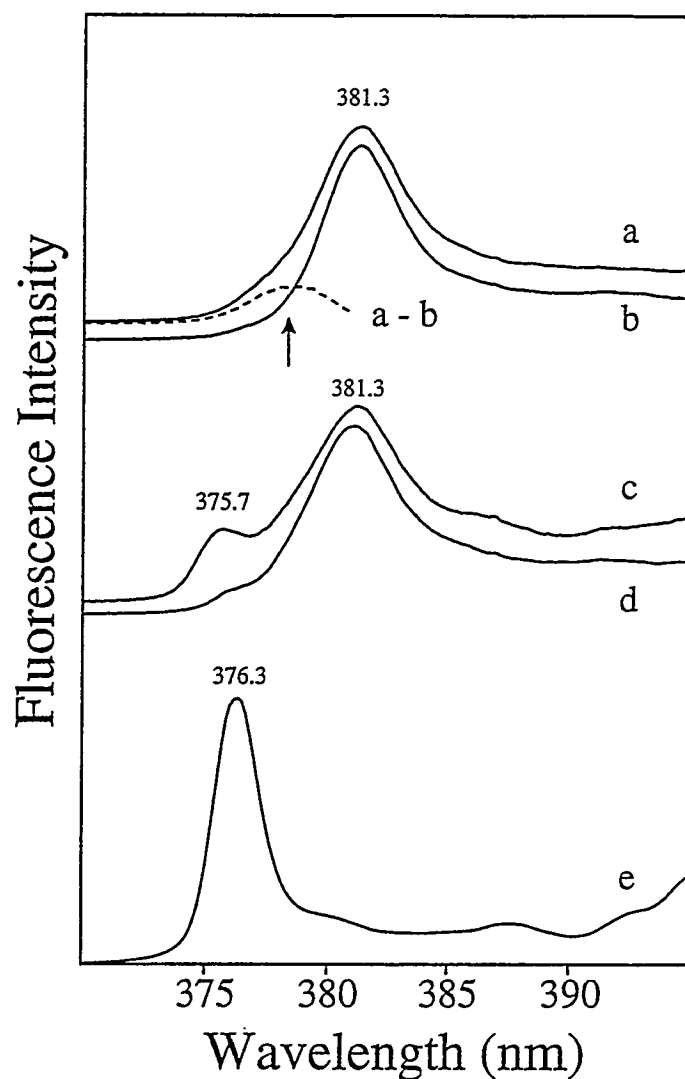
Figure 3-6. Non-line narrowed (0,0) fluorescence origin bands of the (-)-*cis*-adduct of *anti*-BPDE in duplex oligonucleotide (T = 77 K). Curve a: spectrum in aqueous buffer; λex = 308 nm. Curve b: spectrum in aqueous buffer; λex = 355 nm. Dashed curve: difference spectrum 5a - 5b. Curve c: spectrum in 50 % glycerol matrix; λex = 308 nm. Curve d: spectrum in 50 % glycerol matrix; λex = 355 nm. Curve e: spectrum of the same adduct bound to dG only; aqueous buffer; λex = 308 nm.

However, *cis-* and *trans* isomers are easily distinguished under FLN conditions, as will be shown in the next section.

Fluorescence line narrowing spectroscopy

More detailed structural information concerning the different BPDE-adducts can be obtained using fluorescence line narrowing spectroscopy. In the study of carcinogen-DNA adducts this technique may be used to obtain extra conformational information or it can serve chemical/stereochemical identification purposes [26]. Both aspects will now be discussed separately.

In a typical vibronically excited FLN spectrum each S_1 vibrational frequency will appear as a sharp line (the zero-phonon line, ZPL), accompanied by a broader band at longer-wavelength. The latter, so-called phonon side band (PSB), is attributed to molecules that lose part of their excitation energy to lattice vibrations (phonons). The ZPL/PSB intensity ratio strongly depends on temperature and the electronic coupling with the matrix, and can thus provide information on the microenvironment around the chromophore. It was shown by Haarer [39] that π-molecular charge-transfer states are characterized by very strong coupling. Jankowiak and coworkers [27] have shown that the relative intensities of the ZPLs in the FLN excitation spectra of various $(+)$-*anti* BPDE-DNA adducts increases in the order $(+)$-3 intercalated $<$ $(+)$-2 partially base-stacked $<$ $(+)$-1 external, reflecting a decrease in coupling strength between the chromophore and the bases in the same order.

FLN spectra obtained for the four adduct stereoisomers in double-stranded oligonucleotides in aqueous buffer matrix are shown in Fig. 3-7. The spectra were recorded at liquid helium temperature (4.2 K) using 369.48 nm excitation; at this wavelength broadbanded emission due to uncorrelated S_2-S_0 excitation can be ruled out.
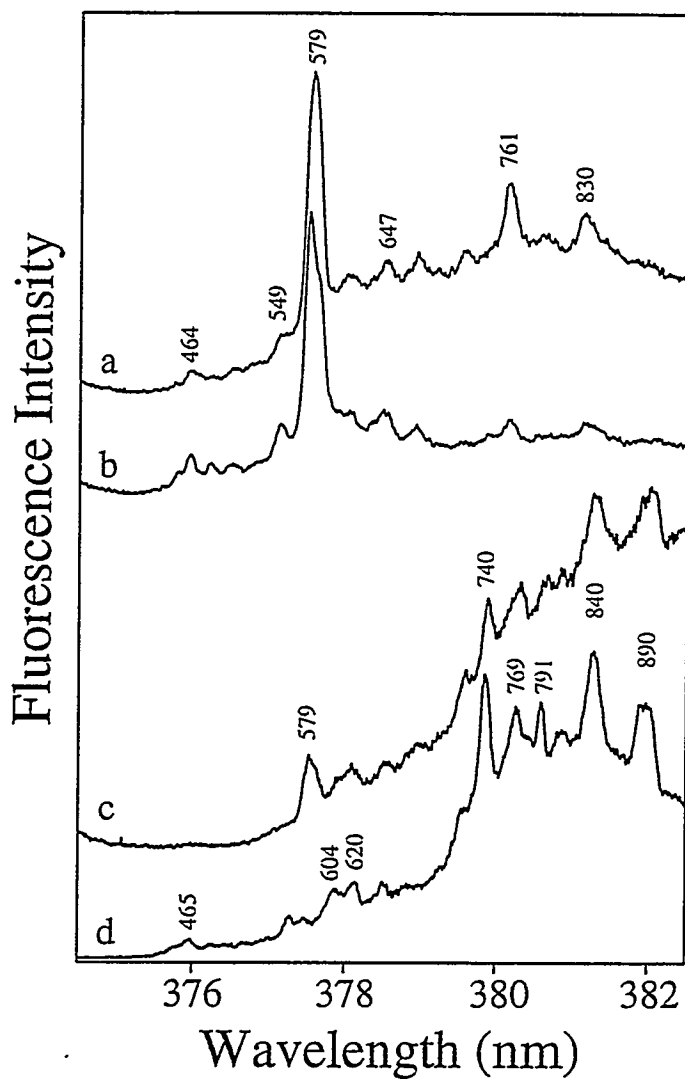
Figure 3-7.   FLN spectra of the duplex oligonucleotides in aqueous buffer, containing different stereoisomeric *anti*-BPDE-N²-dG adducts. Curve a: (+)-*trans*; curve b: (-)-*trans*; curve c: (+)-*cis*; curve d: (-)-*cis* adduct. T = 4.2 K; λex = 369.48 nm. Zero-phonon lines are labeled with their excited-state vibrational frequencies (in cm-1).

In the 378 nm region the (+)-*trans-anti* adduct yields a fairly well resolved FLN spectrum with strong ZPL's (curve 7a; spectra obtained using other excitation wavelengths not shown). This indicates that there are no strong stacking interactions with the bases. These findings for the major adduct are in full agreement with the solution conformation established for the (+)-*trans* adduct by Cosman et al. [20], in which the pyrenyl moiety is situated in the minor groove, with one side interacting with the sugar-phosphate backbone and one side exposed to the solvent. However, the broad emission band underlying the low-energy side of the spectrum (~380 nm) indicates the presence of a second, minor conformation with stronger stacking interactions, in agreement with the NLN results discussed above and shown in Fig. 3-3, spectra a and b.

In contrast, the FLN spectrum of the (-)-*trans-anti* adduct (curve 7b) does not show any broadbanded emission indicative of stacking interactions. This adduct exists in a pure (-)-1 type external conformation. These results are in full agreement with the solution conformation reported by de los Santos et al [24], in which the adduct is located in the minor groove (pointing towards the 3' terminus of the modified strand) and interacts only with the solvent and the sugar-phosphate backbone.

Spectrum 7c shows that the FLN spectrum of the (+)-*cis-anti* adduct is distinctly different. The intensities of the ZPLs are relatively weak and superimposed on a strong broadbanded emission at the low-energy side of the spectrum. This proves that the broad 0-0 band around 381 nm observed at 77 K (Fig. 3-5a) is not due to a broad heterogeneous distribution of adduct conformations, but to strong electron-phonon coupling (π-π interactions). Again, these findings are in full agreement with the intercalated conformation established for this adduct by Cosman et al. [25]. The ZPL's

in the 378 nm region belong to the minor external conformation shown in Fig. 3-5 (difference spectrum 5a-5b).

Curve 7d shows that the FLN spectrum of the (-)-*cis* adduct is very similar to that of its (+)-*cis* counterpart. The (-)-*cis* adduct shows also relatively weak ZPLs with a large contribution from phonon side bands, indicating that also for this adduct the major conformation, assigned as (-)-3, is one in which the chromophore experiences very strong coupling with the bases. These spectra confirm our conclusion of the previous subsection that also the (-)-*cis* adduct adopts primarily an intercalated conformation. Also for this adduct the ZPL's in the 378 nm region belong to the minor external conformation (see Fig. 3-6, difference spectrum 6a-6b).

The FLN spectra obtained in 50 % glycerol matrix are presented in Fig. 3-8 and confirm the NLN results discussed above. In the case of the (+)-*trans-anti* adduct the weak stacking interactions are disrupted, resulting in a purely external (+)1 type conformation (see spectrum 3-8a). The spectrum of (-)-*trans-anti* BPDE is blue-shifted by 30 cm^{-1} upon the addition of glycerol, and as a result the low-frequency modes around 376 nm increase in intensity, while the vibronic lines in the 380 nm region decrease(compare spectra 3-8b and 3-7b). Such behavior is not observed for the (+)-*trans* isomer. These differences could be related to the findings of de los Santos et al. [24], who stated that the interactions between the aromatic moiety and the minor groove are not identical for the two *trans* isomers. Figure 3-8c illustrates again that for the (+)-*cis* adduct even in 50 % glycerol the intercalated structure remains largely intact, but that a minor contribution of an external (+)-1 conformation is also present in this matrix. The relative contribution of this minor fraction is larger in this matrix than in aqueous buffer (compare spectra 8c and 7c). Curve 8d shows the FLN spectrum obtained for the (-)-*cis* adduct. The intercalated conformation remains the major one,
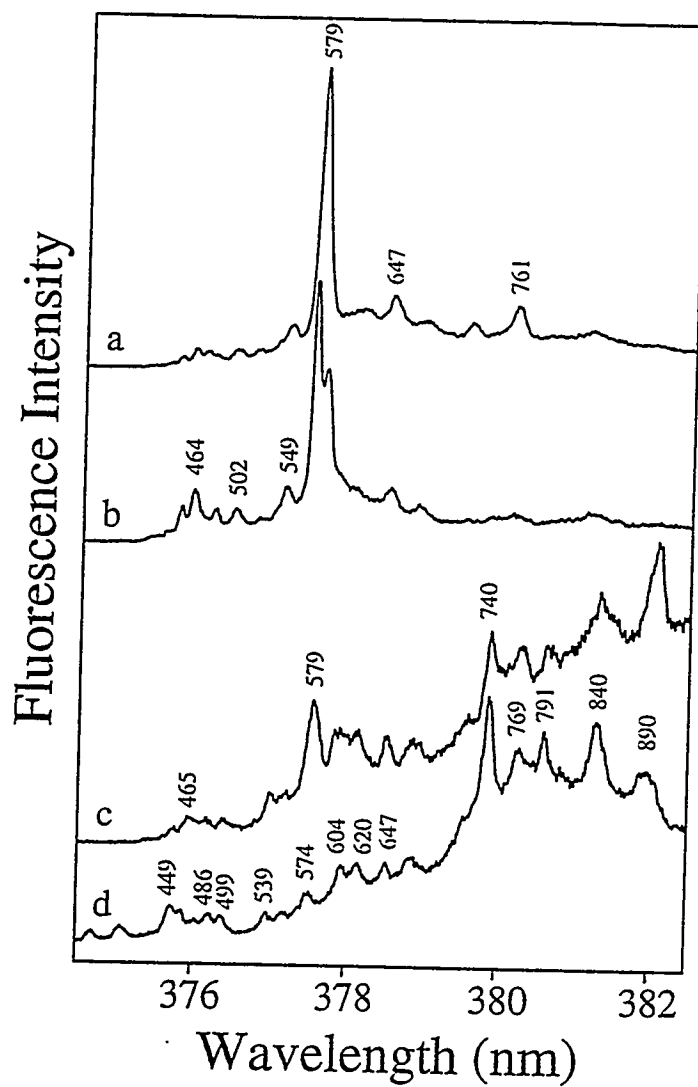
73

Figure 3-8. FLN spectra of the duplex oligonucleotides in 50 % glycerol matrix, containing different stereoisomeric *anti*-BPDE-N^2-dG adducts. Curve a: (+)-*trans*; curve b: (-)-*trans*; curve c: (+)-*cis*; curve d: (-)-*cis* adduct. T = 4.2 K; λex = 369.48 nm. Zero-phonon lines are labeled with their excited-state vibrational frequencies (in cm-1).

but for this adduct, besides the minor external contribution around 378 nm which was also observed in aqueous buffer, the presence of an unknown conformation with an unusually blue-shifted 0-0 band around 376 nm is also observed in this matrix (see below for further details).

When comparing the vibrational frequency patterns of the four adduct stereoisomers in Figures 3-7 and 3-8, it is observed that *trans* and *cis* adducts are very easily distinguished (see also spectra 9b and 9c for the mononucleoside adducts). For example, ZPLs at 549 and 761 cm^{-1} are indicative of *trans* adducts, while strong lines at 539, 740, or 890 cm^{-1} are observed for the *cis* adducts. However, when comparing the vibrational frequencies of the two *trans* spectra there is only a small number of obvious differences (e.g. the 579 cm^{-1} mode) and also for the two *cis* adducts only minor differences were observed (e.g. the 600-620 cm^{-1} region). In the case of the stereoisomeric mononucleoside, (+)-*trans*, (-)-*trans*, (+)-*cis*, and (-)-*cis*-adducts yield the NLN spectra which are similar in all cases, but the FLN spectra are diffirent for the *trans* and the *cis* adducts. However, (+)- and (-)-*trans* or *cis* adducts cannot be distinguished from one another (also when different excitation wavelengths were used to explore other regions of the S$_1$ excited state; spectra not shown). Apparently, the influence of the ribose moiety on the fluorescence characteristics of these stereoisomeric BPDE-mononucleoside adducts is negligible. The major excited state vibrational frequencies are listed in Table 3-2.

Different interactions with the DNA helix, duplex formation, or solvent effects may change the intensity distribution of the ZPLs or increase the intensity of the broad phonon side bands, but the frequencies remain usually unchanged. One of the exceptions observed for these adducts is the splitting of the 579 band for the (-)-*trans* isomer as shown in Figure 3-7b, which is even more pronounced in the 50 % glycerol matrix

Table 3-2: Most prominent excited state vibrational frequencies in FLN spectra of *anti-*BPDE adducts[a]

(+)-*trans*/(-)-*trans*	(+)-*cis*/(-)-*cis*	(-)-*cis*[*b]
453	453	449
464	465	461
483	481	486
502	496	499
549	539	539
579(+);575/583(-)[c]	579(+);574(-)	564
	604/620	601/621
647	647	
720	740	719
761	769	755
	791	784
830	840	842
	890	863
957	949	955
1044	1026	1029
1108	1108	1110
1384	1383	1365/1378
1441	1441	1441

[a] Vibrational frequencies are identical for (+) and (-)-*trans*, and for (+) and (-)-*cis* adducts, unless otherwise indicated. Frequencies are given in wavenumbers; accuracy ± 2 cm^{-1}.

[b] Refers to the blue-shifted component of the (-)-*cis*- adduct spectra (only observed in duplex samples in water/glycerol matrix).

[c] Splitting of the 579 cm^{-1} band depends on duplexation, solvent matrix, and DNA sequence (see also text).

(curve 8b). No splitting was observed in single stranded samples or in the FLN spectra of the (+)-*trans*- and (-)-*trans-anti* BPDE-dG adducts. It appears that the splitting must reflect how this particular duplex structure influences the conformation of the (-)-*trans* adduct. However, it should be mentioned that this effect cannot be used in a general way to distinguish (-)-*trans* from (+)-*trans* adducts, since splitting was also observed for the (+)-*trans* isomer in a d(...TGG...) (...CCA...) sequence [15].

Comparison of the spectra of the two *cis* adducts reveals that in aqueous buffer matrix the vibrational frequencies are very similar. Most frequencies also agree well with those found for the *cis-anti*-BPDE-dG adducts. Only minor differences were observed in the 575-620 cm^{-1} region. Interestingly, in the 50 % glycerol matrix only the low-energy part of the two *cis* spectra (curves 8c and 8d) are similar. The blue-shifted fraction of the (-)-cis adduct, on the other hand, shows an unusual vibrational pattern, different from that observed in aqueous buffer, different from that of the (+)-*cis* adduct, and also different from that of the free (-)-*cis-anti* BPDE-dG adduct. The latter is illustrated in Figure 3-9, comparing the FLN spectra of the (-)-*cis* adduct in duplex oligonucleotide (curve 9a) and bound to dG only (curve 9b). It is clear that for the (-)-*cis* adduct the addition of glycerol has induced more than just a diminished interaction with the bases. It appears that the effect is caused by a structural change in the saturated ring, having a direct influence on the vibrational properties of the aromatic moiety. Multidimensional NMR studies and/or molecular modelling will be needed to test this hypothesis and to help answering the question why this phenomenon is observed for the (-)-*cis* adduct only.
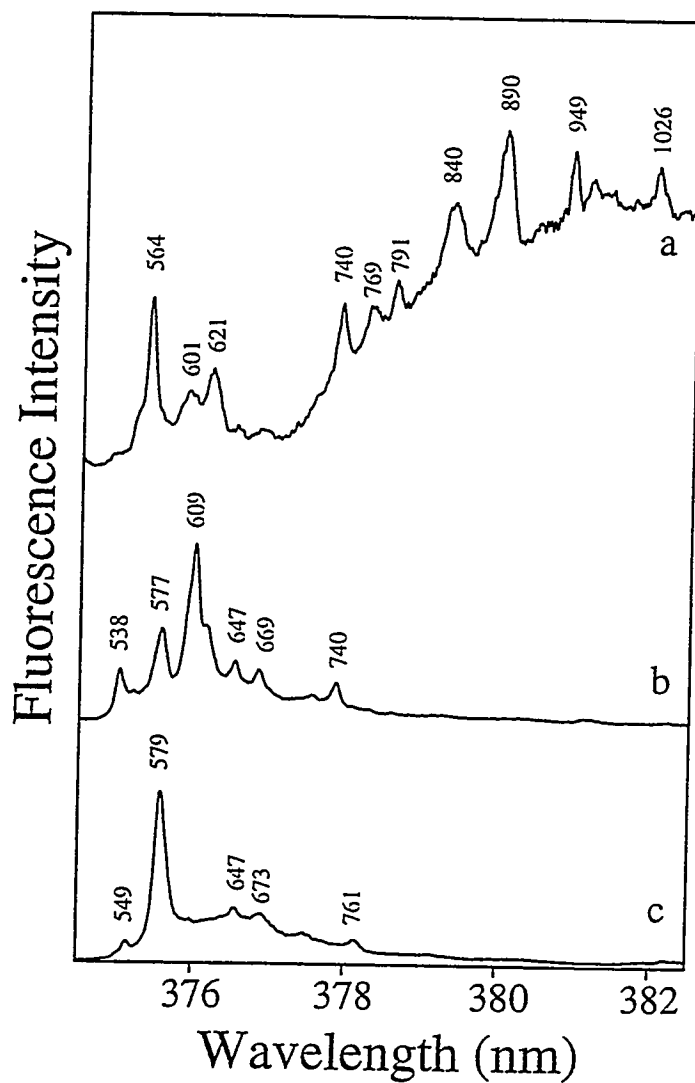
Figure 3-9.   FLN spectra of *anti*-BPDE adducts in 50 % glycerol matrix. Curve a: (-)-*cis* adduct bound to duplex oligonucleotide. Curve b: spectrum of the (-)-*cis* adduct bound to dG only. Curve c: spectrum of the (-)-*trans* adduct bound to dG only. T = 4.2 K, λex = 367.58 nm. Zero-phonon lines are labeled with their excited-state vibrational frequencies (in cm-1).

CONCLUSIONS

The gel electrophoresis experiments of the modified duplex oligonucleotides show that the (+)-*trans* adduct causes a significant retardation, but that the mobility of the other three adducts is similar to that of the unmodified control. On the other hand, the fluorescence data show that the adduct conformation and the extent of solvent exposure are comparable for the two *trans*- and for the two *cis* adducts. For adducted oligonucleotides in double stranded form we conclude that PAGE and fluorescence spectroscopy may be regarded as complementary techniques, the former providing more information on perturbation of the overall helical structure, the latter reflecting the direct environment of the chromophore.

We have demonstrated that using low-temperature fluorescence methods not only major but also minor adduct conformations can be characterized. Compared to room-temperature measurements, e.g. Geacintov et al. [13], the use of cryogenic techniques increases sample stability, reduces spectral broadening, and because of the elimination of quenching processes, all adduct conformations have comparably high fluorescence quantum yields [28]. Another important advantage is that the same techniques can also be employed to study adduct conformations in single stranded oligonucleotides and in whole pieces of intact DNA, in solution or in solid form.

FLN spectroscopy offers additional information on adduct conformations. Based on the extent of electron-phonon coupling one can distinguish between a broad heterogeneous distribution of external, solvent-exposed adducts (as in the case of the (+)-*trans* adduct in aqueous buffer) and a conformation with strong π-π interactions between the chromophore and its microenvironment (as was found for the intercalated *cis* adducts). Furthermore, the vibrational patterns of the FLN spectra are clearly

diffrent, and can be used to distinguish *cis-* from *trans* adducts. However, the FLN technique is often of limited value for distinguishing between (+)- and (-)-*trans*, or (+)- and (-)-*cis* adduct configurations. In principle, however, the FLN method may be capable of distinguishing adducts derived from the binding of enantiomeric diol epoxides to DNA; the configurations of the different OH groups and the orientation of the BPDE-N^2 linkage at chiral binding sites may give rise to different degrees of interactions with neighboring bases, and thus to blue or red shifts in the absorption spectra. However, the vibrational frequencies of the chromophore are usually not affected. An interesting exception to this rule was observed in the case of the (-)-*cis* adduct in 50 % glycerol.

For the (+)-*trans-anti* BPDE-N^2-dG adduct, typically the major stable adduct when DNA is exposed to benzo[*a*]pyrene or BPDE [1,3,40], it was found that the adduct mainly exists in a partially solvent-exposed conformation with little stacking interaction with the bases. These results are, of course, in very good agreement with the solution conformation determined for the same adduct by Cosman et al [20]. However, the sample was not conformationally pure: we also found a minor conformation with a more base-stacked character. The same was observed for the (+)-*trans-anti* BPDE-N^2-dG adduct in oligonucleotide sequences with a 5' guanine neighbor [15].

The data obtained for the (-)-*trans* adduct indicate that the extent of solvent exposure is similar to the major conformation of the (+)-*trans* adduct, but in the case of (-)-*trans* there is only minimal conformational heterogeneity. For this adduct the agreement with the NMR/molecular modelling studies of de los Santos et al. [24] is excellent.

In the case of the (+)-*cis* adduct all spectral evidence indicates an intercalated structure for the major conformation, with only a very minor contribution with a more

solvent-exposed character. Again, these results are in very good agreement with the solution structure reported by Cosman et al [25] and with other spectroscopic studies indicating a base-stacked, internal adduct conformation [13].

For the (-)-*cis* adduct no structure based on NMR data has yet been published. Earlier fluorescence data by Geacintov et al. [13] for this adduct (in a -TGT- sequence) showed a strong red-shift, presumably caused by intercalation. The present results, in particular the strong electron-phonon coupling observed in the FLN spectra and the red-shift of the (0-0) origin band, prove that the (-)-*cis* adduct is indeed intercalated.

In conclusion, we would like to stress that fluorescence techniques cannot be expected to provide the same level of structural detail as two-dimensional NMR studies combined with molecular modelling. Fluorescence-based methods, however, are less time-consuming, require orders of magnitude less material, and are applicable to a wider range of samples, especially larger-sized native DNA molecules. At the same time they do provide very useful structural information including insight on adduct conformations and/or conformational equilibria for adducts with different stereochemistries or for adducts in different base sequence contexts [15]. Such conformational studies could provide important clues as to which factors influence the kinds and frequencies of mutations observed as the result of adduct formation [41,42].

REFERENCES

1. D. H.Phillips, Nature 303 (1983) 468-472.

2. M. R. Osborne and N. T. Crosby, Benzopyrenes. chapters 1-10 (Cambridge University Press, Cambridge, UK,1987).

3. A .H. Conney, Cancer Res. 42 (1982) 4875-4917.

4. E. G. Rogan, P. D. Devanesan, N. V. S. RamaKrishna, S. Higginbotham, N. S. Padmavathi, K. Chapman, E. L. Cavalieri, H. Jeong, R. Jankowiak and G. J. Small, Chem. Res. Toxicol. 6 (1993) 356-363.

5. E. Huberman, L. Sachs, S. K. Yang and H. V. Gelboin, Proc. Natl. Acad. Sci. USA 73 (1976) 607-611.

6. T. Meehan and K. Straub, Nature 277 (1979) 410-412.

7. S. C. Cheng, B. D. Hilton, J. M. Roman and A. Dipple, Chem. Res. Toxicol. 2 (1989) 334-340.

8. R. F. Newbold and P. Brookes, Nature 261 (1976) 52-54.

9. A. W. Wood, R. L. Chang, W. Levin, H. Yagi, D. R. Thakker, D. M. Jerina and A. H. Conney, Biochem. Biophys. Res. Commun.77 (1977) 1389-1396.

10. T. J. Slaga, W. J. Bracken, G. Gleason, W. Levin, H. Yagi, D. M. Jerina and A. H. Conney, Cancer Res. 39 (1979) 67-71.

11. M. K. Buening, P. G. Wislocki, W. Levin, H. Yagi, D. R. Thakker, H. Akagi, M. Koreeda, D. M. Jerina and A. H. Conney, Proc. Natl. Acad. Sci. USA 75 (1978) 5358-5361.

12. P. Brookes and M. R. Osborne, Carcinogenesis 3 (1982) 1223-1226.

13. N. E. Geacintov, M. Cosman, B. Mao, A. Alfano, V. Ibanez and R. G. Harvey, Carcinogenesis 12 (1991) 2099-2108.

14. C. J. Roche, A. M. Jeffrey, B. Mao, A. Alfano, S. K. Kim, V. Ibanez and N. E. Geacintov, Chem. Res. Toxicol. 4 (1991) 311-317.

15. M. Suh, R. Jankowiak, F. Ariese, B. Mao, N. E. Geacintov and G. J. Small, Carcinogenesis (1995) in press.

16. A. Gräslund and B. Jernström, Q. Rev. Biophys. 22 (1989) 1-37.

17. N. E. Geacintov and S. K. Kim, Applications of luminescence techniques in studies of polycyclic carcinogen-nucleic acid interactions. in Practical spectroscopy series vol.12: luminescence techniques on chemical and biochemical analysis, eds. W. R. G. Baeyens, D. De Keukeleire and K. Korkidis (Marcel Dekker, New York, 1991) p.317-338.

18. P. Lu, H. Jeong, R. Jankowiak, G. J. Small, S. K. Kim, M. Cosman and N. E. Geacintov, Chem. Res. Toxicol. 4 (1991) 58-69.

19. G. A. Marsch, R. Jankowiak, M. Suh and G. J. Small, Chem. Res. Toxicol. 7 (1994) 98-109.

20. M. Cosman, C. de los Santos, R. Fiala, B. E. Hingerty, S. B. Singh, V. Ibanez, L. A. Margulis, D. Live, N. E. Geacintov, S. Broyde and D. J. Patel, Proc. Natl. Acad. Sci. USA 89 (1992) 1914-1918.

21. S. B. Singh, B. E. Hingerty, U. C. Singh, J. P. Greenberg, N. E. Geacintov and S. Broyde, Cancer Res. 51 (1991) 3482-3492.

22. M. Cosman, V. Ibanez, N. E. Geacintov and R. G. Harvey, Carcinogenesis 11 (1990) 1667-1672.

23. M. Mao, J. Xu, L. Margulis, S. Smirnov, B. Li, N. Q. Ya and N. E. Geacintov, Carcinogenesis (1995) in press.

24. C. de los Santos, M. Cosman, B. E. Hingerty, V. Ibanez, L. A. Margulis, N. E. Geacintov, S. Broyde and D. J. Patel, Biochemistry 31 (1992) 5245-5252.

25. M. Cosman,, C. de los Santos, R. Fiala, B. E. Hingerty, V. Ibanez, E. Luna, R. G. Harvey, N. E. Geacintov, S. Broyde and D. J. Patel, Biochemistry 32 (1993) 4145-4155.

26. R. Jankowiak and G. J.Small, Chem. Res. Toxicol. 4 (1991) 256-269.

27. R. Jankowiak, P. Lu, G. J. Small and N. E. Geacintov, Chem. Res. Toxicol. 3 (1990) 39-46.

28. R. Zhao, T. Liu, S. K. Kim, M. C. MacLeod and N. E. Geacintov, Carcinogenesis 13 (1992) 1817-1824.

29. N. -Q. Ya, S. Smirnov, M. Cosman, S. Bhanot, V. Ibanez and N. E. Geacintov, in: Structural Biology; The State of the Art. Proceedings of the 8th conversation, R.H.Sarma and M.H.Sarma,Vol.2 (Adenine Press, Schenectady, NY, 1994) p. 349-366.

30. S. Shibutani, L. A. Margulis, N. E. Geacintov and A. P. Grollman, Biochemistry 32 (1993) 7531-7541.

31. M. Eriksson, B. Nordén, B. Jernström and A. Gräslund, Biochemistry 27 (1988) 1213-1221.

32. C. J. Roche, N. E. Geacintov, V. Ibanez and R. G. Harvey, Biophys. Chem. 33 (1989) 277-288.

33. M. E. Hogan, N. Dattagupta and J.P.Whitlock, Jr., J. Biol. Chem. 256 (1981) 4504-4513.

34. B. Mao, Ph.D. thesis, New York University (1993).

35. R. Xu, B. Mao, J. Xu, B. Li, S. Birke, C. E. Swenberg and N. E. Geacintov (1995) To be submitted 12/94

36. P. D. Devanesan, N. V. S. RamaKrishna, R. Todorovic, E. G. Rogan, E. L. Cavalieri, H. Jeong, R. Jankowiak, G. J. Small, Chem. Res. Toxocol. 5 (1992) 302-309.

37. C. A. Angell and E. J. Sare, J. Chem. Phys. 52 (1970) 1058-1068.

38. H. Jeong, Ph.D. thesis, Iowa State University (1991).

39. D. Haarer, J Chem. Phys. 67 (1977) 4076-4085.

40. J. M. Sayer, A. Chadha, S. K. Agarwal, H. J. C. Yeh, H. Yagi and D. M. Jerina, J. Org. Chem. 56 (1991) 20-29.

41. H. Rodriguez and E. L. Loechler, Carcinogenesis 14 (1993) 373-383.

42. H. Rodriguez and E. L. Loechler, Biochemistry 32 (1993) 1759-1769.

CHAPTER 4. FLANKING BASE EFFECTS ON THE STRUCTURAL CONFORMATION OF THE (+)-*TRANS-ANTI* BENZO[*a*]PYRENE DIOLEPOXIDE ADDUCT TO N^2-dG IN SEQUENCE DEFINED OLIGONUCLEOTIDES

M. Suh, R. Jankowiak, F. Ariese, B. Mao, N. E. Geacintov, and G. J. Small

ABSTRACT

Conformations of the *trans*-adduct of (+)-*anti* benzo[*a*]pyrene 7,8-dihydrodiol-9,10-epoxide (BPDE) to N^2-guanine, the major stable DNA-adduct of the environmental carcinogen benzo[*a*]pyrene, were studied as a function of flanking bases in single stranded and in double stranded oligonucleotides. Three 11-mer oligonucleotides d(CTATG$_1$G$_2$G$_3$TATC) were synthesized containing the (+)-*trans-anti* BPDE adduct at one specific guanine of the GGG sequence (a known mutational hot spot). Polyacrylamide gel electrophoresis of the three single stranded oligonucleotides showed that the adduct bound to G$_2$ or G$_3$ (5'-flanking base guanine) causes significantly stronger retardation than the same adduct bound to G$_1$ (5'-flanking base thymine). The strength of the carcinogen-base interactions was reflected in the spectroscopic properties of the pyrenyl moiety. Low temperature fluorescence measurements under line-narrowing (FLN) or non-line narrowing (NLN) conditions showed that in single stranded form the adduct at G$_2$ or G$_3$ (5'-flanking base guanine) adopts a conformation with strong interaction with the bases. This was also observed for the same adduct at the sequence AGA. In contrast, the

(+)-*trans-anti* BPDE adduct with a 5'-flanking thymine exists in a primarily helix-external conformation. Similar differences were observed in the double stranded oligonucleotides: the adducts at G_2 and G_3 were found to exist in similar conformational equilibria, again with significant carcinogen-base interactions , while the adduct at G_1 showed a predominantly external conformation. The nature of the 3'-flanking base appeared to have little influence on the conformational equilibrium of the (+)-*trans-anti* BPDE-guanine adduct. The results could provide insight into the mutational specificity and flanking base effects observed for (+)-*anti* BPDE.

FOOTNOTES

†Abbreviations:

(+)-*anti*-BPDE	(+)-7β,8α-dihydroxy-9α,10α-epoxy-7,8,9,10-tetrahydro-benzo[*a*]pyrene (7R,8S,9S,10R configuration)
NLN	Non-line-narrowed
FLN	Fluorescence line narrowing
PAGE	Polyacrylamide gel electrophoresis
ss	Single stranded
ds	Double stranded

‡ Throughout this paper, deoxynucleotide sequences are listed in the order 5'-...-3'; **bold** typesetting is used to indicate the modified base.

Introduction

Benzo[a]pyrene is a ubiquitous environmental carcinogen which continues to be studied extensively (1-3). Benzo[a]pyrene may be enzymatically activated via one-electron oxidation (4) or monooxygenation pathways. One of the intermediate products of the monooxygenation pathway is the electrophilic and highly reactive metabolite, benzo[a]pyrene diol epoxide (BPDE)[†]. BPDE has been found to bind covalently to DNA (5-7), and this covalent binding is considered to be critical in the initial process of mutagenesis and/or carcinogenesis . The biotransformation of benzo[a]pyrene via the intermediate metabolite (±)-*trans*-7,8-dihydrodiol benzo[a]pyrene results in four stereoisomers; (±)-*anti*-BPDE and (±)-*syn*-BPDE (2,8,9). In mammalian systems, racemic *anti*-BPDE is reported to be more mutagenic than *syn*-BPDE (5,10,11), although the binding rates to DNA are similar (12). Moreover, (+)-*anti*-BPDE is tumorigenic on mouse skin (13) and in new born mouse lung (14,15), while (-)-*anti*-BPDE is not.

It has been suggested that the dramatic differences in carcinogenic potency between closely related stereoisomers must be due to conformational differences (16). Many studies have been devoted to the characterization of BPDE adduct conformations and their effects on biological processes. The opening of the epoxide ring of BPDE can result in *trans*- or *cis* addition; the predominant product is usually the *trans* adduct bound to the exocyclic amino group of guanine (17). It has been demonstrated (18-20) that *trans* and *cis* addition products of (±)-*anti*-BPDE can adopt different conformations in duplex DNA. Also, Geacintov and coworkers (21) showed that the linear dichroism spectra of (+)-*anti*-BPDE adducts depend strongly on the DNA sequence context. Recent NMR studies (22) and theoretical calculations utilizing molecular mechanics methods (23), showed that (+)-*trans*-*anti*-BPDE-N^2-dG in d(CCATCGCTACC) · d(GGTAGCGATGG) duplexes[‡] adopts a helix external conformation with the pyrenyl

residue being situated in the minor groove, pointing towards the 5'-direction of the modified strand. On the other hand, the (-)-*trans-anti*-BPDE-N^2-dG adducts points towards the 3'-direction (24). In addition, recent experiments on the enzymatic digestion of BPDE-modified oligonucleotides by exonucleases indicate that also in single stranded oligonucleotides the (+)-*trans-anti*-BPDE adduct points towards the 5'- end , while in the case of the (-) *trans-anti* adduct it points towards the 3'- end (25), thus paralleling the orientation found in duplexes. One could argue that the adduct conformation in duplex DNA will have an influence on repair efficiency, while the conformation in single strand will more closely resemble the situation during replication. Thus, adduct conformations in both single and double stranded DNA could be important parameters in mutagenesis.

Rodriguez and Loechler found that base sequence plays a role in defining the types of mutations induced by (+)-*anti*-BPDE, and that the nature of the 5'- flanking base next to the guanine undergoing mutation seems to be a key factor (26). The sequences AG, CG, GG showed G→T, G→A and G→C base pairing mutations, while in the sequence TG only G→T mutations were detected. The latter finding was in agreement with other site-specific studies (27) on the major adduct of (+)-*anti*-BPDE formed at N^2-dG in TG sequences, in which G→T mutations were also predominant. Most runs of guanines were found to be mutational hot spots with prevalent frameshift mutations (26). The authors suggested that the sequence context influences adduct conformation, which in turn controls mutagenic specificity. Recently, we have shown that (+)-*anti*-BPDE in binding to the more mutagenically inclined AAGGAA and GAGGAG sequences yielded more internal-type adducts in comparison to other sequences (e.g., CCGG or TGGT) and random sequence DNA (28).

Utilizing high resolution laser-induced fluorescence spectroscopy we have demonstrated in a number of papers (20,28,29), that (±)-*anti*-BPDE adducts can exist in

which the (+)-*trans-anti* BPDE adduct was flanked on the 5'-side by either C, T or A. It will be demonstrated that the 5'-flanking base has a major influence on the conformation(s) of the (+)-*trans-anti*-BPDE-N^2-dG adduct in both ss and ds oligonucleotides.

Materials and methods

Synthesis of BPDE-modified oligodeoxynucleotides

The detailed methods for synthesizing the (+)-*anti*-BPDE modified oligonucleotides using a direct approach (19,31) will be fully described elsewhere (B. Mao et al.; manuscript submitted). The positions of the lesions were established by modified Maxam-Gilbert sequencing procedures (32).

Gel electrophoresis

The oligonucleotide-BPDE adducts and unmodified oligonucleotide were labeled with [γ-^{32}P]ATP purchased from New England Nuclear using T4 polynucleotide kinase from Sigma Inc. 20% native polyacrylamide gel (19:1 acrylamide:bis-acrylamide) in TBE buffer was prepared and used with a 38 cm $\times$ 80 cm Bio-Rad Sequi-Gen Nucleic Acids Sequencing system. The gel was polymerized at ambient temperature, subsequently placed in a cold room (4°C), and incubated in the running buffer (TBE) overnight before the electrophoresis. The labeled oligonucleotide-BPDE adducts were electrophoretically separated for 45 hours at 750 V and $\sim$15 mA; the gel temperature was maintained at 4 ± 1°C throughout the electrophoresis in the cold room. An autoradiogram of the gel was taken at ambient temperature with Kodak XOMAT X-ray films.

Low temperature fluorescence spectroscopy

A detailed description of the apparatus used for FLN and NLN fluorescence spectroscopy is given elsewhere (30). Briefly, the excitation source was a Lambda Physik FL-2002 dye laser (dye solution: DMQ 0.2g/l in dioxane) pumped by a Lambda Physik EMG 102 MSC XeCl excimer laser. For gated detection the output of a reference photodiode triggering an FG-100 high-voltage gate pulse generator was used to define the temporal observation window of a Princeton Instruments IRY 1024/G/B intensified blue-enhanced photodiode array. The detector delay time was set to 45 ns; the gate width was 200 ns. A 1-m focal length McPherson 2016 monochromator was used to disperse the fluorescence. Equipped with a 2400 grooves/mm grating the monochromator provided an 8-nm spectral window with a resolution of ~ 4 cm^{-1}. The broader NLN fluorescence bands were recorded using the same monochromator fitted with a 1200 grooves/mm grating yielding a 19 nm window. NLN spectra were obtained using different excitation wavelengths in order to selectively excite external vs. base-stacked adducts (19). FLN spectra were recorded using many different excitation wavelengths, each revealing a small portion of the S_1 excited state vibrational frequencies. Conformational information can be derived from any single FLN spectrum; typically only one will be shown to illustrate a particular point.

30 µl samples of the oligonucleotide-BPDE adducts dissolved in 20 mM sodium phosphate, 100 mM NaCl, pH 7.0 buffer, were transferred to 2 mm i.d. quartz tubes. "Glass" samples were made by adding an equal volume of glycerol to each aqueous oligonucleotide-BPDE adduct solution. Samples were kept on ice for at least 20 minutes before rapid cooling in liquid helium (for FLN) or liquid nitrogen (for NLN fluorescence spectroscopy). The cryostat was of the double-nested glass type fitted with quartz optical windows.

Results

PAGE of single-stranded BPDE-modified oligonucleotides

Figure 4-1 shows the electrophoretic mobility (in native PAGE) of single stranded d(^{32}P-CTATG$_1$G$_2$G$_3$TATC) oligonucleotides modified by (+)-*trans-anti*-BPDE at different deoxyguanines (dG$_1$-lane 1, dG$_2$-lane 2, dG$_3$-lane 3) and of the unmodified oligonucleotide (lane 4). In agreement with other studies (29,32,33) covalently bound BPDE adducts significantly decrease the electrophoretic mobility of the oligonucleotide strands. However, the three BPDE-modified oligonucleotides show a striking difference in mobility, the adduct covalently bound to dG$_3$ or dG$_2$ causing a significantly greater retardation than the same adduct bound to dG$_1$. A direct interpretation of electrophoretic mobility in terms of sequence-dependent adduct conformation is impossible because in the case of short oligomers the mobility may also depend on the position of the adduct relative to the ends of the strand. Nevertheless, the large differences observed between the dG$_1$ and the dG$_2$, dG$_3$ adducts strongly suggest that the effect may be due to different conformational structures of the DNA-BPDE adducts (see below).

Finally, we would like to mention that the PAGE separation is also an important tool to check sample purity. The autoradiogram in Fig. 4-1 shows the purity of the three adducted oligonucleotides. Overexposure revealed only very minor traces of cross-contamination (ca. 0.1%). Hydrolysis of the adduct into *trans-anti* BP tetraol (which could interfere with the fluorescence measurements) would have yielded the unmodified oligonucleotide, but this was not observed in the overexposed autoradiograms (<0.1%).

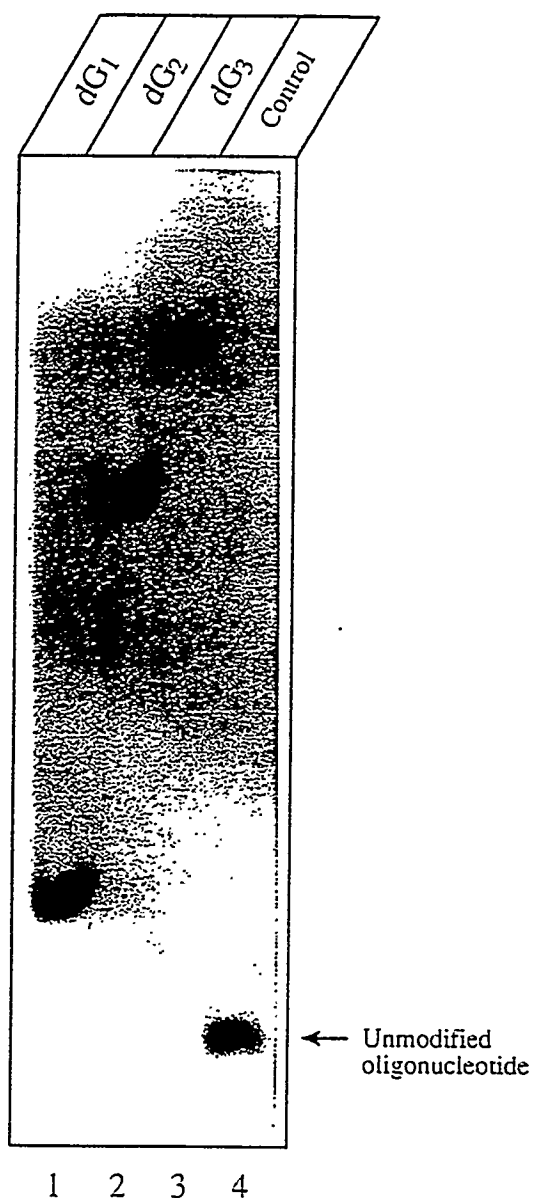Figure 4-1.   Autoradiogram showing electrophoretic mobilities of single stranded d(^{32}P-CTATG$_1$G$_2$G$_3$TATC) oligonucleotides modified by (+)-*trans-anti*-BPDE at dG$_1$ (lane 1; highest mobility), dG$_2$ (lane 2; medium mobility), and dG$_3$ (lane 3; lowest mobility). Lane 4 corresponds to the unmodified oligonucleotide. Conditions: T = 4°C, 20% native polyacrylamide slab gel in TBE buffer.

Cooling rate effects on low temperature fluorescence spectra

Before we describe the non-line-narrowed (NLN) and fluorescence line-narrowed (FLN) spectra of the adducted oligonucleotides, a short discussion of cooling rate dependence is appropriate. During previous low-temperature studies in our laboratory of single-stranded and double-stranded adducted oligonucleotides with relatively high melting temperatures (T_m > 40°C) no cooling rate dependence has been observed [unpublished results]. However, the present study indicated that in the case of adducted oligonucleotides with rather low melting temperatures (T_m < 30°C) the cooling procedure can be a critical parameter for double stranded samples. This is demonstrated in Figure 4-2 showing three FLN spectra of the (+)-*trans-anti*-BPDE adduct at d(...$G_1G_2G_3$...) · d(...CCC...) in aqueous buffer solution. Spectrum a was obtained utilizing fast cooling from approximately 0°C equilibrium; the sample was kept on ice before plunging it into liquid He. An identical spectrum (not shown) was obtained in the case of slow cooling from 0°C, in which case the sample was cooled by helium vapor in the top part of the cryostat before immersion into liquid He. The other spectra of the ds sample were obtained applying slow (curve b) or fast (curve c) cooling to 4.2 K starting from a room temperature (~20°C) equilibrium. The spectra show that slow or fast cooling from 0°C or slow cooling from 20°C led to identical results (compare spectra a and b), whereas fast trapping of a room temperature equilibrium yielded spectra similar to that of the single-stranded oligonucleotide (compare with spectrum d). Thus, we conclude that in case of modified duplexes with low or moderate melting temperatures, one has to utilize slow precooling to 0°C to ensure maximum duplex formation. All fluorescence data presented below were recorded using that procedure.
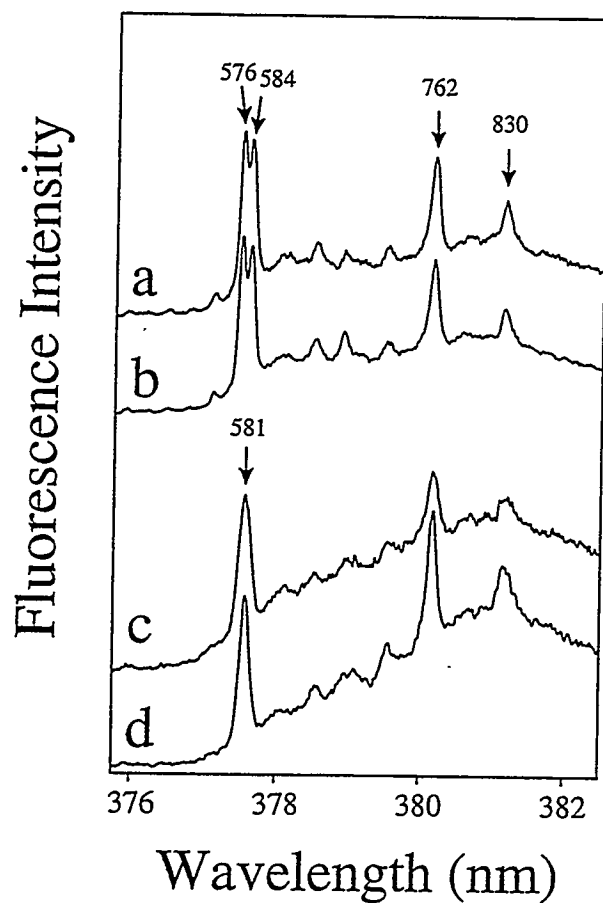
Figure 4-2   Influence of cooling procedure. FLN spectra in aqueous buffer matrix of d(CTATG$_1$G$_2$G$_3$TATC) with the (+)-*trans-anti*-BPDE adduct at dG$_2$ (T = 4.2 K, λ_{ex} = 369.48 nm). Curve a: double stranded, rapidly cooled from 0 °C; curve b: double stranded, slowly cooled from room temperature; curve c: double stranded, rapidly cooled from room temperature; curve d: single stranded sample. Zero-phonon lines are labeled with their excited-state vibrational frequencies.

NLN and FLN spectra of single stranded BPDE-modified oligonucleotides

Figure 4-3 shows NLN fluorescence origin bands (dashed lines, obtained at

T = 77 ; λ_{ex} = 350 nm), and FLN spectra (solid lines, obtained at T = 4.2 K; λ

$_{ex}$ = 365.58 nm). Frames A, B, and C refer to spectra of single-stranded

d(CAATG$_1$G$_2$G$_3$TATC) oligonucleotide in H$_2$O/buffer matrix modified at dG$_1$, dG$_2$, and

dG$_3$, respectively. In single stranded form the major conformation of the BPDE adduct

at dG$_1$, as demonstrated by the NLN spectrum in Fig. 4-3A, shows weaker interactions

with the DNA bases (emission maximum of the 0-0 band ∼ 378 nm) than the other two

oligonucleotides adducted at dG$_2$ and dG$_3$, for which the origin bands are red-shifted to

∼380 nm. High resolution FLN spectra of the (+)-*trans-anti*-BPDE adducts to dG$_2$ and

dG$_3$ are again nearly indistinguishable (frames B and C; solid lines), but very different

from that of the dG$_1$-adduct (frame A, solid line). These data indicate that the adducts

with a guanine as flanking base on the 5¢- side have very similar conformations, assigned

as (+)-3$_s$, in accordance with our previous notation (29). This means that these adducts

show rather strong carcinogen-base stacking interactions even in single stranded form, in

contrast to the (+)-*trans-anti* BPDE adducts in TG$_1$G$_2$ (Figure 4-3A) and in an

oligonucleotide containing a TGT sequence (20), in which the major conformation was

found to be of the external (+)-1$_s$ type.

More detailed FLN/NLN studies of the (+)-*trans-anti* BPDE adduct in the above

mentioned sequences and in other ss oligonucleotides (20, M. Suh et al. in preparation)

revealed that at low temperature often a mixture of conformations is trapped. For

example, selective laser excitation at different wavelengths (data not shown) showed that

in fact the broad NLN spectra in Figure 4-3 (frames A, B, and C; dashed lines) also have

a smaller contribution of a (+)-2$_s$ (partially base-stacked) conformation with an emission

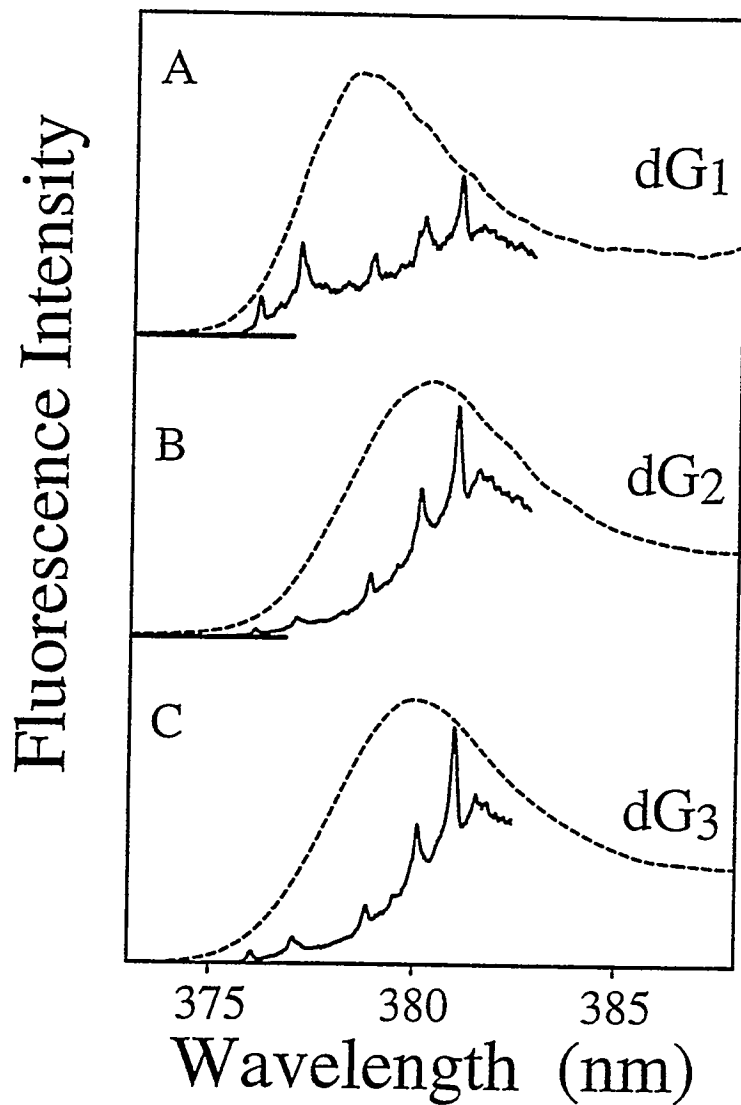maximum around 379 nm. This point can be further illustrated by comparing the FLN

Figure 4-3.   NLN 0-0 fluorescence origin bands (dashed curves; T = 77 K;
λ_{ex} = 350 nm) and FLN spectra (solid curves; T = 4.2 K; λ_{ex} = 365.58 nm) of single stranded d(CTATG$_1$G$_2$G$_3$TATC) oligonucleotides in aqueous buffer with the (+)-*trans-anti*-BPDE adduct at dG$_1$ (frame A), dG$_2$ (frame B), and dG$_3$ (frame C).

spectra in aqueous buffer and 50 % glycerol matrix. Figure 4-4 shows the FLN spectra of $G_1G_2G_3$ (curve a) and TG_1G_2 (curve b) in glycerol/buffer glass . Spectrum b when compared with the corresponding FLN spectrum in H_2O/buffer matrix (solid curve in Figure 4-3A) indicates that glycerol disrupts the carcinogen-base stacking interactions of the $(+)-2_s$ conformation leading to a further blue shift of the origin band $((+)-2_s \rightarrow (+)-1_s$ transformation). This effect is reflected in the spectra by a drastic decrease in the intensity of the emission lines in the 380 nm range whereas the lines in the 377 nm region gained (relative) intensity. In contrast, the adduct at dG_2 (Figure 4-4a), with guanine on its 5'- side, shows only minor differences when compared with the FLN spectrum obtained in aqueous buffer. It appears that the $(+)-3_s$ conformation (with the 0-0 band at ~ 380 nm at low temperature), in which the pyrenyl chromophore has rather strong base stacking interaction, is not very sensitive to the presence of glycerol (34). The same is also observed for the dG_3 adduct (spectra not shown). These data confirm that the $(+)$-*trans-anti*-BPDE adduct to N^2-dG can adopt a $(+)-3_s$ base stacked conformation if the 5'-flanking base is also guanine. In order to establish whether this is also the case when the guanine adduct is flanked by another purine (dA) on the 5'- side, we have studied the d(CTATAGATATC) single stranded oligonucleotide specifically *trans* adducted by $(+)$-*anti*-BPDE at N^2-dG. The fluorescence spectra (not shown here) indicated that also in that sequence the major adduct conformation could be assigned as a $(+)-3_s$ type with strong carcinogen-base stacking interactions.

NLN and FLN spectra of double stranded BPDE-modified oligonucleotides

NLN fluorescence origin bands (dashed curves) and FLN spectra (solid curves) of the $(+)$-*trans-anti*-BPDE adduct covalently bound to dG_1, dG_2, and dG_3 in double stranded oligonucleotides in aqueous buffer matrix are shown in Figure 4-5 in frames A,
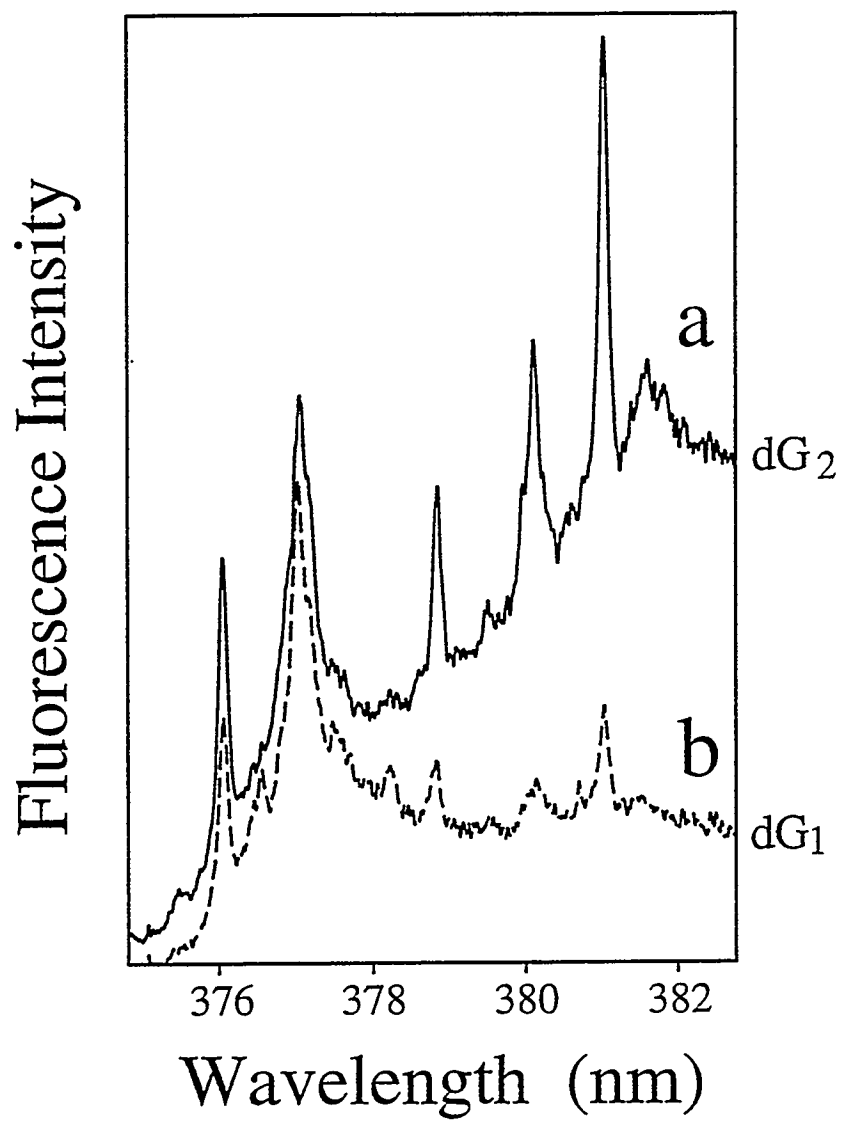
Figure 4-4. FLN spectra (T = 4.2 K, λ_{ex} = 365.58 nm) of single-stranded d(CTATG$_1$G$_2$G$_3$TATC) oligonucleotides in glycerol/aqueous buffer 50:50 matrix with the (+)-*trans-anti*-BPDE adduct at dG$_2$ (curve a), and dG$_1$ (curve b).
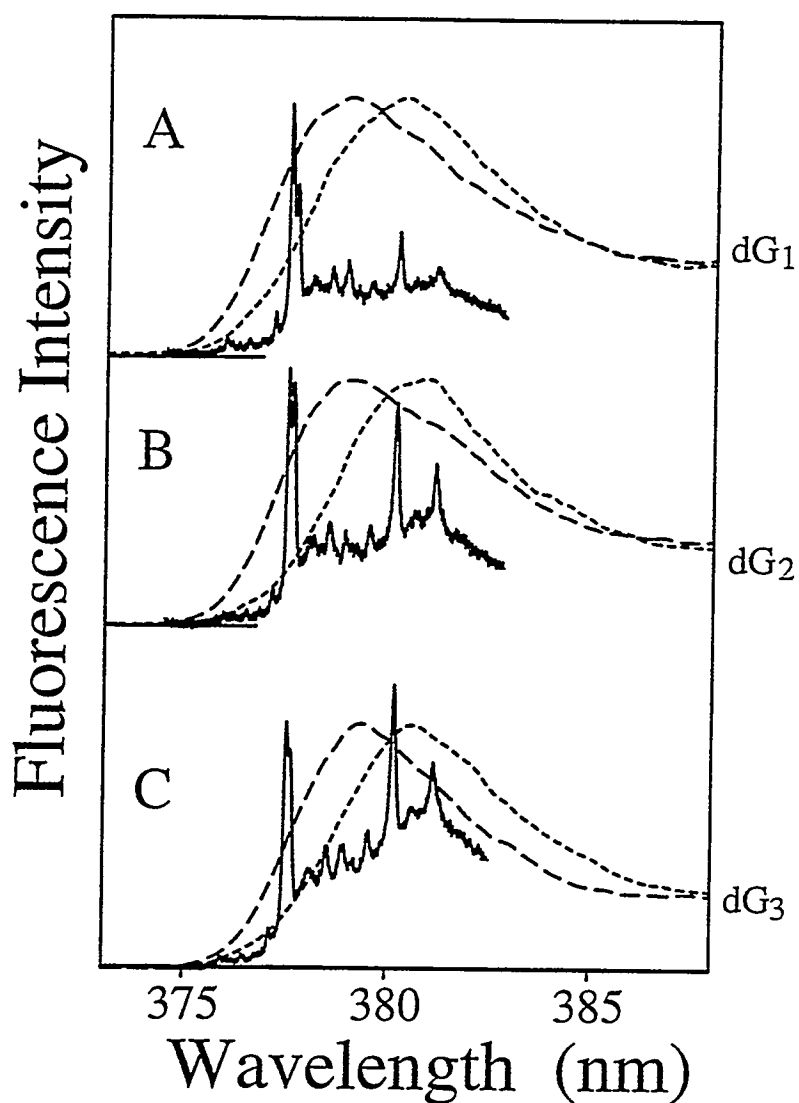
Figure 4-5. FLN and NLN spectra of double stranded d(CTATG₁G₂G₃TATC) oligonucleotides in aqueous buffer matrix. Non-line narrowed 0-0 origin bands obtained for excitation wavelengths of 346 nm (long dashed lines) and 355 nm (short dashed lines). Solid curves represent FLN spectra obtained at T = 4.2 K for λ_{ex} = 369.48 nm. Frames A, B, and C correspond to the (+)-*trans-anti*-BPDE adduct at dG_1, dG_2 and dG_3, respectively.

B, and C, respectively. Long-dashed and short-dashed NLN spectra (normalized) were obtained using excitation at 346 nm and 355 nm, respectively. These wavelengths were chosen based on the absorption spectra presented by Geacintov et al. (19) and provide optimal selectivity for helix-external and base-stacked conformations, respectively. The NLN spectra of all three double stranded oligonucleotides are strongly dependent on excitation wavelength, indicating that the BPDE-adduct exists in a mixture of at least two different conformations. As was the case for the single stranded samples (although the differences are less pronounced) the FLN spectra show that the relative contribution of the base-stacked (+)-3 type adduct is smallest in the $d(...TG_1G_2...) \cdot d(...CCA...)$ duplex (Fig. 4-5A). The FLN spectra obtained for the $d(...G_1G_2G_3...) \cdot d(...CCC...)$ and $d(...G_2G_3T...) \cdot d(...ACC...)$ duplexes, presented in Figs. 4-5B and 5C, show much stronger broadbanded emission around 381 nm, which is typical for a base-stacked (or intercalative) (+)-3 conformation (29).

The above qualitative analysis is supported by the NLN and FLN spectra obtained in 50 % glycerol matrix. Recall, that glycerol may disrupt the weak base-carcinogen interactions of the (+)-2 type conformation, but in the case of strong carcinogen-base interactions the conformational equilibrium should be less sensitive to the presence of glycerol (34). This is demonstrated in Figure 4-6, where we compare the NLN and FLN fluorescence spectra of BPDE-guanine adducts at dG_1 and dG_3. As before, solid lines represent FLN spectra (λ_{ex} = 358.28 nm), while long- and short-dashed lines correspond to NLN fluorescence spectra obtained using 346 nm and 355 nm excitation, respectively. The conformational equilibrium of the adduct at dG_1 is almost entirely shifted to the external (+)-1 type due to the addition of glycerol. The emission maximum has shifted blue and the excitation dependence has decreased considerably compared with the spectra in Fig. 4-5A). The adduct at dG_3 (see Fig. 4-6B) appears to exist in a mixture of (+)-1
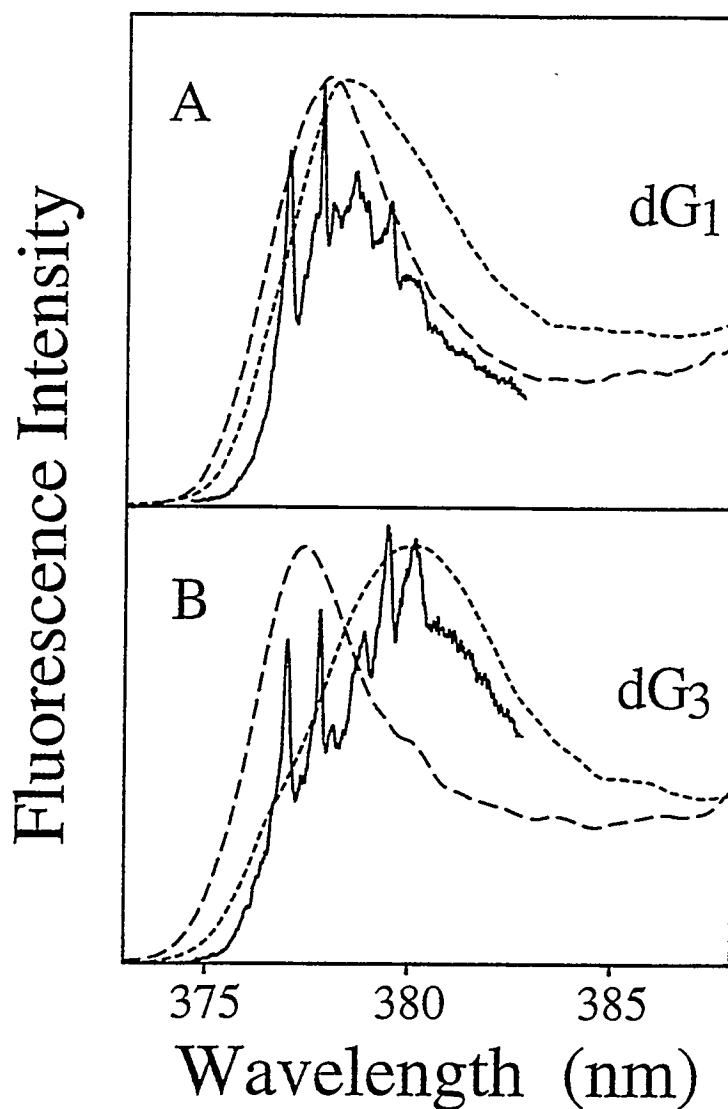
Figure 4-6. FLN and NLN spectra of double stranded d(CTATG$_1$G$_2$G$_3$TATC) oligonucleotides in glycerol/aqueous buffer 50:50 matrix. Non-line narrowed 0-0 origin bands were obtained for excitation wavelengths of 346 nm (long dashed line) and 355 nm (short dashed line). Solid curves represent FLN spectra obtained at T = 4.2 K for λ_{ex} = 358.28 nm. Frames A and B correspond to the (+)-*trans-anti*-BPDE adduct at dG$_1$ and dG$_3$, respectively.

and (+)-3 conformations, preferentially excited at 346 and 355 nm, respectively. The long-dashed spectrum (λ_{exc} = 346 nm) has undergone a strong blue shift compared to Fig. 4-5C, indicating a (+)-2 → (+)-1 transformation, but the relative contribution of the internal (+)-3 type conformation has remained significant in the 50% glycerol matrix, as shown by the short-dashed NLN spectrum and the FLN spectrum of Fig. 4-6B. Spectra obtained for the adduct at dG_2 (not shown) were very similar to those of dG_3; both adducts have a 5'-flanking guanine. These data are consistent with the spectra obtained in aqueous buffer, and demonstrate that also in double stranded oligonucleotides the conformational equilibrium of the (+)-*trans-anti*-BPDE-N^2-dG adduct depends strongly on the nature of the 5' flanking base. If the 5' neighbor is thymine, the major adduct conformation is of the external type. If on the other hand the 5'-flanking base is guanine, the adduct conformation is not purely helix-external but exists in thermal equilibrium with a carcinogen-base stacked conformation. The latter is characterized by strong electron-phonon coupling and a 0-0 fluorescence origin band around 381 nm. These are novel findings, since, until now, strong base stacking interactions were thought to be primarily associated with *cis* adducts of (+)-*anti*-BPDE to dG (19,20,35). At this point we do not know whether the base-stacked conformation of the (+)-*trans-anti* adduct at $G_1G_2G_3$ and G_2G_3T is truly intercalated to the same extent as the above mentioned (+)-*cis-anti* BPDE adduct in double stranded d(...CGC...) · (...GCG...) (35). FLN spectra of the ds (+)-*cis-anti* BPDE-N^2-dG adduct (M. Suh et al.; in preparation) showed stronger coupling and weaker zero-phonon lines than the (+)-*trans* adducts to dG_2 and dG_3, indicating that for the (+)-*cis* adduct the equilibrium is even more strongly dominated by the base-stacked (intercalated) conformation.

More on the 5'- and 3'-flanking base effects

As a final illustration to show that the effect of the 5'-flanking base on the adduct conformation is not limited to one particular sequence, we can compare in Figure 4-7 the FLN spectra of the (+)-*trans-anti*-BPDE adducts in ds samples (Curve a: d(...G_2G_3T...) · d(...ACC...); curve b: d(...$G_1G_2G_3$...) · d(...CCC...); curve c: d(...TG_1G_2...) · d(...CCA...)) with the FLN spectrum obtained for the same adduct (in a different sequence) with neighboring cytosines (curve d: d(...CGC...) · (...GCG...)). Spectra 7a and 7b are nearly identical, and so are spectra 7c and 7d. It appears that in this case the influence of a 5'-flanking cytosine is not very different from that of a 5¢-flanking thymine. At this point we do not know whether this observation can be generalized. Unfortunately, due to the very low melting temperature of the d(CTATAGATATC) · d(GATATCTATAG) oligonucleotide available to us, the conformation of the (+)-*trans-anti* BPDE adduct at N^2-dG with adenine on its 5'-side could not be studied in a well defined duplex structure.

Finally, we would like to illustrate with Figure 4-8 the negligible influence of the 3'-neighbor on the conformational equilibrium of the (+)-*trans-anti* BPDE N^2-dG adduct. The FLN spectra 8a and 8b are nearly indistinguishable and reveal the broad emission around ~381 nm indicating a (+)-3 type base-stacked adduct. Both adducts have the same 5'-neighbor (guanine), but different 3'-flanking bases (thymine in spectrum 8a vs. guanine in spectrum 8b). Similarly, spectra 8c and 8d, obtained for two different oligonucleotides, both with thymine on the 5'-side of the lesion but with different 3'-flanking bases, show very similar spectra indicative of a helix-external (+)-1 conformation. These data confirm that the nature of the 3'-flanking base has little effect on the conformation of this adduct. It will be of interest to see whether or not the diastereomeric (-)-*trans-anti*-BPDE-N^2-dG adduct will show flanking base effects at its

Figure 4-7.   FLN spectra of double stranded (+)-*trans-anti*-BPDE modified oligonucleotides with the following sequences: curve a: d(...G_2G_3T...) · (...ACC...); curve b: d(...$G_1G_2G_3$...) · (...CCC...); curve c: d(...TG_1G_2...) · (...CCA...); curve d: d(...CGC...) · (...GCG...). Aqueous buffer matrix, T = 4.2 K, λ_{ex} = 365.58 nm. Zero-phonon lines are labeled with their excited-state vibrational frequencies.
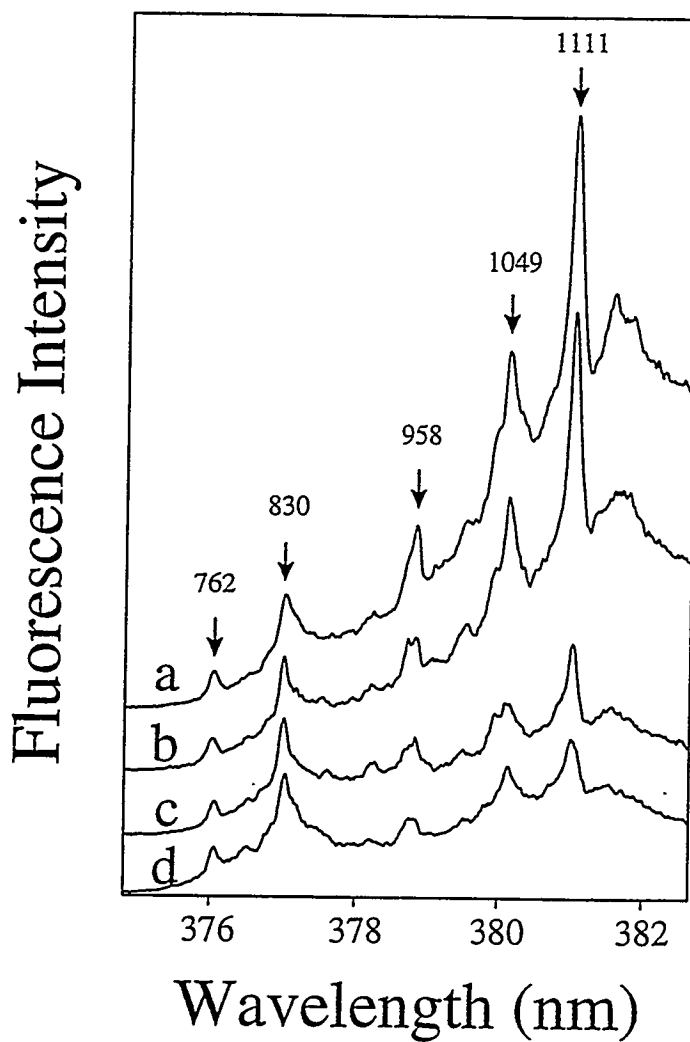
Figure 4-8. FLN spectra of double stranded (+)-*trans-anti*-BPDE modified oligonucleotides with the following sequences: curve a: d(...G_2G_3T...) · (...ACC...); curve b: d(...$G_1G_2G_3$...) · (...CCC...); curve c: d(...TG_1G_2...) · (...CCA...); curve d: d(...TGT...) · (...ACA...). Aqueous buffer matrix, T = 4.2 K, λ_{ex} = 356.78 nm. Zero-phonon lines are labeled with their excited-state vibrational frequencies.
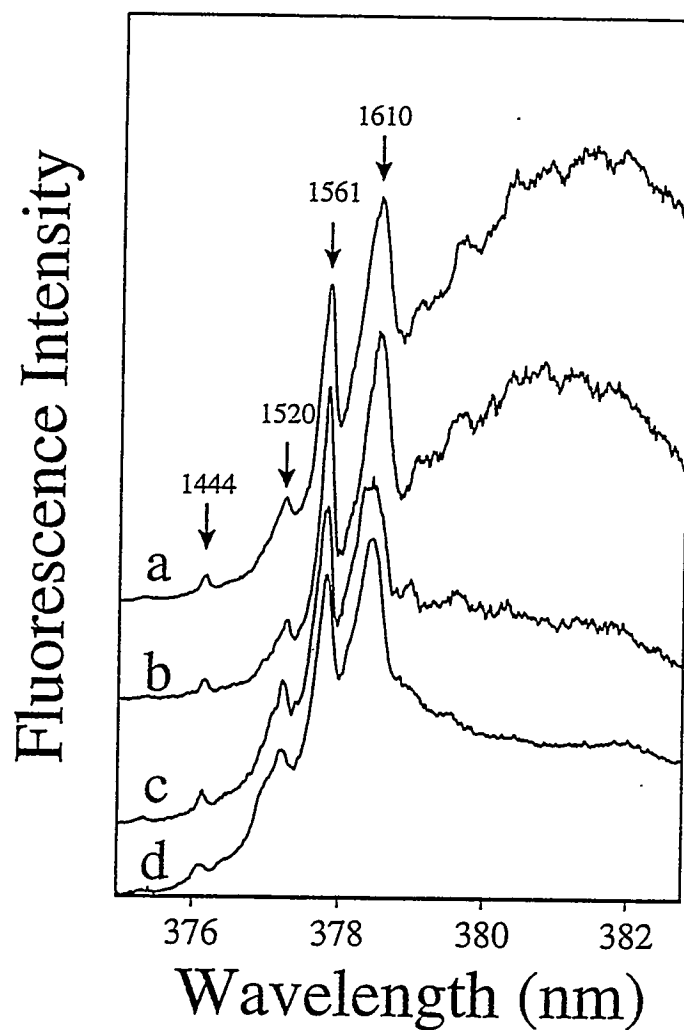
3'-side, since this adduct has been shown to adopt a conformation in which the pyrenyl moiety is pointing towards the 3'-end of the adducted strand (24).

Discussion

As shown by Jankowiak et al (29) and Marsch et al. (28), low-temperature fluorescence techniques are particularly well suited to study adduct conformations, especially if the available amounts are limited. We have shown that not only may the presence of different adduct conformations be revealed, but also that different solvents (e.g., glycerol) may shift the equilibrium, providing more insight into the relative stability of conformations and into conformational heterogeneity.

In this paper, the adduct conformations of (+)-*trans-anti*-BPDE-N^2-dG in different sequence defined oligonucleotides were investigated using FLN and NLN fluorescence spectroscopy. The GGG sequence was selected because runs of guanines appear to be frequently mutated (36,37). The results indicate that the adduct can adopt at least three different conformations both in ss and in ds oligonucleotides. This is in agreement with our previous studies of (±)-*anti*-BPDE adducts in DNA and in different oligonucleotides (20,29). The adduct conformation is strongly influenced by the sequence context. For the (+)-*trans-anti*-BPDE adduct, depending on the 5'-flanking base, the major adduct conformation formed in single stranded DNA is either primarily (+)1$_S$ external for TG, or a mixture of external and (+)3$_S$ base stacked conformations for GG (and AG). Similar flanking base effects were observed in double stranded oligonucleotides.

Most adduct conformations discussed in this paper are very heterogeneous. At room temperature they will be in dynamic thermal equilibrium, which may be either fast or slow. If the thermal equilibrium is fast, as is the case for the (+)-*trans-anti*-BPDE

adduct in the d(...CGC...) · d(...GCG...) duplex, room temperature ^{1}H-NMR studies will reveal only an average structure (22). In contrast, two conformations could be observed for the same adduct in the same oligonucleotide when using low-temperature fluorescence spectroscopy (M. Suh et al.; in preparation). Note that the observation of two or more distinct conformations after cooling to cryogenic temperatures must indicate that these conformations are part of the room-temperature distribution. The conformational equilibrium trapped at low temperature must reflect the major (but not necessarily all) of the conformations that are relevant (thermally accessible) in solution (30). Thus, selective (laser-based) low temperature fluorescence spectroscopy can be very helpful in characterizing adduct conformations which do exist at ambient temperatures, but cannot be readily observed in solution due to various broadening and/or quenching phenomena. In this respect it is important to note that at low temperature external and intercalated BPDE-N^2-dG adducts have similar fluorescence quantum yields, while at room temperature the intercalated adducts may easily escape detection as the result of more efficient quenching (3,19).

The sequence specificity of mutations is in principle attributed to the sequence specific binding, DNA repair and mutagenic translesional synthesis during DNA replication. High mutational frequency by (±)-*anti*-BPDE observed in runs of guanine sequence (36,37) is in agreement with high binding preference of BPDE to guanine bases which have flanking guanines(38,39). However, some discrepancies were also reported. Mazur showed (36) that no mutation occured at some runs of guanines in *aprt* gene treated with (±)-*anti*-BPDE despite the high binding preference at those sites(38). Also prevalent mutations were observed at runs of guanines flanked by adenines notwithstanding the fact that these sites are less prefered binding sites(38,39). Therefore, it is believed that the sequence specificity of the BPDE-indiced mutation depends also on

the biological processing of the lesion site which in turn affected by the conformation of the bound BPDE.

Multiple conformations for a single adduct were also proposed by Loechler and coworkers (40,41), who showed that heating (at 80° C for 10 min) of the (+)-*anti*-BPDE-adducted plasmid PUB3 prior to transformation resulted in different mutations at the particular guanines compared to the unheated control. Our data support their findings, since they indicate that a mixture of adduct conformations can exist. Heating could cause a redistribution of the conformational equilibrium if the energy barriers are relatively high. Also strong sequence-dependent polymorphism in adduct-induced DNA structure with N-2-acetylaminofluorene residue bound to C8-G of the DNA has been reported(42,43). Authors have proposed that the polymorphism plays a major role in the sequence specific responses observed when these regions are processed *in vivo*. This aspect of adduct heterogeneity deserves further study.

At this point we would like to mention that Rodriguez and Loechler (26) found that (+)-*anti*-BPDE induced many mutations, in particular frame-shifts, in sequences with runs of guanines. Thus, tentatively, as a working hypothesis, we suggest that this type of mutation could be induced by carcinogen-base stacked conformations. It was also demonstrated (26) that the specificity of mutagenic activity at a particular guanine residue can be influenced by the base on its immediate 5¢-side; in TG sequences mutations were almost exclusively restricted to G→T. This could be related to the predominantly helix-external adduct conformation. Also relevant are our recently obtained (unpublished) results on DNA adducts from mouse skin treated with benzo[*a*]pyrene, in which (+)-*trans-anti*-BPDE seemed to exist as a mixture of external and internal conformations. We believe that identification of sequence-dependent adduct conformation(s) and study of their repair efficiency in relation to the DNA conformation (i.e., external vs. internal vs.

apurinic site) will be essential to a better understanding of mutagenesis and/or carcinogenesis.

Acknowledgment

References

1. Phillips,D.H. (1983) Fifty years of benzo[a]pyrene. *Nature* **303**, 468-472.

2. Osborne,M.R. and Crosby,N.T. (1987) *Benzopyrenes*. Cambridge University Press, Cambridge, UK (chapters 1-10).

3. Gräslund,A. and Jernström,B. (1989) DNA-carcinogen interaction: covalent DNA adducts of benzo(a)pyrene 7,8 dihydrodiol 9,10 epoxides studied by biochemical and biophysical techniques. *Q. Rev. Biophys.* **22**, 1-37.

4.   Rogan,E.G., Devanesan,P.D., RamaKrishna,N.V.S., Higginbotham,S., Padmavathi,N.S., Chapman,K., Cavalieri,E.L., Jeong,H., Jankowiak,R., and Small,G.J. (1993) Identification and quantitation of benzo[a]pyrene-DNA adducts formed in mouse skin. *Chem. Res. Toxicol.* **6**, 356-363.

5.   Huberman,E., Sachs,L., Yang,S.K., and Gelboin,H.V. (1976) Identification of mutagenic metabolites of benzo[a]pyrene in mammalian cells. *Proc. Natl. Acad. Sci. USA* **73**, 607-611.

6.   Harvey,R.G. (1981) Activated metabolites of carcinogenic hydrocarbons. *Acc. Chem. Res.* **14**, 218-226.

7.   Conney,A.H. (1982) Induction of microsomal enzymes by foreign chemicals and carcinogenesis by polycyclic aromatic compounds. *Cancer Res.* **42**, 4875-4917.

8.   Yang,S.K., McCourt,D.W., Roller,P.P., and Gelboin,H.V. (1976) Enzymatic conversion of benzo[*a*]pyrene leading predominantly to the diol-epoxide *r*-7,*t*-8-dihydroxy-*t*-9,10-oxy-7,8,9,10-tetrahydrobenzo[*a*]pyrene through a single enantiomer of *r*-7,*t*-8-dihydroxy-7,8-dihydrobenzo[*a*]pyrene. *Proc. Natl. Acad. Sci. USA* **73**, 2594-2598.

9.   Thakker,D.R., Yagi,H., Akagi,H., Koreeda,M., Lu,A.Y.H., Levin,W., Wood,A.W., Conney,A.H. and Jerina,D.M. (1977) Metabolism of benzo[*a*]pyrene VI. Stereoselective metabolism of benzo[*a*]pyrene and benzo[*a*]pyrene 7,8-dihydrodiol to diol epoxides. *Chem.-Biol. Interactions* **16**, 281-300.

10. Newbold,R.F.and Brookes,P. (1976) Exceptional mutagenicity of a benzo[*a*]pyrene diol epoxide in cultured mammalian cells. *Nature* **261**, 52-54.

11. Wood,A.W., Chang,R.L., Levin,W., Yagi,H., Thakker,D.R., Jerina,D.M, and Conney,A.H. (1977) Differences in mutagenicity of the optical enantiomers of the diastereomeric benzo[a]pyrene 7,8-diol-9,10-epoxides. *Biochem. Biophys. Res. Commun.* **77**, 1389-1396.

12. Pelling,J.C. and Slaga,T.J. (1982) Comparison of levels of benzo[a]pyrene diol epoxide diastereomers covalently bound *in vivo* to macromolecular components of the whole epidermis *versus* the basal layer. *Carcinogenesis* **3**, 1135-1141.

13. Slaga,T.J., Bracken,W.J., Gleason,G., Levin,W., Yagi,H., Jerina,D.M., and Conney,A.H. (1979) Marked differences in the skin tumor-initiating activities of the optical enatiomers of the diastereomeric benzo(*a*)pyrene 7,8-diol-9,10-epoxides. *Cancer Res.* **39**, 67-71.

14. Kapitulnik,J., Wislocki,P.G., Levin,W., Yagi,H., Thakker,D.R., Akagi,H., Koreeda,M., Jerina,D.M. and Conney,A.H. (1978) Marked differences in the carcinogenic activity of optically pure (+)- and (-)-trans-7,8-dihydroxy-7,8-dihydrobenzo(*a*)pyrene in newborn mice. *Cancer Res.* **38**, 2661-2665.

15. Buening,M.K., Wislocki,P.G., Levin,W., Yagi,H., Thakker,D.R., Akagi,H., Koreeda,M., Jerina,D.M., and Conney,A.H. (1978) Tumorigenicity of the optical enantiomers of the diastereomeric benzo[*a*]pyrene 7,8-diol-9,10-epoxides in newborn mice: Exceptional activity of (+)-7β,8α-dihydroxy-9α,10α-epoxy-7,8,9,10-tetrahydrobenzo[*a*]pyrene. *Proc. Natl. Acad. Sci. USA* **75**, 5358-5361.

16. Brookes,P and Osborne,M.R. (1982) Mutation in mammalian cells by stereoisomers of *anti*-benzo[*a*]pyrene-diolepoxide in relation to the extent and nature of the DNA reaction products. *Carcinogenesis* **3**, 1223-1226.

17. Cheng,S.C., Hilton,B.D., Roman,J.M., and Dipple,A. (1989) DNA adducts from carcinogenic and noncarcinogenic enantiomers of benzo[*a*]pyrene dihydrodiol epoxide. *Chem. Res. Toxicol.* **2**, 334-340.

18. Undeman,O., Lycksell,P.-O., Gräslund,A., Astlind,T., Ehrenberg,A., Jernström,B., Tjerneld,F., and Nordén,B. (1983) Covalent complexes of DNA and two stereoisomers of benzo(*a*)pyrene 7,8-dihydrodiol-9,10-epoxide studied by fluorescence and linear dichroism. *Cancer Res.* **43**, 1851-1860.

19. Geacintov,N.E., Cosman,M., Mao,B., Alfano,A., Ibanez,V., and Harvey,R.G. (1991) Spectroscopic characteristics and site I/site II classification of *cis* and *trans* benzo[*a*]pyrene diolepoxide enantiomer-guanosine adducts in oligonucleotides and polynucleotides. *Carcinogenesis* **12**, 2099-2108.

20. Lu,P., Jeong,H., Jankowiak,R., Small,G.J., Kim,S.K., Cosman,M., and Geacintov,N.E. (1991) Comparative laser spectroscopic study of DNA and polynucleotide adducts from the (+)-*anti*-diol epoxide of benzo[*a*]pyrene. *Chem. Res. Toxicol.* **4**, 58-69.

21. Roche,C.J., Jeffrey,A.M., Mao,B., Alfano,A., Kim,S.K., Ibanez,V., and Geacintov,N.E. (1991) Dependence of conformations of benzo[a]pyrene diol epoxide-DNA adducts derived from stereoisomers of different tumorigenicities on base sequence. *Chem. Res. Toxicol.* **4**, 311-317.

22. Cosman,M., de los Santos,C., Fiala,R., Hingerty,B.E., Singh,S.B., Ibanez,V., Margulis,L.A., Live,D., Geacintov,N.E, Broyde,S., and Patel,D.J. (1992) Solution conformation of the major adduct between the carcinogen (+)-*anti*-benzo[a]pyrene diol epoxide and DNA. *Proc. Natl. Acad. Sci. USA* **89**, 1914-1918.

23. Singh,S.B., Hingerty,B.E., Singh,U.C., Greenberg,J.P., Geacintov,N.E., and Broyde,S. (1991) Structures of the (+)- and (-)- *trans*-7,8-dihydroxy-*anti*-9,10-epoxy-7,8,9,10-tetrahydrobenzo(a)pyrene adducts to guanine-N^2 in a duplex dodecamer. *Cancer Res.* **51**, 3482-3492.

24. de los Santos,C., Cosman,M., Hingerty,B.E., Ibanez,V., Margulis,L.A., Geacintov,N.E., Broyde,S., and Patel,D.J. (1992) Influence of benzo[a]pyrene diol epoxide chirality on solution conformations of DNA covalent adducts: the (-)-*trans-anti*-[BP]G·C adduct structure and comparison with the (+)-*trans-anti*-[BP]G·C enantiomer. *Biochemistry* **31**, 5245-5252.

25. Mao,B., Li,B., Amin,S., Cosman,M., and Geacintov,N.E. (1993) Opposite stereoselective resistance to digestion by phosphodiesterases I and II of benzo[a]pyrene diol epoxide-modified oligonucleotide adducts. *Biochemistry* **32**, 11785-11793.

26. Rodriguez,H. and Loechler,E.L. (1993) Mutational specificity of the (+)-*anti*-diol epoxide of benzo[a]pyrene in a *supF* gene of an *Escherichia coli* plasmid: DNA sequence context influences hotspots, mutagenic specificity and the extent of SOS enhancement of mutagenesis. *Carcinogenesis* **14**, 373-383.

27. Mackay,W., Benasutti,M., Drouin,E., and Loechler,E.L. (1992) Mutagenesis by (+)-*anti*-B[a]P-N^2-Gua, the major adduct of activated benzo[a]pyrene, when studied in an *Escherichia coli* plasmid using site-directed methods. *Carcinogenesis* **13**, 1415-1425.

28. Marsch,G.A., Jankowiak,R., Suh,M., and Small,G.J. (1994) Sequence dependence of benzo[a]pyrene diol epoxide-DNA adduct conformer distribution: a study by laser-induced fluorescence/polyacrylamide gel electrophoresis. *Chem. Res. Toxicol.* **7**, 98-109.

29. Jankowiak,R., Lu,P., Small,G.J., and Geacintov,N.E. (1990) Laser spectroscopic studies of DNA adduct structure types from enantiomeric diol epoxides of benzo[a]pyrene. *Chem. Res. Toxicol.* **3**, 39-46.

30. Jankowiak,R. and Small,G.J. (1991) Fluorescence line narrowing: a high-resolution window on DNA and protein damage from chemical carcinogens. *Chem. Res. Toxicol.* **4**, 256-269.

31. Cosman,M., Ibanez,V., Geacintov,N.E., and Harvey,R.G. (1990) Preparation and isolation of adducts in high yield derived from the binding of two benzo[a]pyrene-7,8-dihydroxy-9,10-oxide stereoisomers to the oligonucleotide d(ATATGTATA). *Carcinogenesis* **11**, 1667-1672.

32. Mao,B., Margulis,L.A., Li,B., Ibanez,V., Lee,H., Harvey,R.G., and Geacintov,N.E. (1992) Direct synthesis and identification of benzo[a]pyrene diol epoxide-deoxyguanosine binding sites in modified oligonucleotides. *Chem. Res. Toxicol.* **5**, 773-778.

33. Hogan,M.E., Dattagupta,N., and Whitlock,J.P., jr. (1981) Carcinogen-induced alteration of DNA structure. *J. Biol. Chem.* **256**, 4504-4513.

34. Jeong,H. (1991) *High resolution fluorescence studies of metabolic pathways of DNA and oligonucleotide adducts from polycyclic aromatic compounds.* Dissertation, Iowa State University.

35. Cosman,M., de los Santos,C., Fiala,R., Hingerty,B.E., Ibanez,V., Luna,E., Harvey,R.G., Geacintov,N.E, Broyde,S., and Patel,D.J. (1993) Solution conformation of the (+)-*cis-anti*-[BP]dG adduct in a DNA duplex: intercalation of the covalently attached benzo[a]pyrenyl ring into the helix and displacement of the modified deoxyguanosine. *Biochemistry* **32**, 4145-4155.

36. Mazur,M. and Glickman,B.W. (1988) Sequence specificity of mutations induced by benzo[a]pyrene-7,8-diol-9,10-epoxide at endogenous *aprt* gene in CHO cells. *Som. Cell Mol. Genet.* **14**,393-400.

37. Yang,J., Maher,V.M. and McCormick J.J. (1987) Kinds of mutations formed when a shuttle vector containing adducts of (±)-7β,8α-dihydroxy-9α,10α-epoxy-7,8,9,10-tetrahydrobenzo[a]pyrene replicates in human cells. *Proc. Natl. Acad. Sci. USA* **84**, 3789-3791.

38.   Boles,C.T. and Hogan,M.E. (1986) High-resolution mapping of carcinogen binding sites on DNA. *Biochemistry* **25**, 3039-3043.

39.   Schwartz,J.J., Lau,H.H.S. and Baird,W.M. (1994) Base sequence selectivity in the binding of 7(R),8(S)-dihydroxy-9(S),10(R)-epoxy-7,8,9,10-tetrahydrobenzo[a]pyrene to oligodeoxyribonucleotide duplexes. *Chem. Res. Toxicol.* **7**, 29-40.

40.   Rodriguez,H. and Loechler,E.L. (1993) Mutagenesis by the (+)-*anti*-diol epoxide of benzo[a]pyrene: what controls mutagenic specificity? *Biochemistry* **32**, 1759-1769.

41.   Drouin,E. and Loechler,E.L. (1993) AP sites are not significantly involved in mutagenesis by the (+)-*anti* diol epoxide of benzo[a]pyrene: the complexity of its mutagenic specificity is likely to arise from adduct conformational polymorphism. *Biochemistry* **32**, 6555-6562.

42.   Belguise-Valladier,P. and Fuchs,R.P.P. (1991) Strong sequence-dependent polymorphism in adduct-induced DNA structure: analysis of single N-2-acetylaminofluorene residues bound within the *Nar*I mutation hot spot. *Biochemistry* **30**, 10091-10100.

43.   Veaute,X. and Fuchs,R.P.P. (1991) Polymorphism in N-2-acetylaminofluorene induced DNA structure as revealed by DNase I footprinting. *Nucleic Acids Res.* **19**, 5603-5606.

CHAPTER 5. FORMATION AND PERSISTENCE OF BENZO[*a*]PYRENE-DNA ADDUCTS IN MOUSE EPIDERMIS *IN VIVO* : IMPORTANCE OF ADDUCT CONFORMATION

M. Suh, F. Ariese, G. J. Small and R. Jankowiak

A. Hewer and D. H. Phillips

ABSTRACT

The formation and repair of benzo[*a*]pyrene diol epoxide-N^2-deoxyguanosine adducts (BPDE-N^2-dG) in DNA isolated from the skin of mice treated topically with benzo[*a*]pyrene (BP) was studied by ^{32}P-postlabeling and by low-temperature fluorescence spectroscopy under low resolution and under high resolution fluorescence line narrowing (FLN) conditions. In agreement with earlier studies, total BP-DNA binding reached a maximum at 24 hours after treatment (dose: 1µmol/mouse), then declined rapidly until 4 days after treatment and much more slowly thereafter. An HPLC method was developed which resolved the ^{32}P-postlabeled (-)-*trans*- from (-)-*cis-anti*-BPDE-N^2-dG, and (+)-*trans*-from (+)-*cis-anti*-BPDE-N^2-dG. HPLC analysis of the major TLC adduct spot (containing >80% of the total adducts) obtained by postlabeling BP-modified mouse skin DNA showed that it consisted of a major component that coeluted with (-)-*cis*-/(+)-*trans-anti*-BPDE-N^2-dG, and a minor component that coeluted with (-)-*trans*-/(+)-*cis-anti*-BPDE-N^2-dG, and that the minor component was repaired at

a slower rate than the major component. Low-temperature fluorescence spectroscopy of the intact DNA identified the major adduct as (+)-*trans-anti*-BPDE-N²-dG, and the minor adduct fraction consisted mainly of (+)-*cis-anti*-BPDE-N²-dG. In agreement with the ³²P-postlabeling results it was observed by fluorescence spectroscopy that the (+)-*cis*-adducts were repaired more slowly than most other adducts. Moreover, the (+)-*trans*-adducts exhibited a broad distribution of base-stacked, partially base-stacked, and helix-external conformations. Mouse skin DNA samples obtained at early timepoints (2 to 8 hrs) after treatment with BP contained substantially more of the 'external' adducts, while samples at later timepoints (24 to 48 hrs) contained relatively more adducts in the base-stacked conformation, indicating also that the latter adducts are repaired less readily than the former. The possible biological significance of these novel observations of conformation-dependent rates of DNA adduct repair, and their possible dependence on DNA sequence, are discussed.

INTRODUCTION

Benzo[*a*]pyrene (BP) is a potent environmental carcinogen. In biological systems, it can be activated enzymatically to the electrophilic metabolite 7,8-dihydroxy-9,10-epoxy-7,8,9,10-tetrahydrobenzo[*a*]pyrene (BPDE) (1,2). The enzymatic transformation of BP to BPDE results in many stereoisomeric BPDEs, of which (+)-*anti*-BPDE ((+)-7β,8α-dihydroxy-9α,10α-epoxy-7,8,9,10-tetrahydrobenzo[*a*]pyrene) is known to be the most mutagenic and tumorigenic in mammalian cells (3-5). *anti*-BPDE forms adducts primarily with the N² -exocyclic amino group of guanine moieties in DNA via either *trans* or *cis* opening of the BPDE epoxide ring (6,7). The covalent binding of BPDE to cellular DNA is believed to be an early event in BP carcinogenesis (8,9).

In order to understand the role of BPDE adduct structures in carcinogenesis, many studies have been carried out with stereochemically pure *anti*-BPDE adducts. Recently, the conformational structures of stereochemically well defined *anti*-BPDE adducts contained in oligonucleotides were characterized by high resolution NMR spectroscopy (10-13), by low-temperature fluorescence spectroscopy (14), optical spectroscopy and thermal stability (15) and fluorescence life time measurements (16). It is conceivable that the conformation of BPDE-DNA adducts is important in determining the biological consequences of BPDE binding to DNA including mutagenesis, and in determining the reparability of BPDE lesions. Different inhibitory effects on DNA and RNA polymerase activities were reported depending on the stereochemical properties of enantiomeric *anti*-BPDE adducts *in vitro* (17-19). Recently, Loechler *et al.* reported that BPDE adduct conformation is a key factor controlling the types of mutation at the lesion site (20). Moreover, BPDE adducts with a given stereochemistry can adopt various conformations depending on the base sequence at the lesion site (14), which in turn results in sequence-specific mutations (21). However, despite the numerous studies on BP or BPDE binding and removal in mouse skin, cells and organ cultures (22-25), there have been no reports characterizing the conformations of DNA adducts formed *in vivo* as a function of the time passed since exposure.

Conventional (26) and laser induced fluorescence (LIF) spectroscopy (27) at cryogenic temperatures can be used for the analysis of DNA damage by PAHs *in vitro* and *in vivo*. For BPDE adducts, the present limit of detection of its pyrene chromophore by fluorescence line-narrowing (FLN) is ≤ 1 adducted base pair per 10^8 base pairs in 100 µg of DNA. For example, FLN spectral analysis of human hemoglobin was used to determine the structure of the major human globin adduct formed *in vivo* from BP (27). FLN spectroscopy can be used to assign adduct stereochemistry and/or adduct

conformation (28), for instance as a function of base sequence (21). We have demonstrated using line-narrowing ($S_1 \leftarrow S_0$ laser excitation at 4.2 K) and non-line-narrowing conditions (NLN; $S_2 \leftarrow S_0$ laser excitation at 77 K) that (±)-*anti*-BPDE adducts can exist in helix-external, partially base-stacked, or base-stacked (intercalated) conformations (28). Based on the extent of the red shift observed for the origin band of the pyrenyl fluorescence spectrum, these three conformations are denoted as (±)-1, (±)-2 and (±)-3, respectively, where the sign indicates whether the adduct is derived from (+)- or from (-)-*anti*-BPDE (28).

In this paper, we present data on the formation and repair of stable BPDE-N^2-dG adducts in DNA in mouse skin, following topical treatment with BP using ^{32}P-postlabeling, HPLC, and laser induced fluorescence techniques. We have found that the rates of repair are different for helix-external and internal adducts. To the best of our knowledge this is the first report indicating that the rate of BPDE-DNA adduct repair may be conformation dependent.

MATERIALS AND METHODS

Chemicals

Benzo[*a*]pyrene (purity >99 %) was purchased from the Community Bureau of Reference (Brussels, Belgium). Polyethyleneimine-cellulose (PEI-cellulose) TLC sheets were manufactured by Macherey-Nagel and supplied by Camlab (Cambridge, U.K.). HPLC grade methanol was purchased from BDH Ltd. (Poole, Dorset, U.K.), and Zorbax phenyl-modified reversed- phase columns were obtained from Hichrom (Reading, U.K.). Samples were filtered prior to HPLC separation using 0.45 μm filters

obtained from Millipore-Waters, Milford, MA. BPDE-N^2-dG standards were obtained by digesting stereochemically pure BPDE-modified oligonucleotides, generously provided by Dr. N. E. Geacintov (New York University, Department of Chemistry). Details of the synthesis of (±)-*anti*-BPDE-modified oligonucleotides using a direct approach (29) are given in reference (30).

Topical Treatment of Mice

Groups of 4 male Parkes mice (6-8 weeks old) purchased from the MRC National Institute for Medical Research (Mill Hill, London, U.K.) were treated with BP; 1 μmol in 150 μl acetone per mouse was applied to shaved areas of their backs. Control animals received acetone only. Groups of four animals were killed by cervical dislocation at different timepoints after treatment (1 hr-7 days). Treated areas of the skin were removed and frozen.

DNA Isolation

The dermal surface of the frozen skin was removed by scraping with a scalpel blade and the remaining frozen epidermal layer was powdered in liquid N_2 (31). The powdered samples were then thawed in 10 mM EDTA, and after homogenization a 10 % solution of SDS (0.1 vol) was added. The DNA was isolated and purified using a previously described phenol/chloroform extraction method (32).

^{32}P-Postlabeling

The general procedure of Randerath and co-workers was used (33,34). DNA digestion and postlabeling using nuclease P1 digestion to enhance the sensitivity of the

assay was carried out essentially as described by Hughes and Phillips (35); 50 μCi [γ-^{32}P]ATP purchased from ICN was used in each labeling reaction.

Thin-Layer Chromatography

In order to resolve the ^{32}P-labeled adducts in digests of DNA from BP-treated mouse skin, a previously described solvent system (36,37) was used with either 10 × 10 or 20 × 20 cm PEI-cellulose TLC plates. Plates were eluted with: D1, 1.0 M sodium phosphate, pH 6.0; D2, 5.3 M lithium formate, 8.5 M urea, pH 3.5; D3, 1.2 M lithium chloride, 0.5 M Tris-HCl, 8.5 M urea, pH 8.0; D4, 1.7 M sodium phosphate, pH 6.0.

For resolution of *cis* and *trans* adducts of the *anti*-BPDE isomers, the chromatography system described by Canella *et al.* (38) was used. ^{32}P-Postlabeled adducts were resolved on 20 × 20 cm PEI-cellulose plates eluted with: D1, 1.0 M sodium phosphate, pH 6.0; D2, 3.6 M lithium formate, 7.5 M urea, pH 3.4, for 20 h on to a paper wick; D3, 0.8 M sodium phosphate, 0.5 M Tris-HCl, 7.5 M urea, pH 8.2, also for 20 hr on to a paper wick.

High-Performance Liquid Chromatography (HPLC)

Radioactive spots of B[*a*]P-DNA adducts were eluted from PEI-cellulose by overnight extraction with 400 μl of 4.0 M pyridinium formate (pH 4.5). Eluates were filtered and then reduced to dryness in a Savant Speed Vac concentrator. Recovery was greater than 90 %. Adduct residues were redissolved in methanol.

HPLC separation of ^{32}P-postlabeled adducts was carried out on a phenyl-modified reversed phase column as described previously (39). Gradients were made using the following solvents: A, 0.3 M sodium dihydrogen orthophosphate and 0.2 M orthophosphoric acid, mixed in proportions to provide a buffer at pH 2.0; B,

methanol:buffer A, 9:1. The gradient program was: 0-12.5 min, a linear gradient of 10-43 % B; 12.5-60 min, a linear gradient of 43-47 % B; 60-80 min, a linear gradient of 47-90 % B; at a flow rate of 1.2 ml/min.

Low-Temperature Fluorescence Spectroscopy

A detailed description of the apparatus used for FLN and NLN fluorescence spectroscopy is given elsewhere (27). Briefly, the excitation source was a Lambda Physik FL-2002 dye laser pumped by a Lambda Physik EMG 102 MSC XeCl excimer laser. The cryostat was of the double-nested glass type fitted with quartz optical windows. For gated detection the output of a reference photodiode triggering an FG-100 high voltage gate pulse generator was used to define the temporal observation window of a Princeton Instruments IRY 1024/G/B intensified blue-enhanced photodiode array. The detector delay time was set to 45 ns; the gate width was 400 ns. A 1-m focal length McPherson 2016 monochromator was used to disperse the fluorescence. For high-resolution measurements the monochromator was equipped with a 2400 grooves/mm grating, providing an 8 nm spectral window with a resolution of ~ 0.08 nm. Low-resolution NLN fluorescence bands were recorded using the same monochromator fitted with a 150 grooves/mm grating yielding a 150 nm window. NLN spectra were obtained using different excitation wavelengths in order to selectively excite helix-external versus base-stacked adducts as described by Geacintov et al. (26,28,30). FLN spectra were obtained using many different excitation wavelengths, each revealing a portion of the S_1 excited-state vibrational frequencies.

DNA isolated from mouse skin treated with BP was precipitated with 0.1 volume of 5 M NaCl and 2 volumes of ethanol precooled to −20 °C. The DNA precipitate containing various amount of adducts was dissolved in 30-40 µl of 20 mM sodium

phosphate buffer (pH 7.0; 100 mM NaCl), and the resulting solution (DNA concentration was ~3mM in base pairs) was transferred to quartz glass tubes (3 mm o.d. × 2 mm i.d. × 1 cm) for spectroscopic analysis at 77 and 4.2 K. In order to determine the DNA concentration of the samples, aliquots of the DNA solutions were diluted and the absorbances at 258 nm were measured using a Hewlett Packard 8452A UV-Vis Spectrometer. Ethanol-precipitated solid pellets of mouse skin DNA were also analyzed for comparison. Synthesized oligonucleotide-BPDE adduct standards were dissolved in 30 μl of 20 mM sodium phosphate, 100 mM NaCl, pH 7.0 buffer. Samples were kept on ice for at least 20 minutes before rapid cooling in liquid helium (for FLN) or liquid nitrogen (for NLN fluorescence spectroscopy).

RESULTS

BP-DNA Adducts on PEI-Cellulose TLC

^{32}P-postlabeling analysis of mouse skin DNA from animals treated topically with BP revealed the expected pattern of BP-DNA adducts on 10 × 10 cm TLC plates at all time-points. This consisted of a major spot, possibly containing more than one compound, and a series of minor spots (data not shown). Adduct resolution was improved further for the 4-h, 6-h, 8-h and 24-h timepoint samples by chromatography of their postlabeled digests on 20 × 20 cm TLC plates, and an example of the profile obtained with the 8-h sample is shown in Figure 5-1. Most of the radioactivity was contained in a major, possibly composite spot (spot 4/5), in addition to which there were a further six minor spots detected: spots 1-3 and 6-8. The relative amounts of radioactivity in each adduct spot is shown for the 4-h, 6-h, 8-h and 24-h samples in Table
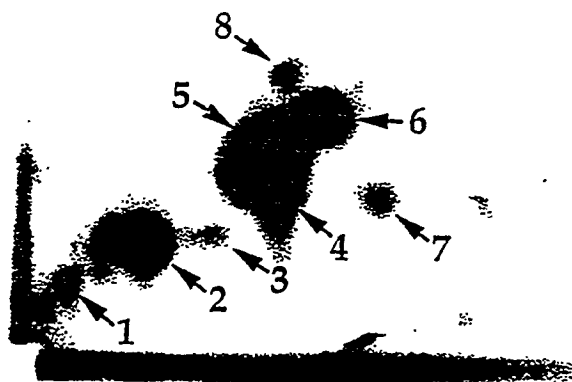
Figure 5-1. Autoradiogram of the PEI-cellulose TLC map (20 × 20 cm) of the ^{32}P-postlabeled digest of DNA isolated from mouse skin 8h after treated with BP (1 μmol). Solvents for chromatography were as described in the text. The origin is located at the bottom left-hand corner. Adduct spot 4 & 5 was excised, eluted and further analyzed by HPLC.

5-1. The major adduct spot (4/5), assumed to be due to the reaction of (+)-*anti*-BPDE with the N^2 position of guanine residues in DNA (33), accounts for >80 % of the total binding detected. The minor adduct spots observed probably result from the reaction of benzo[*a*]pyrene diol-epoxide isomers with adenine residues in DNA, and from the reaction of other reactive intermediates with DNA (40).

Using the TLC conditions described by Canella et al. (38), the four stereochemically distinct *anti*-BPDE-dG adducts (i.e., (+)-*trans*-, (-)-*trans*-, (+)-*cis*- and (-)-*cis*-) derived from *anti*-BPDE-modified duplexes 5'-d(CCATCGCTACC')- (GGTAGCGATGG), modified by *trans* or *cis* addition of the exocyclic amino group of G to the C10 position of either (+)- or (–)-*anti*-BPDE, were also analyzed by ^{32}P-postlabeling. In agreement with previous reports (38), our results indicated that the *cis* and *trans* adducts of both the (+)- and (–) isomers could be resolved from each other on TLC (data not shown). However, the (–)-*cis* adduct comigrated with the (+)-*trans* adduct; and the (–)-*trans* adduct comigrated with the (+)-*cis* adduct.

For subsequent HPLC analysis of these adducts, the TLC spots were excised and the radioactive material was eluted to provide material for injection onto HPLC.

HPLC of Adduct Standards

The ^{32}P-postlabeled *trans*- and *cis*- adducts of (–)-*anti*-BPDE with guanine residues were well resolved on HPLC, eluting around 29 and 36 minutes, respectively (Figure5-2A). The *trans*- and *cis*- adducts of (+) *anti*-BPDE to guanine were also well resolved from each other (Figure 5-2B), with elution times of around 36 and 29 minutes, respectively. A UV marker compound, 9,10-dihydro-9,10-dihydroxyphenanthrene, eluted at ~ 46 minutes. These results indicate that the *cis* adduct of (+)-*anti*-BPDE had a retention time very similar to that of the *trans* adduct of (–)-*anti*-BPDE, and the *trans*

Table 5-1. Quantitation of adduct spots in mouse skin DNA obtained 4,6,8, and 24 hours after topical application of BP

Spot number	% of total radioactivity			
	4 h	6 h	8 h	24 h
1	1.3	0.9	0.9	0.8
2	8.3	9.5	12.2	10.0
3	2.1	0.8	0.8	2.6
4 & 5	81.2	82.9	81.0	82.0
6	5.7	4.4	3.8	3.4
7	1.3	0.5	0.5	0.4
8	0.0	1.0	0.8	0.8

adduct of (+)-*anti*-BPDE had a retention time very similar to that of the *cis* adduct of (-)-*anti*-BPDE. Indeed, in co-injection experiments, it was not possible to separate these adduct pairs adequately (data not shown).

HPLC of the Major BP-DNA Adduct Spot

HPLC profiles of the adducts extracted from TLC spot 4&5 (see Figure 5-1) were obtained for each time point. Figure 5-2C shows the result obtained with the sample collected at 4 hr after treatment. A major peak at ~36 minutes and a minor peak at ~ 29 minutes were found. The retention time of the major peak corresponds to that of the *trans* adduct of (+)-*anti*-BPDE (but also that of the *cis* adduct of (-)-*anti*-BPDE) and the retention time of the minor peak corresponds to that of the *cis* adduct of (+)-*anti*-BPDE (but also the *trans* adduct of (-)-*anti*-BPDE). However, fluorescence line narrowing data (see below) indicate that the major BP-DNA adduct is (+)-*trans-anti*-BPDE and not (-)-*cis-anti*-BPDE, in agreement with previously reported findings (41). Similarly, the minor HPLC peak is believed to contain primarily the (+)-*cis-anti*-BPDE adduct (see the following section on FLNS).

The relative amounts of *trans*- and *cis*- guanine adducts of (+)-*anti*-BPDE found in mouse skin DNA at different times after treatment with BP are depicted in Figure 5-3B. These two curves are contrasted with the total BP binding to DNA as shown in Figure 5-3A. Since the (+)-*trans-anti*-BPDE-dG is the major adduct found with ^{32}P postlabeling (about 70-75 % of the total adduct level), it is not surprising that the time profiles of the (+)-*trans-anti*-BPDE adduct (curve a of frame B) and that of the total BP adduct level (frame A) are nearly indistinguishable. These data, in agreement with our earlier works (37), show that the (+)-*trans-anti*-BPDE adduct (~ 13 fmol/μg of DNA) was at its highest level at 24 hours and had declined significantly by 48 hours. In
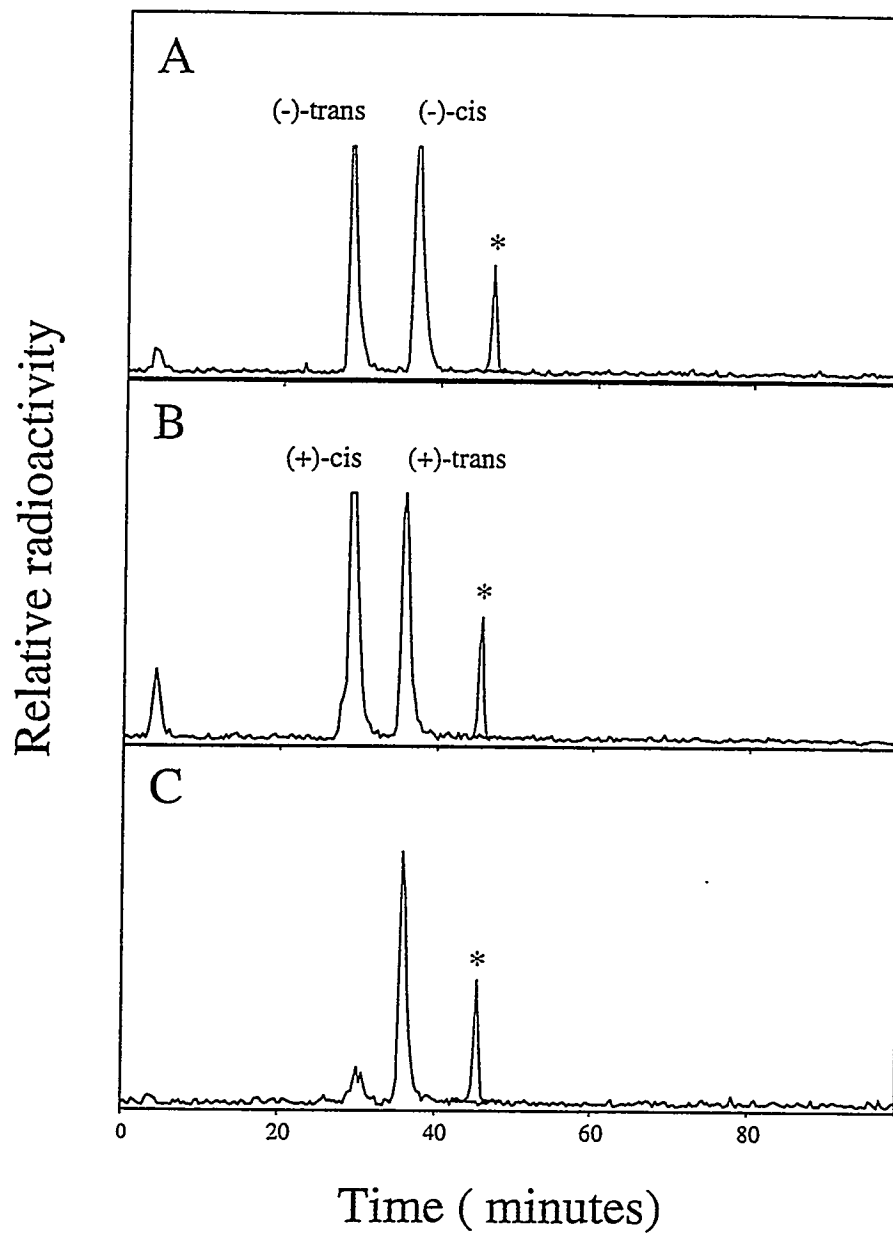
Figure 5-2. HPLC of ³²P-postlabeled *trans-* and *cis-anti*-BPDE adducts obtained from stereochemically pure BPDE modified oligonucleotides (frames A and B) and from mouse skin DNA at 4 hours after BP treatment *in vivo* (frame C). The HPLC peaks with elution times at around 29 and 37 minutes correspond to (-)-*trans*-/(+)-*cis*- and (-)-*cis*-/(+)-*trans*-adducts, respectively. The peak around 46 minutes corresponds to the UV marker (see text for explanation).
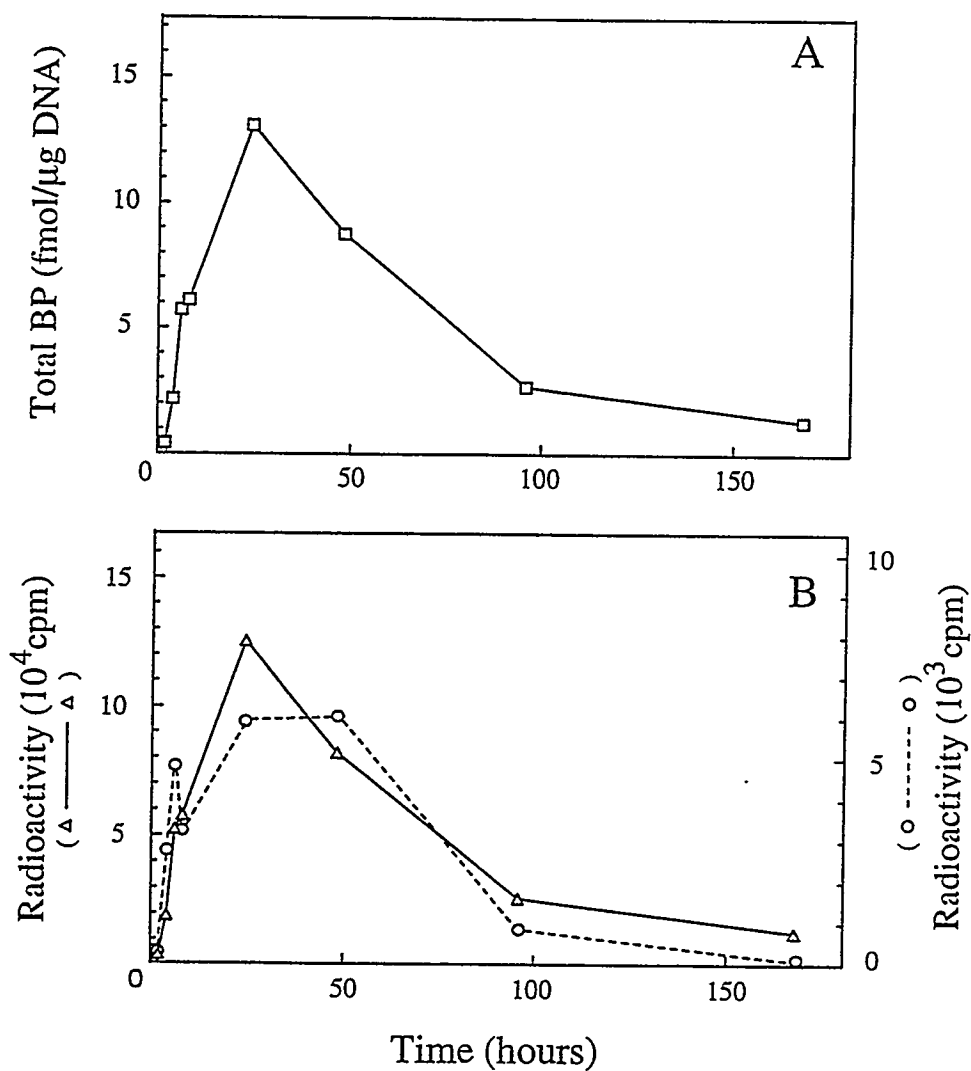
Figure 5-3.   Formation and removal of BP-DNA adducts in mouse skin as a function of time after BP application. (A) Total BP binding to DNA, as determined from TLC maps, in fmol adducts/μg of DNA (B) Relative intensity of radioactivity (in cpm) of $(+)$-*trans*- (solid line, left-hand axis) and $(+)$-*cis-anti*-BPDE-N^2-dG adducts (dashed line, right-hand axis), obtained after HPLC separation of the major adduct spot.

contrast, the level of the (+)-*cis-anti*-BPDE adduct at 48 hours was as high as that observed at 24 hours.

Low-Temperature Fluorescence Spectroscopy Studies

The stereochemical characteristics of the BPDE adducts were determined by fluorescence line narrowing spectroscopy (FLNS). This technique is used to obtain high-resolution, vibrationally resolved fluorescence spectra from samples cooled to 4.2 K (28). It has been established (14,42) that when a tunable dye laser is used to probe the vibrational frequencies of the first electronically excited state S_1, the 579 cm^{-1} mode is very strong for ($\pm$)- *trans-anti*-BPDE adducts to N^2-dG, while the 612 cm^{-1} mode is rather weak. For *cis* addition products of the exocyclic amino group of guanine moieties to ($\pm$)-anti-BPDE, those two modes exhibit comparable intensities and the 740 cm^{-1} mode becomes readily noticeable. This is illustrated in Figure 5-4 presenting the FLN spectra of the (+)-*trans*- and the (+)-*cis-anti*-BPDE-N^2-dG adduct contained in the oligonucleotide d(CCATC<u>G</u>CTACC) · (CCATCGCTACC) (curve b and c, respectively). The FLN spectrum of the mouse skin DNA sample obtained 24 hours after topical application (curve a) is almost identical to that of the (+)-*trans-anti*-BPDE adduct to the oligonucleotide (curve b) but very different from that of the (+)-*cis-anti*-BPDE adduct bound to the same oligonucleotide (curve c). Spectrum a shows the very strong 579 cm^{-1} mode that is characteristic of *trans-anti*-BPDE adducts. Also a minor contribution of a *cis* addition product in mouse skin DNA can be noticed by the presence of a weak 740 cm^{-1} mode (indicated by the asterisk). All other mouse skin DNA samples from different timepoints showed very similar spectra indicating that the *trans* adduct is the major adduct throughout the whole time course (data not shown). Therefore, the major adduct separated by HPLC (Figure 5-2, frame C) can be safely assigned as (+)-*trans-anti*-
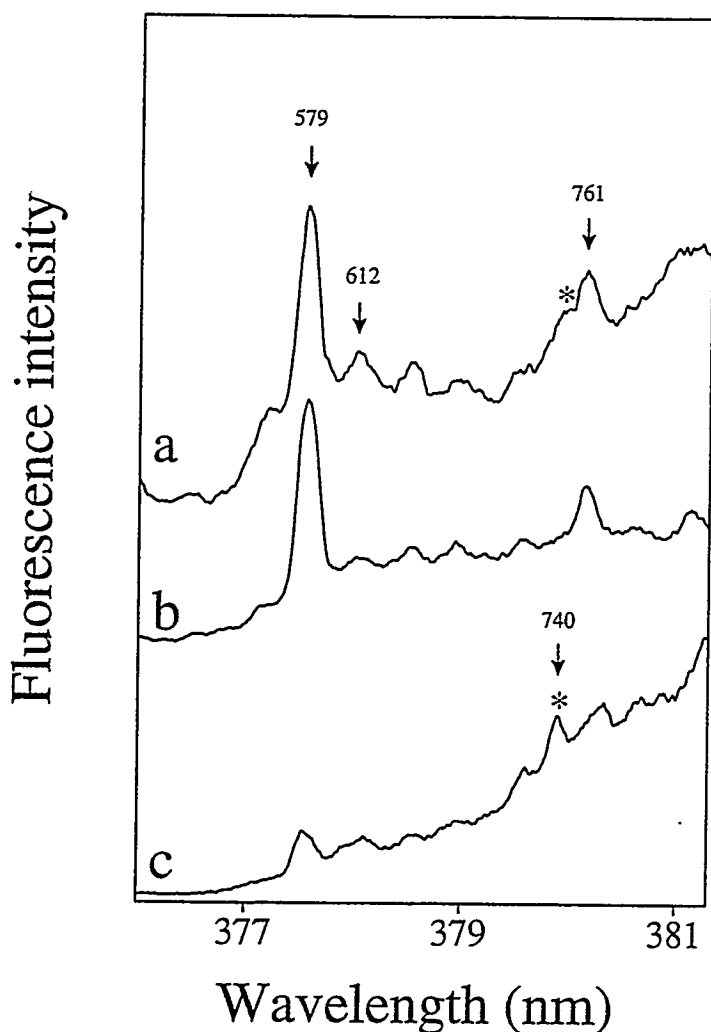
Figure 5-4. Fluorescence line narrowing spectra of BPDE-DNA adducts, λ_{ex} = 369.48 nm; T = 4.2 K. Curve a: ethanol precipitated solid DNA from mouse skin obtained 24 hours after BP treatment; curve b: (+)-*trans-anti*-BPDE-N^2-dG adduct to double stranded d(CCATCGCTACC) · d(GGTAGCGATGG) oligonucleotide, dissolved in 20 mM sodium phosphate, 100 mM NaCl, pH 7.0 buffer; curve c: (+)-*cis-anti*-BPDE-N^2-dG adduct to the same double-stranded oligonucleotide in the same buffer matrix. The underlines are used to indicate the residues modified by BPDE. Vibrational modes are labeled with their excited state vibrational frequencies in cm^{-1}. An asterisk is used to label the mode which is typical for the *cis*-adduct.

BPDE-N^2-dG and not as a (-)-*cis* adduct. The absence of the 557 cm^{-1} and 616 cm^{-1} modes indicates that there is no significant contribution from *syn* adducts (43).

Low-resolution fluorescence emission spectra of adducted mouse skin DNA samples in aqueous buffer solution at 77K revealed that the conformational distribution of the adducts changes throughout the time course. The fluorescence origin bands of the adducted mouse skin DNA showed a gradual red shift up to 24 hours after the application of BP and then shifted blue for later timepoints (see Figure 5-5, curves a,b of frame A and curve a of frame B, non-selectively excited at 350 nm). The same trend was observed for solid pellet samples of ethanol precipitated mouse skin DNA (data not shown). The maximum red shift was observed at 1 day after the application of BP, independent of the excitation wavelength except when a wavelength selective to intercalated conformations was used, i.e., 355 nm. The red shift can be explained generally by increased contributions from (+)-2 and (+)-3 adduct conformations, i.e. adducts with partially base-stacked or base-stacked (intercalated) conformations, respectively. We have already reported (21) that the conformational distributions of (+)-*trans-anti*-BPDE-N^2-dG adducts to double stranded oligonucleotides depend on the neighboring base sequences. The origin band of the mouse skin DNA samples is broader and strongly red-shifted compared to all (+)-*trans-anti*-BPDE-N^2-dG adducts studied so far in calf thymus DNA and in various double stranded oligonucleotides *in vitro* (14,21,42) (see discussion below). This indicates that in mouse skin DNA there is a broad, heterogeneous distribution of adduct conformations, of which a large fraction shows considerable base-stacking. Since about 75 % of the total adduct population has the same stereochemistry, we suggest that the conformational heterogeneity is related to the various base sequences around the lesion sites.
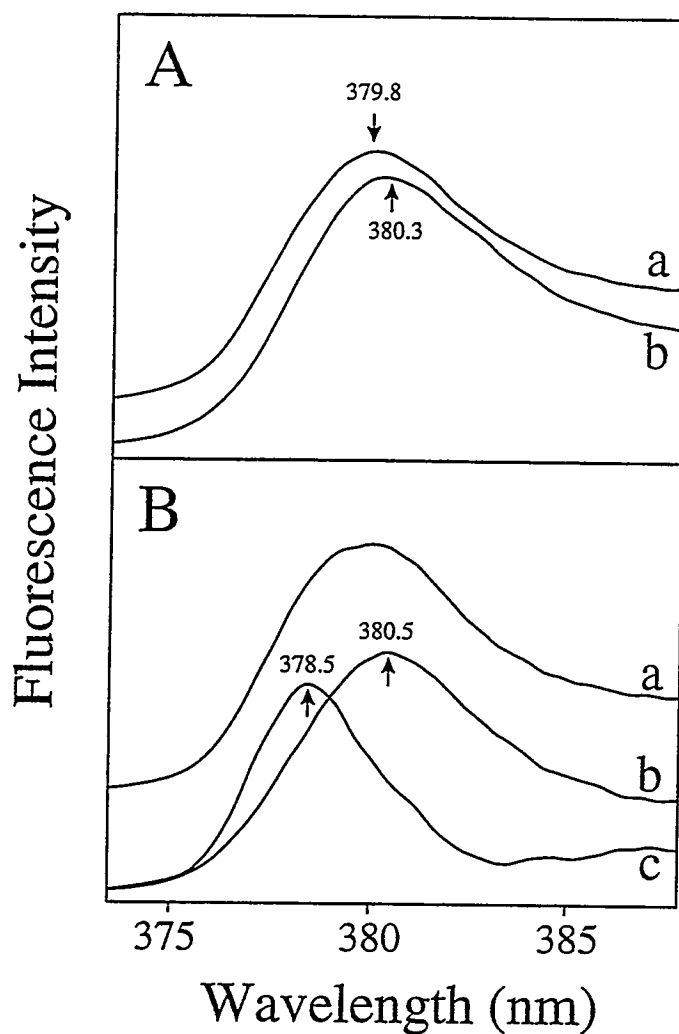
Figure 5-5. NLN fluorescence origin bands of BPDE-DNA adducts from mouse skin. Frame A shows a shift in the conformational distribution in time: curves a and b correspond to mouse skin DNA obtained at 4 hours and 24 hours, respectively. λ_{ex} = 350. Frame B illustrates adduct heterogeneity: curve a and b correspond to the 4 day sample, excited at 350 nm and 355 nm, respectively. Curve c is the difference spectrum (curve a minus curve b), showing the minor adduct fraction with helix-external character. Solvent matrix: 20 mM sodium phosphate buffer (pH 7.0) with 100 mM NaCl; T = 77 K.

Adduct heterogeneity is further illustrated in Figure 5-5B, presenting the NLN
fluorescence spectra of the 4-day sample using non-selective excitation at 350 nm (curve
a) and more selective excitation at 355 nm (curve b). As shown by Geacintov *et al.* (30),
355 nm radiation preferentially excites intercalative BPDE adducts. However, the
emission maximum and width of curve b do not agree completely with the emission band
measured for the intercalated (+)-*cis-anti*-BPDE-N^2-dG adduct in duplex oligonucleotides
(14). We conclude that the adduct population excited at 355 nm contains not only truly
intercalated adducts, but also adducts experiencing weaker stacking interactions ((+)-2
type conformation). The difference spectrum (curve a minus curve b = curve c) shows
the existence of a smaller adduct fraction with a helix-external character and an emission
maximum at 378.5 nm. At this point it should be mentioned that at cryogenic
temperatures all BPDE adducts show very similar fluorescence lifetimes and must
therefore have comparable fluorescence quantum yields. Thus, the relative fluorescence
intensities of the various adduct types provide a direct indication of their contribution to
the total adduct population if non-selective excitation is used.

In order to investigate the formation and removal of BPDE lesions in mouse skin
DNA, the broad fluorescence emission band was integrated over the 370-500 nm range;
the resulting total fluorescence intensity was normalized by the absorbance of the
corresponding DNA solution at 258 nm. When non-selective excitation is utilized, the
integrated fluorescence intensity reflects the total BPDE level bound to the DNA. As
illustrated in Figure 5-6A, at most time points the fluorescence intensity profile (shown as
circles) of mouse skin DNA excited at 350 nm is very similar to the total BP profile
obtained by postlabeling (compare with Figure 5-3A). For the 4-day and 7-day samples,
however, the fluorescence intensity profile reveals higher adduct levels than the ones
obtained via the ^{32}P postlabeling method. The total adduct level obtained by fluorescence
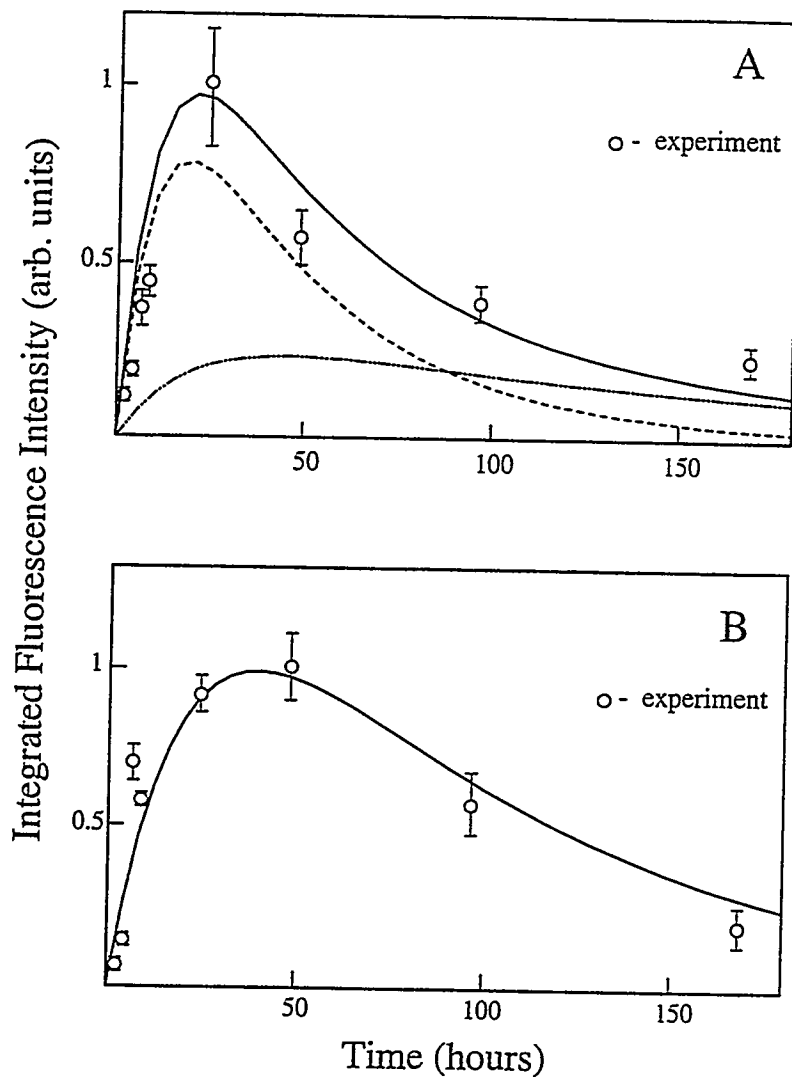
Figure 5-6. Fluorescence intensity profiles of mouse skin DNA after topical application of BP. Epidermal DNA from each timepoint was dissolved in 20 mM sodium phosphate buffer (pH 7.0; 100 mM NaCl). NLN fluorescence spectra at 77 K were integrated over the 370 nm - 500 nm range and normalized by DNA concentrations. Frames A and B show the intensities obtained at λ_{ex} = 350 and 355 nm, respectively. Experimental data are shown as circles; error bars represent the standard deviations from three different measurements. Line curves are best fits obtained with the following parameters: Frame A, dashed line (fast component): τ_f = 18 hrs, τ_{ro} = 19 hrs, σ = 7 hrs; dashed/dotted line (slow component): τ_f = 18 hrs, τ_{ro} = 100 hrs, σ = 20 hrs; the solid line is the sum of the two component curves. Frame B: τ_f = 18 hrs, τ_{ro} = 57 hrs, σ = 10 hrs.

spectrometry reaches the maximum at 24 hour after BP treatment. Moreover, when selective excitation at 355 nm is employed, the fluorescence intensity profile as a function of time reflects the formation and removal of BPDE adducts adopting base-stacked and/or intercalated conformations (see Figure 5-6B). Interestingly, the overall profile is similar to that of the (+)-*cis-anti*-BPDE-N^2-dG adduct as measured by HPLC, except for the 4-day and 7-day samples (see Figure 5-3B). The similarity can be explained by the fact that the (+)-*cis-anti*-BPDE-N^2-dG adduct has been shown to adopt primarily an intercalated conformation in double-stranded oligonucleotides (12,14,30). The intercalated conformation reaches the maximum level at 48 hour after BP application and the overall profile is broader than the total BP level profile shown in Figure 5-3A. FLN spectra, obtained with excitation wavelength 356.78 nm, confirm the intercalated character of these adducts. Figure 5-7 shows that the intensity of the broad emission intercalated BPDE adducts (14), varies depending on the time passed after BP treatment, and follows the time profile obtained by NLN fluorescence spectrometry at 355 nm (Figure 5-3B).

Analysis of Formation and Repair Kinetics

In an attempt to obtain more insight into the observed time profiles in terms of apparent rates of formation and removal, we tried to fit the experimentally obtained fluorimetric data assuming, for simplicity, single exponential kinetics for adduct formation and repair. It is straightforward to show that the time course of adduct formation/repair can be described as:

$$A(t) = A_o \frac{k_f}{k_f - k_r} [\exp(-k_f t) - \exp(-k_r t)] \qquad (1)$$
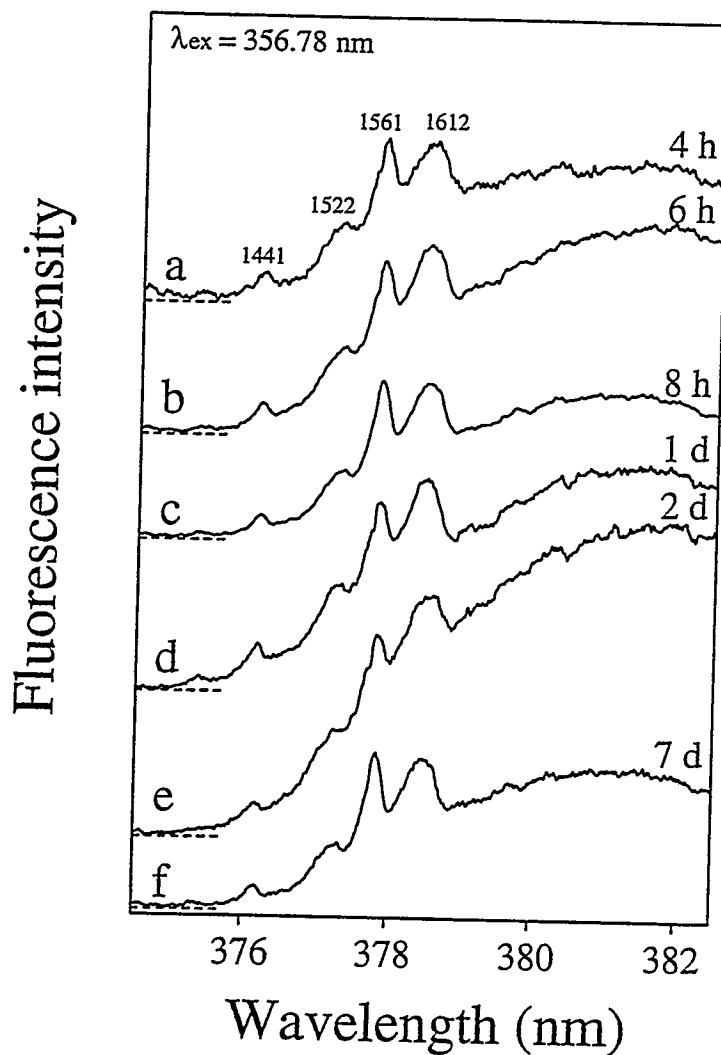
Figure 5-7. FLN spectra of mouse skin DNA obtained at different time points after BP application. Curve a: 4 hrs; curve b: 6 hrs; curve c: 8 hrs; curve d: 24 hrs; curve e: 48 hrs; curve f: 196 hrs. Ethanol-precipitated solid DNA was used to obtain a better signal-to-noise ratio. Base-lines are marked as dotted lines at the left edge of the curves; intensities are normalized to the 1561 cm^{-1} mode. Vibrational modes are labeled with their excited states vibrational frequencies in cm^{-1}. λ_{ex} = 356.78 nm; T = 4.2 K.

where $k_f = \ln2/\tau_f$ and $k_r = \ln2/\tau_r$, τ_f and τ_r being the half lives of adduct formation and repair, respectively. A(t) is the time-dependent adduct concentration; A_o is a constant.

In order to take into consideration the adduct heterogeneity of the sample, due to the various base sequences and the inhomogeneous character of the DNA environment, we assume the repair to have a Gaussian distribution of half-life values τ_r with variance σ^2 . We average A(t) of Eq. 1 over the distribution $f(\Delta\tau_r)$ of repair half-lives: $\Delta\tau = \tau_r - \tau_{ro}$, where τ_{ro} is the mean value for the repair half-life. Thus,

$$A'(\Delta\tau_r, t) = \int_{-\infty}^{+\infty} d(\Delta\tau_r) \cdot f(\Delta\tau_r) \cdot A(t) \qquad (2)$$

Eq. 2 may be solved yielding the concentration of adducts being formed and repaired via nonconstrained first-order reactions. Normalized fits to the experimental results are presented as line curves in Figure 5-6. As shown in Figure 6-6B the time profile of the intercalated adducts can be fitted reasonably well when substituting an apparent half-life of formation of 18 hrs, a half-life of removal of 57 hrs, and a relatively small value for σ , set to 10 hrs. The experimental data do not indicate a very broad distribution of repair rates. In the case of the total adduct levels, however, the time profile cannot be fitted very well with single exponential kinetics, not even when a very large σ value is assumed. The experimental data clearly indicate a rapid initial phase, followed by a much slower removal of the remaining (minor) fraction, which we attempted to fit assuming a bimodal repair rate distribution, as shown in Figure 5-6A: dashed line (fast component): $\tau_f = 18$ hrs, $\tau_{ro} = 19$ hrs, $\sigma = 7$ hrs; dashed/dotted line (slow component): $\tau_f = 18$ hrs, $\tau_{ro} = 100$ hrs, $\sigma = 20$ hrs; the solid line is the sum of the two component curves. We conclude that the major adduct fraction is relatively quickly repaired, which might be due to the fact that (+)-*trans-anti*-BPDE adducts (the major contribution to the total adduct population) tend to disturb the overall helical structure (bending (44) and /or unwinding

(45)) and are therefore presumably more easily recognized by cellular repair mechanisms. The time profile is very similar to that found for the (+)-*trans-anti*-BPDE-N^2-dG adduct measured by HPLC (solid line in Fig. 5-3B). The remaining minor fraction that is less easily repaired is of course partly due to the intercalated species of time profile 6B. However, since the total adduct profile represents a very heterogeneous mixture, also other adduct species with a more external, partially base-stacked character (less efficiently excited at 355 nm) could be difficult to recognize and/or repair. Finally, a leveling off of the repair rate could also be due to a decrease in enzyme activity after the initial (induced) active phase. At this point it is not clear as to what extent this effect plays a significant role in the overall kinetics. We did not attempt to correct for the contribution from cell turnover to the adduct removal process because mouse epidermis cell turnover, even though it is faster than for other tissues (i.e. heart, lung), is much slower than active enzymatic repair (22).

DISCUSSION

In this paper the BPDE-DNA adducts formed in mouse skin were assessed by ^{32}P-postlabeling, HPLC, and laser-excited fluorescence spectroscopy performed under line-narrowing ($S_1 \leftarrow S_0$ laser excitation at 4.2 K) and non-line narrowing conditions ($S_2 \leftarrow S_0$ laser excitation at 77 K) (28). The study shows that laser induced fluorescence spectroscopy can provide new insights into the importance of adduct conformation for DNA repair.

The major stable adduct formed in mouse skin DNA was found to be the (+)-*trans-anti*-BPDE-N^2-dG adduct (Figure 5-4) in agreement with previously reported results (7,41). The time profile of total BP adduct formation and repair, as measured by postlabeling, is fairly consistent with our fluorescence spectrometry results (compare

Figure 5-3A with Figure 5-6A) and previous *in vivo* studies of BP-treated mouse skin DNA (37) where the maximum BP adduct level was also observed 24 hours after BP application. The time profiles obtained by fluorescence spectrometry and the ones obtained by postlabeling/HPLC are not necessarily identical. The former method analyzes the whole mouse skin DNA after minimal sample handling, while the other methods involve digestion, ^{32}P-labeling, and TLC separation, followed by adduct spot extraction from the PEI-cellulose plates for HPLC analysis. Considering the fact that some adducts may be less completely recovered than others (total recovery of the postlabeling method for BP adducts is ~50% (46)), and that for HPLC analysis only the major spot (about 80% of the total adducts) was recovered from the TLC plates, the data obtained by using fluorescence spectrometry may reflect more closely the total adduct profile. A possible explanation for the fact that for the 4-day and 7-day samples the total adduct levels obtained via ^{32}P-postlabeling are lower than those measured by non-selectively excited fluorimetry (see Figure 5-6A), or by tritium counting as reported by DiGiovanni *et al.* (22), could be related to one or more steps in the postlabeling procedure that might cause a lower recovery for the most persistent adducts.

The stereoisomeric (+)-*trans* and (+)-*cis-anti*-BPDE-N^2-dG adducts constitute at least 80% of the total BP adducts found in mouse epidermal DNA by postlabeling (table 5-1). Interestingly, the time courses of the *trans-* and *cis* adduct levels, as determined by HPLC, show remarkable differences. The shift of the maximum level to later time and the broader profile are indicative of a slower repair process for the (+)-*cis-anti*-BPDE-N^2-dG adduct compared to the (+)-*trans-anti*-BPDE-N^2-dG adduct. When we examined the *in vivo* formation and repair of BP adducts in terms of adduct conformations by means of low-temperature fluorescence spectroscopy, we found that adducts with internal (base-stacked) conformations are repaired more slowly than external (solvent exposed) adducts

(see Figure 5-6). For internal adducts the apparent half-life of repair, τ_{ro}, is estimated to be about 57 hours while that of external adducts is about 19 hours. However, the most persistent adducts that were still present 7 days after the treatment featured a rather external character, indicating a bimodal distrubution of repair rates for these adducts (see Figure 5-6). The estimated τ_{ro} values are comparable to the removal half-life of 28.3 hours measured for (+)-*anti*-BPDE adducts from a DNA-repair-proficient line of Chinese hamster ovary (CHO) cells (24). The apparent half-life of formation, τ_f, obtained by fitting the experimental data, is 18 hours for both external and internal adducts. This is to be expected as the rate-limiting step for adduct formation *in vivo* is believed to be metabolic activation of BP to the electrophilic metabolite BPDE rather than BPDE binding to the DNA which is accomplished within a few minutes *in vivo* and *in vitro* (24).

We have shown earlier that the conformational distribution of the (+)-*trans-anti*-BPDE-N^2-dG adduct depends on the 5'-flanking base of the adducted guanine (21). The conformational distribution of the (+)-*trans-anti*-BPDE-N^2-dG adduct in duplex oligonucleotides consists primarily of (+)-1 (external; solvent exposed) and (+)-2 (partially base-stacked) conformations with fluorescence origin bands located at 378 and 380.3 nm, respectively (14). In this study, the fluorescence origin bands of mouse skin DNA samples were found to be red-shifted compared to that of (+)-*anti*-BPDE adducts to calf-thymus DNA formed *in vitro* (28) or typical (+)-*trans-anti*-BPDE-N^2-dG adducts to various duplex oligonucleotides (14,21). This suggests that in mouse skin DNA the major, (+)-*trans-anti*-BPDE-N^2-dG adduct experiences very strong base-stacking interactions. The 24-hours sample shows the largest contribution of these base-stacked conformations (maximum of origin band is 380.3 nm for 350 nm excitation). The contribution from intercalated *cis*- adducts alone cannot account for this red shift since the *cis*- adduct level is still at its maximum value at 48 hours after BP application. In

addition, the (+)-*cis-anti*-BPDE-N^2-dG adduct constitutes less than 10 % of the total *anti*-BPDE adducts as determined by HPLC. The shifts of the conformational distribution in time observed for the total adduct fluorescence (consisting mainly of (+)-*trans-anti*-BPDE-N^2-dG adducts) may be explained by different repair rates for adducts with different conformations, depending on the base sequences around the adducted sites. Our findings are consistent with the sequence-specific incision repair of BPDE lesions, which was suggested by Tang *et al.* (47) in their study of UVRABC nuclease activity on ($\pm$)-*anti*-BPDE adducts to DNA *in vivo* and *in vitro*. They found that when $\phi X178$ RF DNA modified with ($\pm$)-*anti*-BPDE was treated with UVRABC nuclease from *E. coli,* the incision repair activity of the enzyme depended on the base sequence at the BPDE lesion site, suggesting that sequence-specific conformations of BPDE adducts affect protein binding and/or processing.

Our findings that the intercalated (base-stacked) adducts and (+)-*cis-anti*-BPDE-N^2-dG adducts in mouse epidermis are repaired approximately 3 times more slowly than the major fraction of external adducts and (+)-*trans-anti*-BPDE-N^2-dG adducts are in agreement with previously reported data on transcription elongation by T7 RNA polymerase (19). In their study, Choi and coworkers reported that the (+)-*trans-anti*-BPDE-N^2-dG adduct inhibited elongation by T7 RNA polymerase more efficiently than the (+)-*cis-anti*-BPDE-N^2-dG adduct when oligonucleotides with stereoisomerically pure BPDE-guanine adducts were used as templates. They also suggested that the premature termination of RNA synthesis occurring at or near the lesion site might be perceived by the cell as a signal to clear the adduct. Therefore, (+)-*trans-anti*-BPDE-N^2-dG adduct, being an efficient inhibitor of transcription, would be removed preferentially. Evidence for such a mechanism has been provided by Chen *et al.* (48), who reported preferential removal of BPDE adducts from the transcribed strand compared with the non-transcribed

strand of the *hprt* gene in human diploid fibroblasts exposed to (±)-*anti*-BPDE. However, it remains to be established whether the observed repair kinetics in mouse skin are also a consequence of this mechanism. The preferential recognition of the (+)-*trans-anti*-BPDE-dG adduct by repair systems may be related to the change in DNA structure induced by BPDE binding. The tertiary structure of BPDE-modified duplex oligonucleotides was found to be altered most significantly in case of the (+)-*trans-anti*-BPDE-dG adduct, as shown by the strong reduction of electrophoretic mobility in native polyacrylamide gel electrophoresis when compared with oligonucleotides containing (-)-*trans*, (+)-*cis* and (-)-*cis-anti*-BPDE-dG adducts (14). Also, the flexible hinge joint or bent/kinked structure (10,44,49,50) induced by (+)-*anti*-BPDE adducts (which are primarily (+)-*trans-anti*-BPDE-dG adducts) indicate tertiary DNA structure changes around this particular lesion.

In summary, our results demonstrate that the rate of removal of BPDE-DNA adducts in mouse skin, a target organ for BP carcinogenesis, depends on adduct conformation. Taken together with evidence that adduct conformation is influenced by the neighboring base(s) in the DNA sequence, our results provide the first *in vivo* evidence that adduct conformation and/or base sequence determines the reparability of BPDE-DNA adducts.

ACKNOWLEDGEMENT

REFERENCES

1. Huberman,E., Sachs,L., Yang,S.K., and Gelboin,H.V. (1976) Identification of mutagenic metabolites of benzo[a]pyrene in mammalian cells. *Proc. Natl. Acad. Sci. USA* **73**, 607-611.

2. Conney,A.H. (1982) Induction of microsomal enzymes by foreign chemicals and carcinogenesis by polycyclic aromatic compounds. *Cancer Res.* **42**, 4875-4917.

3. Newbold,R.F. and Brookes,P. (1976) Exceptional mutagenicity of a benzo[*a*]pyrene diol epoxide in cultured mammalian cells. *Nature* **261**, 52-54.

4. Buening,M.K., Wislocki,P.G., Levin,W., Yagi,H., Thakker,D.R., Akagi,H., Koreeda,M., Jerina,D.M., and Conney,A.H. (1978) Tumorigenicity of the optical enantiomers of the diastereomeric benzo[*a*]pyrene 7,8-diol-9,10-epoxides in newborn mice: Exceptional activity of (+)-7β,8α-dihydroxy-9α,10α-epoxy-7,8,9,10-tetrahydrobenzo[*a*]pyrene. *Proc. Natl. Acad. Sci. USA* **75**, 5358-5361.

5. Slaga,T.J., Bracken,W.J., Gleason,G., Levin,W., Yagi,H., Jerina,D.M., and Conney,A.H. (1979) Marked differences in the skin tumor-initiating activities of the optical enatiomers of the diastereomeric benzo(*a*)pyrene 7,8-diol-9,10-epoxides. *Cancer Res.* **39**, 67-71.

6. Meehan,T., Straub,K. (1979) Double-stranded DNA stereoselectively binds benzo(*a*)pyrene diol epoxides. *Nature* **277**, 410-412.

7. Cheng,S.C., Hilton,B.D., Roman,J.M., and Dipple,A. (1989) DNA adducts from carcinogenic and noncarcinogenic enantiomers of benzo[*a*]pyrene dihydrodiol epoxide. *Chem. Res. Toxicol.* **2**, 334-340.

8. Phillips,D.H. (1983) Fifty years of benzo[*a*]pyrene. *Nature* **303**, 468-472.

9. Gelboin,H.V. (1969) A microsome-dependent binding of benzo[*a*]pyrene to DNA *Cancer Res.* **29**, 1272-1276.

10. Cosman,M., de los Santos,C., Fiala,R., Hingerty,B.E., Singh,S.B., Ibanez,V., Margulis,L.A., Live,D., Geacintov,N.E, Broyde,S., and Patel,D.J. (1992) Solution conformation of the major adduct between the carcinogen (+)-*anti*-benzo[*a*]pyrene diol epoxide and DNA. *Proc. Natl. Acad. Sci. USA* **89**, 1914-1918.

11. de los Santos,C., Cosman,M., Hingerty,B.E., Ibanez,V., Margulis,L.A., Geacintov,N.E., Broyde,S., and Patel,D.J. (1992) Influence of benzo[*a*]pyrene diol epoxide chirality on solution conformations of DNA covalent adducts: the (-)-*trans-anti*-[BP]G·C adduct structure and comparison with the (+)-*trans-anti*-[BP]G·C enantiomer. *Biochemistry* **31**, 5245-5252.

12. Cosman,M., de los Santos,C., Fiala,R., Hingerty,B.E., Ibanez,V., Luna,E., Harvey,R.G., Geacintov,N.E, Broyde,S., and Patel,D.J. (1993) Solution conformation of the (+)-*cis-anti*-[BP]dG adduct in a DNA duplex: intercalation of the covalently attached benzo[*a*]pyrenyl ring into the helix and displacement of the modified deoxyguanosine. *Biochemistry* **32**, 4145-4155.

13. Fountain,M.A., and Krugh,T.R. (1995) Structural characterization of a (+)-*trans-anti*-benzo[*a*]pyrene-DNA adduct using NMR, restrained energy minimization, and molecular dynamics. *Biochemistry* **34**, 3152-3161.

14. Suh,M., Ariese,F., Small,G.J., Jankowiak,R., Liu,T.-M., and Geacintov,N.E. (1995) Conformational studies of the (+)-*trans*-, (-)-*trans*-, (+)-*cis*-, and (-)-*cis* adducts of *anti*-benzo[*a*]pyrene diolepoxide to N²-dG in duplex oligonucleotides using polyacrylamide gel electrophoresis and low-temperature fluorescence spectroscopy. *Biophys. Chem.* in press.

15. Pontén,I., Seidel,A., Gräslund,A., and Jernström,B. (1994) Spectroscopic studies of the *trans* adducts derived from (+)- and (-)-*anti*-benzo[*a*]pyrene-7,8-dihydrodiol-9,10-epoxide and the oligonucleotide 5'-d(CCTATAGATATCC). *Carcinogenesis* **15**, 2207-2213.

16. LeBreton,P.R., Huang,C.-R., Fernando,H., Zajc,B., Lakshman,M.K., Sayer,J.M., and Jerina,D.M. (1995) Multiple fluorescence lifetimes for oligonucleotides containing single, site-specific modifications at guanine and adenine corresponding to *trans* addition of exocyclic amino groups to (+)-(7*R*,8*S*,9*S*,10*R*)- and (-)-(7*S*,8*R*,9*R*,10*S*)-7,8,-dihydroxy-9,10-epoxy-7,8,9,10-tetrahydrobenzo[*a*]pyrene. *Chem. Res. Toxicol.* **8**, 338-348.

17. Hruszkewycz,A.M., Canella,K.A., Peltonen,K., Kotrappa,L., and Dipple,A. (1992) DNA polymerase action on benzo[a]pyrene-DNA adducts. *Carcinogenesis* 13, 2347-2352.

18. Shibutani, S., Margulis, L. A., Geacintov, N. E., and Grollman, A. (1993) Translesional synthesis on a DNA template containing a single stereoisomer of dG-(+)- or dG-(-)-*anti*-BPDE (7,8-dihydroxy-*anti*-9,10-epoxy-7,8,9,10-tetrahydrobenzo[a]pyrene). *Biochemistry* 32, 7531-7541.

19. Choi,D.-J., Marino-Alessandri,D.J, Geacintov,N.E., and Scicchitano,D.A. (1994) Site-specific benzo[a]pyrene diol epoxide-DNA adducts inhibit transcription elongation by bacteriophase T7 RNA polymerase. *Biochemistry* 33, 780-787.

20. Drouin,E. and Loechler,E.L. (1993) AP sites are not significantly involved in mutagenesis by the (+)-*anti* diol epoxide of benzo[a]pyrene: the complexity of its mutagenic specificity is likely to arise from adduct conformational polymorphism. *Biochemistry* 32, 6555-6562.

21. Suh,M., Jankowiak,R., Ariese,F., Mao,B., Geacintov,N.E., and Small,G.J. (1994) Flanking base effects on the structural conformation of the (+)-*trans-anti*-benzo[a]pyrene diolepoxide adduct to N^2-dG in sequence-defined oligonucleotides. *Carcinogenesis* 15, 2891-2898.

22. DiGiovanni,J., Decina.P.C., Prichett,W.P., Fisher,E.P., and Aalfs,K.K. (1985) Formation and disappearance of benzo[a]pyrene DNA-adducts in mouse epidermis. *Carcinogenesis.* 6, 741-747.

23. Tang,M., Pao,A., and Zhang,X. (1994) Repair of benzo[a]pyrene diol epoxide- and UV-induced DNA damage in dihydrofolate reductase and adenine phosphoribosyltransferase genes of CHO cells. *J. Biol. Chem.* 269, 12749-12754.

24. MacLeod,M.C., Daylong,A., Adair,G., and Humphrey,R.M. (1991) Differences in the rate of DNA adduct removal and the efficiency of mutagnesis for two benzo[a]pyrene diol epoxide in CHO cells. *Mutation Res.* 261, 267-279.

25. Wolterbeek,A.P.M., Roggeband,R., Steenwinkel,M-J.S.T., Baan,R.A., and Rutten,A.A.J.J.L. (1993) Formation and repair of benzo[a]pyrene-DNA adducts in cultured hamster tracheal epithelium determined by ^{32}P-postlabeling analysis and unscheduled DNA synthesis. *Carcinogenesis*, 14, 463-467.

26. Zhao,R., Liu,T.-M., Kim,S.K., MacLeod,M.C., and Geacintov,N.E. (1992) Identification and quatitative detection of isomeric benzo[a]pyrene diolepoxide-DNA adducts by low-temperature conventional fluorescence methods. *Carcinogenesis*, 13, 1817-1824.

27. Jankowiak,R. and Small,G.J. (1991) Fluorescence line narrowing: a high-resolution window on DNA and protein damage from chemical carcinogens. *Chem. Res. Toxicol.* 4, 256-269.

28. Jankowiak,R., Lu,P., Small,G.J., and Geacintov,N.E. (1990) Laser spectroscopic studies of DNA adduct structure types from enantiomeric diol epoxides of benzo[a]pyrene. *Chem. Res. Toxicol.* 3, 39-46.

29. Cosman,M., Ibanez,V., Geacintov,N.E., and Harvey,R.G. (1990) Preparation and isolation of adducts in high yield derived from the binding of two benzo[a]pyrene-7,8-dihydroxy-9,10-oxide stereoisomers to the oligonucleotide d(ATATGTATA). *Carcinogenesis* 11, 1667-1672.

30. Geacintov,N.E., Cosman,M., Mao,B., Alfano,A., Ibanez,V., and Harvey,R.G. (1991) Spectroscopic characteristics and site I/site II classification of *cis* and *trans* benzo[a]pyrene diolepoxide enantiomer-guanosine adducts in oligonucleotides and polynucleotides. *Carcinogenesis* 12, 2099-2108.

31. Phillips,D.H., Glover,P.L., and Sims,P. (1978) The covalent binding of polycyclic hydrocarbons to DNA in the skin of mice of different strains. *Int. J. Cancer*, 22, 487-494.

32. Gupta,R.C. (1984) Non-random binding of the carcinogen N-hydroxy-2-acetylaminofluorene to repetitive sequences of rat liver DNA *in vivo*. *Proc. Natl. Acad. Sci. USA*, 81, 6943-6947.

33. Gupta,R.C., Reddy,M.V., and Randerath,K. (1982) ^{32}P-Postlabeling analysis of non-radioactive carcinogen-DNA adducts. *Carcinogenesis* 3, 1081-1092.

34. Reddy,M.V., and Randerath,K. (1986) Nuclease P1-mediated enhancement of sensitivity of ^{32}P-postlabeling test for structurally diverse DNA adducts. *Carcinogenesis* 7, 1543-1551.

35. Hughes,N.C., and Phillips,D.H. (1993) ^{32}P-Postlabeling analysis of the covalent binding of benzo[ghi]perylene to DNA *in vivo* and *in vitro*. *Carcinogenesis* 14, 127-133.

36. Dunn,B.P., and Stich,H.F. (1986) ^{32}P-Postlabeling analysis of aromatic DNA adducts in human oral mucosal cells. *Carcinogenesis* **7**, 1115-1120.

37. Hughes,N.C., and Phillips,D.H. (1990) Covalent binding of dibenzpyrenes and benzo[*a*]pyrene to DNA: evidence for synergistic and inhibitory interactions when applied in combination to mouse skin. *Carcinogenesis* **11**, 1611-1619.

38. Canella,K., Peltonen,K., and Dipple,A. (1991) Identification of (+) and (-) *anti* benzo[*a*]pyrene dihydrodiol epoxide-nucleic acid adducts by the ^{32}P-postlabeling assay. *Carcinogenesis* **12**, 1109-1114.

39. Pfau,W., and Phillips,D.H. (1991) Improved reversed-phase high-performance liquid chromatographic separation of ^{32}P-labeled nucleoside 3',5'-bisphosphate adducts of polycyclic hydrocarbons. *J. Chromatogr.* **570**, 65-76.

40. Osborne,M.R. and Crosby,N.T. (1987) *Benzopyrenes*. Cambridge University Press, Cambridge, UK (chapters 1-10).

41. Thakker,D.R., Yagi,H., Akagi,H., Koreeda,M., Lu,A.Y.H., Levin,W., Wood,A.W., Conney,A.H. and Jerina,D.M. (1977) Metabolism of benzo[*a*]pyrene VI. Stereoselective metabolism of benzo[*a*]pyrene and benzo[*a*]pyrene 7,8-dihydrodiol to diol epoxides. *Chem.-Biol. Interactions* **16**, 281-300.

42. Lu,P., Jeong,H., Jankowiak,R., Small,G.J., Kim,S.K., Cosman,M., and Geacintov,N.E. (1991) Comparative laser spectroscopic study of DNA and polynucleotide adducts from the (+)-*anti*-diol epoxide of benzo[*a*]pyrene. *Chem. Res. Toxicol.* **4**, 58-69.

43. Jankowiak,R., Lu,P., Small,G.J., Nishimoto,M., Varanasi,U., Kim,S.K., and Geacintov,N.E. (1990) Fluorescence line-narrowing spectrometry: a versatile tool for the study of chemically initiated carcinogenesis. *J. Pharm. Biomed. Anal.* **8**, 113-121.

44. Hogan,M.E., Dattagupta,N., and Whitlock,J.P., jr. (1981) Carcinogen-induced alteration of DNA structure. *J. Biol. Chem.* **256**, 4504-4513.

45. Xu,R., Birke,S., Carberry,S.E., Geacintov.N.E., Swenberg,C.E., and Harvey,R.G. (1992) Differences in unwinding of supercoiled DNA induced by the two enantiomers of anti-benzo[*a*]pyrene diol epoxide. *Nucleic. Acids. Res.* **20**, 6167-6176.

46. Segerbäck,D., and Vodicka,P. (1993) Recoveries of DNA adducts of polycyclic aromatic hydrocarbons in the ^{32}P-postlabeling assay. *Carcinogenesis* **14**, 2463-2469.

47. Tang,M., Pierce,J.R., Doisy,R.P., Nazimiec,M.E., and MacLeod,M.C. (1992) Differences and similarities in the repair of two benzo[*a*]pyrene diol epoxide isomers induced DNA adducts by *uvrA, uvrB*, and *uvrC* gene products. *Biochemistry* **31**, 8429-8436.

48. Chen,R.-H., Maher,V.M., Brouwer,J., van de Putte,P., and McCormick,J.J. (1992) Preferential repair and strand-specific repair of benzo[*a*]pyrene diol epoxide adducts in the *HPRT* gene of diploid human fibroblasts. *Proc. Natl. Acad. Sci. USA.* **89**, 5413-5417.

49. Roche,C.J., Geacintov,N.E., Ibanez,V., and Harvey,R.G. (1989) Linear dichroism properties and orientations of different ultraviolet transition moments of benzo[*a*]pyrene derivatives bound noncovalently and covalently to DNA. *Biophys. Chem.* **33**, 277-288.

50. Eriksson,M., Nordén,B., Jernström,B., and Gräslund,A. (1988) Binding geometries of benzo[a]pyrene diol epoxide isomers covalently bound to DNA. Orientational distribution. *Biochemistry* **27**, 1213-1221.

149

CHAPTER 6. SPECTROSCOPIC STUDY OF TO-PRO-3-DNA COMPLEXES

6.1 Introduction

During the past several years, it has been established that nonphotochemical hole burning is a general and facile phenomenon for chromophores in biological systems, such as proteins (chlorophylls, carotenoids, pheophytins and hemes) [1] and DNA (PAH-DNA adducts [2], intercalated dyes [3]). Recently, Hayes and Small [4] showed that nonphotochemical hole burning can be used as a probe of the molecular environment in their studies with oxazine 720 in two different forms of glassy ethanol [5] and aluminum-phthalocyanine-tetrasulfonate in glassy water matrices [6]. There are many studies which show that the zero phonon hole (ZPH) width depends strongly on the amorphous host in which the chromophore is imbedded [7-9]. In the case of polymer hosts, the ZPH width was reduced as the rigidity of the polymer increased [10]. Friedrich and coworkers [11] showed that the compressibilities of several tautomeric forms of mesoporphyrine IX substituted horseradish peroxidase differ by as much as a factor of 3 between tautomers resulting in different ZPH width shift upon pressure change. It was shown that the hole burning efficiency of an intercalating dye, daunomycin, is 60 times larger when it is bound to $(dA-dT)_5 \cdot (dA-dT)_5$ than when bound to $(dG-dC)_5 \cdot (dG-dC)_5$ [3]. Hole growth rates were also reported to depend strongly on the host environment [6]. Since the nonphotochemical hole burning has proven to be sensitive to the molecular environment and has been applied successfully to various biological systems, it was also suggested by Small and coworkers that the technique may be applicable to imaging biological systems with high sensitivity and resolution, and to diagnosis of normal and abnormal cells [4].

Currently, many fluorescent dyes that selectively associate with specific organelles (mitochondria, endoplasmic reticulum, Golgi apparatus, nucleus, cytoskeleton (F- and G-actin), plasma membranes etc.) and with biological molecules (DNA, protein) are

available [12 and references therein]. A series of Rhodamine, lipophilic acridine orange, oxacarbocyanine, benzimidazolylcarbocyanine and styryl derivatives are known to stain mitochondria [13-15]. Short and long-chain carbocyanine derivatives are used for staining the endoplasmic reticulum (ER) to study structural interactions and dynamics of the ER [16,17]. NBD hexanoic ceramide, BODIPY ceramide and their sphingomyelin derivatives are available for staining Golgi apparatus [18-20]. For F-actin specific dyes, several fluorescent chromophores (BODIPY, Coumarin, fluorescein, rhodamine derivatives, Texas red etc.) are attached to phallotoxins which are bicyclic peptides that bind to F-actin [21,22]. For G-actin staining, DNase I is used instead of phallotoxins [23,24]. There are large numbers of DNA, protein and membrane binding dyes with fluorescence excitation and emission at various wavelengths (for review see reference 12).

Among the numerous DNA binding dyes, the two recently synthesized cyanine dyes YO-YO and TO-TO, which form extremely stable and highly fluorescent complexes with DNA, are considered to be the most promising in the development of DNA probes [25,26]. They are homodimeric derivatives of oxazole yellow (YO) and thiazole orange (TO), which are unsymmetric cyanine dyes with a conjugated chain connecting a quinoline moiety with a benzo-1,3-oxazole and a benzo-1,3-thiazole moiety, respectively. The dyes have excellent properties: high binding constants to DNA (10^8 - 10^{12} M^{-1}) and a high kinetic stability of dye-DNA complex, a large enhancement in fluorescence (3000 times) upon binding to double-stranded DNA, high extinction coefficients ($\sim 10^5 M^{-1} cm^{-1}$) [25,27,28]. It was reported that the binding of the dyes to double-stranded DNA occur via bis-intercalation of the two monomeric units [29,30]. Recently, a detailed solution structure of the TO-TO-DNA complex was reported [31]. The large enhancement of the fluorescence is believed to be the result of decreased rotational mobility around the

internuclear bridge between the two aromatic ring systems [32]. A series of dyes derived from YO-YO and TO-TO have been synthesized with fluorescence emission maxima spanning from 450 nm to 700 nm [12].

TO-PRO-3 is a dye which has the quinoline moiety connected to the benzo-1,3-thiazole moiety (see Figure 6-1 for the chemical structures) and has its absorption maximum at 642 nm and emission maximum at 661 nm when it binds to double stranded DNA in solution [12]. TO-TO-3 is a homodimer of two TO-PRO-3 units for which the binding constant to DNA is 40 times larger than that of TO-PRO-3. Both dyes can be excited by commercially available He-Ne lasers. The aims of the present study are to characterize the optical, hole burning properties of TO-PRO-3 and their changes upon binding to DNAs in order to explore the feasibility of using the nonphotochemical hole burning technique for imaging and diagnosis of biological systems. We are interested in whether the hole burning characteristics of the dye (hole growth kinetics, hole width, electron phonon coupling) change depending on the biological environment (in this study we will focus on DNA) and how they are affected in terms of the interaction between the dye and DNA. We used high resolution absorption and fluorescence spectroscopy in conjunction with nonphotochemical hole burning spectroscopy at low temperature. Also the optical and hole burning properties of the homodimeric dye, TO-TO-3, were measured and compared with those of the monomeric dye, TO-PRO-3.
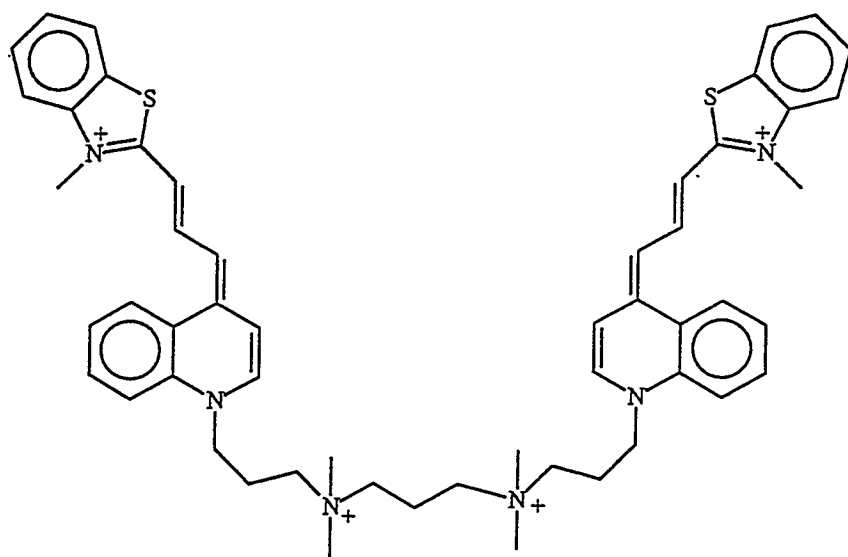
6.2 Materials and methods

Chemicals and sample preparations

TO-PRO-3 and TO-TO-3 iodide were purchased from Molecular Probes, Inc. as a 1mM solution in DMSO and were used without further purification. Double and single
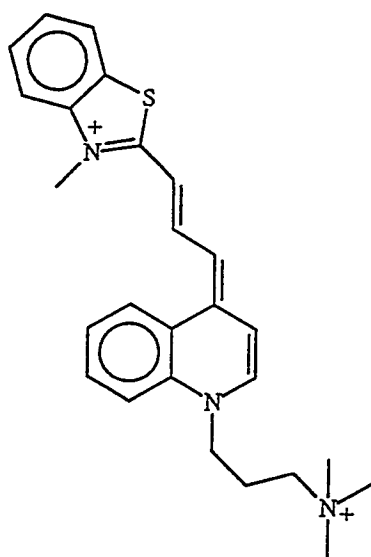
TO-PRO-3

TO-TO-3

Figure 6-1. Chemical structures of TO-PRO-3 and TO-TO-3.

stranded calf thymus DNA were purchased from Sigma Inc. Phosphate buffer was used for DNA sample preparation (20 mM disodium phosphate, 100 mM NaCl, pH 7.0 filtered through a 0.22 μm pore size filter for sterilization). DNA concentration was determined by measuring the absorbance of corresponding solutions at 258 nm. The following extinction coefficients at 258 nm were used for each DNA solution [33]: double-stranded calf thymus DNA, 6.6×10^3 $M^{-1}cm^{-1}$; single-stranded calf thymus DNA, 1.0×10^4 $M^{-1}cm^{-1}$. Samples were made as follows unless stated otherwise. For absorption measurement, TO-PRO-3 sample was made by adding 30 % water and 70 % glycerol to make a final dye concentration of 30 μM. TO-PRO-3 with DNA solutions were made in 60 % phosphate buffer and 40 % glycerol with dye and DNA concentration of, 30 μM and 600 μM of base pairs ($1:20_{bp}$), respectively. For fluorescence excitation and emission measurements, dye and DNA concentrations were reduced to 3 μM and 60 $μM_{bp}$, respectively. In order to avoid the precipitation of dye-DNA complexes and possible artifacts due to slow binding equilibrium kinetics, the aqueous DNA solution was added to the aqueous dye solution followed by glycerol. For TO-TO-3 absorption measurements, 50 μM TO-TO-3 solutions were made in a 1:4:5 (v/v/v) DMSO:water:glycerol solvent, and 10 μM TO-TO-3 with 500 $μM_{bp}$ DNA solutions were made in 60 % phosphate buffer and 40 % glycerol. For TO-TO-3 fluorescence measurements, the dye concentration was reduced to 5 μM and the DNA concentration was increased to 900 $μM_{bp}$.

Absorption measurements

Absorption spectra of samples were measured with Bruker IFS 120 HR Fourier transform infrared spectrometer (FT-IR) over the range from 25000 to 10000 cm^{-1} . The spectra were measured with a 1 cm^{-1} resolution for the hole burning experiments and with

a 4 cm-1 resolution for simple absorption measurements. The sample solution was placed between two quartz plates separated by an o-shaped teflon spacer (1 mm thick) and the quartz plates were mounted in a copper sample holder with screws. The sample solution was first cooled slowly to 77 K by cold nitrogen vapor in order to produce an optically clear glass, then cooled further to liquid helium temperature in a cryostat for hole burning studies or kept at liquid nitrogen temperature for a simple low temperature absorption measurements. The sample temperature was measured with a silicon diode thermometer mounted on the copper sample holder. The hole burning light source was a Coherent 699-29 ring dye laser (DCM Special dye) pumped by an argon ion laser (6 W output). With the intracavity etalons installed, the hole burning laser line width was ≤ 20 MHz. The sample was placed at a 45 degree angle to both the burning laser beam and the probe beam from the FT-IR. The burning laser beam was defocused to illuminate the whole sample while the probe beam was not.

Fluorescence excitation measurements

A Coherent 699-29 ring dye laser pumped by an argon ion laser (6 W output) was used for the hole burning and as the fluorescence excitation source. DCM Special dye was used giving a tuning range from 615 nm to 706 nm. For hole burning and high resolution scans (scanning for hole width), the intracavity etalons were installed giving a laser line width of ≤ 20 MHz. The wavelength was continuously monitored with a Burleigh wavemeter. The dye laser output power was stabilized with a laser amplitude stabilizer and monitored with a power meter equipped with a diode. The laser power density for the hole burning was varied with density filters within the range of 250 nW/cm^2 to 300 $\mu W/cm^2$. For the fluorescence excitation spectra before and after burning, the laser was attenuated to ~ 250 nW/cm^2. The laser illuminated ~ 0.35 cm^2 area of a sample. The sample solutions in quartz tubes (2 mm i.d.) were first cooled

slowly to liquid nitrogen temperature then cooled to liquid helium temperature in a cryostat. The temperature was measured with a silicon diode thermometer mounted on the copper frame which holds the sample. Fluorescence from the sample was long pass filtered and detected with an RCA C31034 photomultiplier tube. The signal from the photomultiplier tube was amplified and digitized with a Stanford Research Systems SR-400 photon counter.

Fluorescence emission measurements

The excitation source used for fluorescence emission measurements was a Lambda-Physik Lextra 100 XeCl excimer laser system providing high energy (200 mJ/pulse) pulses with a repetition rate of up to 100 Hz at 308 nm. Typically, attenuated laser output (30 mW/cm^2 intensity) was used. A double-nested glass low temperature cryostat was used for optical experiments at 77 K. Sample in quartz tubes (2 mm i.d.) were directly immersed in liquid nitrogen to obtain spectra at 77 K. The collected fluorescence was dispersed by a McPherson 2016 1-meter focal length monochromator and detected by a Princeton Instruments IRY 1024/G/B intensified photodiode array. A 150 grooves/mm grating was employed providing 150 nm window and 0.8 nm resolution. No time resolved detection system was employed.

6.3   Results and Discussions

Absorption and Fluorescence emission measurements

Absorption (frame A) and fluorescence emission (frame B) spectra of TO-PRO-3 free in solution, TO-PRO-3 bound to double-, and TO-PRO-3 bound to single-stranded

calf thymus DNA at low temperature are shown in Figure 6-2. TO-PRO-3, and TO-PRO-3 bound to DNAs exhibit similar absorption maxima around 640 nm at 4.2 K. The emission maxima at 77 K, however, are very different: ~642.3 nm, 649.5 nm and 660.6 nm for the dye, the dye bound to double-stranded calf thymus DNA, and to single-stranded calf thymus DNA, respectively. The fluorescence emission band of the free dye gradually shifted blue when its concentration was varied from 30 μM to 0.5 μM. The most blue shifted emission resulting in the smallest Stoke's shift 39 cm^{-1} is shown in the figure. The dye bound to double-stranded calf thymus DNA has similar FWHM as free dye in absorption, but there is an extra contribution on the red side of the absorption band. Fluorescence emission band of the dye bound to the double-strand DNA is very broad and its maximun is shifted red than that of the free dye. The dye bound to single-stranded calf thymus DNA shows the largest FWHM of absorption band because of an additional absorption on the red side of the absorption band, and the most red shifted emission.

Spectral hole burning measurement

A hole burned spectrum for TO-PRO-3 bound to double-stranded calf thymus DNA is shown in Figure 6-3. At the fluence used, the zero phonon hole (ZPH) is not saturated. The broad pseudo-phonon side band hole (see the inset of the figure) is located at ~30 cm^{-1} lower energy side of the ZPH. The anti-hole structure is not very clear due to interference by the real phonon side band hole to the high energy side of the ZPH. Hole burned spectra with deeper ZPH reveal the anti-hole structure more clearly indicating that the hole burning mechanism of the dye is nonphotochemical (see Figure 6-4).
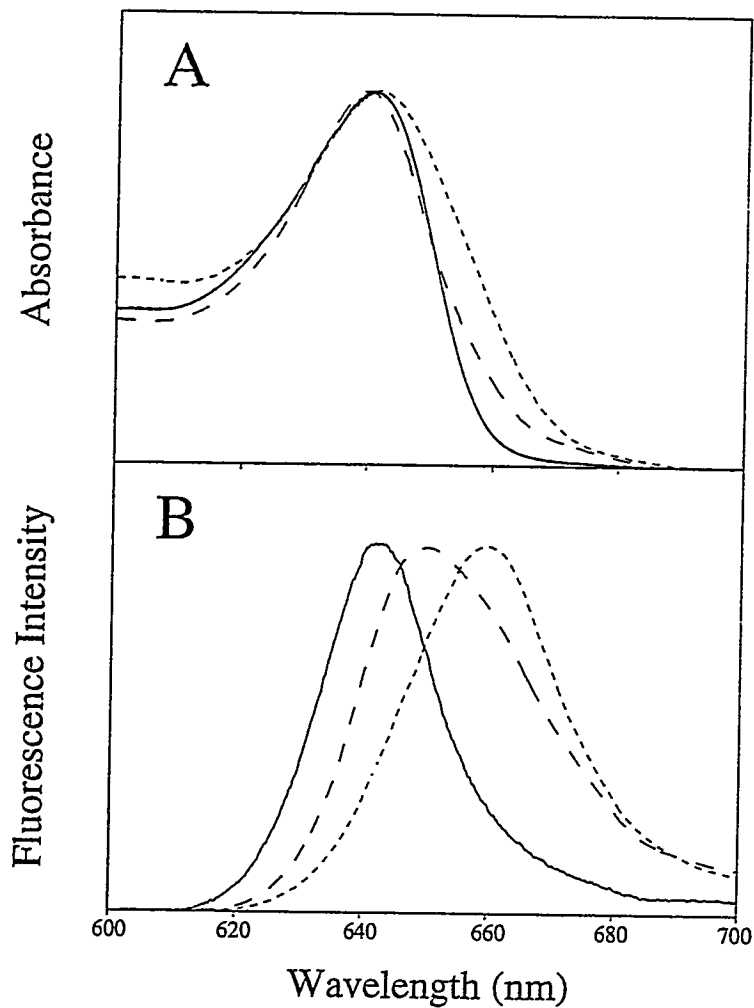
Figure 6-2. Absorption (frame A) and fluorescence emission (frame B) spectra of TO-PRO-3 (solid line) and TO-PRO-3 bound to double-stranded calf thymus DNA (dashed line) and single-stranded calf thymus DNA (dotted line). Absorption spectra are acquired at 4.2 K. For fluorescence emission measurement at 77 K, excitation wavelength was 308 nm.
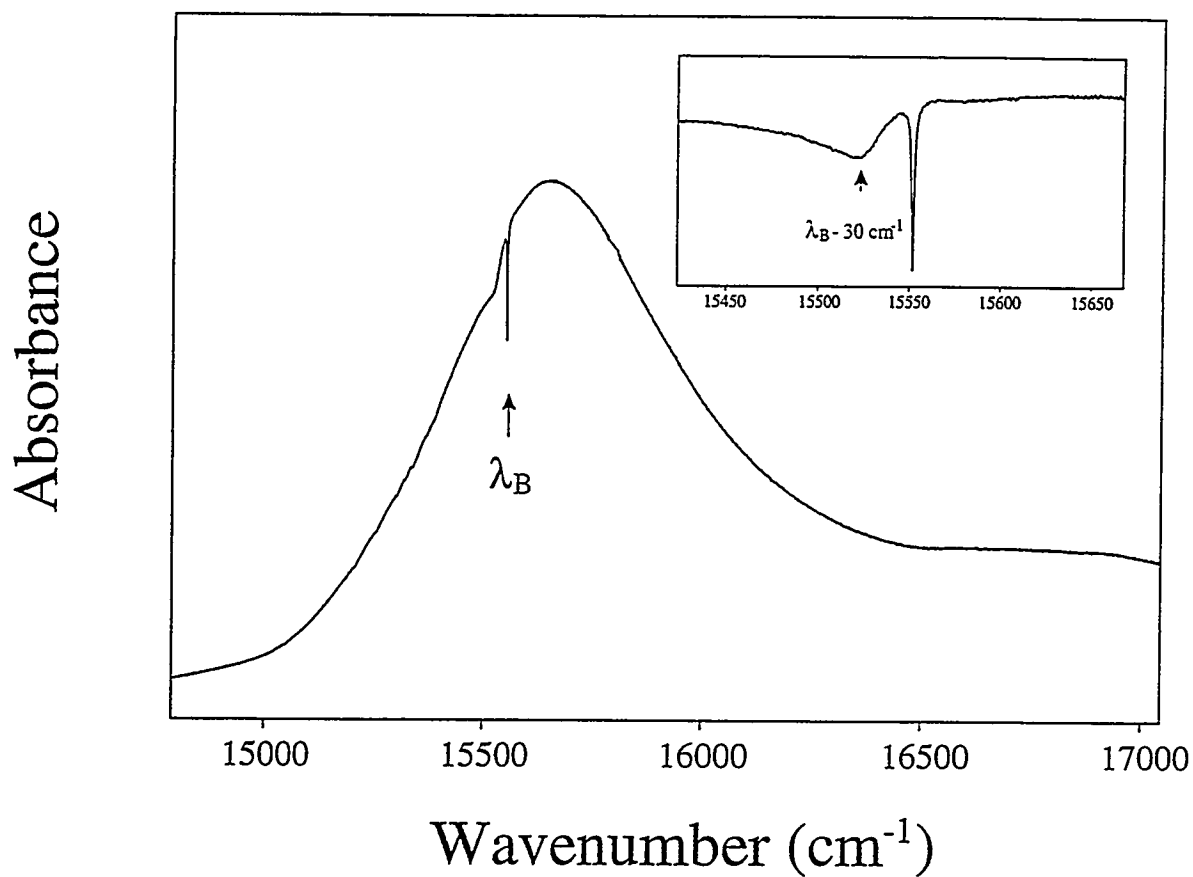
Figure 6-3. Hole-burned spectrum of TO-PRO-3 bound to double-stranded calf thymus DNA at 5 K. The burn wavelength ,λ_B = 643 nm; burn intensity, 20 mW/cm^2; burn time, 5 sec. The inset shows the difference spectrum of hole-burned and preburn absorption spectra. The broad pseudo-phonon side band hole is displaced to the red side of λ_B by ~30 cm^{-1}.

In nonphotochemical hole burning, excitation (ω_L) in the origin band yields the ZPH burned at ω_L accompanied by higher energy vibronic satellite holes. If excitation into congested vibronic absorption regions is utilized, vibronic satellite hole structures which are burned into the origin bands are generated in addition to the ZPH at the burn frequency. The displacement of the satellite holes from the burn frequency yields the excited-state frequencies of the Franck-Condon active modes. This is illustrated in Figure 6-4 and Figure 6-5. Figure 6-4 shows difference spectra of TO-PRO-3 and TO-PRO-3 bound to double- and single-stranded calf thymus DNA for λ_B = 650 nm. The figure shows the ZPH at ω_B (laser burn frequency), a broad pseudo-PSBH at the lower energy side of the ZPH, broad real vibronic satellite holes at the higher energy side and pseudo-vibronic holes at the lower energy side of the ZPH. The antihole structure at energies just above ω_B provides evidence that the spectra are produced by nonphotochemical hole burning. It should be noted that the vibronic contribution to the absorption at this wavelength, λ_B, is observed only for the dye bound to DNA as evidenced by the pseudo-vibronic satellite holes at the red side of burn frequency (see curves b and c of Figure 6-4). For the dye without DNA, however, no vibronic contribution to the absorption at this wavelength is observed since no pseudo-vibronic hole exists. Therefore, the observed pseudo-vibronic holes must be from the dye adopting a conformation that is available only when bound to DNA. And the origin band maximum of the dye adopting that conformation must be red shifted compared to the absorpton band maximum ($\sim$ 640 nm, see Figure 6-2) in order to be excited vibronically with λ_B = 650 nm.

Difference spectra for λ_B = 628 nm are shown in Figure 6-5. Satellite hole frequencies of the dye and the dye bound to DNAs are identical except for a few low frequency modes. The 162 cm^{-1} mode exists in free dye and single-stranded calf thymus
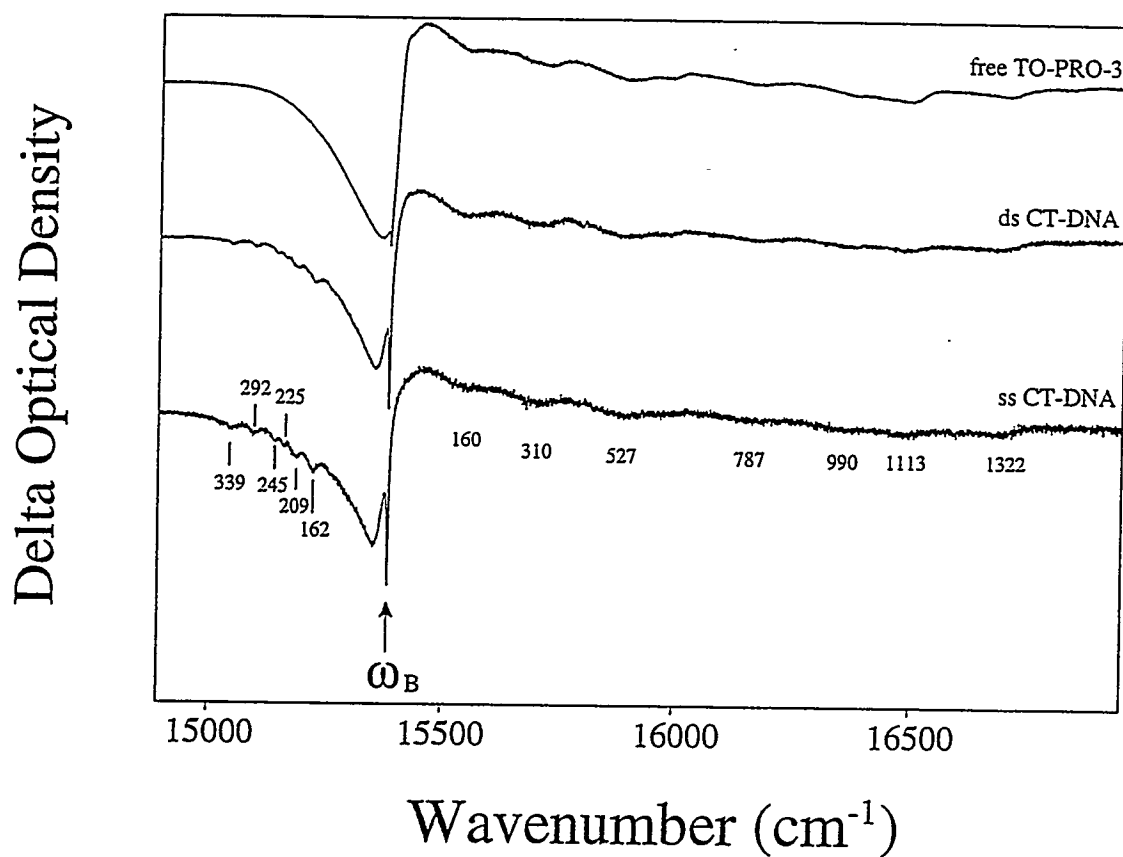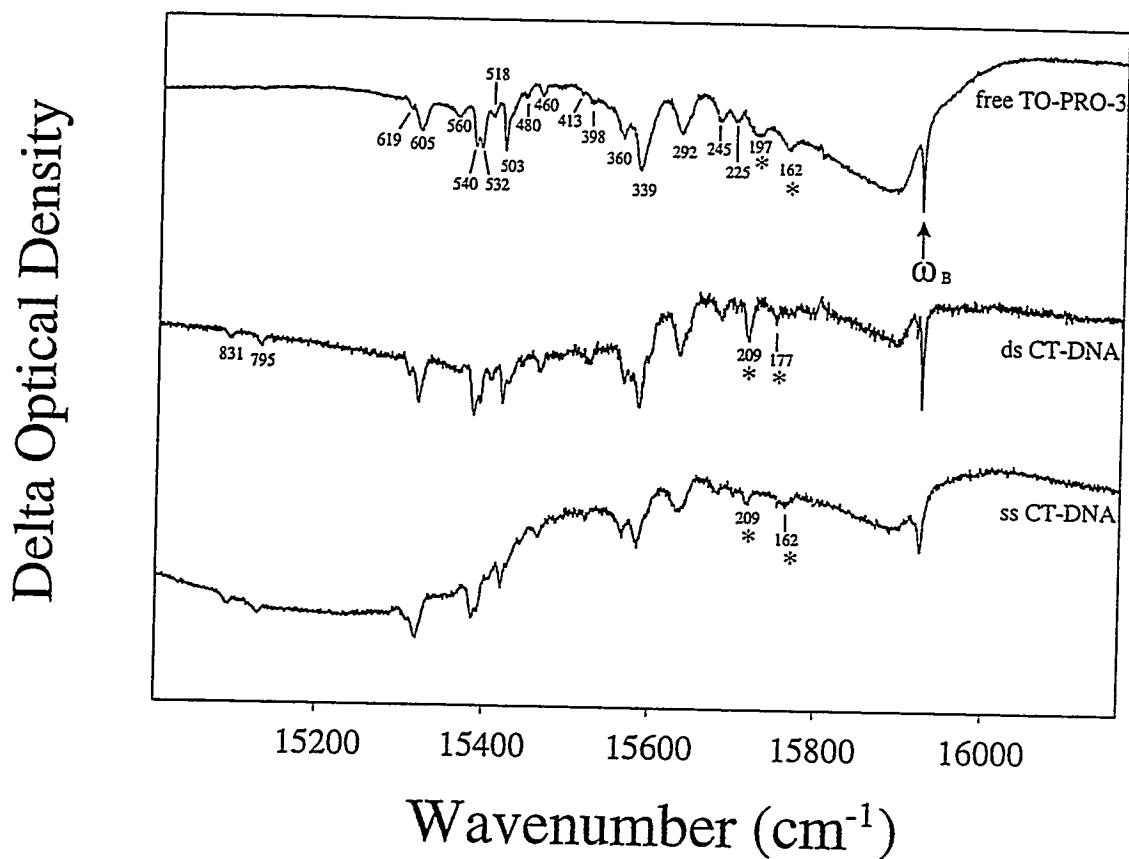
Figure 6-4. Difference hole-burned spectra of TO-PRO-3, and TO-PRO-3 bound to double-stranded and single-stranded calf thymus DNA at 4.2 K. The burn wavelength , λ_B = 650 nm (15384 cm^{-1}); burn intensity, 200 mW/cm^2. Satellite holes are labeled with the excited-state vibrational frequencies (cm^{-1}).

Figure 6-5. Difference hole-burned spectra of TO-PRO-3, and TO-PRO-3 bound to double-stranded and single-stranded calf thymus DNA at 4.2 K. The burn wavelength $,\lambda_B$ = 628 nm (15924 cm^{-1}); burn intensity, 200 mW/cm^2. Satellite holes are labeled with excited-state vibrational frequencies (cm^{-1}). An asterisk is used to label the mode which is distinctive (see the text).

DNA but loses its intensity in double-stranded calf thymus DNA. The 177 cm^{-1} mode is more active in double-stranded CT-DNA. The 197 cm^{-1} mode is active only in free dye while the 209 cm^{-1} mode is active only in DNA samples. These distinctive modes are labeled with an asterisk in the spectra of Figure 6-5. The relative intensity distributions of the satellite holes in the spectra are different, indicating that the Franck-Condon factor of each vibrational mode varies depending on the environment of the dye molecule. It is noted that very broad satellite holes exist at ∼ 15400 cm^{-1} and ∼ 15250 cm^{-1} in the cases of the dye bound to double- and single-stranded calf thymus DNA, respectively. The broad holes must be related to the dye adopting a conformation which is different from the ones producing sharp satellite holes. The position of the broad holes corresponds to shoulder (at ∼ 655 nm) in the absorption band of DNA samples (compare to Figure 6-2). Considering the broadness and the position of the holes, the conformation(s) responsible for the broad holes seems to have strong stacking interaction with DNA bases which may eventually results in a charge transfer between the DNA base and the dye.

The excited-state fundamental vibrational frequencies and their measured Franck-Condon factors for TO-PRO-3 without DNA are shown in Table 6-1. These Franck-Condon factors were obtained using the method described by Gillie and Small [34]. The table illustrates that all intramolecular Franck-Condon factors are small. Therefore, we conclude that the linear electron-intramolecular vibration coupling for TO-PRO-3 is very weak, with the maximum Frank-Condon factor (equivalent to Huang-Rhys factor S contributed from intramolecular vibration) measured being ∼0.09. The linear electron-phonon coupling (S, intermolecular) estimated from the Stoke's shift 39 cm^{-1} = $2S\omega_m$ (ω_m = 30 cm^{-1}) is 0.65, and is considerably stronger than any of the intramolecular vibrations.

Table 6-1. Vibrational frequencies and Franck-Condon factors for TO-PRO-3 obtained by nonphotochemical hole burning at 4.2 K.

S_1 vibrational frequencies (cm-1)	Franck-Condon factors
158*	0.0241
162	0.0115
197	0.0183
225	0.0069
245	0.0115
292	0.0340
310*	0.0195
339	0.0600
360	0.0316
398	0.0031
413	0.0008
460	0.0050
480	0.0007
503	0.0044
518	0.0006
527*	0.0299
532	0.0025
540	0.0027
560	0.0132
605	0.0374
614*	0.0040
619	0.0050
787*	0.0221
990*	a
1113*	0.0906
1322*	0.0208

Frequencies labeled with an asterisk were obtained from vibronic holes (Figure 6-4). Franck-Condon factors were obtained from pseudo-vibronic holes (Figure 6-5).
a. The calculated value is included in the value of 1113 cm^{-1} mode.

164

Conformational equilibrium of TO-PRO-3 bound to DNA

A shoulder in the absorption band, the broad and skew shaped emission band of the TO-PRO-3 bound to double-stranded calf thymus DNA indicate that the dye adopts more than one conformation. As indicated by the broad hole observed in vibronically excited hole burning spectrum, the dye binds to the double-stranded DNA with a strong base stacking interaction in addition to an external binding. Figure 6-6 shows the two different dye conformations contributing to an emission spectrum of the dye bound to double-stranded calf thymus DNA. The curve a is the emission spectrum of the dye bound to double-stranded calf thymus DNA, and the curve b is the emission spectrum of TO-PRO-3 free in solution representing the emission from the dye externally bound to DNA. Note that the curve a -b can generate the emission from the dye adopting a conformation(s) other than the external conformation; an base-stacked conformation because the maximum is red shifted and the band is broader than those of the external conformaion. A similar conformational equilibrium was observed in the case of the dye bound to single-stranded calf thymus DNA with more contribution from a base stacked conformation than when bound to double-stranded DNA (data not shown).

It would be reasonable to assume that TO-PRO-3 strongly interacting with the DNA (base-stacked conformation) is responsible for the broad satellite holes produced when burned at λ_B = 650 nm (see Figure 6-5), and TO-PRO-3 weakly interacting with the DNA (externally bound conformation) is responsible for the sharp satellite holes. As an attempt to verify this assumption, the linear electron phonon coupling constants of the dye adopting the former and the latter conformation were estimated. Figure 6-7 shows the observed broad satellite hole (maximum at 656.0 nm) of the dye bound to single-stranded calf thymus DNA, and the emission (maximum at 662.9 nm) spectrum of the
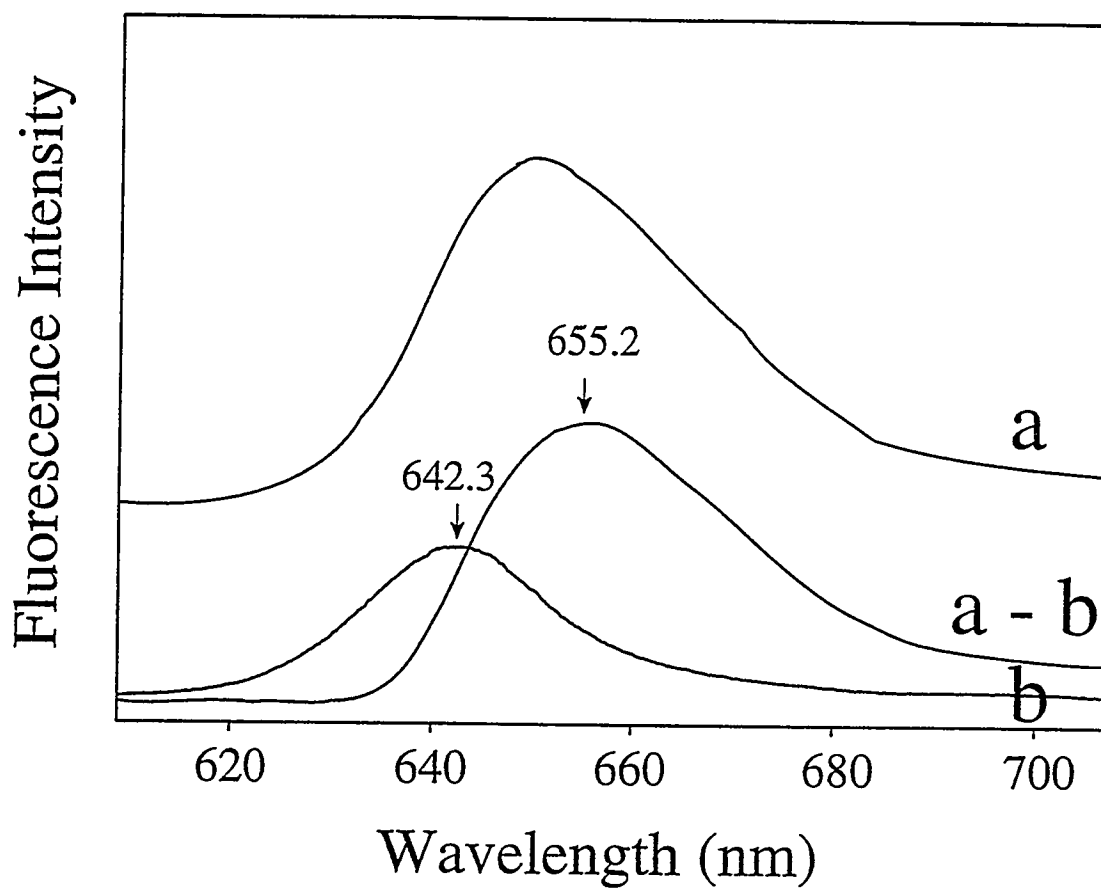
Figure 6-6. The conformational equilibrium of TO-PRO-3 bound to double-stranded calf thymus DNA. The fluorescence emission spectrum of TO-PRO-3 bound to double-stranded calf thymus DNA (curve a), and the emission spectrum of 0.5 μM free TO-PRO-3 solution (curve b). Curve a - b is obtained by subtracting the curve b from the curve a. T = 77 K, λ_{ex} = 308 nm.
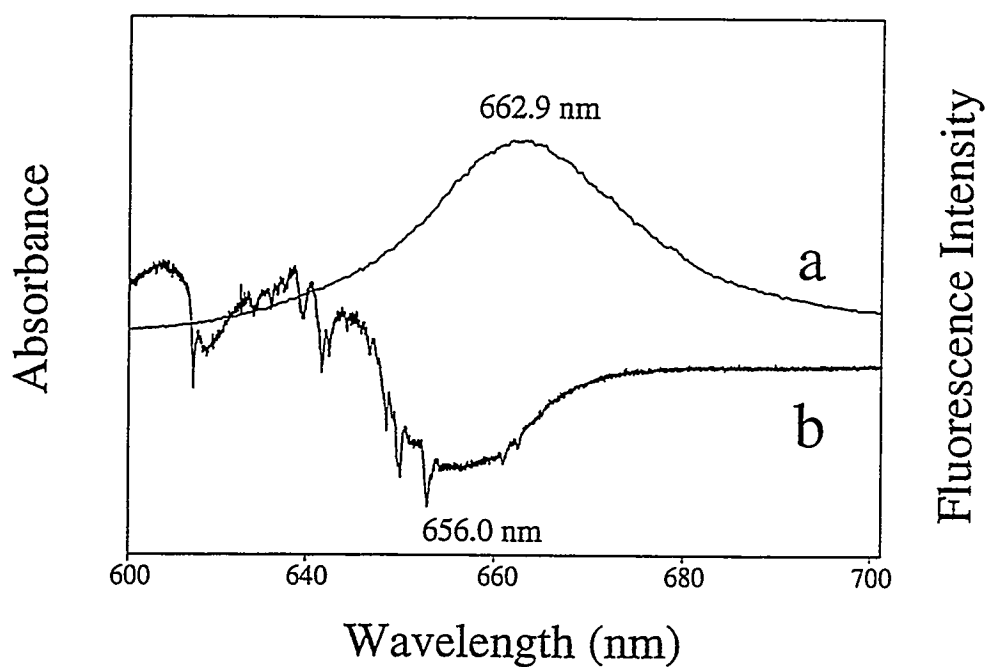
Figure 6-7. Base-stacked conformation of TO-PRO-3 bound to single-stranded calf thymus DNA. The fluorescence emission spectrum (curve a) of TO-PRO-3 bound to single-stranded calf thymus DNA and difference hole-burned absorption spectrum (curve b) at 4.2 K. The emission spectrum was obtained by subtracting the contribution from the externally bound dye at T = 77 K.

dye bound to single-stranded calf thymus DNA after subtracting the contribution from the externally bound dye. The Stoke's shift form the two spectra is estimated to be 159 cm^{-1} resulting in S value (a measure of linear electron phonon coupling) as 2.64 for the base-stacked conformation. Similarly, the S value for the dye bound to double-stranded DNA was calculated from the broad satellite hole observed with $\lambda_B = 650$ nm (curve b of figure 6-5) and from the fluorescence emission of the dye after subtracting the contribution from the externally bound dye (curve a - b of figure 6-6). For S value of the dye externally bound to the DNA, the absorption maximum the dye bound to DNA and the emission maximum of the free dye were used. The estimated Stoke's shifts and S values are listed in Table 6-2. As indicated in S values, the linear electron phonon coupling strength of the base-stacked conformation (strong, S > 1) are much larger than that of the external conformation (weak, S < 1).

Dispersive hole growth kinetics

Hole growth kinetics curves of free TO-PRO-3 and of TO-PRO-3 bound to double- and single-stranded calf thymus DNA at 4.2 K are shown in Figure 6-8. Considering dispersion of hole formation kinetics, the time-dependent hole depth, 1 - D(t), is described by D(t) [35]:

$$D(t) = (2\pi)^{-1/2} \int_{-\infty}^{\infty} dx \exp[-x^2/2] \exp[-\Sigma_0 \xi(x)t]$$

with $\Sigma_0 = P\sigma\Omega_0\tau$ where P is the burn photon flux, σ is the peak absorption cross section, τ is the excited state lifetime, and Ω_0 is the prefactor in the Fermi-Golden rule expression for the extrinsic two level system (TLS$_{ext}$) relaxation rate, R, for nonphotochemical hole burning, $R = \Omega_0 \exp(-2\lambda)$ where λ is the tunnel parameter for TLS$_{ext}$ assumed to be a Gaussian with a center at λ_0 and a standard deviation σ_λ [36]. The integration variables $x = (\lambda - \lambda_0)/\sigma_\lambda$ and $\xi(x) = \exp[-2(\lambda_0-\sigma_\lambda x)]$. As pointed out by

Table 6-2. Absorption and emission characteristics of TO-PRO-3 bound to DNAs at low temperature.

Conformation	λ_{max} (abs.) in nm	λ_{max} (em.) [a] in nm	Stoke's shift in cm^{-1}	Huang-Rhys factor (S) [b]
without DNA	640.7	642.3	39	0.65
ds DNA / External	640.2	642.3	51	0.85
ds DNA / Base-stacked	649.0	655.2	146	2.43
ss DNA / External	641.0	642.3	32	0.53
ss DNA / Base-stacked	656.0	662.9	159	2.64

a. For the emission maximum of the external conformation of the dye bound to DNAs, the emission maximum of the dye without DNA is used.

b. Huang-Rhys factors (S) are estimated from Stoke's shift $= 2S\omega_m$, where ω_m is the mean phonon frequency.
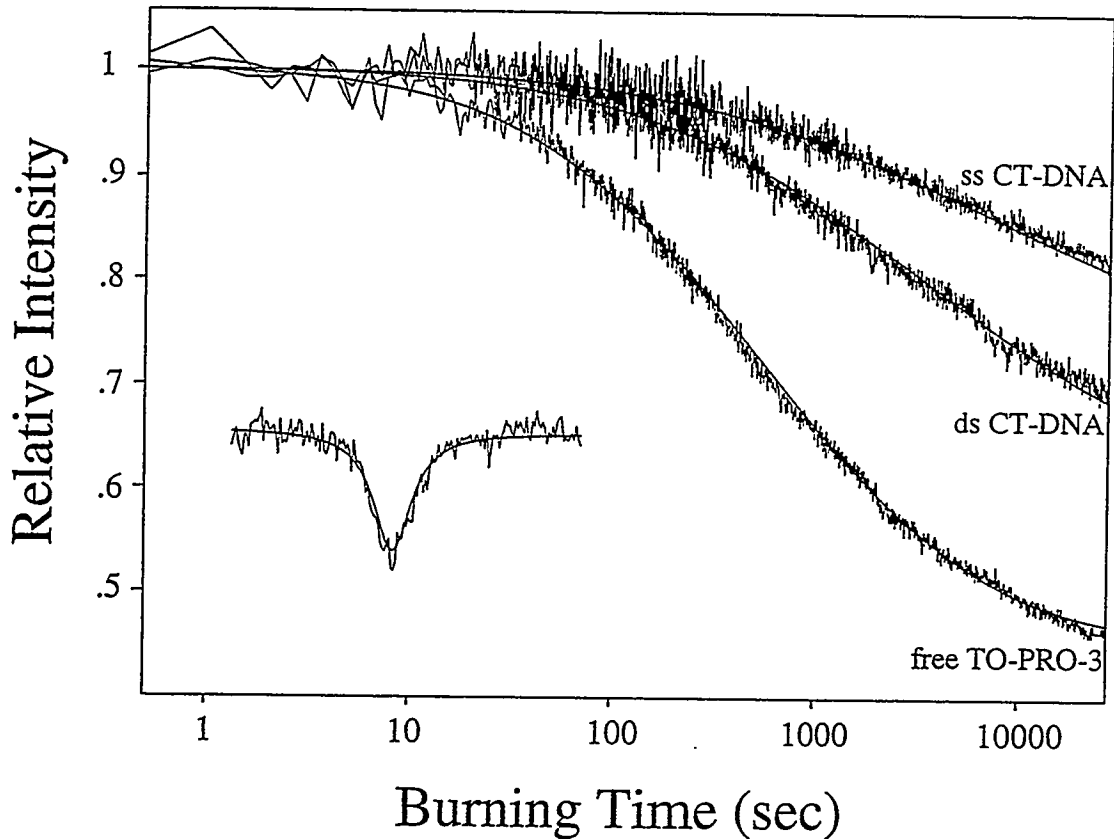
Figure 6-8. Hole growth curves (noisy lines) and theoretical fits (smooth lines) of TO-PRO-3, and TO-PRO-3 bound to double-stranded and single-stranded calf thymus DNA at 4.2 K.   The burn wavelength ,λ_B = 650 nm; burn intensity, 270 nW/cm^2. The fits are obtained with the following parameters: S = 0.61, λ_0 = 7.8 and σ_λ = 0.86 for dye with no DNA, and 0.94, 8.8, 1.1 for with double-stranded DNA, and 1.3, 9.1, 1.3 for with single-stranded DNA, respectively (for detailed fitting equation and parameter values, see the text). The inset is the hole shape for single-stranded calf thymus sample with the hole width 6.0 GHz estimated from a hole burned less than 5 %.

Kenney et al. [35], when fitting hole growth data, the measured depth of the ZPH peak is normalized to the maximum hole depth given by e^{-S} (S is the Huang-Rhys factor). The value of σ, the absorption cross section, was determined by scaling the room temperature to low-temperature homogeneous widths as determined from the room temperature absorption width and the hole width measured at low temperature. It was observed that the hole widths ranged from 6 GHz to 11 GHz depending on the depth of the hole. The narrowest width observed in the short burn limit, 6.0 GHz, was used for the fit. The same hole width, 6.0 GHz, was used for all 4.2 K kinetic curve fittings since the hole widths of various samples- TO-PRO-3 and TO-PRO-3 with various DNAs- were practically identical within the limit of experimental error. The fluorescence lifetime, τ, was measured at 77 K as 3.5 ns for free TO-PRO-3 and 3.9 ns for TO-PRO-3 bound to double-stranded calf thymus DNA (data not shown). For single-stranded and other DNAs, 3.9 ns was also used for fitting. For Ω_0 value, 7.6×10^{12} s^{-1} was used as in reference [37]. The hole growth kinetics data are fit to 1 - D(t) in order to determine S, λ_0 and σ_λ. Excellent fits of the calculated curves with the experimental data were obtained. The parameters used for the fits are S = 0.61, λ_0 = 7.8 and σ_λ = 0.86 for the dye without DNA, and 0.94, 8.8, 1.1 for the dye bound to double-stranded calf thymus DNA, and 1.3, 9.1, 1.3 for the dye bound to single-stranded calf thymus DNA, respectively. Uncertainty of the calculated parameters is ≤ 10 %. λ_0 value is less accurate than S and σ_λ values since all possible experimental uncertainties (e.g. hole width, life time of excited state and burn photon flux) will influence this value while other parameters are hardly affected. It is also worth noting that the calculated S value may be underestimated since we used a high laser power densities for the later time points of the kinetic curves, where burning may occur through the absorption by phonon side bands even after the ZPH has reached its saturation depth.

The dye molecule can exist in several conformations (due to various binding modes, sites etc.), therefore, it is likely that we burn a certain conformation(s) more than others at this burn wavelength (650 nm). The dye bound externally to DNA will be burned more through its ZPH than the dye intercalated (or base-stacked) since the linear electron phonon coupling of the dye adopting the latter conformation is much larger than that adopting the former conformation. The calculated S values from hole growth kinetics contain information on the conformation burned through ZPH (the coupling strength between the dye and DNAs), and of a conformation(s) where the dye is coupled very strongly to its environment. Note the S value of the free dye obtained from the saturated hole depth (0.61) is in good agreement with the S value estimated from Stoke's shift (0.65, see Table 2) since there is only one conformation in the case of the free dye. However, for the dye bound to double- and single-stranded calf thymus DNA, S values obtained from hole growth kinetics are between those of external and of base-stacked conformations obtained from Stoke's shifts; compare 0.94 with 0.85 and 2.43, and 1.3 with 0.53 and 2.64 for double- and single-stranded DNA, respectively. This discrepancy in S values indicates that the dye exists in a mixture of conformations when bound to DNA. The S value of the dye bound to single-stranded DNA obtained from hole growth kinetics is larger than that of the dye bound to double-stranded DNA, indicating that the contribution from the dye adopting base-stacked conformation in the single-stranded DNA is larger than that in the double-stranded DNA. The calculated λ_0 and σ_λ values primarily represent the average dispersive kinetic behavior of the dye adopting the conformation(s) which can be burned through ZPH (external conformation). It is noted that σ_λ is larger in the single-stranded DNA (1.3) than in the double-stranded DNA (1.1).

Spectroscopic studies of TO-TO-3

The absorption and the fluorescence emission spectra of the homodimeric dye TO-TO-3, and the dye bound to double-stranded calf thymus DNA are shown in Figure 6-9. The absorption maximum is 648.9 nm for the free dye and 643.7 nm for the dye bound to double-stranded DNA. It is noted that the absorption maximum of the free TO-TO-3 is red shifted compared to the monomeric dye (TO-PRO-3, ~641 nm), indicating that there is an intramolecular stacking interaction in the dimeric dye (compare with figure 6-2 frame A). Also the spectral shape of TO-TO-3 bound to DNA is very similar to that of the TO-PRO-3 spectrum, but free TO-TO-3 shows more absorption at the high energy side of the band. The similar intramolecular stacking interaction (exciton coupling) was observed with YOYO and other cyanine dyes [38] and explained in terms of a charge transfer between two monomeric systems stacked with parallel orientation [32]. A very similar charge transfer may also occur with the monomeric dye (TO-PRO-3) since the fluorescence emission of the monomeric dye shifts red as the dye concentration increases (data not shown).

The hole growth kinetic curves for TO-TO-3 and TO-TO-3 bound to double- and single-stranded calf thymus DNA are shown in Figure 6-10. The dye bound to double- and single-stranded DNA show the hole formation kinetic behavior similar to the monomeric dye: the dye bound to double-stranded calf thymus DNA burns deeper than the one bound to single-stranded calf thymus DNA. However, the hole formation kinetic behavior of TO-TO-3 without DNA is very different compared to monomeric TO-PRO-3 (compare figure 6-10 with 6-8). TO-TO-3 burns much less deep than TO-PRO-3 due to intramolecular stacking interaction between the two monomeric units. Another indication of the intramolecular stacking interaction is provided by the fluorescence life times of the dimeric dye and the monomeric dye measured at 77 K. Fluorescence life times were 2.9
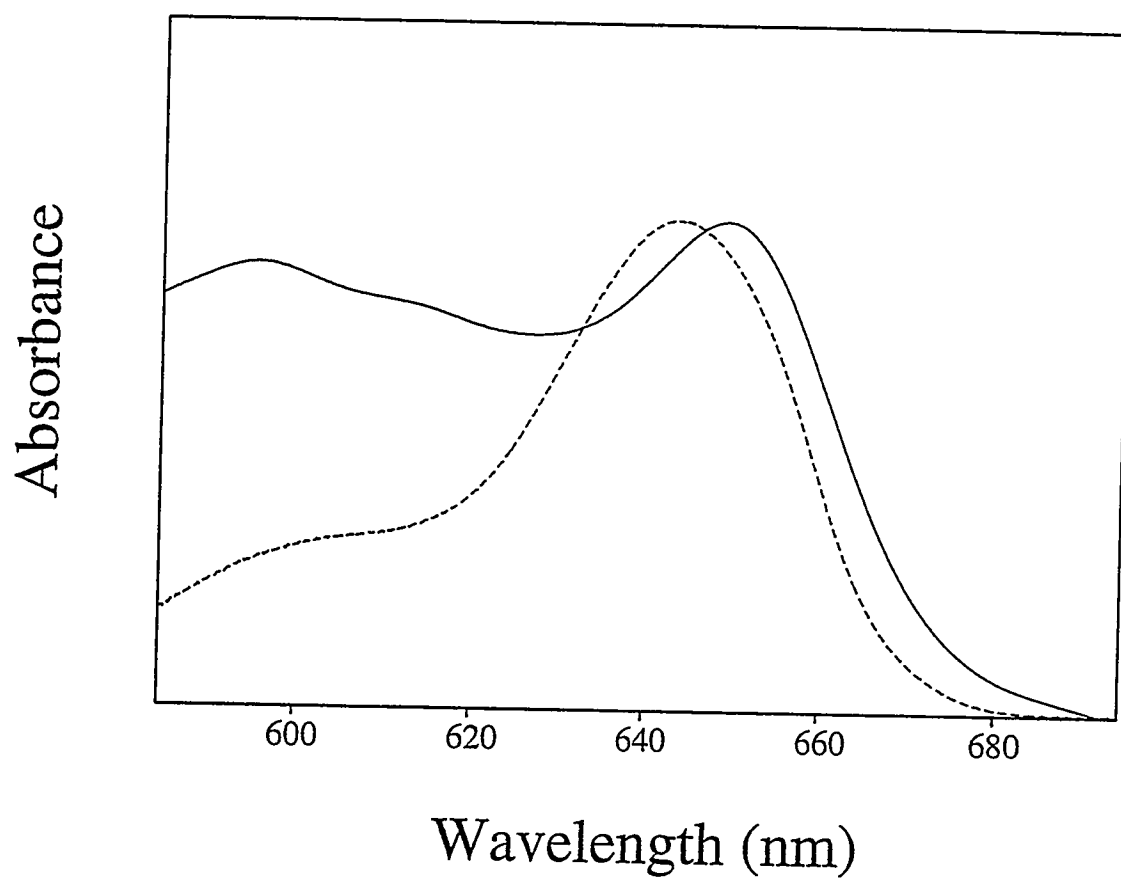
Figure 6-9. Absorption spectra of TO-TO-3 (solid line) and TO-TO-3 bound to double-stranded calf thymus DNA (dashed line) at 77K.
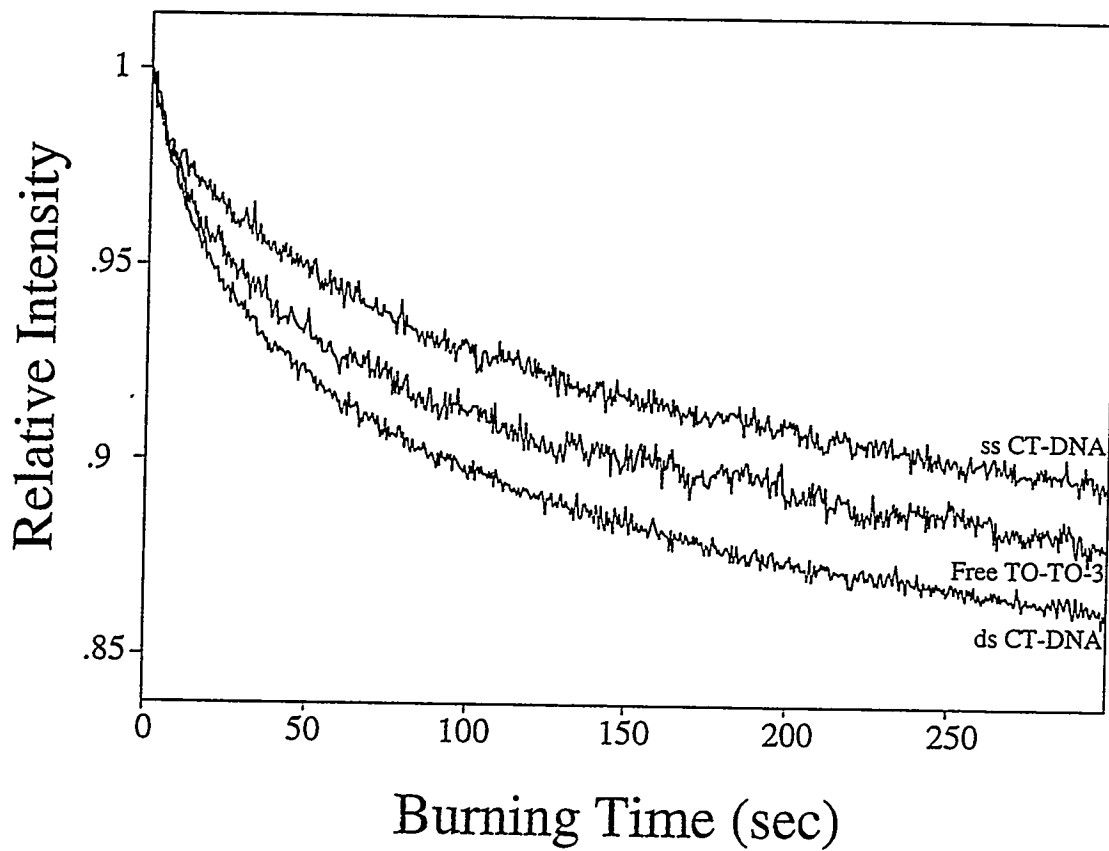
Figure 6-10. Hole growth curves of TO-TO-3, and TO-TO-3 with double-stranded and single-stranded calf thymus DNA at 5 K. The burn wavelength ,λ_B = 659 nm; burn intensity, 1.4 μW/cm².

ns and 4.0 ns for free TO-TO-3 and TO-TO-3 with ds CT-DNA, respectively. The fluorescence life time of TO-TO-3 with ds CT-DNA, 4.0 ns, is very similar to that of TO-PRO-3 with ds CT-DNA, 3.9 ns, while the free dyes show substantial differences in life time, 2.9 ns for TO-TO-3 and 3.5 ns for TO-PRO-3 (data not shown). No further investigation was carried out because of the poor solubility of the dye-DNA complexes at low temperatures.

Structure of TO-PRO-3 bound to DNAs

Unlike the structures of their mother compounds (TO-PRO-1 and TO-TO-1 which is a homodimeric form of TO-PRO-1, both compounds have the chromophore made with benzothiazol and quinolinium rings linked by a methylene unit) which have been investigated by high resolution NMR spectroscopy in solution recently [31], the detailed structures of TO-PRO-3 and TO-TO-3 have not been established. It was found [31] that TO-TO-1 bisintercalated between base pairs in solution with an unwinding of the DNA helix by 60 ° and an increase in base pair stacking distance from 3.6 to 6.7 Å. Also the propeller twist angle of DNA bases increased at and near the binding sites. The two rings (benzothiazol and quinolinium ring) showed sequence preferences- benzothiazol ring preferred to intercalate between two pyrimidine bases while quinolinium ring intercalated between purine bases. Since the only difference between the molecular formula of TO-PRO-3 and TO-PRO-1 is an extra ethylene unit added between the benzothiazol and the quinolinium ring for TO-PRO-3, it has been assumed that the binding geometry of two molecules are similar [39]. However, the extra ethylene unit of TO-PRO-3 is very critical in determining whether the chromophore unit (two rings and the link) can intercalate between base pairs or not. It is obvious that the whole chromophore unit can not be accommodated between base pairs since the size change by the extra ethylene unit

is significant, ~3 Å, unless the DNA undergoes an extreme structural distortion such as melting of the duplex structure. Therefore the dye primarily binds externally to DNA followed by a slow conversion to the base-stacked conformation. The observed base-stacked conformation of the TO-PRO-3 when bound to double-stranded DNA is probably a partial intercalation of the chromophore unit (either a quinoline ring or a benzo-1,3-thiazole ring) . Similarly, a partial bisintercalation of the dimeric dye TO-TO-3 can be suggested.

It is evident that there is more contribution from base-stacked conformation in the case of single-stranded calf thymus DNA than in the case of double-stranded calf thymus DNA. The absorption and emission spectrum of TO-PRO-3 bound to single-stranded DNA show more contribution at the red side of the bands. Dispersive hole growth kinetics of TO-PRO-3 bound to single-stranded calf thymus DNA showed a S value 1.3 that is larger than that of the dye bound to double-stranded DNA (0.94). A similar trend in saturated hole depth was observed with TO-TO-3. Also, the absorption and emission maxima of the base-stacked conformation of TO-PRO-3 bound to single-stranded DNA are red shifted compared to those of the dye bound to double-stranded DNA. This is probably due to the structural flexibility of single-stranded DNA. The more flexible single-stranded DNA can arrange bases to interact more with the dye than double-stranded DNA.

6.4 Concluding Remarks

In this study, we have shown that optical and hole burning properties of TO-PRO-3 depend on its environment. We found that the saturated hole depth of TO-PRO-3 decreased dramatically when bound to DNA, and the saturated hole depth of the dye bound to double-stranded calf thymus DNA is deeper than that in single-stranded calf

thymus DNA. Hole growth kinetic parameters λ_0 and σ_λ of TO-PRO-3 increased when the dye bound to DNA. Unlike the saturated hole depth and hole growth kinetics, the hole width of TO-PRO-3 bound to DNA remained practically the same. The absorption bands maxima of the free dye, the dye bound to double-stranded DNA and the dye bound to single-stranded DNA are very similar while the emission maxima are different; in an increasing order of red shift, free dye < dye bound to double-stranded DNA < dye bound to single-stranded DNA. From the very broad satellite holes in vibronic hole burning spectra and the red shifted emission bands of TO-PRO-3 bound to double- and single-stranded DNAs, it is concluded that there is a binding mode(s) which results in a strong coupling between the dye and DNA (base-stacked conformation) in addition to an external binding mode. The conformational distribution of the dye bound to DNA is found to be responsible for the observed optical and hole burning properties. The homodimeric dye TO-TO-3 also showed that the hole growth kinetic property depended on its environment. Without DNA, the dimeric dye seems to have the stacking interaction between two intramolecular monomeric units. The stacking interaction is disrupted by forming a complex with DNA.

Since the hole burning properties are sensitive to the environment of the probe molecule, by selecting appropriate probe molecule, it would be highly possible that this technique can be applied to imaging and diagnosis of biological systems. In order to understand the detailed nature of changes of optical and hole burning properties, further investigation is necessary.

6.5 Prospect of Nonphotochemical Hole Burning for Imaging and Diagnosis

There are many chemical and physical characteristics of cancer cells that can distinguish them from normal cells [40,41]. Among them, high nucleus-to-cytoplasm

ratio and prominent nucleoli [42,43] are the characteristics that may be utilized for hole burning imaging and diagnosis. When transformed cells in culture are studied, the following characteristics are found with malignant cells: lost requirement for adherence, alteration of cell surface and change in cytoskeleton [44-47]. Transformed cells generally lose the requirement for adherence; they grow without attachment to a substratum, therefore, they are more round shaped. Since the properties of transformed cells relating to growth and behavior are probably consequences of cell surface events, cell surface changes are becoming important subject for studying cell transformation. Probably the most important difference is that the proteins of the cell surface are much more mobile in transformed cells than in normal cells. Because the lipids are not intrinsically more mobile, it is believed that links between surface proteins and the underlying cytoskeletal elements are modified by transformation. Also, there are differences in the cytoskeleton. The actin microfilaments that span the length of normal cells are either diffusely distributed or concentrated beneath the cell surface.

It is possible to choose a dye molecule that binds specifically to target biological systems. Based on the chemical and physical changes of cancer cells or transformed cells, many investigations using nonphotochemical hole burning of organelle or biological molecule specific dyes are possible. For example, an investigation of nuclei using DNA and RNA binding dyes and nonphotochemical hole burning for imaging and diagnosis is feasible. Many membrane binding dyes and protein binding dyes can be used to study the critical cell surface alteration upon transformation. For the cytoskeleton changes, actin specific dyes can be utilized. Nonphotochemical hole burning as a function of pressure is certainly applicable to study surface alteration and cytoskeleton changes, which are often accompanied by a change in compressibility.

References

1. Jankowiak,R., Hayes,J.M., and Small,G.J. (1993) *Chem. Rev.* **93**, 1472.

2. Jankowiak,R., Cooper,R.S., Zamzow,D., Small,G.J., Doskocil.J., and Jeffrey,A.M. (1988) *Chem. Res. Toxixol.* **1**, 60.

3. Flöser,G., and Haarer,D. (1988) *Chem. Phys. Lett.* **147**, 288.

4. Hayes,J.M. and Small,G.J. (1995) *SPIE* **2385**, 115.

5. Kenney,M.J., Jankowiak,R., and Small,G.J. (1990) *Chem. Phys.*, **146**, 40.

6. Kim,W.-H., Reinot,T., Hayes,J.M. and Small,G.J. (1995) *J. Phys. Chem.* **99**, 7300.

7. Narasimhan,L.R., Littau,K.A., Pack,D.W., Bai,Y.S., Elschner,A., and Fayer,M.D. (1990) *Chem. Rev.* **90**, 439.

8. Völker,S. (1989) *Annu. Rev. Phys. Chem.* **40**, 499.

9. Meijers,H.C., and Wiersma,D., (1992) *Phys. Rev. Lett.* **68**, 381.

10. Furusawa,A. Horie,K., Suzuki,T., Madrida,S., and Mita,I. (1990) *Appl. Phys. Lett.* **57**, 1.

11. Zollfrank,J., Friedrich,J., and Parak,F. (1992) *Biophys. J.* **61**, 716.

12. Haugland,R.P. (1992) *Handbook of Fluorescent Probes and Research Chemicals, 5th ed.* (Larison, K.D. Ed.) Molecular Probes, Inc.

13. Liu,Z., Bushnell,W.R., and Brambl,R. (1987) *Plant Physiol.* **84**, 1385.

14. Septinus,M., Seiffert,W., and Zimmermann,H.W. (1983) *Histochemistry* **79**, 443.

15. Bereiter-Hahn, J. (1976) *Biochim. Biophys. Acta* **423**, 1.

16. Terasaki,M., Chen,L.B., and Fujiwara,K. (1986) *J. Cell Biol.* **103**,1557.

17. Terasaki,M., and Jaffe,L.A. (1991) *J. Cell Biol.* **114**, 929.

18. Pagano,R.E., Sepanski,M.A., and Martin,O.C. (1989) *J. Cell Biol.* **109**, 2067.

19. Lipsky,N.G., and Pagano,R.E. (1985) *Science* **228**, 745.

20. Koval,M., and Pagano,R.E. (1989) *J. Cell Biol.* **108**, 2169.

21. Persky,B. and McGarvey,T. (1990) *Histochem. J.* **22**, 624.

22. Young,V.B., Falkow,S., and Schoolnik,G.K. (1992) *J. Cell. Biol.* **116**, 197.

23. Sanger,J.M. (1990) *Proc. Natl. Acad. Sci. USA* **87**, 5474.

24. Polzar,B. (1989) *Eur. J. Biochem.* **182**, 267.

25. Rye,H.S., Yue,S., Wemmer,D.E., Quesada,M.A. Haugland,R.P., Mathies,R.A., Glazer,A.N. (1992) *Nucleic Acids Res.* **20**, 2803.

26. Selvin,P. (1992) *Science* **257**, 885.

27. Glazer,A.N., and Rye,H.S. (1992) *Nature*, **359**, 859.

28. Rye,H.S., Debora,J.M., Quesada,M.A., Mathies,R.A., and Glazer,A.N. (1993) *Anal. Biochem.* **208**, 144.

29. Larsson,A. Carlsson,C., Jonsson,M., and Albinsson,B. (1994) *J. Am. Chem. Soc.* **116**, 8459.

30. Jacobsen,J.P., Pedersen,J.B., Hansen,L.F., and Wemmer,D.E. (1995) *Nucleic Acids Res.* **23**, 753.

31. Spielmann,H.P., Wemmer,D.E., and Jacobsen,J.P. (1995) *Biochemistry* **34**, 8542.

32. Carlsson,C., Larsson,A., Jonsson,M., Albinsson,B., and Nordén,B. (1994) *J. Phys. Chem.* **98**, 10313.

33. Wells et al. (1970) *J. Mol. Biol.* **54**, 465.

34. Gillie,J.K., and Small,G.J. (1989) *J.Phys. Chem.* **93**, 1620.

35. Kenney,M.J., Jankowiak,R., and Small,G.J. (1990) *Chem. Phys.*, **146**, 40.

36. Jankowiak,R., Small,G.J., and Athreya,K.B. (1986) *J. Phys. Chem.* **90**, 3896.

37. Moerner,W.E., Lenth,W., Bjorklund,G.C. (1988) In *Topics in Current Physics, Persistent Spectral Hole Burning: Science and Applications* (Moerner,W.E.,Ed) Springer-Verlag. Berlin, Heidelberg, Vol. 44, Chapter 7, p251.

38. West,W., Pearce,S. (1965) *J. Phys. Chem.* **69**, 1894.

39. Benson,S.C., Mathies,R.A., and Glazer,A.N. (1993) *Nucleic Acid Res.* **21**, 5720.

40. Liss,A.R. (1985) *Molecular Basis of Cancer* (Rein,R. Ed.) Part A and B.

41. Darnell,J.E., Lodish,H., and Baltimore,D. (1986) *Molecular Cell Biology*, Scientific American Books, New York, Chapter 23.

42. Cairns,J. (1975) *Nature* **255**,197.

43. Nicholson,G.L. (1979) *Sci. Am.* **240**(3), 66.

44. Abercrombie,M. (1970) *In Vitro* **6**, 128.

45. Holley,R.W., and Kiernan,J.A. (1968) *Proc. Nat'l. Acad. Sci. USA* **60**, 300.

46. Hynes,R.O. Ed. (1979) *Surface of Normal and Malignant Cells*, Wiley

47. Hynes,R.O. (1976) *Biochim. Biophys. Acta* **458**, 73.

CHAPTER 7. GENERAL CONCLUSIONS

The conformational characteristics of the four stereochemically distinct *anti*-BPDE modified duplexes d(CCATCGCTACC)·(GGTAGCGATGG) by *trans* or *cis* addition of the exocyclic amino group of guanine to the C10 posion of either (+)- or (-)-*anti* BPDE depend on the stereochemistry of the bound BPDE. The (+)-*trans* adduct adopts primarily an external conformation with only minor interactions with the helix, but a smaller fraction (~25 %) appears to exists in a partially base-stacked conformation while the (-)-*trans* adduct exists almost exclusively (~ 97 %) in an external conformation. Both *cis* adducts adopt an intercated conformation with only a very minor contribution with a more solvent-exposed character. It is also concluded that perturbation of the overall helical structure is the most significant for the (+)-*trans* adduct than the other adducts.

5'-Flanking base of the BPDE lesion site affects the conformations of the *trans* adduct of (+)-*anti*-BPDE to N^2-guanine in the 11-mer oligonucleotides, d(CTATG$_1$G$_2$G$_3$TATC). In single-stranded form, the adduct at G$_2$ or G$_3$ (5'-flanking base is guanine) adopts a conformation with strong interaction with the bases. In contrast, the (+)-*trans-anti*-BPDE adduct with a 5'-flanking thymine exists in a primarily helix-external conformation. Similar conformational equilibria exist in the double-stranded oligonucleotides. 3'-Flanking base has little influence on the conformational equilibrium of the (+)-*trans-anti*-BPDE adduct.

More than 80 % of BPDE adducts formed after topical application of benzo[*a*]pyrene (BP) to the skin of mice are (+)-*trans*- and (+)-*cis-anti*-BPDE-N^2-dG adduct to DNA. Total BPDE adduct level formed in DNA isolated from the skin of mice reaches the maximum at 24 hours after the BP treatment, then declines rapidly until 4

days after the treatment and much more slowly thereafter. The (+)-*cis-anti*-BPDE-N^2-dG adducts are repaired more slowly than most other adducts. The (+)-*trans-anti*-BPDE-N^2-dG adducts adopts base-stacked, partially base-stacked and helix external conformations *in vivo*. The adducts in the base-stacked conformation are repaired less readily than the external adducts.

Optical and hole burning properties of fluorescent DNA binding dyes TO-PRO-3 and TO-TO-3 depend on their DNA environment. Stoke's Shifts, saturation hole depths and dispersivenesses of hole growth kinetics of TO-PRO-3 change as the DNA types, sequences and lengths change. However, the hole width remains practically the same unlike the other hole burning properties. The dye can exist in various conformations depending on the binding modes, and the conformational equilibrium depends on the DNA types, sequences and lengths. Among the conformations of the dye, there is a conformation(s) that is strongly coupled to the DNA resulting in the charge transfer between the dye and DNA bases. TO-TO-3 have the stacking interaction between two intramolecular monomeric units which is disrupted by forming a complex with DNA.

ACKNOWLEDGMENTS

APPENDIX A. OPTICAL AND HOLE BURNING CHARACTERISTICS OF TO-PRO-3 BOUND TO DNA; EFFECTS OF DNA SEQUENCE AND SIZE

Introduction

TO-PRO-3 is a DNA binding dye with a quinoline moiety connected to a benzo-1,3-thiazole moiety (see Figure 6-1 for the chemical structures) [1]. TO-TO-3 is a homodimer of two TO-PRO-3 units. The aims of the present study are to characterize the optical, hole burning properties of TO-PRO-3 bound to DNAs as a function of DNA sequences and sizes. The optical and hole burning characteristics of the dye (hole growth kinetics, hole width, electron phonon coupling, HB efficiency) change depending on the biological environment (such as DNA types, sequences, lengths etc.) were studied using high resolution absorption and fluorescence spectroscopy in conjunction with nonphotochemical hole burning spectroscopy at low temperature. The conformational equilibrium of the dye bound to DNA will be discussed with observed spectroscopic data.

Materials and methods

Chemicals and sample preparations

TO-PRO-3 and TO-TO-3 iodide were purchased from Molecular Probes, Inc. as a 1 mM solution in DMSO and were used without further purification. Double and single stranded calf thymus DNA were purchased from Sigma Inc.. Poly(dA-dT)·poly(dA-dT) and poly(dG-dC)·poly(dG-dC) were also purchased from Sigma Inc.. Oligonucleotides were synthesized and subsequently purified by HPLC at Nucleic Acid Facility of Iowa State University. Phosphate buffer was used for DNA sample preparation (20 mM disodium phosphate, 100 mM NaCl, pH 7.0 filtered through a 0.22 μm pore size filter for sterilization). DNA concentration was determined by measuring the absorbance of corresponding solutions at 258 nm. The following extinction coefficients at 258 nm were used for each DNA solution [2]: double-stranded calf thymus DNA, 6.6×10^3 $M^{-1}cm^{-1}$; single-stranded calf thymus DNA, 1.0×10^4 $M^{-1}cm^{-1}$; poly(dA-dT)·poly(dA-dT), 6.8×10^3 $M^{-1}cm^{-1}$; poly(dG-dC)·poly(dG-dC), 8.4×10^3 $M^{-1}cm^{-1}$; single stranded oligonucleotides, 1.0×10^4 $M^{-1}cm^{-1}$.

Samples were made as follows unless stated otherwise. For absorption measurement, TO-PRO-3 sample was made by adding 30 % water and 70 % glycerol to make a final dye concentration of 30 μM. TO-PRO-3 with DNA solutions were made in 60 % phosphate buffer and 40 % glycerol with dye and DNA concentration of, 30 μM and 600 μM of base pairs ($1:20_{bp}$), respectively. For fluorescence excitation and emission measurements, dye and DNA concentrations were reduced to 3 μM and 60 $μM_{bp}$, respectively. In order to avoid the precipitation of dye-DNA complexes and possible artifacts due to slow binding equilibrium kinetics, the aqueous DNA solution was added to the aqueous dye solution followed by glycerol.

Absorption measurements

Absorption spectra of samples were measured with Bruker IFS 120 HR Fourier transform infrared spectrometer (FT-IR) over the range from 25000 to 10000 cm^{-1} . The spectra were measured with a 4 cm-1 resolution. The sample solution was placed between two quartz plates separated by an o-shaped teflon spacer (1 mm thick) and the quartz plates were mounted in a copper sample holder with screws. The sample solution was first cooled slowly to 77 K by cold nitrogen vapor in order to produce an optically clear glass, then kept at liquid nitrogen temperature for a low temperature absorption measurements. The sample temperature was measured with a silicon diode thermometer mounted on the copper sample holder.

Fluorescence excitation measurements

A Coherent 699-29 ring dye laser pumped by an argon ion laser (6 W output) was used for the hole burning and as the fluorescence excitation source. DCM Special dye was used giving a tuning range from 615 nm to 706 nm. For hole burning, the intracavity etalons were installed giving a laser line width of ≤ 20 MHz. For the fluorescence line narrowing measurement, the intracavity etalon was removed from the ring dye laser system and the wavelength was scanned by rotating the birefringent filter stack. In this configuration, the laser line width was 0.1 cm^{-1}. The wavelength was continuously monitored with a Burleigh wavemeter. The dye laser output power was stabilized with a laser amplitude stabilizer and monitored with a power meter equipped with a diode. The laser power density for the hole burning was varied with density filters within the range of 250 nW/cm^2 to 300 μW/cm^2. For the fluorescence excitation spectra before and after burning, the laser was attenuated to $\sim$250 nW/cm^2. The laser illuminated $\sim$0.35 cm^2 area of a sample. The sample solutions in quartz tubes (2 mm i.d.) were first cooled slowly to liquid nitrogen temperature then cooled to liquid helium

temperature in a cryostat. Temperatures lower than 4.2 K were achieved by pumping the cryostat filled with liquid helium. The temperature was measured with a silicon diode thermometer mounted on the copper frame which holds the sample. Fluorescence from the sample was long pass filtered and detected with an RCA C31034 photomultiplier tube. The signal from the photomultiplier tube was amplified and digitized with a Stanford Research Systems SR-400 photon counter.

Fluorescence emission measurements-NLN and FLN

The excitation source used for low resolution fluorescence emission measurements (non-line narrowing, NLN) was a Lambda-Physik Lextra 100 XeCl excimer laser system providing high energy (200 mJ/pulse) pulses with a repetition rate of up to 100 Hz at 308 nm. Typically, attenuated laser output (30 mW/cm^2 intensity) was used for the low resolution fluorescence emission measurement. For fluorescence line narrowing measurements (FLN), a Coherent 699-29 ring dye laser pumped by an argon ion laser (6 W output) with the laser line width ~0.1 cm^{-1} was used as an excitation source. A double-nested glass low temperature cryostat was used for both 4.2 K (FLN) and 77 K (NLN) optical experiments. Sample in quartz tubes (2 mm i.d.) were directly immersed in liquid helium (or liquid nitrogen) to obtain spectra at 4.2 K (or 77 K). The collected fluorescence was dispersed by a McPherson 2016 1-meter focal length monochromator and detected by a Princeton Instruments IRY 1024/G/B intensified photodiode array. For FLN measurement, the monochromator was equipped with a 2400 grooves/mm grating providing 18 nm spectral window at 0.1 nm resolution. For low resolution fluorescence emission spectra (NLN), a 150 grooves/mm grating was employed (150 nm window and 0.8 nm resolution). In both cases, no time resolved detection system was employed.

Results and Discussions

Absorption and Fluorescence emission measurements

Absorption and fluorescence emission spectra of TO-PRO-3 bound to DNAs are illustrated in Figures A-1 and A-2 (for TO-PRO-3, TO-PRO-3 bound to double- and single-stranded calf thymus DNA, see Figure 6-2). The absorption and the fluorescence emission bands of the dye with poly(dG-dC)·poly(dG-dC) in Figure A-1 are red shifted compared to those of the dye with poly(dA-dT)·poly(dA-dT) indicating that the interaction of the dye with DNA depends on the base sequences of the DNA. Interestingly, the absorption and the emission spectra of the double-stranded calf thymus DNA sample are similar to those of poly(dA-dT)·poly(dA-dT) sample but differ from those of poly(dG-dC)·poly(dG-dC) sample. Absorption spectra of duplex 11-mer oligonucleotide sample (d-(CCATCGCTACC)·d-(GGTAGCGATGG)), and poly(dG-dC)· poly(dG-dC) are very similar but their emission spectra are different implying that the interaction of TO-PRO-3 with these DNAs is not the same.

Absorption and emission spectra of TO-PRO-3 bound to single-stranded calf thymus DNA and to 11-mer oligonucleotides are shown in Figure A-2. Note that the DNA length appears to affect the interactions of the dye with DNAs since absorption bands of the dye bound to oligonucleotides are red shifted while emission bands of the dye bound to oligonucleotides are blue shifted compared to those of the dye bound to single-stranded calf thymus DNA. Also, differences in the emission spectra of two 11-mer oligonucleotides samples are noted- the emission band of the d-(GGTAGCGATGG) sample is red shifted and broader than that of the d-(CCATCGCTACC) sample. The difference may be due to a base sequence effect on the interaction of the dye with single-
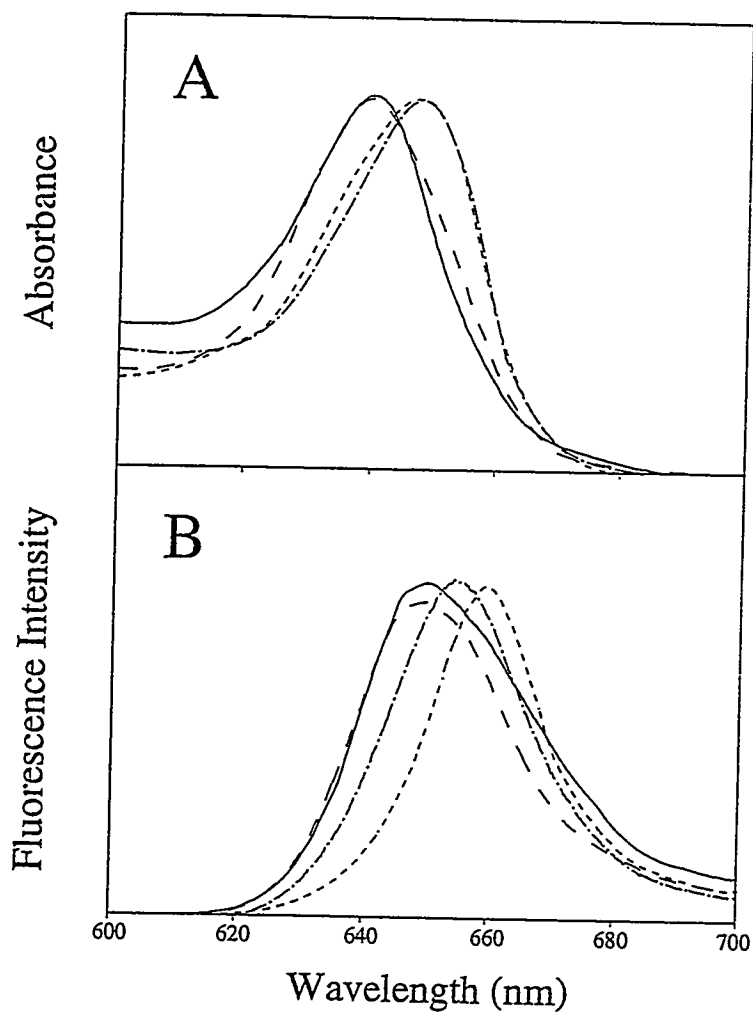
190

Figure A-1. Absorption (frame A) and fluorescence emission (frame B) spectra of TO-PRO-3 bound to double-stranded calf thymus DNA (solid line), poly(dA-dT)·poly(dA-dT) (dashed line), poly(dG-dC)·poly(dG-dC) (dotted line), d-(CCATCGCTACC)·d-(GGTAGCGATGG) (dashed and dotted line); T = 77 K, excitation wavelength was 308 nm.
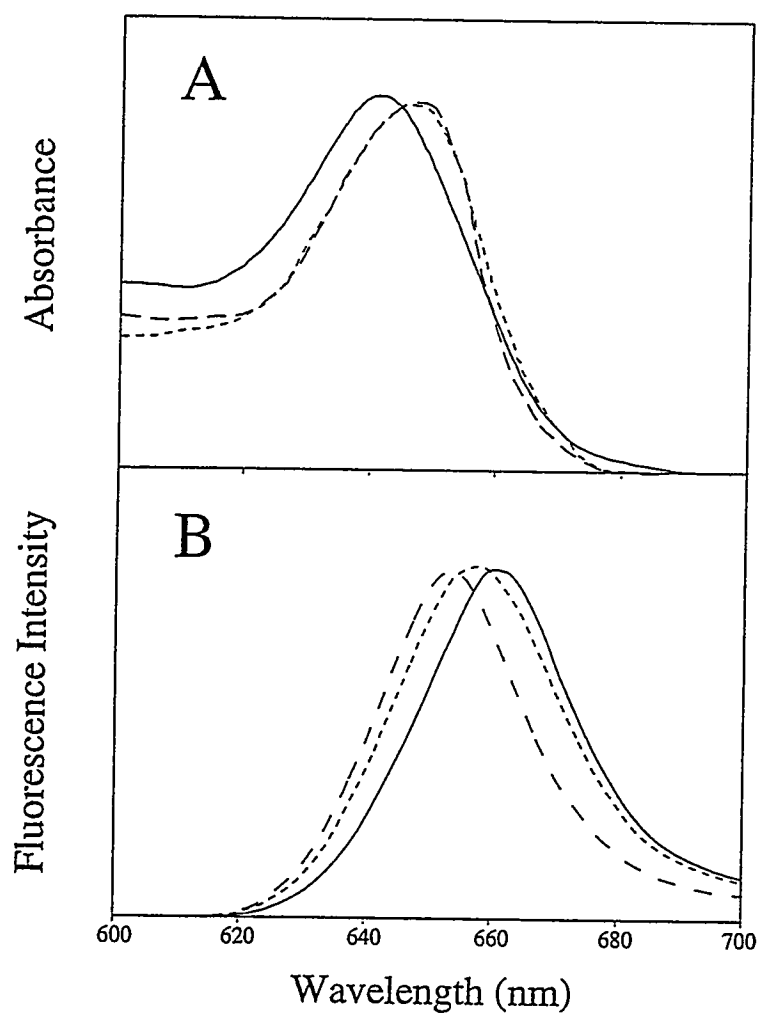
191

Figure A-2. Absorption (frame A) and fluorescence emission (frame B) spectra of TO-PRO-3 bound to single-stranded calf thymus DNA (solid line), d-(CCATCGCTACC) (dashed line) and d-(GGTAGCGATGG) (dotted line); T = 77 K, excitation wavelength was 308 nm.

stranded DNAs. In Table A-1, the absorption and the emission maxima of TO-PRO-3 with various DNAs are summarized.

Spectral hole burning measurement; Hole growth kinetics

The time-dependent hole depth, 1 - D(t), is described by D(t) [3]:

$$D(t) = (2\pi)^{-1/2} \int_{-\infty}^{\infty} dx \exp[-x^2/2] \exp[-\Sigma_0 \xi(x) t]$$

with $\Sigma_0 = P\sigma\Omega_0\tau$ where P is the burn photon flux, σ is the peak absorption cross section, τ is the excited state lifetime, and Ω_0 is the prefactor in the Fermi-Golden rule expression for the extrinsic two level system (TLS_{ext}) relaxation rate, R, for nonphotochemical hole burning, $R = \Omega_0 \exp(-2\lambda)$ where λ is the tunnel parameter for TLS_{ext} assumed to be a Gaussian with a center at λ_0 and a standard deviation σ_λ [4]. The integration variables $x = (\lambda - \lambda_0)/\sigma_\lambda$ and $\xi(x) = \exp[-2(\lambda_0 - \sigma_\lambda x)]$. As pointed out by Kenney et al. [3], in fitting the hole growth data, the measured depth of the ZPH peak is normalized to the maximum hole depth given by e^{-s} (S is Huang-Rhys factor which is a measure of the electron-phonon coupling strength). The same value of σ, the absorption cross section, the hole width, 6.0 GHz, fluorescence life time measured at 77 K (3.9 n) that are used in chapter 6 of this dissertation were used for all 4.2 K kinetic curve fittings. For Ω_0 value, 7.6×10^{12} s^{-1} was used as in reference [5]. The hole growth kinetics data are fit to 1 - D(t) in order to determine S, λ_0 and σ_λ.

Calculated dispersive hole growth kinetic parameters of TO-PRO-3 bound to various DNAs are summarized in Table A-2. Uncertainty of the calculated parameters is less than 10 %. S values of the dye with various DNAs are different reflecting the differences in saturated hole depth. Dispersion of the hole growth kinetics- represented by σ_λ- also depends on the DNA. As mentioned in chapter 6, the calculated S values from hole growth kinetics contain information on the conformation burned through ZPH

Table A-1. Absorption and fluorescence emission characteristics of TO-PRO-3 with various DNAs at low temperature (77 K).

	λ_{max}(abs.) [a] in nm	λ_{max}(em.) [b] in nm
free dye	640.7	642.3
ds CT-DNA	640.2	649.5
poly(dA-dT)·poly(dA-dT)	639.0	649.0
poly(dG-dC)·poly(dG-dC)	647.0	658.0
d(CCATCGCTACC)·d(GGTAGCGATGG)	647.9	654.4
ss CT-DNA	641.0	660.6
d(CCATCGCTACC)	646.8	653.1
d(GGTAGCGATGG)	646.6	657.3

a. TO-PRO-3 and DNA concentrations, except oligonucleotides samples, were 30 μM and 600 μM$_{bp}$ in 60 % phosphate buffer (20 mM disodium phosphate, 100 mM NaCl, pH 7.0) and 40 % glycerol, respectively. For both single and double oligonucleotide samples, 3 μM TO-PRO-3 and 60 μM$_{bp}$ oligonucleotide were used. The free dye, the dye bound to double-stranded calf thymus DNA, and the dye bound to single-stranded calf thymus DNA were measured at T = 4.2 K.

b. For the dye with DNA samples, TO-PRO-3 and DNA concentrations were 3 μM and 60 μM$_{bp}$, respectively. For the free dye sample, 0.5 μM solution was used.

Table A-2. Calculated dispersive hole-growth parameters S, λ_0, and σ_λ of TO-PRO-3 with various DNAs. Holes were burned at 4.2K; burning wavelength, 650 nm; burn intensity, 270 nW/cm^2.

	S	λ_0	σ_λ
free dye	0.61	7.8	0.86
poly(dA-dT)·poly(dA-dT)	0.83	8.9	0.96
ds CT-DNA	0.94	8.8	1.1
poly(dG-dC)·poly(dG-dC)	1.1	8.9	1.2
d(CCATCGCTACC)·d(GGTAGCGATGG)	1.1	9.0	1.2
ss CT-DNA	1.3	9.1	1.3
d(GGTAGCGATGG)	1.8	9.1	1.5

(the coupling strength between the dye and DNAs), and of a conformation(s) where the dye is coupled very strongly to its environment. The calculated λ_0 and σ_λ values represent the average dispersive kinetic behavior of the dye adopting the conformation(s) which can be burned through ZPH.

Hole growth kinetics of TO-PRO-3 bound to poly(dA-dT)·poly(dA-dT) and to poly(dG-dC)·poly(dG-dC) at 2.1 K are shown in Figure A-3. The saturated hole depth of the dye bound to poly(dA-dT)·poly(dA-dT) is deeper than that of the dye bound to poly(dG-dC)·poly(dG-dC). This indicates that the electron phonon coupling of externally bound TO-PRO-3 to GC base pairs is stronger than that to AT base pairs, and/or the contribution from a base-stacked conformation is larger in case of poly(dG-dC)·poly(dG-dC) than for poly(dA-dT)·poly(dA-dT). Parameters for the fit are the same ones used for the fit of hole growth curves measured at 4.2 K except the hole width was corrected according to $T^{1.3}$ law [6] (6.0 GHz at 4.2 K was reduced to 2.4 GHz at 2.1 K). Also λ_0 value was slightly adjusted for a better fit.

The effect of base sequences in hole burning is further demonstrated in Figure A-4. Identical hole formation kinetics for two different double-stranded DNAs, poly(dG-dC)·poly(dG-dC) and d-(CCATCGCTACC)·d-(GGTAGCGATGGA), were observed indicating that DNA sequence is a key factor for hole formation kinetics in the case of double-stranded DNA. The oligonucleotide contains 7 GC base pairs out of 11 base pairs.

Figure A-5 illustrates the dependence of hole formation kinetics on the amount of DNA. It is tempting to speculate that energy transfer between dyes can explain the observed difference. However, we concluded that no energy transfer occurs since no fluorescence emission spectra change was observed when dye to DNA ratio was varied
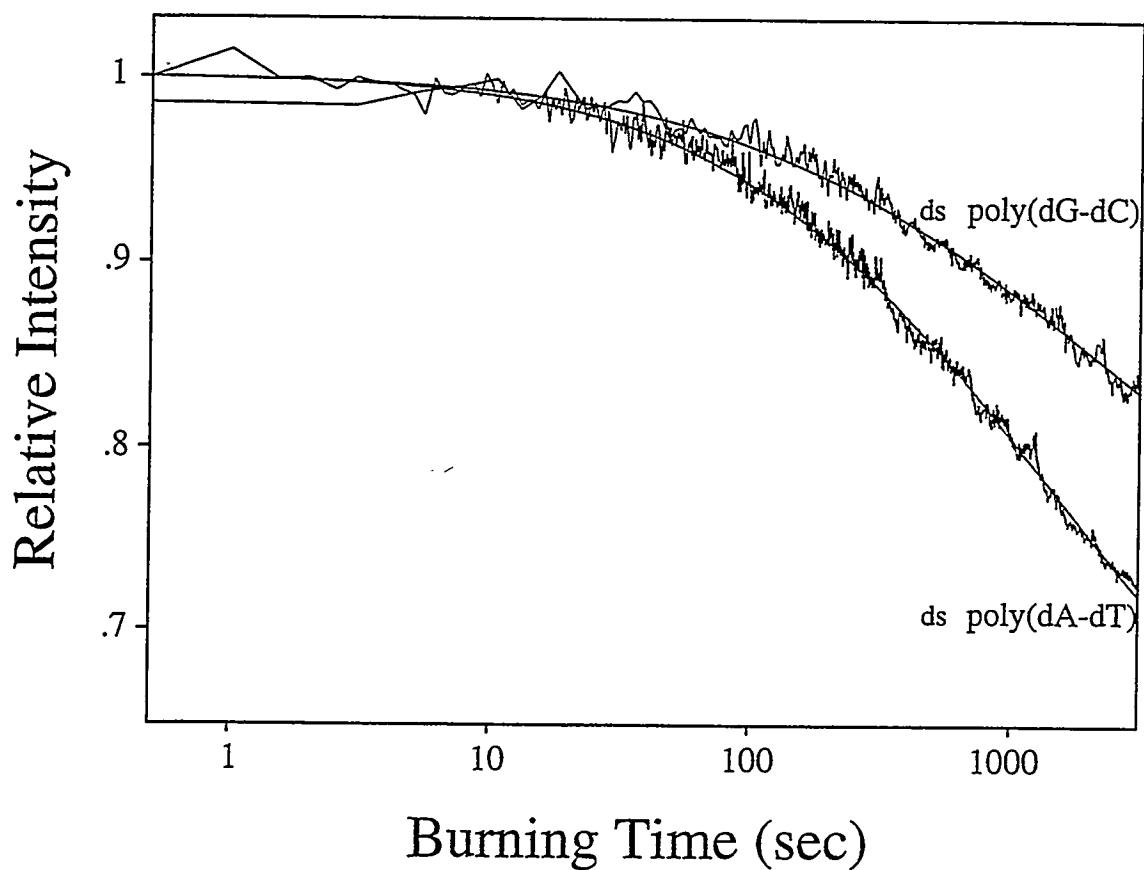
Figure A-3. Hole growth curves with theoretical fits of TO-PRO-3 bound to poly(dA-dT)·poly(dA-dT) and poly(dG-dC)·poly(dG-dC) at 2.1 K. The burn wavelength, λ_B, is 649 nm and the burn intensity is 320 nW/cm^2. The fits are obtained with the following parameters: $S = 0.83$, $\lambda_0 = 8.8$ and $\sigma_\lambda = 0.96$ for poly(dA-dT)·poly(dA-dT), and 1.1, 9.0, 1.2 for poly(dG-dC)·poly(dG-dC), respectively.
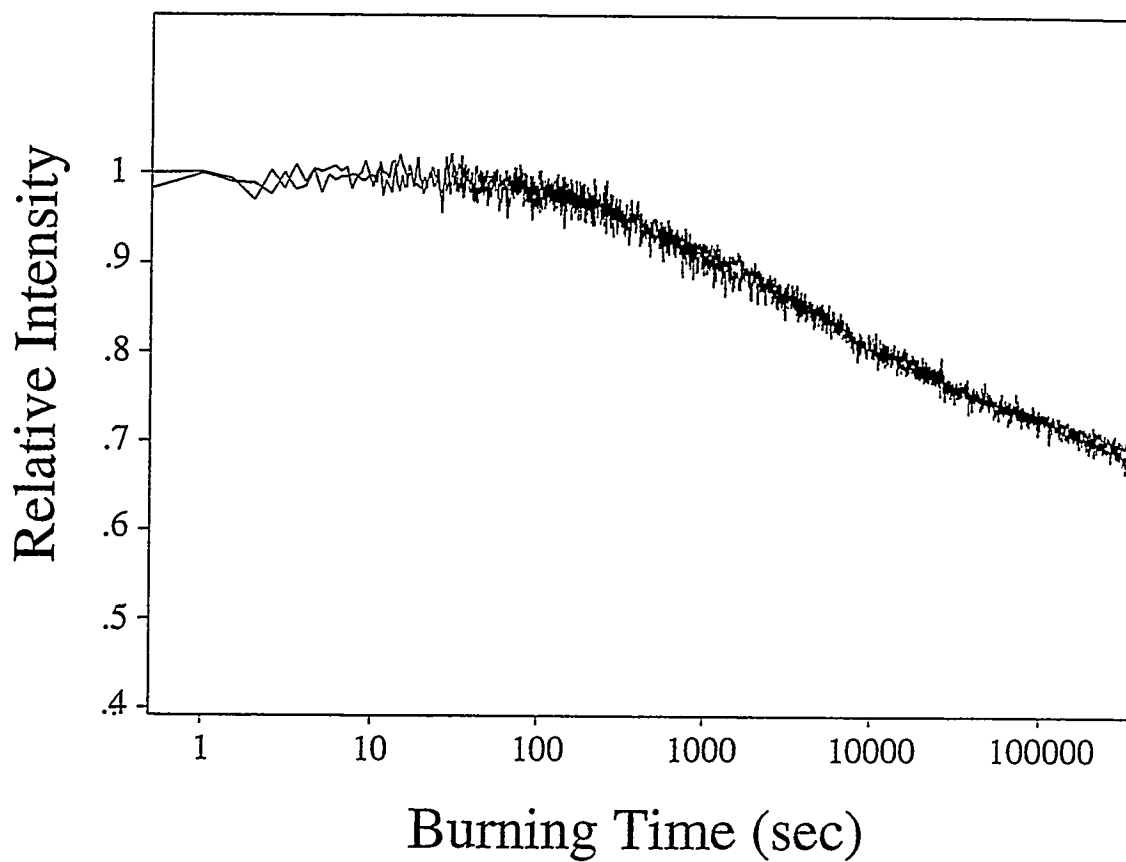
Figure A-4. Hole growth kinetics of TO-PRO-3 bound to poly(dG-dC)·poly(dG-dC) and d-(CCATCGCTACC)·d-(GGTAGCGATGG) AT 4.2 K. The burn wavelength, λ_B = 650 nm, burn intensity, 270 nW/cm^2.
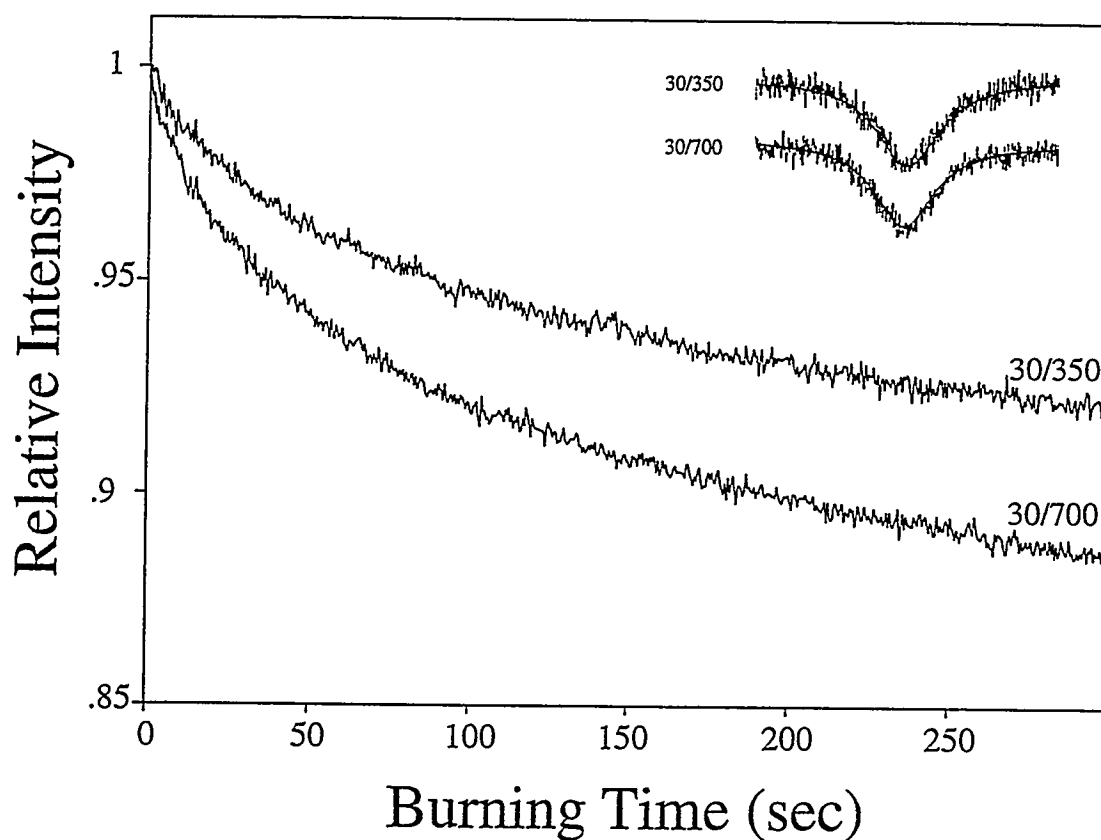
Figure A-5. Hole growth curves and hole shapes of TO-PRO-3 bound to double-stranded calf thymus DNA with different dye to DNA ratios at 4.2 K. The inset shows hole shapes of two samples after 300 sec burning. Upper curve and hole shape correspond to 30 μM TO-PRO-3 and 350 μM_{bp} double-stranded calf thymus DNA. Bottom curve and hole shape correspond to 30 μM TO-PRO-3 and 700 μM_{bp} double-stranded calf thymus DNA. Hole widths are 10.4 and 9.7 GHz, respectively. The burn wavelength, λ_B = 652 nm; burn intensity, 1.8 μW/cm^2.

from $1/5_{bp}$ to $1/20_{bp}$. The observed difference in the hole formation kinetics may be due to changes in binding modes and/or sites.

Fluorescence line narrowing spectroscopy

Fluorescence line narrowing (FLN) spectra of TO-PRO-3 and TO-PRO-3 bound to various DNAs are shown in Figure A-6. The vibrational frequencies in the FLN spectra, are the same as the ones observed in vibronic hole burning. Distinctive modes are also observed and labeled with an asterisk. Curves b and d correspond to double- and single-stranded DNA samples, respectively. Broad emission underneath the zero phonon lines is noted in curves of DNA samples. The broad emission is more clearly noticed in single-stranded calf thymus DNA and poly(dG-dC)·poly(dG-dC) samples with the emission maxima around 660 nm (curves d and e in frame B, respectively).

Dispersive kinetics of nonphotochemical hole growth and quantum yield

We found that the hole growth kinetics of TO-PRO-3 is independent of the burning temperature, in the temperature range 4.2 K to 2.1 K in agreement with the findings of Kenney et al. [3]. Since kT (at T = 4.2 K or 2.1 K) $<<$ ω_m = 30 cm^{-1} (mean phonon frequency), the value for S must be the same at both temperatures studied. The temperature dependence of the hole growth kinetics was attributed to the temperature dependence of the peak absorption cross section, which is inversely proportional to homogeneous linewidth of the ZPH, Γ_{hom}, at low temperature. At low temperature it was established that Γ_{hom} is proportional to T$^{1.3}$ [6]. Therefore, when the homogeneous linewidth of the ZPH is taken into account according to T$^{1.3}$ law, the excellent fit shown in Figure 6-7 (kinetic curves measured at 2.1 K) using the same parameters as those
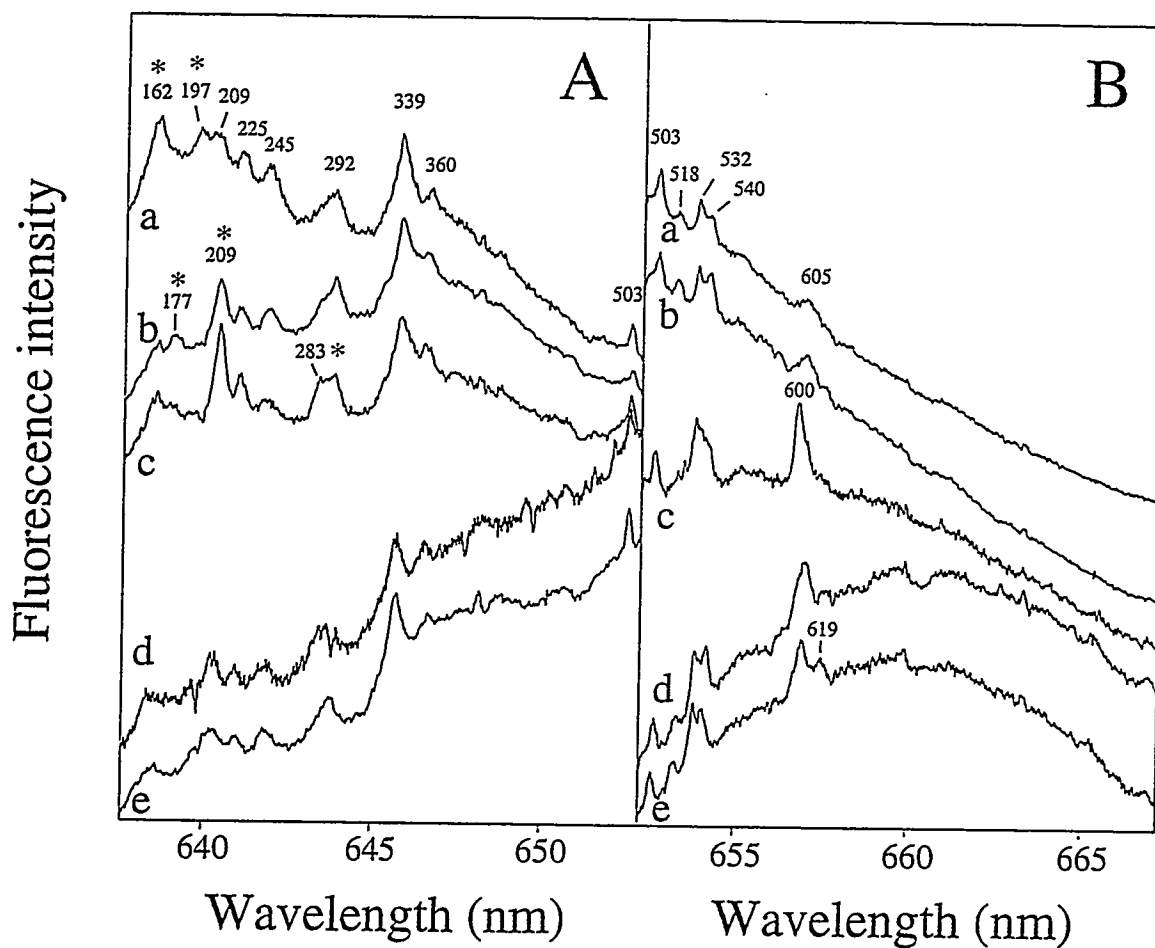
Figure A-6. Fluorescence line-narrowing spectra of TO-PRO-3 and TO-PRO-3 bound to various DNAs at 4.2 K. Curve a, the free dye; curve b, the dye bound to double-stranded calf thymus DNA; curve c, the dye bound to poly(dA-dT)·poly(dA-dT); curve d, the dye bound to single-stranded calf thymus DNA; curve e, the dye bound to poly(dG-dC)·poly(dG-dC). λ_{ex} = 632.01 nm. An asterisk is used to label the mode which is distinctive (see the text).

obtained for the kinetics at 4.2 K indicates that the hole burning efficiency is the same at those two temperatures.

The average relaxation rates associated with hole burning and the average quantum yields for hole burning can be calculated based on the kinetic parameters obtained. The average relaxation rate, $<R>$, is [3]:

$$<R> = R_0 \exp(2\sigma_\lambda^2)$$

where $R_0 = \Omega_0 \exp(-2\lambda_0)$. For free TO-PRO-3, using $\lambda_0 = 7.8$ and $\sigma_\lambda = 0.86$, $<R>$ is calculated to be 5.6×10^6 s^{-1}. For poly(dA-dT)·poly(dA-dT) and poly(dG-dC)·poly(dG-dC), $<R>$ values are 8.9×10^6 s^{-1} and 2.5×10^6 s^{-1}, respectively. The average hole burning quantum yield, $<\phi>$, can be calculated from the average relaxation rate by the relationship:

$$<\phi> = <R>/(<R> + 1/\tau)$$

where τ is the life time of the excited state. For free TO-PRO-3, and TO-PRO-3 bound to poly(dA-dT)·poly(dA-dT) and poly(dG-dC)·poly(dG-dC), the average hole burning quantum yields are 1.9×10^{-2}, 3.5×10^{-3} and 9.7×10^{-3}, respectively. These values are comparable to the hole burning quantum yields of other organic dyes in glassy matrices (10^{-2} or 10^{-3}) [3]. The average hole burning quantum yields of TO-PRO-3 bound to poly(dA-dT)·poly(dA-dT) and poly(dG-dC)·poly(dG-dC) are different from the values reported for daunomycin bound to (dA-dT)$_5$·(dA-dT)$_5$ and (dG-dC)$_5$·(dG-dC)$_5$ by Flöser and Haarer [7]. For daunomycin, the quantum yield of the system with (dA-dT)$_5$·(dA-dT)$_5$ is 0.029 while that of (dG-dC)$_5$·(dG-dC)$_5$ is 4.8×10^{-4} indicating daunomycin bound to (dA-dT)$_5$·(dA-dT)$_5$ burns 60 times more efficiently than when bound to (dG-dC)$_5$·(dG-dC)$_5$. On the contrary, TO-PRO-3 showed 2.8 times more efficient burning when it is bound to poly(dG-dC)·poly(dG-dC) than when bound to poly(dA-dT)·poly(dA-dT). The differences in hole burning efficiencies of daunomycin and TO-PRO-3 indicate that the

interaction of the chromophore with DNA is different due to structural differences of chromophores. Daunomycin intercalates its planar aromatic ring system between the base pairs. Considering the size of the chromophore of TO-PRO-3, it would be reasonable to assume that the chromophore can be accommodated only partially between base pairs or binds in grooves instead of between base pairs.

It is worth speculating the observed differences in hole-burning (saturated hole depth) and fluorescence emission properties of TO-PRO-3 bound to poly(dG-dC)· poly(dG-dC) and to poly(dA-dT)·poly(dA-dT) in terms of the binding structure of the dye molecule. The observed Huang-Rhys parameter (S) of the dye bound to poly(dG-dC)· poly(dG-dC) is larger than that of the dye bound to poly(dA-dT)·poly(dA-dT). This imply that there are more TO-PRO-3 intercalated partially in the case of poly(dG-dC)· poly(dG-dC) while the externally bound (including groove binding) TO-PRO-3 prevails in the case of poly(dA-dT)·poly(dA-dT). The increased contribution from partially intercalated dyes can also explain the red shifted emission spectrum in the poly(dG-dC)· poly(dG-dC) sample. The conformational differences of the dyes bound to the two polynucleotides may be due to the stronger interaction between the dye and guanine-cytidine bases than that between the dye and adenine-thymine bases. It should be mentioned that the estimated hole burning efficiency of TO-PRO-3 bound to DNA from hole growth kinetics represents only the dye adopting a external conformation(s). In this external conformation(s), TO-PRO-3 bound to poly(dA-dT)·poly(dA-dT) and poly(dG-dC)·poly(dG-dC) seem to show the similar hole burning efficiencies. A more detailed explanation at the molecular level requires further investigation including the structure of TO-PRO-3 bound to DNA. Nevertheless, it is evident that the hole burning efficiency is sensitive to dye-DNA interactions.

It should be noted that the length of the DNA also plays an important role in the interaction of the dye with DNA. TO-PRO-3 bound to poly(dG-dC)·poly(dG-dC) and double-stranded 11-mer oligonucleotide exhibit the very similar absorption spectra and hole growth kinetic parameters, however, their emission spectra showed different maxima and band widths. The discrepancy in fluorescence emission spectra may indicate that the strongly coupled states of the dye bound to oligonucleotide is different from the one bound to polynucleotide. The DNA length effect was also observed when comparing single-stranded polynucleotide and oligonucleotide samples. Both single-stranded oligonucleotide samples studied, d-(CCATCGCTACC) and d-(GGTAGCGATGG), showed smaller Stoke's shifts (149 and 252 cm^{-1}, respectively) than single-stranded calf thymus DNA sample (463 cm^{-1}) while the S value of d-GGTAGCGATGG sample (1.8) was larger than that of single-stranded calf thymus DNA (1.3). Therefore, in the case of single-stranded DNA, the interaction of the dye with DNA seems to be affected even more by the length of the DNA than in the case of double-stranded DNA. Also the base sequence effect of the single-stranded oligonucleotide was observed. d-(GGTAGCGATGG) sample showed a larger S value (more contribution from base-stacked conformation) than d-(CCATCGCTACC) sample. The former oligonucleotide contains 8 purines and 3 pyrimidines while the latter one contains 3 purines and 8 pyrimidines implying that the observed base sequence effect may correlate with the content of purine/pyrimidine bases.

Concluding Remarks

In this study, we have shown that optical and hole burning properties of TO-PRO-3 depend on DNA types, sequences and lengths all of which affect the interaction between TO-PRO-3 and DNA. Purine bases appear to interact more with the dye resulting in the dye adopting the base-stacked conformation more than external conformation. Contribution from the dye adopting base-stacked conformation is larger when bound to long DNA than when bound to oligonucleotides.

References

1. Haugland,R.P. (1992) *Handbook of Fluorescent Probes and Research Chemicals, 5th ed.* (Larison, K.D. Ed.) Molecular Probes, Inc.

2. Wells,R.D., Larson,J.E., and Grant,R.C. (1970) *J. Mol. Biol.* **54**, 465.

3. Kenney,M.J., Jankowiak,R., and Small,G.J. (1990) *Chem. Phys.*, **146**, 47.

4. Jankowiak,R., Small,G.J., and Athreya,K.B. (1986) *J. Phys. Chem.* **90**, 3896.

5. Moerner,W.E., Lenth,W., Bjorklund,G.C. (1988) In *Topics in Current Physics, Persistent Spectral Hole Burning: Science and Applications* (Moerner,W.E.,Ed) Springer-Verlag. Berlin, Heidelberg, Vol. 44, Chapter 7, p251.

6. Völker,S. (1989) In *Relaxation Processes in Molecular Excited States*, (Fünfschilling,J., Ed.) Kluwer Academic Publisher, Dordrecht, p 113 and references therein.

7. Flöser,G., and Haarer,D. (1988) *Chem. Phys. Lett.* **147**, 288.